

Durham E-Theses

Fluorinated Benzylphosphonic Acid Derivatives for Work Function Modification

ABRAHAM, FFION

How to cite:

ABRAHAM, FFION (2014) *Fluorinated Benzylphosphonic Acid Derivatives for Work Function Modification*, Durham theses, Durham University. Available at Durham E-Theses Online:
<http://etheses.dur.ac.uk/10622/>

Use policy

The full-text may be used and/or reproduced, and given to third parties in any format or medium, without prior permission or charge, for personal research or study, educational, or not-for-profit purposes provided that:

- a full bibliographic reference is made to the original source
- a [link](#) is made to the metadata record in Durham E-Theses
- the full-text is not changed in any way

The full-text must not be sold in any format or medium without the formal permission of the copyright holders.

Please consult the [full Durham E-Theses policy](#) for further details.

Durham University

A Thesis Entitled

Fluorinated Benzylphosphonic Acid Derivatives for Work Function Modification

By

FFION ABRAHAM

(Ustinov College)

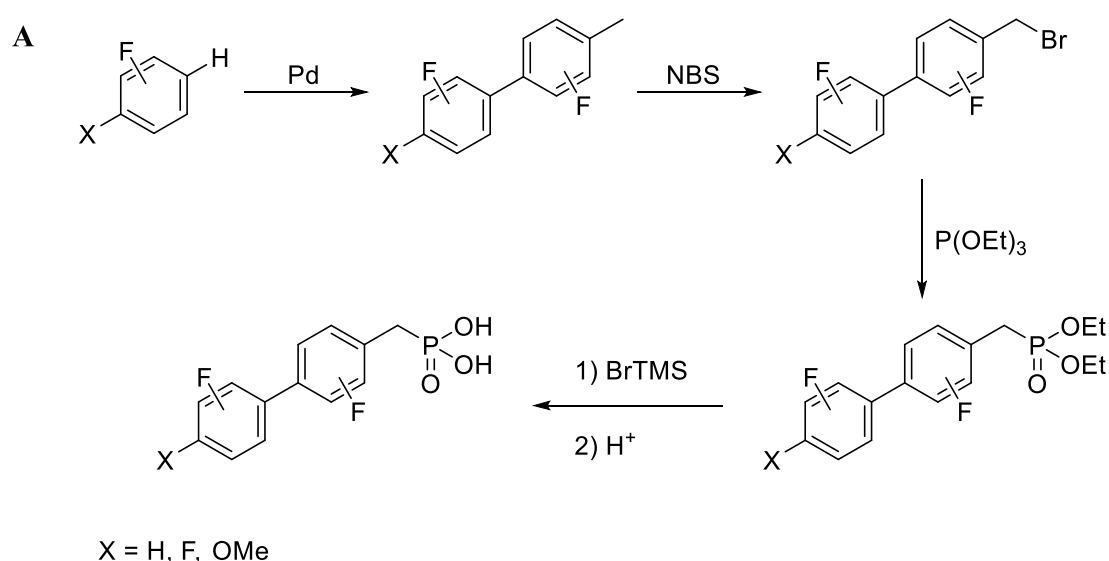
A candidate for the degree of Doctor of Philosophy

Department of Chemistry, Durham University

2014

Abstract

Methodology for the synthesis of polyfluorinated biphenyl benzylphosphonic acids was developed and various highly fluorinated phosphonic acid derivatives may be synthesised from the corresponding fluorobenzene system. (A) Synthesis of analogous benzylphosphonic acids from corresponding benzyl bromides is also described. The use of these systems as self-assembled monolayers on AlO_x was assessed by a range of surface-sensitive analytical techniques.



The surface energy and work function of aluminium oxide (AlO_x) may be altered upon the adsorption of monolayers formed of partially fluorinated benzylphosphonic acids. Replacement of surface hydroxyl groups by hydro- and fluorocarbon modifiers significantly lowers the surface energy of AlO_x , increasing its compatibility with suitable organic layers for applications such as organic light emitting diodes (OLEDs) and organic thin film transistors (OTFTs). Fluorinated self-assembled monolayers can alter the work function of AlO_x by inducing a surface dipole upon adsorption. Depending on the nature of the dipole, the work function can either be increased or decreased over a total range of 0.91 eV.

In addition, the synthesis of related, highly polar, piperazine based biaryl benzylphosphonic acids, and their biphenyl counterparts, is described.

Acknowledgements

Firstly, I would like to thank Professor Graham Sandford, my academic supervisor, for his invaluable help, support and encouragement throughout the course of my Ph.D. I would also like to thank Dr. Florian von Wrochem, Dr. William Ford, Dr. Frank Scholz and Miss. Gabriele Nelles for their advice and contributions towards my project and for their hospitality during my time in Germany and SONY for funding.

This research would not have been possible without the help of the highly professional technical staff at Durham University, namely: Dr. Alan Kenwright, Mr. Ian McKeag, Mrs. Catherine Heffernan, Dr. Juan Malavia (NMR); Dr. Jackie Mosely, Dr. David Parker, Mr. Peter Stokes (Mass spectrometry); Miss. Judith Magee (Elemental analysis); Dr. Dmitrii Yufit (X-ray crystallography) and Mr. Peter Coyne, Mr. Malcom Richardson and Mr. Aaron Brown (Glassblowing).

I would like to thank all members of Team Fluorine, both past and present, particularly Dr. Jessica Breen, Dr. Katharine Linton, Mr. Robert Goodwill, Mr. Tony Harsanyi, Mr. Matthew Didsbury, Mr. Adam Hope and Mr. Bear. I would also like to thank anyone who has found time to share a beer and a game of pool with me over my time in Durham, providing me with much entertainment along the way. Special mention must go to the Back Row Bandits, Al and Cecily.

Finally, I would like to thank my mum and dad for always encouraging me to do my best and pursue my ambitions, Siân, Elin and Bryn for their love and support, and Andy for making the last year of my Ph.D. by far the best.

Memorandum

The work described in this thesis was carried out at Durham University between October 2010 and December 2013. This thesis is the work of the author, except where acknowledged by reference and has not been submitted for any other degree. The copyright of this thesis rests with the author. No quotation from it should be published without the prior written consent and information derived from it should be acknowledged.

Nomenclature and Abbreviations

Ac	Acetyl
acac	Acetylacetonate
AIBN	Azobisisobutyronitrile
AlO _x	Aluminium oxide
aq.	Aqueous
Ar	Aryl
ASAP	Accurate solids analysis probe
D	Debye
DCM	Dichloromethane
DBA	Dibenzylideneacetone
DFT	Density functional theory
DMA	Dimethylacetamide
DME	Dimethoxyethane
DMF	<i>N,N</i> -Dimethylformamide
DMSO	Dimethylsulfoxide
dppe	1,2-Bis(diphenylphosphino)ethane
DSSC	Dye sensitised solar cell
E_B	binding energy
E_F	Conduction band energy level
EI	Electron ionisation
E_K	Kinetic energy
eq.	equivalents
Et	Ethyl
eV	Electron volts
E_{vac}	Vacuum energy level
GC-MS	Gas chromatography-mass spectrometry
HOMO	Highest occupied molecular orbital
hrs	Hours
<i>i</i> Pr	Isopropyl
IR	Infrared
IRRAS	Infrared reflectance absorption spectroscopy

J	Coupling constant, Hz
LCD	Liquid crystal display
LUMO	Lowest occupied molecular orbital
m.p.	Melting point
M	Metal
Me	Methyl
MeCN	Acetonitrile
mins	Minutes
mmol	Millimoles
mol	Moles
NBS	<i>N</i> -Bromosuccinimide
<i>n</i> Bu	Butyl
NMR	Nuclear magnetic resonance
Oct	Octyl
OLED	Organic light emitting diode
OP	Oxygen plasma
OTFT	Organic thin film transistor
PES	Photoemission spectroscopy
Ph	Phenyl
pK_a	Acid dissociation constant
PM-IRRAS	Polarisation modulation infrared reflectance absorption spectroscopy
ppm	Parts per million
Pr	Propyl
rt	Room temperature
SAM	Self-assembled monolayer
SC	Solvent clean
SEE	Secondary electron edge
S_NAr	Nucleophilic aromatic substitution
SPB	Spherical polyelectrolyte brushes
T-BAG	Tethering by aggregation and growth
<i>t</i> -Bu	Tertiary butyl
TFA	Trifluoroacetic acid
TFT	Thin film transistor
THF	Tetrahydrofuran

TMEDA	Tetramethylethylenediamine
TMS	Trimethylsilyl
u.v.	Ultraviolet
UVO	Ultraviolet-ozone
W	Work function of spectrometer
XPS	X-ray photoelectron spectroscopy
γ	Surface tension
Δ	Heat
δ	Chemical shift / ppm
μ	Dipole moment
μW	Microwave irradiation
Φ	Work function
Φ_e	Barrier for electron injection
Φ_h	Barrier for hole injection

Contents

Abstract	i
Acknowledgements	ii
Memorandum	iii
Nomenclature and Abbreviations.....	iv
Chapter 1: Introduction	1
1.1 Overview	1
1.2 Self-Assembled Monolayers	1
1.2.1 Structures of SAMs.....	1
1.2.2 Altering Metal Surface Properties Through The Use of SAMs.....	5
1.3 Aspects of Organofluorine Chemistry	8
1.3.1 Overview.....	8
1.3.2 Syntheses of Perfluorinated Aromatic Systems.....	9
1.3.2.1 Sources of Fluorine	9
1.3.2.2 Saturation Rearomatisation Processes.....	10
1.3.2.3 Direct Replacement of Chlorine for Fluorine	11
1.3.3 Reactivity Profile of Perfluorinated Aromatic Systems	12
1.3.3.1 S _N Ar Reactions of Highly Fluorinated Aromatic Systems	14
1.4 Synthesis of Highly Fluorinated Biphenyl Systems.....	17
1.4.1 Reaction at an Aryl C–F Bond.....	17
1.4.1.1 S _N Ar Reactions.....	17
1.4.1.2 Radical Reactions.....	18
1.4.2 Suzuki-Miyaura Cross-Coupling Reactions	19
1.4.2.1 Introduction	19
1.4.2.2 Uses of Pentafluorophenylboronic Acid	20
1.4.2.3 Uses of Fluorinated Borate and Boronate Salts	23
1.4.2.4 Uses of Fluorinated Aryl Halides.....	26
1.4.3 C–F Bond Activation Reactions	28
1.4.4 C–H Bond Activation Reactions.....	30
1.4.4.1 Coupling Polyfluorobenzenes with Aryl Halides	30
1.4.4.2 Reactions of Polyfluorobenzenes with Alternative, Preactivated Coupling Partners.....	35

1.4.4.3 Coupling Polyfluorobenzenes with Simple Arenes	37
1.4.5 Decarboxylation Reactions	39
1.5 Summary	42
1.6 References to Chapter 1.....	44
Chapter 2: Synthesis of Fluorinated Biphenylphosphonic Acids	50
2.1 Introduction	50
2.2 Aims and Objectives	50
2.3 Synthetic Strategy.....	54
2.4 Results and Discussion	56
2.4.1 Synthesis of Fluorinated Phosphonic Acid Precursors	56
2.4.1.1 Palladium Catalysed Synthesis of Fluorinated Biphenyl Systems.....	56
2.4.1.2 Synthesis of an Acetylene Bridged Fluorinated Biphenyl	64
2.4.2 Attachment of a Phosphonic Acid Moiety by S_NAr	66
2.5 Conclusions	68
2.6 References to Chapter 2.....	70
Chapter 3: Synthesis of Fluorinated Benzylphosphonic Acids.....	72
3.1 Introduction	72
3.2 Aims and Objectives	72
3.3 Synthetic Strategy.....	75
3.4 Results and Discussion	76
3.4.1 DFT Calculations of Benzylphosphonic Acids	76
3.4.2 Synthesis of Benzylphosphonate Esters by Michaelis-Arbuzov Reactions....	78
3.4.3 Hydrolysis to Benzylphosphonic Acids.....	79
3.4.4 Synthesis of Benzylphosphonic Acids with Alternative Terminal Substituents	82
3.5 Conclusions	85
3.6 References to Chapter 3.....	87
Chapter 4: Synthesis of Fluorinated Biaryl Benzylphosphonic Acids	88
4.1 Introduction	88
4.2 Aims and Approach.....	88
4.3 Synthetic Strategy.....	90
4.4 Results and Discussion	92
4.4.1 DFT Calculations of Biphenyl Benzylphosphonic Acids.....	92
4.4.2 Synthesis of Non-Fluorinated Biphenyl Benzylphosphonic Acids	93

4.4.3 Synthesis of Fluorinated Biphenyl Benzylphosphonic Acids.....	94
4.4.3.1 Reactions of 4-Bromobenzyl Bromide.....	94
4.4.3.2 C–H Bond Activation Reactions.....	98
4.4.3.3 Synthesis of Alternative Fluorinated Benzylphosphonic Acids.....	103
4.4.4 Incorporation of a Carboxylic Acid Anchor Group.....	106
4.4.5 Synthesis of Alternative Biaryl Phosphonic Acids.....	108
4.4.5.1 Synthesis of Aminomethylphosphonic Acids.....	109
4.4.5.2 Synthesis of Analogous Phenyl Derivatives.....	114
4.5 Conclusions.....	116
4.6 References to Chapter 4.....	118
Chapter 5: Surface Modification of Aluminium Oxide by Fluorinated Phosphonic Acid Derivatives.....	
120	
5.1 Introduction.....	120
5.2 Aims and Approach.....	120
5.3 Methods of Surface Characterisation for Monolayer Studies.....	122
5.3.1 Contact Angle Goniometry.....	122
5.3.2 PM-IRRAS.....	123
5.3.3 XPS.....	125
5.4 Results and Discussion.....	126
5.4.1 Sample Preparation.....	126
5.4.2 SAM studies.....	129
5.4.2.1 Contact Angle Goniometry and Surface Coverage.....	130
5.4.2.2 PM-IRRAS Measurements.....	135
5.4.2.2.1 General Considerations for Measurements on AlO _x	135
5.4.2.2.2 PM-IRRAS Results.....	135
5.4.2.3 Work Function Tuning.....	150
5.5 Conclusions.....	153
5.6 References to Chapter 5.....	159
Chapter 6: Experimental.....	
161	
6.1 General.....	161
6.2 Experimental Data to Chapter 2.....	162
6.3 Experimental Data to Chapter 3.....	171
6.4 Experimental Data to Chapter 4.....	188
6.5 Experimental Data to Chapter 5.....	219

6.6 Experimental Data for Calculated Dipole Moments	223
6.7 References	224
Appendix A	226
Appendix B	231
Appendix C	243

Chapter 1

Introduction

1.1 Overview

Fluoroorganic molecules have already found many applications within electronic products, notably in liquid crystal display (LCD) devices, due to the high electronegativity of the fluorine atom capable of inducing a strong dipole on any organic system, and the strong C–F bond being stable under many operating conditions. The use of self-assembled monolayers (SAMs) find widespread applications within photovoltaic and (opto)electronic devices through their ability to alter specific properties of the metal surfaces to which they are attached. The focus of this thesis is the synthesis of a range of fluorinated aromatic derivatives, and their subsequent testing as SAMs on aluminium oxide (AlO_x), in a project in collaboration with the SONY Corporation. Consequently, this introduction will provide background information on the relevant aspects of SAMs and fluoroaromatic chemistry.

1.2 Self-Assembled Monolayers

1.2.1 Structures of SAMs

The ability to control and manipulate the physical and electronic properties of semiconductors and metals is of key significance when incorporating such materials into electronic devices. A SAM is an ordered structure, formed by the chemisorption of specific molecules onto surfaces, which can be specifically designed to exhibit certain properties.¹

Compounds that are used for the formation of monolayers on metal surfaces, such as those described in this thesis, can have their basic structures simplified into three distinct components; the anchor group, the core spacer group and the terminal functional group. [Figure 1]

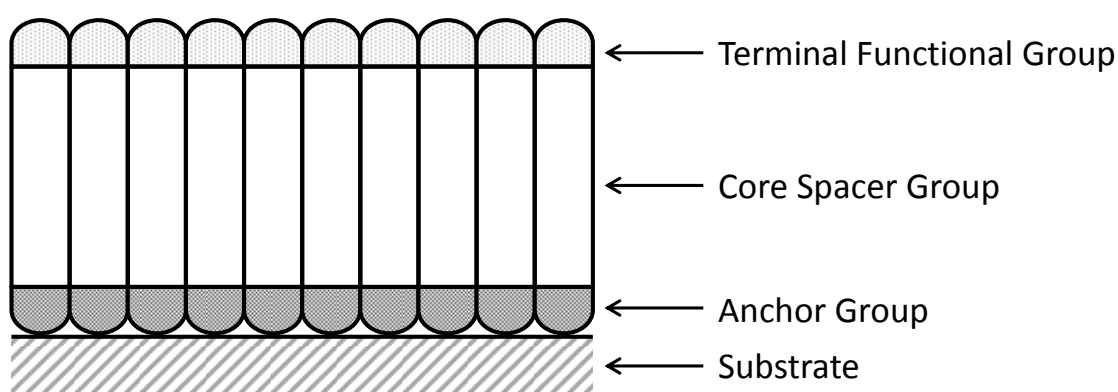


Figure 1. Schematic of an organic monolayer attached to a substrate. Figure adapted from Ulman.¹

The anchor group allows for the covalent linkage of organic systems to the metal surface, the strength of this binding being dependent upon the nature of the interaction between the anchor group and the substrate. An anchor group is required to couple the organic molecules to the substrate as metal-carbon bonds are generally not sufficiently stable toward hydrolysis. The spacer group, as well as providing a connection between the anchor group and the terminal functional group, determines the thickness and stability of the monolayer and may alter the electronic properties of the substrate. The terminal functional group, like the spacer group, can contribute to altering the electronic properties of the substrate, but also provides a potential site for further chemical reactions, thus determining the surface properties and chemistry observed at this interface.²

Many different inorganic materials such as metals, metal oxides and alloys can be modified using monolayers in this way. Each possess different surface chemistries and properties, and for this reason a number of different anchor groups have been used for the functionalisation of metal surfaces. Whilst each anchor group may possess advantages and disadvantages for certain surfaces, there often exists more than one moiety capable of binding effectively to a specific substrate. Although many more exist,² the most commonly utilised anchor groups include those derived from thiols, silanes, carboxylic acids and phosphonic acids. The various advantages and disadvantages of each of these anchor groups, along with examples of their uses, will now, briefly, be discussed.

Organosulfur derivatives have a high affinity for transition metal surfaces, and as such can form highly ordered, dense monolayers.² The most widely studied monolayer-substrate systems are those of alkanethiols on metals, particularly gold.^{3–11} The well-characterised, uniform SAMs of alkanethiols have been used for selective chemical etching of thin metal films,¹² as well as for model, biological surfaces¹³ and in a number of electronic applications.² It has, however, been shown that, when heated, the gold-thiol bond is easily broken and desorption of the monolayer from the substrate is observed in solution.¹⁴

Organosilane derivatives are also widely used for the modification of surfaces, in particular silicon-containing substrates. Silane based monolayers possess many desirable properties, including their thermal and chemical stability for attachment to a variety of substrates. This robustness stems from linkages between the silane and the substrate as well as between neighbouring silane molecules. Unlike other monolayer-substrate systems, the formation of silane monolayers involves an irreversible covalent cross-linking step.¹⁵ However, production of high-quality silane monolayers is far from simplistic as the formation of complete, robust monolayers is heavily dependent upon the hydrolysis of the organosilane derivative. This requires the careful control of water levels present during monolayer formation; in the absence of water, incomplete monolayers are formed whereas an excess of water can result in self-condensation and polymerisation leading to the formation of multilayers. [Figure 2] Self-condensation may also occur over time and so, to ensure long-term performance, monolayers must be stored in anhydrous conditions.^{1,16,17}

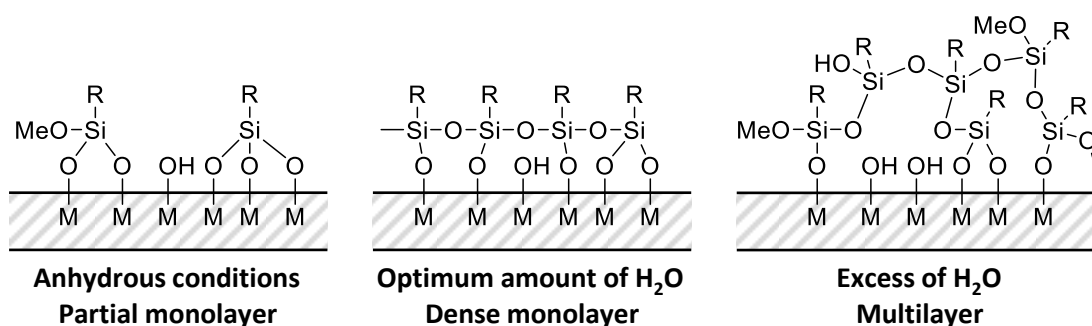


Figure 2. Schematic showing the effects of no, optimum, and excess water on the modification of an oxide surface by a silane. Figure adapted from Mutin et al.¹⁷

Organosilane monolayers have found use in a variety of applications, including ultrathin dielectric materials for thin film transistors (TFTs)^{18–20} and the modification of ZnO, a candidate for hybrid solar cells.²¹ Densely packed silanes have also been shown to behave as excellent insulators suitable for nanoscale electronic device fabrication.²²

Although much of the current literature focuses upon thiol- and silane- based monolayer-substrate systems, there also exist a number of monolayer systems based on organic acid monolayers.¹⁵

Carboxylic acids have been used successfully for the modification of semiconductor surfaces. Monolayers bound to TiO₂ and ZnO via carboxylic acid groups have been used extensively for the fabrication and study of dye-sensitised solar cells (DSSCs), providing enhanced surface light absorption and improved photoelectric conversion efficiencies.^{23–27} When compared to the surface bonds observed between thiols on gold and siloxanes on silica, discussed above, the interaction between carboxylic acids and many metal oxides is relatively weak. Furthermore, in the case of functionalised acids, competition for surface sites can exist between the anchor group and terminal functional group resulting in undesirable looped structures and poor quality monolayers.^{28,29} Although high coverage monolayers of carboxylic acids have been reported, the relative weakness of their binding has resulted in observations of significant monolayer removal simply through rinsing with solvents.³⁰

Although the concept of organic monolayer formation on substrates has existed since the 1920s,³¹ the use of phosphonic acids for the modification of metal oxide surfaces only began development in the early '90s. Since this time, phosphonic acid derivatives have been utilised for a variety of applications due to the robust nature of the monolayers they form. Compared to carboxylic acids, phosphonic acids have lower pK_a values and, consequently, have been shown to bind to the surfaces of metal oxides with much stronger interactions.^{32,33} In the case of TiO₂, increased Ti–O–P bond strengths have allowed for the production of solar cells which possess better long-term stabilities.²⁹ Phosphonic acids form extremely well-packed monolayers on a variety of metal oxide surfaces, are stable under ambient conditions and are not hydrolytically sensitive.^{34,35} Unlike carboxylic acids, they form strong bonds to metal oxide surfaces, resulting in a robust monolayer. The formation of M–O–P bonds through

heterocondensation and coordination is kinetically favoured and, unlike their silicon counterparts, homocondensation of P–O–H bonds to P–O–P bonds occurs only at high temperatures.¹⁶ Phosphonic acid monolayers have been reported for use in, amongst others, organic thin-film transistors (OTFTs),^{36,37} corrosion resistance applications³⁸ and as biomaterials.³⁹

The terminal functional group of a SAM (Figure 1) can provide further functionality capable of conducting chemistry that may otherwise have proven difficult at the surface of a metal substrate. The use of alcohol and carboxylic acid terminated SAMs allow for a wide range of further transformations and reactions to be conducted, with the formation of highly ordered bilayers possible.¹ Adler *et al.* have also reported the cross-linking of aliphatic isocyanates with long chain phosphonic acid SAMs bearing a terminal amino group, to form superior corrosion resistant surfaces.⁴⁰

Finally, the core spacer group within a SAM (Figure 1), as well as providing a connection between the anchor group and terminal functional group, often determines the thickness of a SAM, as well as providing stability. For these reasons, traditionally, the core spacer group of a SAM often consists of functionalised long chain hydrocarbons capable of close packing to provide a dense, stable monolayer.¹

1.2.2 Altering Metal Surface Properties Through The Use of SAMs

Since 1971, and the first reported practice of a monolayer to alter the electronic properties of metal electrodes⁴¹, research into altering specific properties of metal surfaces through the attachment of self-assembled monolayers (SAMs) has grown exponentially. As discussed in the previous section, the use of SAM modified metal oxide substrates has gathered significant interest due to their wide applicability in the area of materials science.

A key property that can be altered through the attachment of a SAM, and one that is of particular interest within this thesis, is the shifting of the work function of a metal substrate. The work function (Φ) of a metal, or metal oxide, corresponds to the amount of energy that must be expended in order to excite an electron from its bound state, within the conduction band (E_F), to an energy level just outside of the metal, the

vacuum level (E_{vac}).⁴² It has been demonstrated that a layer of electrical dipoles on the surface of a metal can produce a substantial shift in various surface potentials, including the work function, provided that there is a net layer dipole moment perpendicular to the substrate surface.⁴³

In organic light emitting diodes (OLEDs), electrons and accompanying holes are injected into an organic layer sandwiched between two metal contacts. The recombination of an electron and a hole in this layer is accompanied by the emission of light and the key to this process is accomplishing efficient injections from the metal substrate. This can be achieved by the contacts possessing a small Schottky energy barrier; determined by the energy difference between the work function of the metal and the electron affinity of the organic material. The insertion of a SAM with an oriented dipole (μ) between the metal and organic material allows for the tuning and manipulation of the energy barrier through the tuning of the work function of the metal. This modification provides a significant degree of control of the electrical characteristics of the system since electronic transport in many electronic devices depends on the properties of the interfaces through which the electrons pass.^{44,45} [Figure 3]

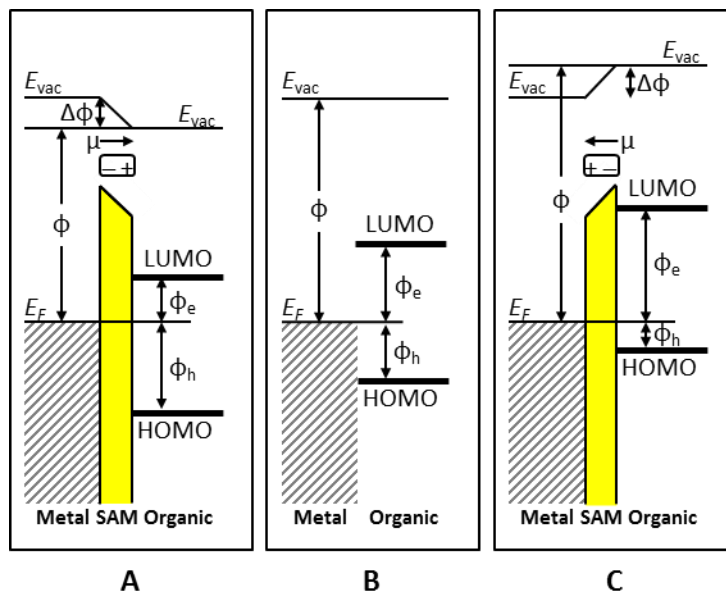


Figure 3. The dependence of the work function of a metal on the insertion of an oriented dipole moment.

The insertion of a SAM with a positive dipole moment, pointing away from the metal surface, decreases the work function of the metal and subsequently lowers the barrier for electron injection, Φ_e . [Figure 3, scheme A] Similarly, the insertion of a SAM with a negative net dipole moment increases the work function of the metal and subsequently lowers the barrier for hole injection, Φ_h . [Figure 3, scheme C]

As well as tuning the way in which two materials can interact at their interface through the alteration of the electronic characteristics of surfaces, the insertion of a SAM can also alter the surface properties of a substrate. Bare metal oxide substrates often possess extremely high surface energies due to the presence of hydroxyl groups which greatly increase the hydrophilicity of the surface. From a device perspective, high surface energies are highly undesirable as subsequently deposited organic layers often possess much lower surface energies and consequently the wetting of the metal substrate is not optimal, the adhesion is poor, and causes device failure.⁴⁶ By covalently bonding a SAM to the surface of the metal, depending on the terminal functional group, the surface energy can be substantially lowered. This can control and improve the subsequent wetting with an organic layer and provide a more even coverage, resulting in better device performance and long term stability. Alongside tuning the surface energy to increase the adhesion force between a metal surface and organic layer, this interaction can be further strengthened through the presence of stacking interactions between the SAM and organic layer. By tuning the terminal functional group of the SAM to resemble functional groups present within the organic layer, enhanced interactions between layers may be achieved and for this reason many SAMs used within electronic devices contain pendent aromatic substrates, a common feature of the organic layer employed within such systems.⁴⁶

In this work, the inclusion of fluorine substituents within compounds designed for SAM formation will be probed to determine the effects of fluorinated systems on, for example, dipole moment, monolayer formation and the modification of metal oxide properties compared to their non-fluorinated counterparts. To aid with the understanding of this work, a discussion concerning the relevant aspects of organofluorine chemistry will be presented in the following section to provide background to the synthetic work presented in this thesis in the preparation of substrates for SAM formation and device application.

1.3 Aspects of Organofluorine Chemistry

This thesis is concerned with reactions of highly fluorinated aromatics, including nucleophilic aromatic substitution and palladium catalysed C–C bond formation, for the synthesis of biphenyls for use as SAMs for electronic applications. Of particular interest is the effect of fluorine substituents in these aromatic structures upon subsequently deposited SAMs on metal oxide surfaces. Reviewed within the following section are the relevant aspects of general organofluorine chemistry and the reactivity profiles of highly fluorinated aromatics of particular interest to the synthetic chemistry studied.

1.3.1 Overview

Fluorine is the 17th most abundant element, yet molecules containing a C–F bond are rarely found in nature. Owing to this, the vast majority of molecules that contain C–F bonds originate from a laboratory synthesis.

With a value of 4 on the Pauling scale⁴⁷, fluorine is the most electronegative element within the periodic table and, due to the large difference in electronegativities, the C–F bond is highly polarised. This polarisation leads to a large dipole, which subsequently results in favourable interaction between the lone pairs on fluorine and the partial positive charge on carbon. This electrostatic attraction makes the C–F bond unusually stable and it is, in fact, the strongest covalent bond in organic chemistry.^{48,49} [Table 1]

Table 1. Bond dissociation energies of common covalent bonds.⁴⁸

Bond	Bond Dissociation Energy/ <i>kJ mol⁻¹</i>
C–F	440.7
C–H	413.4
C–O	351.5
C–C	347.7
C–Cl	328.4
C–N	291.6

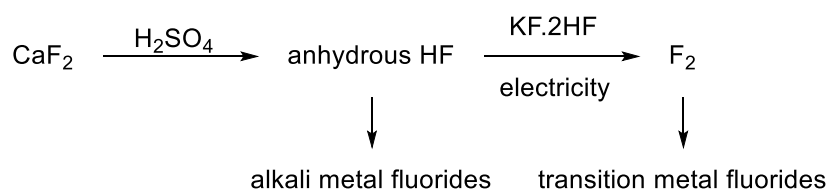
In terms of size, fluorine lies between the boundaries set by hydrogen and oxygen. This similarity means that replacement of either of these atoms for fluorine within a structure can dramatically alter the chemical properties of a compound without overly affecting the related geometry of the system. For example, the replacement of a hydrogen for a fluorine atom can alter the chemical stability as well as properties, such as pK_a , of neighbouring functional groups in a molecule.⁴⁹ Unlike oxygen, the lone pairs possessed by fluorine are reluctant to participate within resonance or hydrogen bonding due to fluorine's high electronegativity. Therefore, replacement of oxygen with fluorine, although retaining the basic shape, can give rise to the drastic alteration of the reactivity of certain molecules.

The chemical variations that accompany such structural alterations have proven, in many cases, to be extremely beneficial and the introduction of fluorine substituents within many chemical systems has become critical to on-going research conducted by many industrial and pharmaceutical industries.⁴⁸

1.3.2 Syntheses of Perfluorinated Aromatic Systems

1.3.2.1 Sources of Fluorine

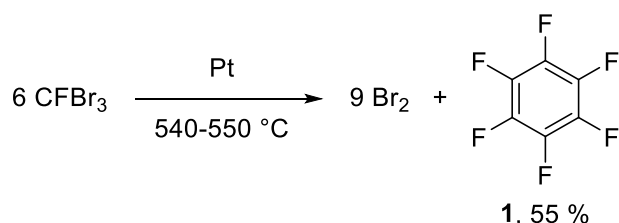
In many fluorination reactions, the key starting material, and the source of fluorine, is anhydrous HF. Formed from the reaction between fluorspar (CaF_2) and concentrated sulfuric acid, anhydrous HF can be reacted to form alkali metal fluorides, F_2 and transition metal fluorides.⁵⁰ [Scheme 1] The synthesis of fluorinated molecules can be achieved through careful, direct reaction with anhydrous HF or with the associated metal fluorides, such as cobalt trifluorides and antimony pentafluoride, or fluorine gas.



Scheme 1. Preparation of various sources of fluorine.

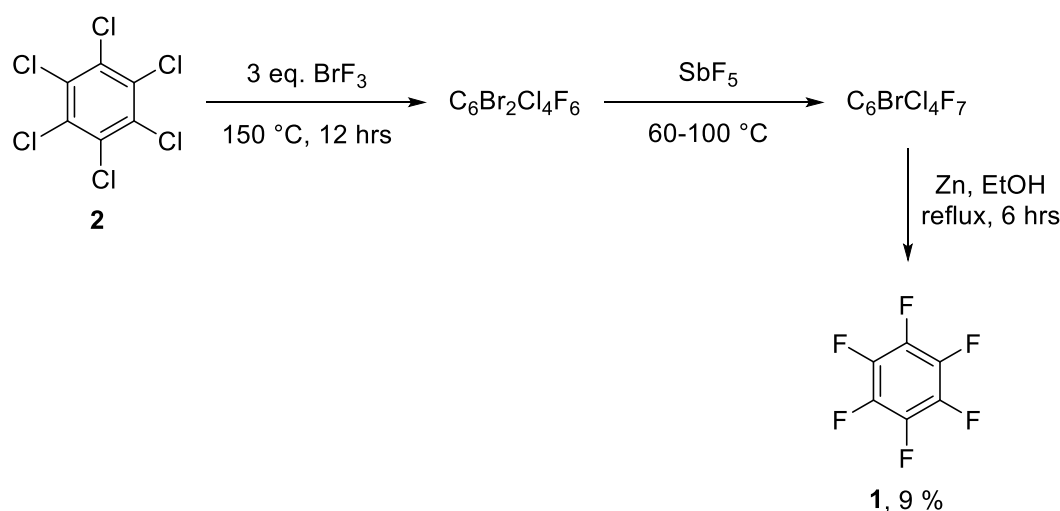
1.3.2.2 Saturation Rearomatisation Processes

Although not reported straight away, it is widely acknowledged that the first relatively simple synthesis of hexafluorobenzene **1** was achieved via the pyrolysis of tribromofluoromethane.⁵¹ [Scheme 2]



Scheme 2. Synthesis of hexafluorobenzene **1** by the pyrolysis of tribromofluoromethane.

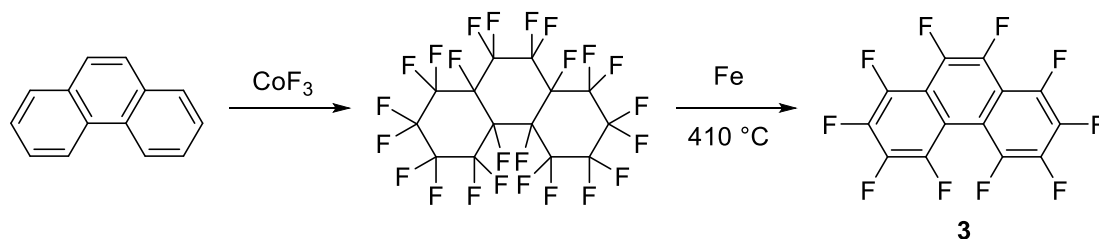
Prior to this publication, however, McBee *et al.* reported in 1947 the synthesis of hexafluorobenzene from hexachlorobenzene **2** at much lower temperatures.⁵² [Scheme 3] Fluorination of hexachlorobenzene by bromine trifluoride, followed by partial replacement of bromine, and dehalogenation of the resulting compound led to the synthesis of hexafluorobenzene by an overall saturation-reductive dehalogenation reaction, albeit in low yield.



Scheme 3. Synthesis of hexafluorobenzene from hexachlorobenzene.

In 1959, a new two-step saturation-rearomatisation procedure was reported for the synthesis of perfluoroaromatic compounds from the corresponding hydrocarbons.⁵³

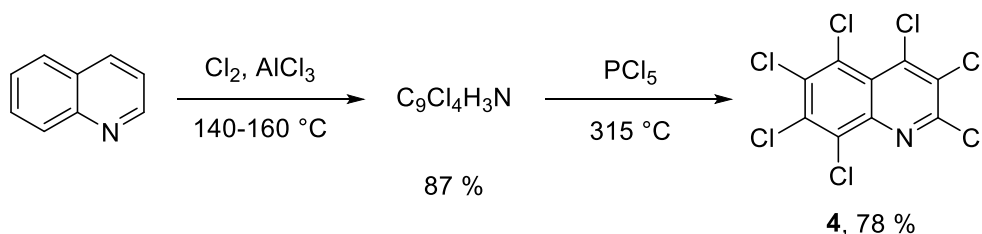
Perfluorinated saturated systems are synthesised by the reaction of an aromatic hydrocarbon with cobalt trifluoride and subsequently defluorinated via heating with iron or nickel, and is still used today on the industrial scale. [Scheme 4]



Scheme 4. Synthesis of perfluorophenanthrene **3** from phenanthrene.⁵⁴

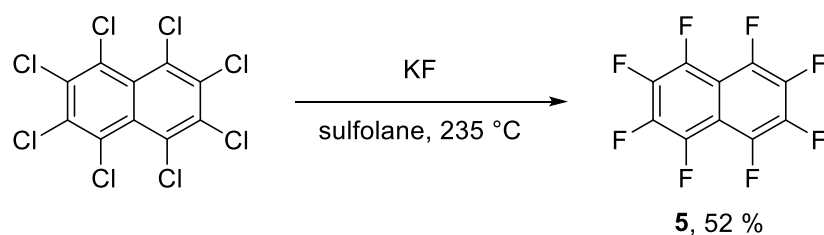
1.3.2.3 Direct Replacement of Chlorine for Fluorine

Fluorination of perchlorinated starting materials (the Halex process) provides another common route towards the synthesis of perfluorinated aromatics. In turn, perchlorinated starting materials are synthesised by the chlorination of hydrocarbons through consecutive reactions with chlorine gas and phosphorous pentachloride at elevated temperatures. [Scheme 5]



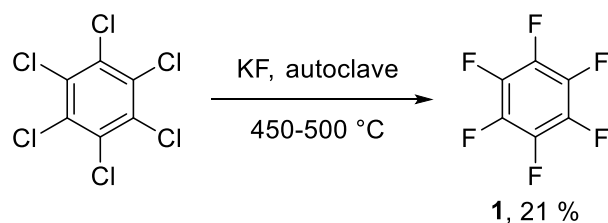
Scheme 5. Synthesis of perchloroquinoline **4** from quinolone.⁵⁵

Subsequent reactions of perchloroaromatics with alkali metal fluorides in highly polar solvents, produces the associated perfluorinated systems through the nucleophilic displacement of chlorine for fluorine. To maintain the level of nucleophilicity required for the reaction to occur, it is essential that water is excluded from the reaction system so as not to solvate the fluoride ion. The first such syntheses of this nature involved the use of KF in sulfolane at high temperatures, as represented in the synthesis of perfluoronaphthalene **5**.⁵⁶ [Scheme 6]



Scheme 6. *Synthesis of perfluoronaphthalene 5.*⁵⁶

The use of sulfolane as a solvent permits Halex reactions to be carried out at high temperatures however the extent of fluorination can be limited by the thermal stability of the solvent. Development of solvent free, high pressure methodology allows for the synthesis of a wide range of polyfluoroaromatic compounds, including hexafluorobenzene **1**.⁵⁷ [Scheme 7]



Scheme 7. *Fluorination of hexachlorobenzene with KF.*

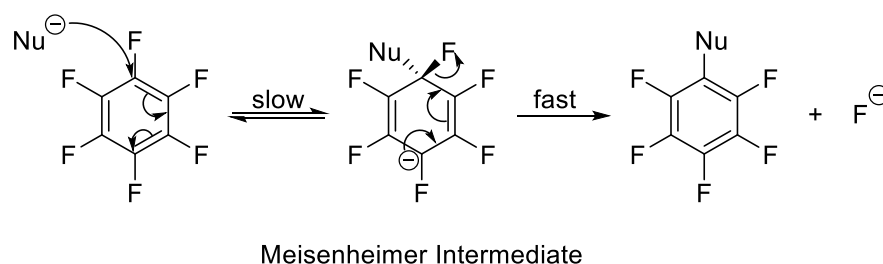
The methods of fluorination discussed here represent the most common methodologies for the syntheses of perfluorinated aromatic systems. The chemistry of these molecules will be discussed within the next section of this chapter.

1.3.3 Reactivity Profile of Perfluorinated Aromatic Systems

Many of the molecules that are described within this thesis contain a perfluorinated aromatic core and such systems have been well studied and reviewed.⁵⁸ Background information on reactivity will be presented from appropriate reviews on the subject.

Whereas unsaturated hydrocarbons are prone to reactions with electrophilic species, the corresponding fluorocarbons display a mirror-image chemistry, being highly reactive towards nucleophilic attack. Due to the high electronegativity of fluorine the majority of

nucleophilic reactions proceed through a two-step addition-elimination nucleophilic aromatic substitution (S_NAr) mechanism. [Scheme 8]



Scheme 8. Mechanism of nucleophilic aromatic substitution (S_NAr).

Initial attack of the nucleophile and subsequent formation of the Meisenheimer intermediate is the rate determining step of the reaction as it involves breaking the aromaticity of the fluoroaromatic ring. Conversely, the loss of fluoride *ipso* to the site of attack is fast due to the restoration of aromaticity in the final product. For successful nucleophilic attack to occur, two key requirements must be satisfied. Firstly, any substituents present must be capable of effectively stabilising the Meisenheimer intermediate and secondly, there must also be a suitable leaving group present. Highly fluorinated aromatic systems satisfy both of these criteria.⁵⁰

Generally, ring fluorine substituents positioned *ortho* and *meta* to the initial site of nucleophilic attack are found to increase the rates of typical S_NAr reactions of fluoroaromatic systems.⁵⁰ Fluorine substituents positioned *ortho* to the site of attack do so by increasing the electrophilicity of the proximal carbon atoms and although fluorine atoms positioned *meta* and *para* will also display this effect, it is less influential. [Figure 4]

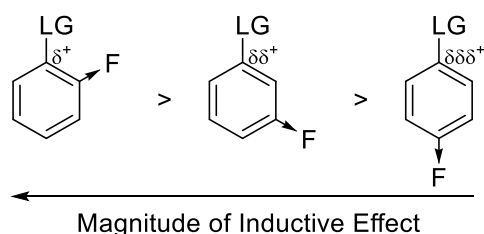
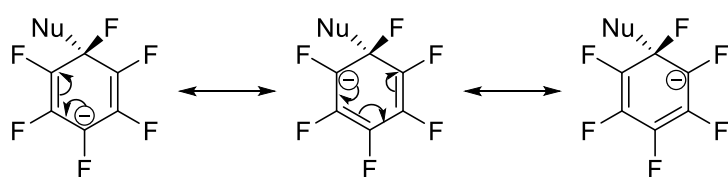


Figure 4. Activating effects of fluorine substituents towards S_NAr .⁵⁸

Ring fluorine substituents positioned *meta* to the site of attack increase the rate of reaction through the stabilisation of the negative charge in the Meisenheimer intermediate. This negative charge can be delocalised onto any of the three carbon atoms situated *ortho* and *para* to the nucleophilic attack. [Scheme 9] In these positions, electron pair repulsion from the fluorine lone pairs effectively counteract any inductive stabilisation gained and so fluorine atoms located *para* to the site of substitution are found to be deactivating. Fluorine substituents β - to the negative charge, *meta* to the nucleophile, are strongly inductively stabilising and reduce the activation energy of the reaction.⁵⁹



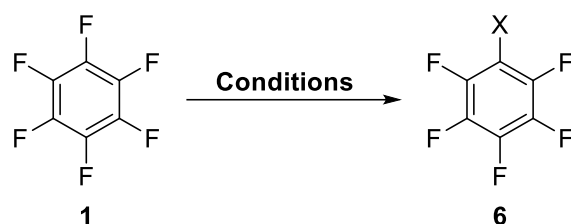
Scheme 9. Resonance structures of Meisenheimer intermediates.

Although, by this rationale, *ortho* fluorine substituents would be expected to destabilise the Meisenheimer intermediate, their powerful activation of the initial site of attack dominates and they are strongly activating substituents. It is found that an incoming nucleophile will react preferentially at the C–F bond with the greatest number of fluorine substituents positioned at sites *ortho* and *meta* to itself.⁶⁰

Having rationalised the reactivity profile of perfluorinated aromatics, the next section of this chapter will focus on the S_NAr reactions of hexa- and pentafluorobenzene derivatives since these systems were used in the research aspect of this project.

1.3.3.1 S_NAr Reactions of Highly Fluorinated Aromatic Systems

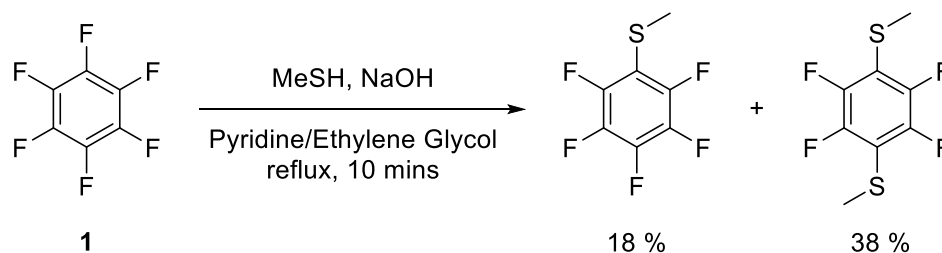
S_NAr reactions of hexafluorobenzene to form monosubstituted pentafluorobenzene derivatives **6** have been studied in great detail and a range of examples are provided here. [Table 2]

Table 2. Representative S_NAr reactions of hexafluorobenzene.

X	Conditions	Yield / %	Ref.
H	LiAlH ₄ , diethyl ether, reflux, 8 hrs	61	[61]
Et	EtMgBr, THF, rt, 23 hrs	56	[62]
<i>n</i> Bu	<i>n</i> BuLi, THF, -60 °C, 2 hrs	53	[63]
OH	NaOH, cyclohexane, reflux, 2 hrs	71	[64]
OEt	KOEt, ethanol, reflux, 1 hr	56	[65]
Ph	PhMgBr, THF, reflux, 11 hrs	7	[62]
NMe ₂	Me ₂ NH, water, 235 °C, 2 hrs	71	[61]

Although initial attempts to arylate hexafluorobenzene using lithium and Grignard reagents were low yielding, there now exists a number of protocols for the synthesis of C–C bonds formed by reactions with other aryl species and these will be discussed in greater depth later in this chapter.

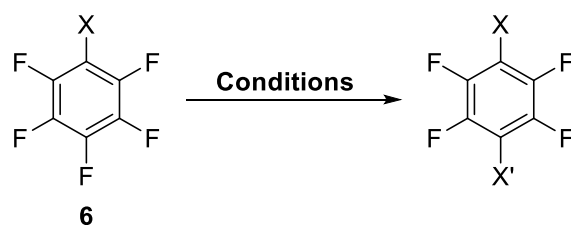
As is shown, a broad range of mono-substituted pentafluorobenzene derivatives **6** are attainable through simple, one-step reactions of hexafluorobenzene. No regioselectivity issues are encountered for these reactions due to the symmetrical nature of the starting material, however problems may arise if the mono-substituted derivative is more activated towards further S_NAr reaction than the starting material. An example of such a situation can be seen in the reaction of hexafluorobenzene and an equimolar quantity of sodium thiomethoxide.⁶⁶ [Scheme 10] With an excess of hexafluorobenzene present the disubstituted product is isolated in a 38 % yield and when the thiomethoxide nucleophile is used in excess the only product detected is that of a tetra-thiolated aromatic derivative.



Scheme 10. S_NAr reactions of hexafluorobenzene with sodium thiomethoxide.⁶⁶

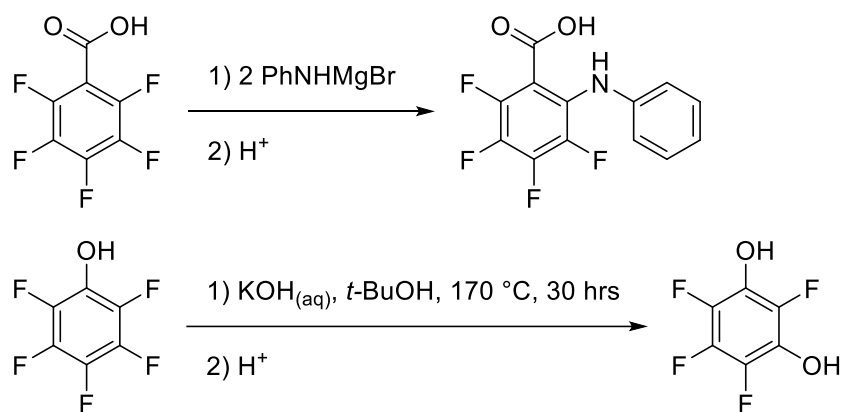
Many monosubstituted perfluorinated aromatics **6** remain highly activated towards further S_NAr reactions due to the remaining electron withdrawing ring fluorine substituents. Whereas the symmetry of hexafluorobenzene provides six equivalent fluorine environments, the subsequent pentafluorobenzene derivative **6** possess three chemically inequivalent C–F bonds, all of which are capable of further S_NAr reactions. As discussed previously, it is found that a nucleophilic species will preferentially attack the C–F bond with the greatest number of fluorine substituents *ortho* and *meta* to it, therefore the majority of S_NAr reactions will occur at the site *para* to the substituent X. [Table 3]

Table 3. Representative S_NAr reactions of pentafluorobenzene derivatives.



X	X'	Conditions	Yield / %	Ref.
H	OH	KOH, pyridine, water, reflux, 25 hrs	32	[61]
Br	NH ₂	NH ₄ OH, 200 °C, 2 hrs	77	[61]
C ₆ F ₅	Et	EtMgBr, THF, 0 °C – rt, 30 mins	56	[67]

The occurrence of the second substitution reaction *para* to the initial site of attack underlines the dominance of the activating effect of the ring fluorine atoms. There are, however, examples of reactions in which a variation from *para* selectivity does occur, with these reactions often governed by X either being a powerful electron-donating substituent or capable of directing an incoming nucleophiles.^{68–70} [Scheme 11]



Scheme 11. Examples of ortho and meta selectivity in S_NAr reactions of pentafluorobenzene derivatives.^{68,70}

It is important when designing organic syntheses of perfluorinated aromatic systems to take into consideration the effects of ring fluorine substituents on the reactivity of such products towards certain species.

1.4 Synthesis of Highly Fluorinated Biphenyl Systems

This next section will review the appropriate literature for the synthesis of biphenyl structures containing a highly fluorinated aromatic ring.

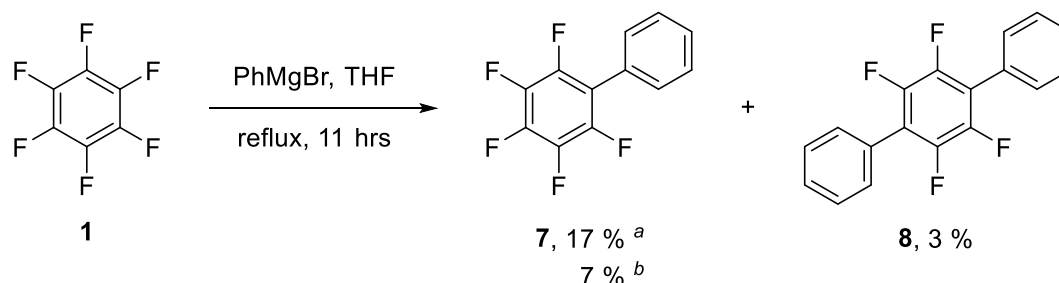
1.4.1 Reaction at an Aryl C–F Bond

1.4.1.1 S_NAr Reactions

Nucleophilic aromatic substitution (S_NAr) reactions provide an extremely useful means to add functionality to fluorinated aromatic systems. [Table 2] However, it has been shown that the reactivity of Grignard reagents towards hexafluorobenzene decreases in the order allyl or benzyl > alkyl > aryl.⁶² For this reason, along with the potential for numerous side-reactions to occur, the formation of highly fluorinated biphenyl derivatives via this route is not common and there exists very little data on the synthesis of such compounds via a S_NAr reaction pathway.

Whilst many reactions between non-aryl Grignard reagents and hexafluorobenzene occur at room temperature, or require cooling, it has been shown that the addition of a

solution of hexafluorobenzene **1** to phenylmagnesium bromide, at room temperature, results in no apparent reaction. Upon heating, the desired fluorinated biphenyl **7** is obtained in a low yield along with trace amounts of the disubstituted product **8**.⁶² [Scheme 12]



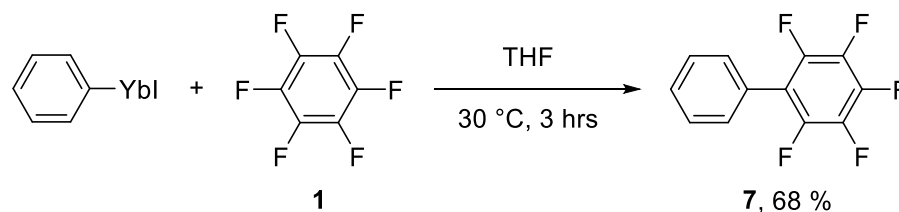
^aCrude product yield.

^bPure product yield.

Scheme 12. *S_NAr* reaction of hexafluorobenzene and phenylmagnesium bromide.⁶²

Two separate accounts have shown that exchanging the Grignard reagent for the related phenyl-lithium compound increased the yield of the desired fluorinated biphenyl **7** to 36 %⁷¹ and 70 %⁶¹, along with 15 and 17 % disubstituted product **8** respectively.

Reports have also described lanthanide complexes, similar to Grignard reagents, as suitable reaction partners for the synthesis of pentafluorobiphenyl **7**. Upon reaction of a ytterbium derivative with hexafluorobenzene **1**, biphenyl **7** was isolated in the highest yield reported for the synthesis of **7** via a *S_NAr* reaction pathway.⁷² [Scheme 13]

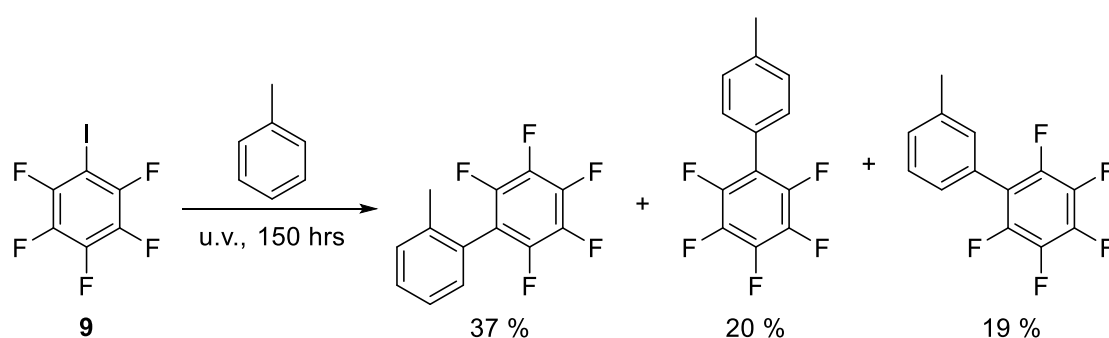


Scheme 13. *S_NAr* reaction of hexafluorobenzene and phenyl ytterbium iodide.⁷²

1.4.1.2 Radical Reactions

In 1967, Birchall *et al.* reported the use of pentafluoroiodobenzene as a precursor to the pentafluorophenyl radical in an attempt to further expand polyfluoroarene chemistry. Although initial testing showed that photochemical decomposition under UV light

proceeded slowly, and subsequent recombination of the radicals preferred, in the presence of certain aromatic compounds, high yields of fluorinated biphenyls were obtained. Irradiation of pentafluoroiodobenzene **9** in the presence of benzene and toluene yielded the relevant biphenyls in high conversions along with trace amounts of pentafluorobenzene.⁷³ [Scheme 14]

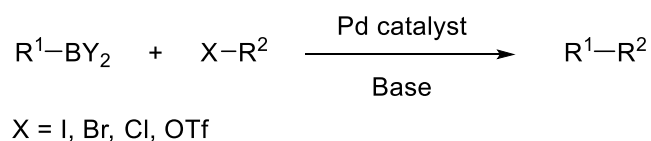


Scheme 14. Synthesis of highly fluorinated biphenyls from pentafluoroiodobenzene.⁷³

1.4.2 Suzuki-Miyaura Cross-Coupling Reactions

1.4.2.1 Introduction

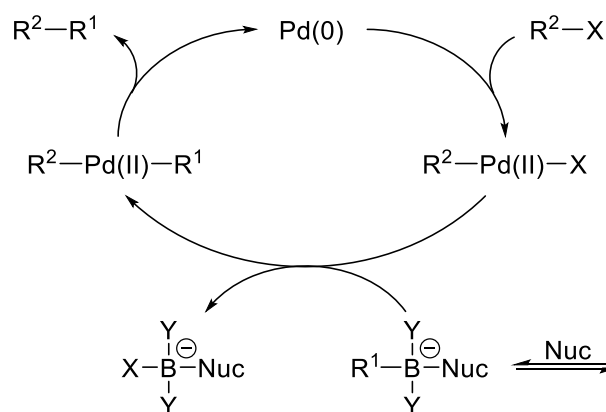
A powerful methodology for the formation of aryl C–C bonds is the Suzuki-Miyaura reaction, which couples organoboron compounds with organic halides (or triflates) in the presence of a palladium catalyst.⁷⁴ [Scheme 15]



Scheme 15. Standard Suzuki-Miyaura cross-coupling reaction.⁷⁵

In conventional Suzuki-Miyaura cross-couplings there are three key steps. Firstly, oxidative addition of the organic halide to the active Pd(0) species yields a stable *trans*-Pd(II) species. The second step involves the transfer of an organic substituent, from an organoboron species, to the palladium intermediate. This transmetalation step is aided by the *in situ* activation of the precursor organoboron reagent, through reaction with a suitable base/nucleophile. Without this activation process, the reaction fails as the

organoboron system does itself not undergo transmetalation due to the low nucleophilicity of the organic groups on the boron atom. Finally, reductive elimination of the cross-coupled product reproduces the active Pd(0) complex and the catalytic cycle completes.⁷⁵ [Scheme 16]



Scheme 16. Simplified catalytic cycle for the Suzuki-Miyaura cross-coupling reaction. Figure adapted from Suzuki et al.⁷⁵

The Suzuki-Miyaura cross-coupling reaction presents an efficient method for the formation of C–C bonds, using mild operating conditions and readily-available, easy to handle substrates. Through toleration of a broad range of functionality this synthetic procedure provides a general and diverse methodology for the synthesis of a wide range of compounds.⁷⁵ However, there exist very few general procedures for the synthesis of highly fluorinated biphenyl derivatives via a Suzuki-Miyaura reaction pathway, with many literature examples conducted to test the efficiencies of new, catalytic palladium complexes. The remainder of this section will discuss the relevant examples that have been reported.

1.4.2.2 Uses of Pentafluorophenylboronic Acid

There is a potential for either of the two components of the Suzuki-Miyaura reaction, the organoboron compound or the halide, to provide the perfluorinated functionality desired for the synthesis of a highly fluorinated biphenyl. One viable option is the use of pentafluorophenylboronic acid **10** within the cross-coupling reaction. [Figure 5]

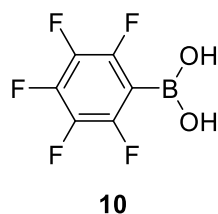
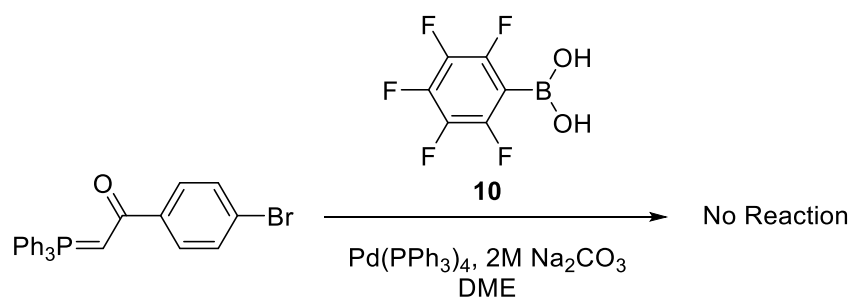


Figure 5. Pentafluorophenylboronic acid.

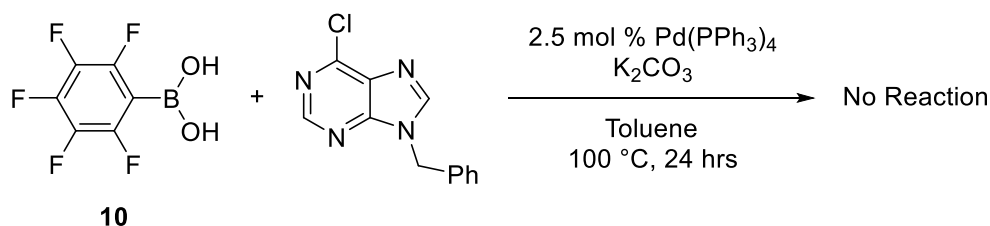
Unlike the analogous hydrocarbon compounds, polyfluorinated arylboronic acids remain uncommon reagents within cross-coupling reactions. In general, the presence of more fluorine atoms, especially in close proximity to the boronic functionality, significantly affects reactivity. 3,4,5-Trifluorophenylboronic acid remains an exception, displaying reactivities similar to the non-fluorinated counterpart.⁷⁶ Under ‘standard’ Suzuki-Miyaura reaction conditions, the use of **10** to provide the perfluorinated aryl functionality is problematic due to the difficulties encountered during the transmetalation of the highly electron deficient C₆F₅ moiety and subsequent undesired side reactions.⁷⁷

Thiemann *et al.* reported a procedure for the synthesis of biarylcarbonylmethylidenephosphoranes using a Suzuki-Miyaura cross-coupling reaction, however no coupling was observed with pentafluorophenylboronic acid.⁷⁸ [Scheme 17] The lack of observed reactivity was attributed to a competing hydrolysis reaction of the boronic acid, due to the introduction of a fluorine substituent at the 2-position, however no experimental data was provided for this claim. When repeated in non-aqueous media, pentafluorophenylboronic acid, again, failed to undergo the coupling reaction.



Scheme 17. Attempted cross-coupling reaction of pentafluorophenylboronic acid and an arylphosphorane.⁷⁸

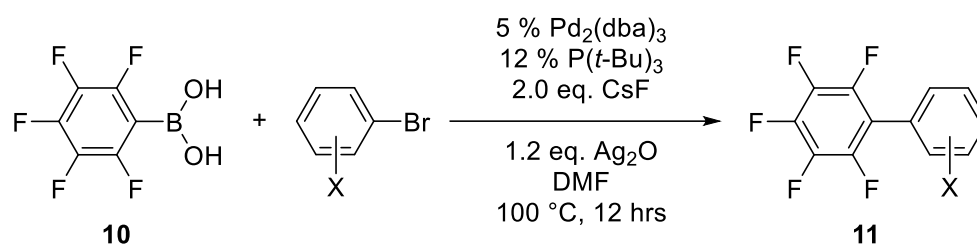
Similarly, Havelková *et al.* reported the lack of reactivity of pentafluorophenylboronic acid **10** in the Suzuki-Miyaura cross-coupling reaction for the synthesis of 6-alkylated purines.⁷⁹ The presence of weak acceptor substituents on the boronic acid ring led to isolation of products in good to excellent yields, with the introduction of stronger electron acceptors lowering this yield. The extreme case of pentafluorophenyl boronic acid **10**, under the same reaction conditions, did not react at all. [Scheme 18]



Scheme 18. Attempted cross-coupling reaction of pentafluorophenylboronic acid and a substituted purine.⁷⁹

When employed within cross-coupling reactions, highly fluorinated arylboronic acids are often consumed by competitive hydrodeboration reactions whereby the (dihydroxy)boryl group is replaced by hydrogen. In the case of pentafluorophenylboronic acid in aqueous solution, hydrodeboration is slow, with no decomposition observed in acidic solution.⁸⁰ However, for fluorine containing arylboronic acids of the form C₆H_(5-n)F_nB(OH)₂, in the presence of numerous bases, there is a significant acceleration in hydrodeboration with an increasing number of fluorine atoms from n = 1 to 5. The rate at which hydrodeboration occurs is dependent upon both the number and positioning of the fluorine substituents relative to boron, with pentafluorophenylboronic acid displaying the highest reactivity.⁸¹

In 2005, Korenaga *et al.* described new conditions for a Suzuki-Miyaura reaction capable of coupling pentafluorophenylboronic acid **10** with a variety of aryl bromides to yield the fluorinated biphenyls **11**.⁷⁷ [Scheme 19]



Scheme 19. Suzuki-Miyaura cross-coupling reaction of pentafluorophenylboronic acid and aryl bromides.⁷⁷

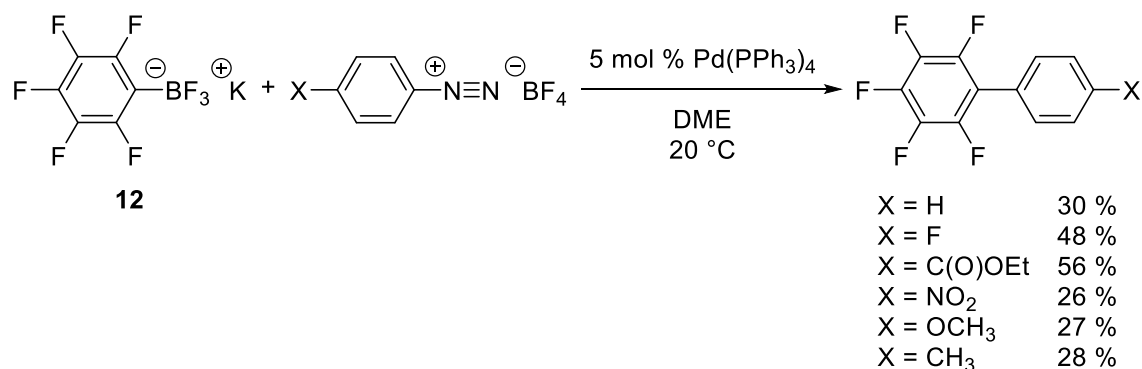
Absence of a base in the reaction gave very low yields of product and use of the commonly employed base (K₂CO₃) had very little effect on this. Although the reaction rate could be increased through the use of KO*t*-Bu, competing S_NAr reactions were observed through the formation of the 4-substituted product. For these reasons, a mild fluoride ion base was employed, and the use of bulkier, basic ligands accelerated the reaction rate further. These conditions were employed for a variety of bromides possessing both electron withdrawing and donating groups. Although there are reports of successful catalyst systems developed for the use of polyfluorophenylboronic acids in Suzuki-Miyaura cross-couplings,⁸² this particular synthetic protocol remains the only example of the use of pentafluorophenylboronic acid for the synthesis of fluorinated biphenyls using palladium catalysis; and has been applied for the synthesis of fluorinated molecular tweezers.⁸³

1.4.2.3 Uses of Fluorinated Borate and Boronate Salts

As discussed in the previous section, the range of usable, fluorinated boronic acids within Suzuki-Miyaura cross-coupling reactions is limited to those that do not undergo competing side-reactions, especially considering many protocols are performed at elevated temperatures for several hours. One potential alternative is the use of borate or boronate salts as cross-coupling partners. Many of these compounds display higher protolytic stability than their related boronic acids, which would aid the transmetalation of such weakly nucleophilic substrates within the catalytic cycle.⁷⁶

In 2002, Frohn *et al.* demonstrated the use of a (pentafluorophenyl)trifluoroborate salt **12**, along with other (polyfluorophenyl)trifluoroborate salts, in aryl C–C bond forming methodology through reactions with benzenediazonium tetrafluoroborates.⁷⁶ [Scheme

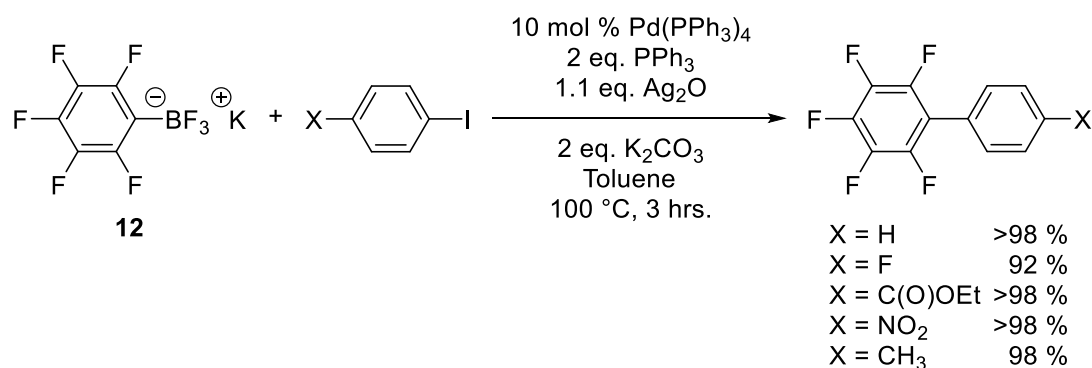
20] Such borate salts are easily prepared through the reaction of the precursor boronic acid and aqueous potassium bifluoride. Studies have shown that the trifluoroborate salt itself acts as a reservoir for the boronic acid within the reaction and in doing so reduces the formation of certain side-products due to protodeboronation and homocoupling. For this reason many reactions of trifluoroborate salts have been shown to be more efficient than their related boronic acids in Suzuki-Miyaura cross-coupling reactions.⁸⁴



Scheme 20. Synthesis of fluorinated biphenyls through Suzuki-Miyaura cross-couplings of potassium (pentafluorophenyl)trifluoroborate **12**.⁷⁶

Although only moderate yields were obtained with the highly reactive benzenediazonium tetrafluoroborates, this reaction protocol demonstrated the possibility of utilising boron salts for the synthesis of highly fluorinated biphenyls from Suzuki-Miyaura cross-coupling reactions.

The same research group subsequently published optimised conditions for the synthesis of the same compounds through reaction of potassium (pentafluorophenyl)trifluoroborate with the precursor aryl iodides, in far greater yields.⁸⁵ [Scheme 21] Similar reactions with the related aryl bromides required longer reaction times and displayed lower conversions and yields.



Scheme 21. Alternative synthesis of fluorinated biphenyls through Suzuki-Miyaura cross-couplings of potassium (pentafluorophenyl)trifluoroborate.⁸⁵

Reactions of structurally similar lithium (polyfluorophenyl)trimethoxyborates (Figure 6) with 4-fluoroiodobenzene have also been reported, to investigate the effect of the number and position of fluorine atoms on the aryl ring on the reactivity in the Suzuki-Miyaura cross-coupling reaction. Under optimised conditions, the highest yield of pentafluorobiphenyl achieved was 60 %. The stability of the lithium salt within certain solvents was found to be an important factor in overall yield often with the best results obtained in toluene, due to the salts insolubility and subsequent lack of degradation.⁸⁶

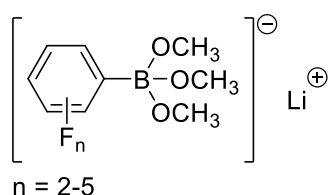
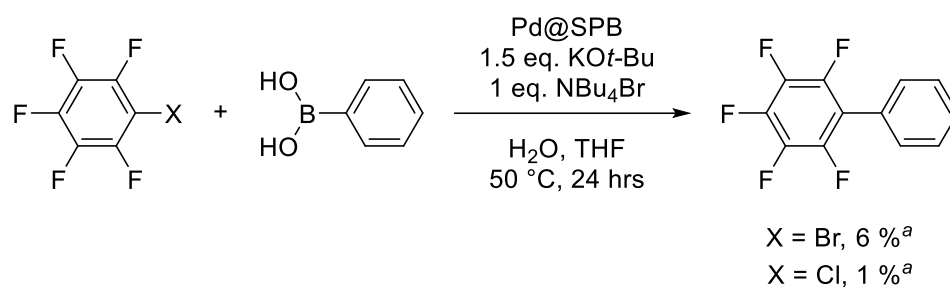


Figure 6. General structure of lithium (polyfluorophenyl)trimethoxyborate salts.

Following on from the work published regarding the reaction of (polyfluorophenyl)trifluoroborates with aryl halides (Scheme 21), Frohn *et al.* investigated the effect that various palladium catalysts and *N*-heterocyclic carbene ligands had on such cross-coupling reactions.⁸⁷ As was observed previously, aryl iodides proved more reactive than the related bromides with a broad range of substituted, fluorinated biphenyls isolated in varying yields, dependent upon the reaction conditions used.



^aGC conversion.

Scheme 23. Pd nanoparticles immobilised on spherical polyelectrolyte brushes (Pd@SPB) as catalysts in the synthesis of polyfluorinated biphenyls.⁹⁰

A similar synthesis was reported in 2010 by Buchmeiser *et al.* using Pd nanoparticles immobilised within the pores of a monolithic polymer support. Using this catalyst system, pentafluorobiphenyl **7** could be synthesised in a 71 % yield from pentafluorobromobenzene and phenylboronic acid.⁹¹

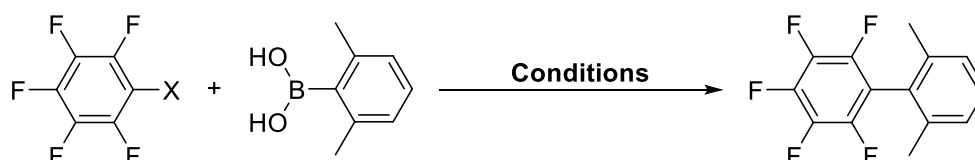
Similar to this method, Ramón *et al.* used palladium impregnated magnetite (Fe $_3$ O $_4$), which could be easily removed from the reaction mixture using a simple magnet, to synthesise a number of biaryl compounds. Using pentafluoroiodobenzene as an example of an electron deficient aryl iodide, reaction with phenylboronic acid yielded **7** in an 87 % yield.⁹²

Another synthesis of biphenyl **7** came from the group of Protasiewicz *et al.* who reported the use of palladium complexes of *trans*-spanning diphosphines within Suzuki-Miyaura cross-couplings of phenylboronic acid. The increased flexibility provided by their unique chelating ligand enabled the reaction with pentafluorobromobenzene to afford pentafluorobiphenyl **7** in up to 100 % yield.⁹³

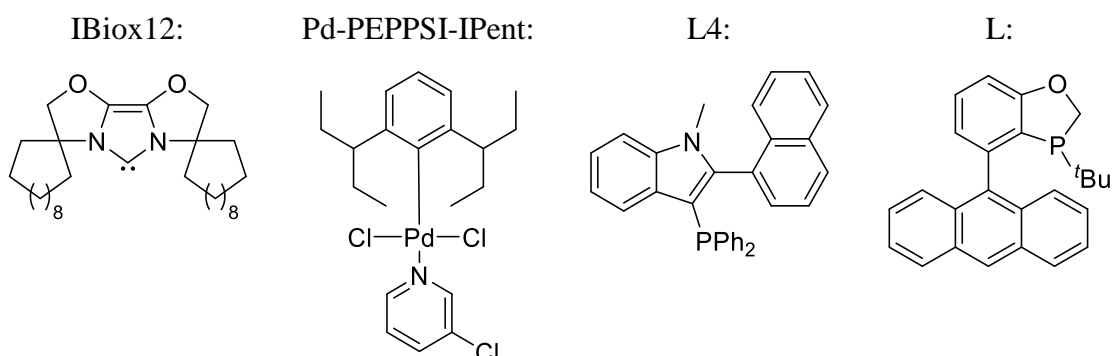
The remaining examples, utilising perfluorohalobenzenes, are all described as protocols for the synthesis of *ortho*-disubstituted biphenyls in the literature. Although sterically demanding halides have no major effect on the outcome of the Suzuki-Miyaura cross-coupling reaction, the use of *ortho*-disubstituted arylboronic acids in the reactions often result in diminished product yields.⁷⁵ This loss in reactivity is the result of a slowing in the rate of transmetalation to the palladium halide complex as well as protodeboronation, a common side reaction of sterically demanding boronic acids, as

discussed previously.⁹⁴ As sterically hindered biaryls structures have been found in many natural products, synthetic protocols able of synthesising such compounds are highly desired yet often require complicated catalytic complexes. Examples of such syntheses with a perfluorinated aryl halide are summarised in Table 4.

Table 4. Suzuki-Miyaura syntheses of tetraortho-disubstituted biphenyls with a perfluorinated aryl ring.



Entry	X	Conditions	Yield / %	Ref.
1	Cl	K ₃ PO ₄ , Pd(OAc) ₂ , IBiox12, toluene, 110 °C, 16 hrs.	89	[94]
2	Cl	KOH, Pd-PEPPSI-IPent, dioxane, 65 °C, 24 hrs.	59	[95]
3	Cl	Cs ₂ CO ₃ , [Pd ₂ (dba) ₃]/L4, dioxane, 110 °C, 24 hrs.	82	[96]
4	Br	K ₃ PO ₄ , [Pd(OAc) ₂]/L, dioxane, 110 °C, 24 hrs.	87	[97]



Although all of the examples discussed in this section demonstrate the use of perfluorohalobenzenes within the Suzuki-Miyaura cross-coupling reaction, at present, there have been no publications demonstrating the use of pentafluorohalobenzenes with a range of organoborane derivatives for the synthesis of functional highly fluorinated systems.

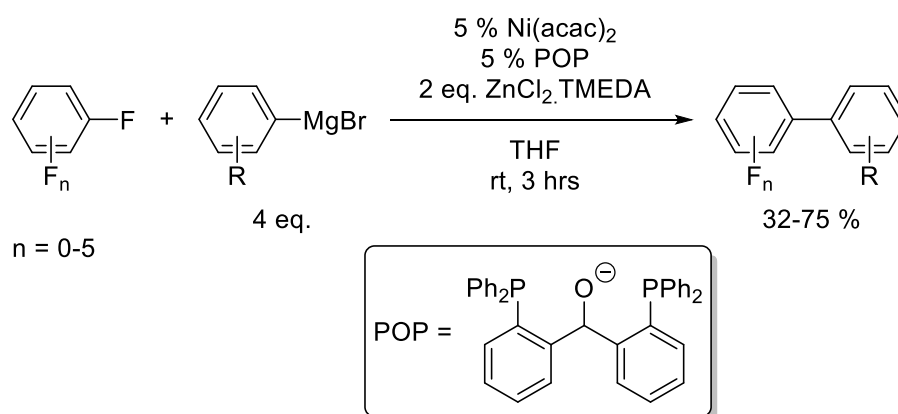
1.4.3 C–F Bond Activation Reactions

The previous section discussed numerous variations of the Suzuki-Miyaura cross-coupling reaction for the synthesis of highly fluorinated biphenyls, with specific

examples given for the use of aryl-iodides, -bromides, and -chlorides. Traditionally, iodo- and bromobenzenes are used preferentially to the related chloro-compounds due to the relatively high bond strength of C–Cl bonds and for this reason, metal catalysed C–F bond activation is significantly challenging. Much research in this area of chemistry has focused upon the functionalisation of monofluorinated compounds to yield the related non-fluorinated products and although there are literature examples utilising di- and trifluorobenzenes⁹⁸, very little research exists for the monosubstitution of polyfluorinated arenes by catalytic C–F bond activation reactions.

The selective monosubstitution of polyfluorinated arenes, utilising conventional nickel and palladium substrates, poses problems due to “ring-walking” within the catalytic complex. This process involves the catalytic metal centre “walking” over the conjugated π -system of the aryl ring and activating numerous C–F bonds, making the selective activation of a singular C–F bond in a polyfluorinated compound extremely difficult.⁹⁹

A recent publication by Nakamura *et al.* described the use of an alkoxydiphosphine ligand within a Kumada-type coupling for the monosubstitution of polyfluoroarenes.¹⁰⁰ [Scheme 24] The tridentate POP ligand used within the reaction helps to stabilise an intermediate nickel species within the catalytic cycle and prevents “ring-walking” from occurring.

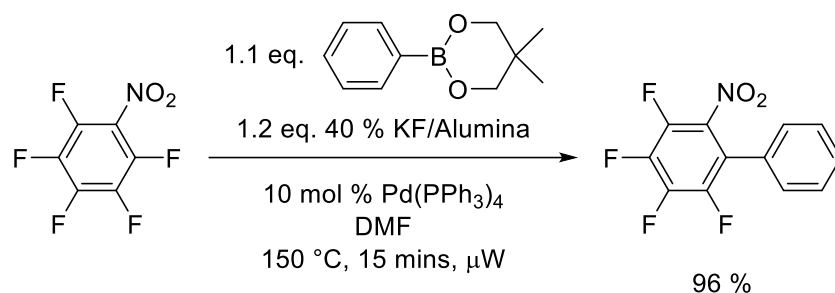


Scheme 24. Monofunctionalisation of polyfluoroarenes with organomagnesium reagents.¹⁰⁰

Although only one example is provided for the monofunctionalisation of hexafluorobenzene, it is known to be a particularly difficult substrate to functionalise in

this manner and the reaction occurs in a satisfactory yield (52 %) with high selectivity for monoarylation.

Previous research within the Durham fluorine group has shown highly fluorinated nitrobenzene derivatives to be suitable coupling partners within catalytic C–F bond activation reactions.¹⁰¹ [Scheme 25] The presence of an *ortho* nitro group directs the incoming nucleophilic palladium centre towards the adjacent C–F bond, providing highly fluorinated biphenyl derivatives in moderate to excellent yields.



Scheme 25. Palladium catalyzed C–F bond activation of pentafluoronitrobenzene.¹⁰¹

1.4.4 C–H Bond Activation Reactions

As mentioned previously, the high bond strength of C–F bonds along with difficulties regarding monoarylation makes the synthesis of highly fluorinated biphenyls by catalytic C–F bond activation particularly challenging. Another potential complication arises with similar reactions of polyfluorobenzenes, as transition metal complexes capable of oxidative addition to a C–F bond possess a higher reactivity towards C–H bonds, forming highly reactive C–M bonds.¹⁰² This observed reactivity allows for the synthesis of highly fluorinated biphenyls through C–H bond activation reactions, an area of research that has grown significantly in the last 5 years with a number of literature procedures reported.

1.4.4.1 Coupling Polyfluorobenzenes with Aryl Halides

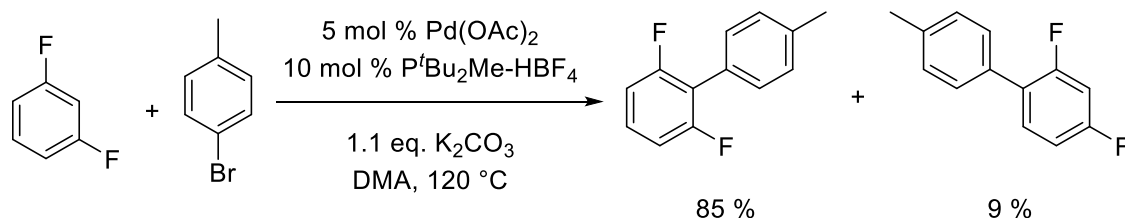
The first reported synthesis for the arylation of electron deficient polyfluorobenzenes came from the group of Fagnou, and showed that the reaction favoured the activation of acidic protons, a key feature of highly fluorinated benzenes.¹⁰³ [Scheme 26]



Scheme 26. Catalytic intermolecular direct arylation of polyfluorobenzenes.¹⁰³

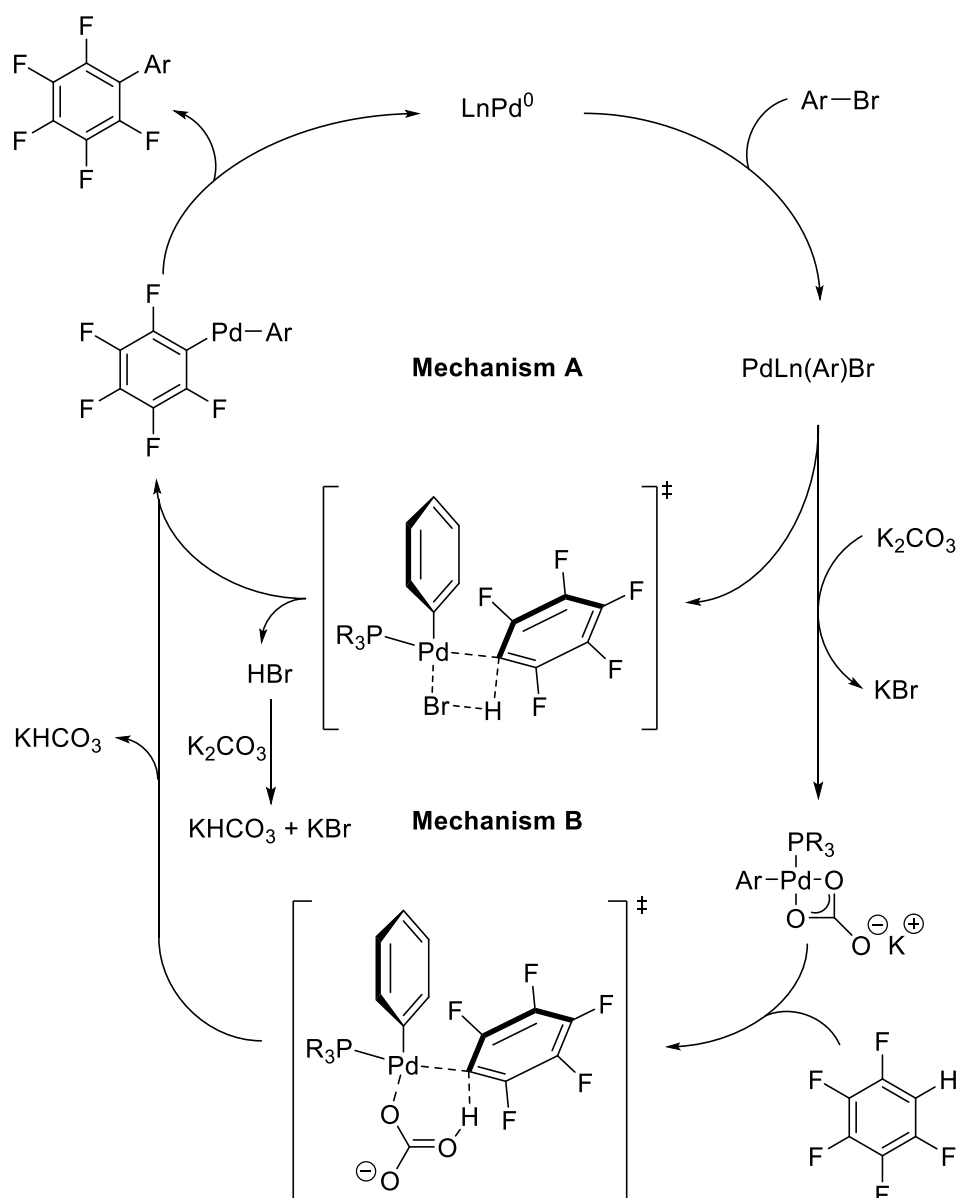
Reactions with substituted aryl bromides yielded the best results, although the related chlorides and iodides were also shown to be viable coupling partners under the reaction conditions and the addition of silver triflate improved yields for couplings.

Reactions of pentafluorobenzene proceeded in good to excellent yields, with the relative reactivities of other polyfluorobenzenes paralleling the relative acidities of the C–H bond undergoing the reaction. [Scheme 27] In the case of fluorobenzenes possessing more than one potential reaction site, mixtures of mono-, bis-, and in certain cases trisarylated products were obtained, however the formation of polyarylated products could be suppressed through the use of a slight excess of the starting fluoroaromatic.



Scheme 27. Arylation of 1,3-difluorobenzene.¹⁰³

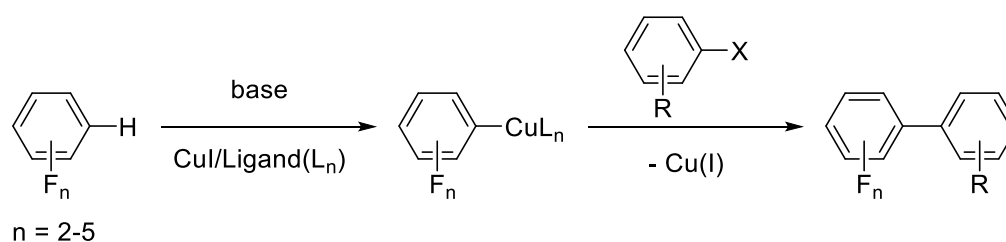
Computational studies performed to investigate the mechanism of the reaction indicated that the selectivity was determined solely by the acidity of the C–H bond reacting and not due to stabilisation between fluorine and palladium in any intermediates. A number of potential reaction pathways were investigated, with the proposed mechanism occurring via concerted metalation and proton abstraction with either a ligated bromide (Mechanism A) or bicarbonate ion (Mechanism B) acting as the base. [Scheme 28]



Scheme 28. Proposed catalytic cycle for the direct arylation of perfluorobenzenes.¹⁰³

Although this protocol provided the first method for the coupling of polyfluorinated benzenes with aryl halides, lower yields were obtained with aryl chlorides or sterically demanding aryl bromides. A revised procedure was published shortly after by the same group, using *S*-Phos as the catalytic ligand, enabling the use of these more challenging substrates within the cross-coupling procedure.¹⁰⁴ As well as increasing the substrate scope, the coupling reaction was shown to proceed at 80 °C, lower than the initially reported 120 °C.

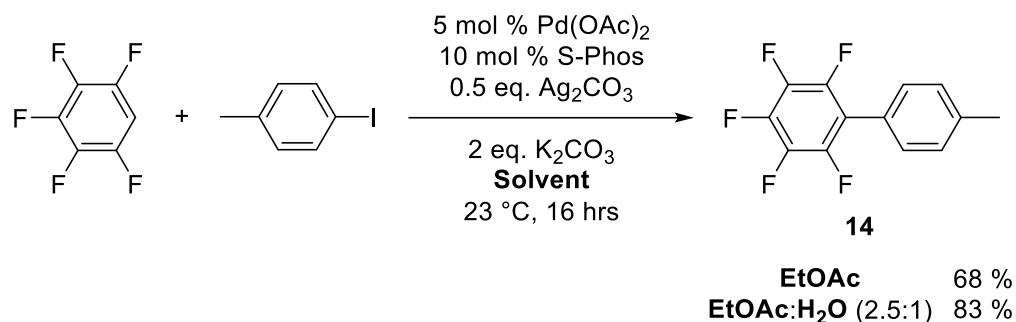
Additionally, the group of Daugulis reported a related procedure for the synthesis of highly fluorinated biphenyls.^{105,106} The employment of copper as the catalytic species within the cross-coupling reaction provides a cheaper alternative to palladium, whilst maintaining the high reaction yields reported previously. The coupling is reported to proceed via the base-promoted formation of a fluoroarylcopper intermediate which subsequently reacts with the aryl halide, with the acidity of the substrate responsible for determining the site of reaction. [Scheme 29]



Scheme 29. Proposed mechanism for the copper catalysed arylation of polyfluorobenzenes.¹⁰⁵

For reactions of pentafluorobenzene, the highest yields were afforded when employing K_3PO_4 as the base. For less acidic arenes (generally possessing less than 3 fluorine substituents) it was necessary to employ stronger lithium alkoxide bases to allow high yielding reactions.

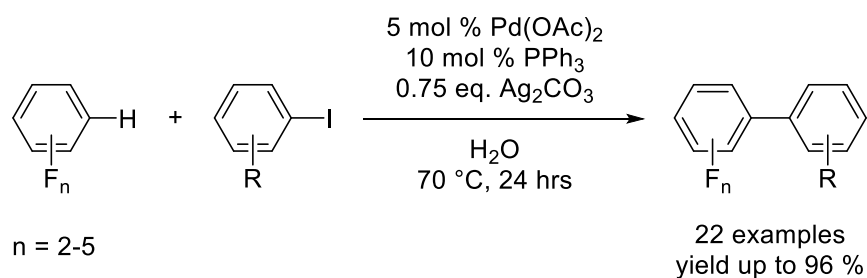
With both Fagnou and Daugulis highlighting the potential to synthesise polyfluorobiphenyl derivatives through metal catalysed C–H bond activation with an aryl halide, much attention then focused on developing milder reaction conditions to facilitate substrate compatibility and reaction applications. The Fagnou group itself published new reaction conditions to facilitate the arylation of polyfluorinated arenes at room temperature utilising biphasic solvent conditions.¹⁰⁷ The use of water as a co-solvent was shown to increase the yield of a test reaction between pentafluorobenzene and 4-iodotoluene, with the ratio of solvents critical to maximum conversion. [Scheme 30] The use of aqueous media ensures the complete solubilisation of all reaction components.



Scheme 30. The effect of biphasic solvent conditions on yields achieved for C–H bond activation in polyfluoroarenes.¹⁰⁷

The yields achieved could further be enhanced through the use of alternative phosphine ligands, with MePhos increasing the isolated yield of **14** to 90 %. The use of silver carbonate as an additive proved crucial, with no reaction observed in its absence. The role of the silver salt has been attributed to the abstraction of the iodine ligand from the palladium intermediate since Ag(I)⁺ possesses a strong affinity towards iodide, yielding an electrophilic, cationic palladium intermediate.^{77,107} These optimised reaction conditions were subsequently applied to a wide range of aryl iodides and polyfluorobenzenes for the synthesis of substituted, fluorinated biphenyl systems.

Recently Zhang *et al.* published a new range of mild conditions for the synthesis of similar, fluorinated biphenyls.¹⁰⁸ Unlike the group of Fagnou, Zhang used water as the sole reaction medium and, although this required moderate heating of the reaction solution to 70 °C, this presents a number of beneficial points including the low-cost, ready availability and nontoxicity of water. Other alterations to Fagnou's reaction conditions¹⁰⁷ includes the use of triphenylphosphine as the ligand, a cheaper alternative to the phosphines employed previously, along with the employment of silver carbonate as the base as well as the halide scavenger. [Scheme 31]

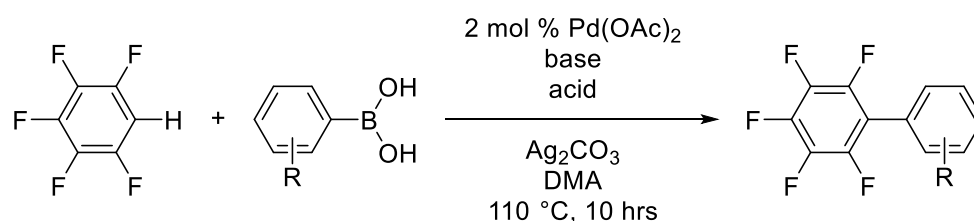


Scheme 31. Palladium catalyzed direct arylation of polyfluoroarenes on water.¹⁰⁷

Although stating that the reaction mechanism remained unclear, it was proposed that the arylation proceeded in a manner matching that suggested by Fagnou (Scheme 28, Mechanism B), with abstraction of the iodide ligand by silver carbonate.

1.4.4.2 Reactions of Polyfluorobenzenes with Alternative, Preactivated Coupling Partners

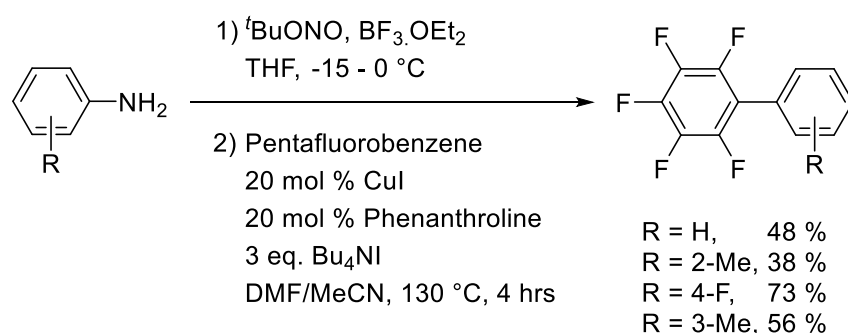
As well as reactions with aryl halides, polyfluorobenzenes are also capable of undergoing cross-couplings with a variety of arylating reagents. Su *et al.* devised a novel cross-coupling procedure involving pentafluorobenzene and numerous arylboronic acids, with a broad range of substrates accommodated by the variation of certain reaction conditions.¹⁰⁹ [Scheme 32]



Scheme 32. Direct arylation of pentafluorobenzene with arylboronic acids.¹⁰⁹

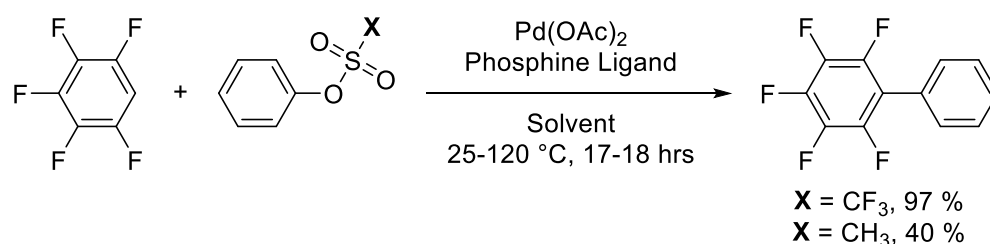
C–H activation of electron deficient fluorobenzenes occurs under basic conditions, a parameter that could potentially promote homocoupling of the boronic acid. Su proposed that the simultaneous addition of a weak acid to the reaction solution would slow the rate of transmetalation of the boronic acid, thereby preventing the occurrence of this unwanted side-reaction. Selection of an appropriate acid/base combination was attributed to the success of the cross-coupling reaction with a variety of substrates. Although the reaction conditions could be extended to substituted polyfluorobenzenes, they were unsuitable for substrates containing more than one activated C–H bond, with mixtures of products obtained in such cases. One proposed reaction mechanism for the transformation involves transmetalation of the boron species to palladium, followed by palladation of the polyfluorobenzene in a concerted metalation-deprotonation step. Reductive elimination subsequently yields the fluorinated biphenyl product.

Related syntheses with aryltrifluoroborates¹¹⁰ and arenediazonium tetrafluoroborates¹¹¹ have also recently been reported, yielding a variety of substituted, fluorinated biphenyls. Although yields decreased in reactions between arenediazonium tetrafluoroborates and less fluorinated benzenes, examples were given whereby the reaction could be conducted as a one-pot procedure from the starting aniline, without the necessity to isolate the intermediate salt. [Scheme 33] During reaction optimisation it was noted that in the absence of iodide ions, homo-coupling of the arenediazonium tetrafluoroborates yielded the major product of the reaction. Control experiments confirmed that the arenediazonium tetrafluoroborate salts were in fact rapidly converted to the respective aryl iodides in the presence of iodide ions.



Scheme 33. One-pot cross-couplings of anilines with pentafluorobenzene.¹¹¹

The final example of using alternative activated benzenes comes with the use of aryl triflates as coupling partners for polyfluorobenzenes.¹¹² Reactions of pentafluorobenzene with various substituted aryl triflates proceeded in good to excellent yields at ambient temperatures. As with previous reaction procedures, reactivities decreased with less fluorinated benzenes, as the relative acidities of the C–H bond decreased. The reaction was extended to the related mesylate compounds, however only trace amounts of product were obtained under the same reaction conditions. Further optimisation did increase yields of the cross-coupling products but generally remained comparatively lower. [Scheme 34]

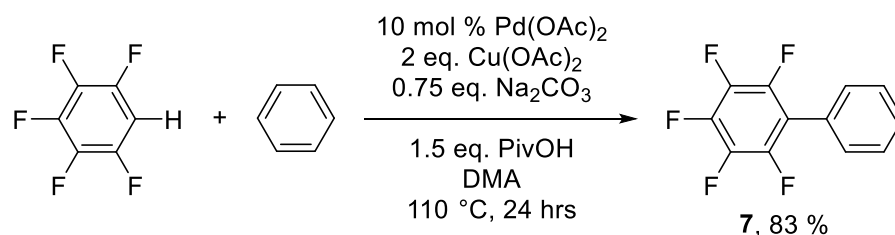


Scheme 34. Comparison of phenyl -triflate and -mesylate in C–H bond activations.¹¹²

1.4.4.3 Coupling Polyfluorobenzenes with Simple Arenes

Whilst C–H bond activation reactions of polyfluorobenzenes circumnavigate the necessity to synthesise fluorinated- arylhalide or boronic species, all the reactions discussed previously remain reliant upon a preactivated arene as a second coupling partner. An even more efficient method for the synthesis of fluorinated biphenyls by C–H bond activation reactions would occur between two non-prefunctionalised arenes. The main synthetic challenge posed by such a dehydrogenative cross-coupling reaction centres around maintaining control of the regioselectivity of the reaction, to obtain the desired product ahead of unwanted homocoupling products.¹¹³

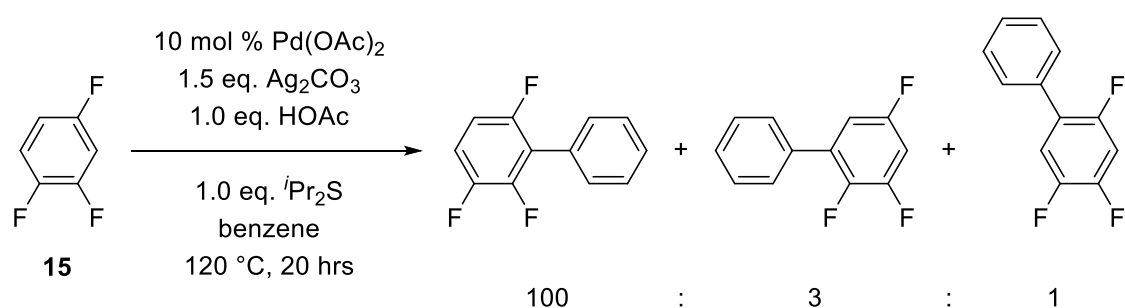
Continuing on from their work with pentafluorobenzene and arylboronic acids, Su *et al.* targeted this problem, choosing to couple electronically distinct arenes in an attempt to overcome issues surrounding unwanted homocoupling reactions.¹¹³ They postulated that the reaction of a simple, electron-rich arene with a palladium catalyst would occur preferentially to an electron deficient fluoroarene, thereby generating a relatively electron-rich complex, which would subsequently react with the fluoroarene. Their hypothesis was proven with the cross-coupling of pentafluorobenzene and benzene to yield pentafluorobiphenyl **7** in good yield, with only trace amounts of biphenyl and decafluorobiphenyl observed. [Scheme 35]



Scheme 35. Cross-coupling reaction between pentafluorobenzene and benzene.¹¹³

The reaction was expanded to include the reaction of substituted polyfluorobenzenes with benzene, albeit with an increase in side-products, as well as the reactions of monosubstituted benzenes. In the latter case, mixtures of both *meta*- and *para*-regioisomers were obtained, regardless of the nature of the substituent.

A similar reaction procedure was published shortly after by the group of Shi, in which they showed the use of dialkyl sulfides as ligands to accelerate C–H bond activation which gave complete conversions with only trace amounts of homocoupling observed.¹¹⁴ A number of examples were also given that highlighted Fagnou's previous findings that for polyfluoroarenes possessing chemically distinct C–H bonds, arylation will occur preferentially at the most acidic site, as exemplified by the reaction of 1,2,4-trifluorobenzene **15**. [Scheme 36]



Scheme 36. Regioisomers obtained from the C–H bond activation reaction of 1,2,4-trifluorobenzene with benzene.¹¹⁴

Contrary to the hypothesis of Su *et al.*, Shi proposed a reaction mechanism whereby the initial aryl-palladium complex was formed from the activated palladium catalyst and deprotonated polyfluorobenzene. C–H bond activation of the simple arene by a concerted metalation-deprotonation pathway subsequently gives a biaryl-palladium complex, with reductive elimination forming the fluorinated biphenyl product.

Other procedures have also been reported for the cross-coupling of simple aromatics including the use of imidazolium ionic liquids as reaction solvents¹¹⁵, and replacement of the traditionally employed palladium catalyst with gold salts.¹¹⁶ The use of ionic liquids as solvents allows the reactions to proceed without the need for additional oxidants or additives, with the reaction catalysed purely by Pd(OAc)₂ and acetic acid, albeit in slightly lower yields than certain other protocols. The use of gold salts as

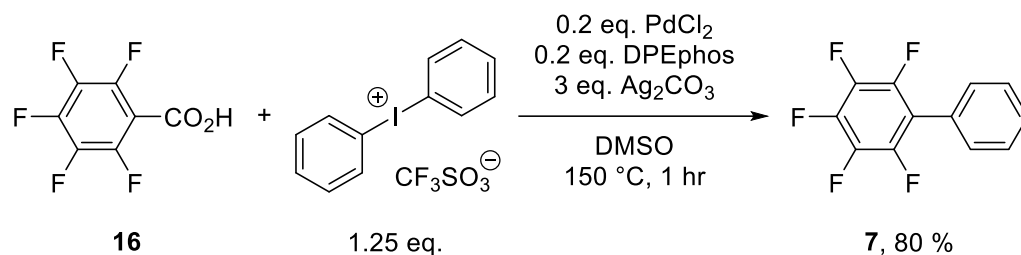
replacements for palladium complexes has the potential to solve any selectivity issues within the cross-coupling reactions as Au(I) salts are capable of mediating C–H bond activations of electron deficient arenes whilst Au(III) salts preferentially react with electron-rich arenes. It should however be noted that current research into this area of chemistry is at an early stage, with compatible conditions for the desired one-pot reactions still under optimisation.

C–H bond activation reactions of polyfluorobenzenes enable the synthesis of highly fluorinated biphenyls in a similar manner to Suzuki-Miyaura cross-coupling reactions whilst lessening the dependence on fluorinated substrates such as arylboronic acids and halides, which require multiple steps for synthesis and often have low reactivity. As well as couplings with substituted aryl species to product highly fluorinated biphenyls, there also exist a number of protocols for cross-couplings of polyfluorobenzenes with aromatic heterocycles.^{106,107,117} The wide substrate scope displayed by polyfluorobenzenes within the discussed reactions is a direct result of employing electron deficient arenes within base-catalysed arylation reactions, instead of as nucleophilic species in traditional cross-coupling reactions.

1.4.5 Decarboxylation Reactions

The final method for the synthesis of polyfluorinated biaryls that will be discussed in this chapter involves palladium catalysed, decarboxylative cross-coupling reactions. Syntheses of biaryls using benzoic acids as an aryl source has become an attractive and growing area of research over recent years, due in part to the replacement of, often expensive, organometallic reagents and the generation of gaseous CO₂ as a by-product.

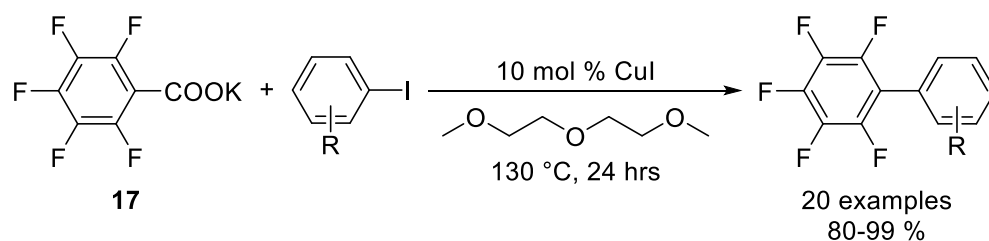
One of the earliest examples of the use of pentafluorobenzoic acid **16** as an arylating partner was conducted to demonstrate the successful coupling of electron deficient benzoic acids with diaryliodonium triflates.¹¹⁸ [Scheme 37]



Scheme 37. Synthesis of **7** via a decarboxylative cross-coupling reaction of pentafluorobenzoic acid and diphenyliodonium triflate.¹¹⁸

Although only one example was provided for the synthesis of a highly fluorinated biphenyl, this procedure demonstrated the use of pentafluorobenzoic acid as a promising alternative to the related boronic acid.

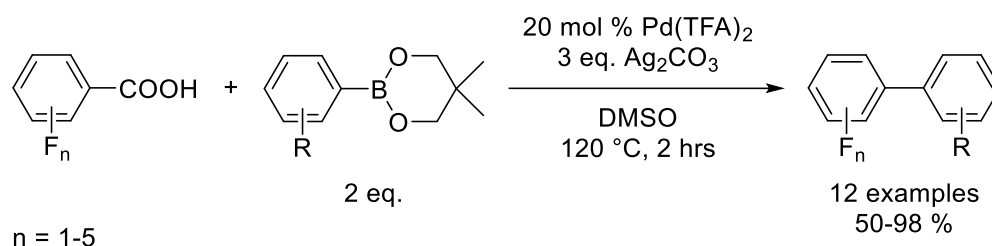
Liu *et al.* later published research into the copper catalysed decarboxylative couplings of potassium pentafluorobenzoate **17** with aryl iodides.¹¹⁹ [Scheme 38] A broad range of functional groups were tolerated under the reaction conditions, producing fluorinated biaryls in good to excellent yields. The use of diglyme as a solvent gave optimum yields, even without the addition of a ligand species. Aryl bromides were also tolerated within the reaction parameters, again producing biaryls in good to excellent yields, but required the addition of phenanthroline as a ligand.



Scheme 38. Copper catalysed decarboxylative cross-coupling between potassium pentafluorobenzoate and aryl iodides.¹¹⁹

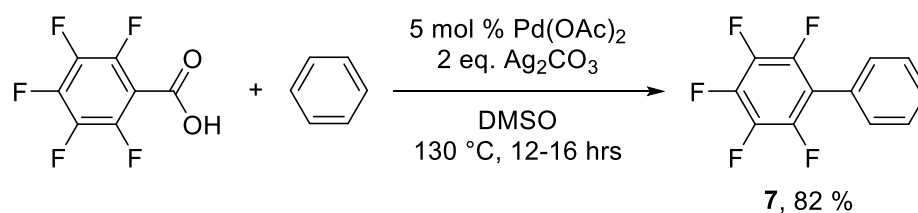
Fluorinated benzoic acids have also been used for decarboxylative Suzuki-Miyaura cross-coupling reactions.¹²⁰ [Scheme 39] The use of 6-membered boronic esters aided the suppression of the formation of homo-coupled side-products, as the rate of transmetalation of such boronic species is slower than the related acids. It was also found that alteration of the reaction catalyst could drastically affect the reaction

outcome. Exchange of the palladium catalyst for a copper-based species yielded the esterification product rather than the Suzuki-Miyaura cross-coupled biaryl.



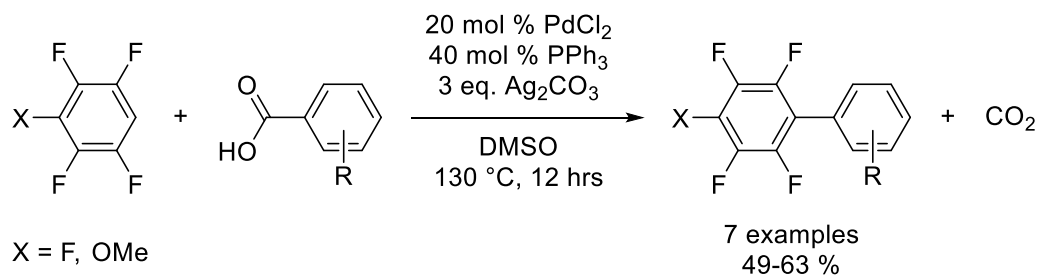
Scheme 39. Decarboxylative Suzuki-Miyaura cross-couplings between polyfluorinated benzoic acids and boronic acid esters.¹²⁰

More recently, Luo *et al.* utilised perfluorobenzoic acids for palladium catalysed decarboxylative C–H bond functionalisations of simple arenes for the synthesis of polyfluorobiphenyls.¹²¹ [Scheme 40]



Scheme 40. Decarboxylative arylation of polyfluorobenzoic acid with benzene.¹²¹

There also exist synthetic protocols whereby the fluorinated aryl ring is provided by the non-carboxylated starting material in the cross-coupling reaction. A number of penta- and tetrafluoro substituted biaryls have been synthesised by the palladium catalysed cross-coupling of polyfluorobenzenes with various, substituted nitrobenzoic acids.¹²² [Scheme 41]



Scheme 41. *Palladium catalyzed decarboxylative arylation of polyfluorobenzenes with benzoic acids.*¹²²

1.5 Summary

The use of self-assembled monolayers on metal surfaces is widespread due to their ability to tune key properties such as work function of the metal and surface wettability. For these reasons SAMs are widely applied within electronic device fabrication. The unique chemistry associated with the incorporation of fluorine substituents; high electronegativity and subsequent dipole moments, and high bond strength of the C–F bond; has the potential to provide favourable properties to SAMs compared to their non-fluorinated counterparts.

The synthesis of perfluorinated aromatics is well known, with the subsequent reactions of nucleophilic species by a nucleophilic aromatic substitution pathway well studied and developed. The syntheses of highly fluorine biphenyls by S_NAr methodology is limited, with a number of alternative metal-catalysed syntheses developed to account for this.

The use of highly fluorinated reagents within standard Suzuki-Miyaura cross-coupling reactions is problematic due to the low nucleophilicity of pentafluorophenylboronic acid and the susceptibility of this reagent to undergo hydrodeboration. The use of alternative borate salts provides one alternative to this problem. Although there also exist a number of literature examples for the use of perfluorohalobenzenes within such reactions, many involve the use of complicated catalyst systems. As such, a robust and cheap coupling process, using readily available palladium catalysts, would be highly advantageous.

More recently, research has developed in the area of catalytic C–H bond activation reactions of highly fluorinated benzenes to form biaryls, with the process strongly dependent on the relative acidities of the C–H bonds undergoing arylation.

1.6 References to Chapter 1

- (1) Ulman, A. *Chem. Rev.* **1996**, *96*, 1533–1554.
- (2) Love, J. C.; Estroff, L. A.; Kriebel, J. K.; Nuzzo, R. G.; Whitesides, G. M. *Chem. Rev.* **2005**, *105*, 1103–1170.
- (3) Nuzzo, R. G.; Allara, D. L. *J. Am. Chem. Soc.* **1983**, *105*, 4481–4483.
- (4) Poirier, G.; Pylant, E. *Science* **1996**, 1145–1147.
- (5) Biebuyck, H. A.; Bain, C. D.; Whitesides, G. M. *Langmuir* **1994**, *10*, 1825–1831.
- (6) Dubois, L. H.; Zegarski, B. R.; Nuzzo, R. G. *J. Chem. Phys.* **1993**, *98*, 678–688.
- (7) Laibinis, P. E.; Whitesides, G. M.; Allara, D. L.; Tao, Y. T.; Parikh, A. N.; Nuzzo, R. G. *J. Am. Chem. Soc.* **1991**, *113*, 7152–7167.
- (8) Bain, C. D.; Evall, J.; Whitesides, G. M. *J. Am. Chem. Soc.* **1989**, *111*, 7155–7164.
- (9) Bain, C. D.; Whitesides, G. M. *Science* **1988**, *240*, 62–63.
- (10) Porter, M. D.; Bright, T. B.; Allara, D. L.; Chidsey, C. E. *J. Am. Chem. Soc.* **1987**, *109*, 3559–3568.
- (11) Dubois, L. H.; Nuzzo, R. G. *Annu. Rev. Phys. Chem.* **1992**, *43*, 437–463.
- (12) Xia, Y.; Zhao, X.-M.; Whitesides, G. M. *Microelectron. Eng.* **1996**, *32*, 255–268.
- (13) Valiokas, R.; Svedhem, S.; Svensson, S. C.; Liedberg, B. *Langmuir* **1999**, *15*, 3390–3394.
- (14) Bain, C. D.; Troughton, E. B.; Tao, Y. T.; Evall, J.; Whitesides, G. M.; Nuzzo, R. G. *J. Am. Chem. Soc.* **1989**, *111*, 321–335.
- (15) Schwartz, D. K. *Annu. Rev. Phys. Chem.* **2001**, *52*, 107–137.
- (16) Mutin, P. H.; Guerrero, G.; Vioux, A. *J. Mater. Chem.* **2005**, *15*, 3761–3768.
- (17) Mutin, P. H.; Guerrero, G.; Vioux, A. *C. R. Chim.* **2003**, *6*, 1153–1164.
- (18) Facchetti, A.; Yoon, M.-H.; Marks, T. J. *Adv. Mater.* **2005**, *17*, 1705–1725.
- (19) DiBenedetto, S. A.; Frattarelli, D.; Ratner, M. A.; Facchetti, A.; Marks, T. J. *J. Am. Chem. Soc.* **2008**, *130*, 7528–7529.
- (20) Byrne, P. D.; Facchetti, A.; Marks, T. J. *Adv. Mater.* **2008**, *20*, 2319–2324.
- (21) Allen, C.; Baker, D.; Albin, J.; Oertli, H.; Gillaspie, D.; Olson, D.; Furtak, T.; Collins, R. *Langmuir* **2008**, *24*, 13393–13398.

- (22) Koide, Y.; Such, M. W.; Basu, R.; Evmenenko, G.; Cui, J.; Dutta, P.; Hersam, M. C.; Marks, T. J. *Langmuir* **2003**, *19*, 86–93.
- (23) Persson, P.; Lunell, S.; Ojamäe, L. *Int. J. Quantum Chem.* **2002**, *89*, 172–180.
- (24) Tian, X.; Xu, J.; Xie, W. *J. Phys. Chem. C* **2010**, *114*, 3973–3980.
- (25) Chen, Y.-S.; Li, C.; Zeng, Z.-H.; Wang, W.-B.; Wang, X.-S.; Zhang, B.-W. *J. Mater. Chem.* **2005**, *15*, 1654–1661.
- (26) Yip, H.-L.; Hau, S. K.; Baek, N. S.; Jen, A. K.-Y. *Appl. Phys. Lett.* **2008**, *92*, 193313.
- (27) Xu, W.; Peng, B.; Chen, J.; Liang, M.; Cai, F. *J. Phys. Chem. C* **2008**, *112*, 874–880.
- (28) Laibinis, P. E.; Hickman, J. J.; Wrighton, M. S.; Whitesides, G. M. *Science* **1989**, *245*, 845–847.
- (29) Lushtinetz, R.; Frenzel, J.; Milek, T.; Seifert, G. *J. Phys. Chem. C* **2009**, *113*, 5730–5740.
- (30) Taylor, C. E.; Schwartz, D. K. *Langmuir* **2003**, *19*, 2665–2672.
- (31) Langmuir, I. *Trans. Faraday Soc.* **1920**, *15*, 62–74.
- (32) Bae, E.; Choi, W.; Park, J.; Shin, H. S.; Kim, S. B.; Lee, J. S. *J. Phys. Chem. B* **2004**, *108*, 14093–14101.
- (33) Badia, A.; Lennox, R. B.; Reven, L. *Acc. Chem. Res.* **2000**, *33*, 475–481.
- (34) Ma, H.; Yip, H.-L.; Huang, F.; Jen, A. K.-Y. *Adv. Funct. Mater.* **2010**, *20*, 1371–1388.
- (35) Hotchkiss, P. J.; Malicki, M.; Giordano, A. J.; Armstrong, N. R.; Marder, S. R. *J. Mater. Chem.* **2011**, *21*, 3107–3112.
- (36) Klauk, H.; Zschieschang, U.; Pflaum, J.; Halik, M. *Nature* **2007**, *445*, 745–748.
- (37) Klauk, H.; Zschieschang, U.; Halik, M. *J. Appl. Phys.* **2007**, *102*, 074514–074514.
- (38) Quiñones, R.; Gawalt, E. S. *Langmuir* **2008**, *24*, 10858–64.
- (39) Gawalt, E. S.; Avaltroni, M. J.; Danahy, M. P.; Silverman, B. M.; Hanson, E. L.; Midwood, K. S.; Schwarzbauer, J. E.; Schwartz, J. *Langmuir* **2003**, *19*, 200–204.
- (40) Maegerle, I.; Jaehne, E.; Henke, A.; Adler, H.-J. P.; Bram, C.; Jung, C.; Stratmann, M. *Prog. Org. Coat.* **1998**, *34*, 1–12.
- (41) Mann, B.; Kuhn, H. *J. Appl. Phys.* **1971**, *42*, 4398–4405.

- (42) Würfel, P.; Würfel, U. *Physics of Solar Cells: From Basic Principles to Advanced Concepts*; John Wiley & Sons Inc., 2009.
- (43) Haick, H.; Ambrico, M.; Ligonzo, T.; Tung, R. T.; Cahen, D. *J. Am. Chem. Soc.* **2006**, *128*, 6854–6869.
- (44) Campbell, I.; Rubin, S.; Zawodzinski, T.; Kress, J.; Martin, R.; Smith, D.; Barashkov, N.; Ferraris, J. *Phys. Rev. B* **1996**, *54*, R14321.
- (45) Shirota, Y. *J. Mater. Chem.* **2000**, *10*, 1–25.
- (46) Lee, J.; Jung, B.-J.; Lee, J.-I.; Chu, H. Y.; Do, L.-M.; Shim, H.-K. *J. Mater. Chem.* **2002**, *12*, 3494–3498.
- (47) Pauling, L. *The Nature of the Chemical Bond and the Structure of Molecules and Crystals: An Introduction to Modern Structural Chemistry*; Cornell University Press, 1939.
- (48) O'Hagan, D. *Chem. Soc. Rev.* **2008**, *37*, 308–319.
- (49) Park, B. K.; Kitteringham, N. R.; O'Neill, P. M. *Annu. Rev. Pharmacol.* **2001**, *41*, 443–470.
- (50) Chambers, R. D. *Fluorine in Organic Chemistry*; John Wiley & Sons Inc., 1974.
- (51) Hellmann, M.; Peters, E.; Pummer, W.; Wall, L. *J. Am. Chem. Soc.* **1957**, *79*, 5654–5656.
- (52) McBee, E.; Lindgren, V.; Liggett, W. *Ind. Eng. Chem.* **1947**, *39*, 378–380.
- (53) Gething, B.; Patrick, C.; Stacey, M.; Tatlow, J. *Nature* **1959**, *183*, 588–589.
- (54) Harrison, D.; Stacey, M.; Stephens, R.; Tatlow, J. *Tetrahedron* **1963**, *19*, 1893–1901.
- (55) Chambers, R.; Hole, M.; Iddon, B.; Musgrave, W.; Storey, R. *J. Chem. Soc. C* **1966**, 2328–2331.
- (56) Fuller, G. *J. Chem. Soc.* **1965**, 6264–6267.
- (57) Vorozhtsov, N.; Platonov, V.; Yakobson, G. *Russ. Chem. B.* **1963**, *12*, 1389–1389.
- (58) Brooke, G. M. *J. Fluorine Chem.* **1997**, *86*, 1–76.
- (59) Chambers, R. D. *J. Fluorine Chem.* **2010**, *131*, 665–675.
- (60) Chambers, R. D.; Martin, P. A.; Sandford, G.; Williams, D. L. H. *J. Fluorine Chem.* **2008**, *129*, 998–1002.
- (61) Wall, L. A.; Pummer, W. J.; Fearn, J. E.; Antonucci, J. M. *J. Res. Nat. Inst. Stand. Technol. A.* **1963**, *67A*, 481–497.

- (62) Harper Jr, R. J.; Soloski, E. J.; Tamborski, C. *J. Org. Chem.* **1964**, *29*, 2385–2389.
- (63) Birchall, J.; Haszeldine, R. *J. Chem. Soc.* **1961**, 3719–3727.
- (64) Feldman, D.; Segal-Lew, D.; Rabinovitz, M. *J. Org. Chem.* **1991**, *56*, 7350–7354.
- (65) Birchall, J.; Haszeldine, R. *J. Chem. Soc.* **1959**, 13–17.
- (66) Langille, K.; Peach, M. *J. Fluorine Chem.* **1972**, *1*, 407–414.
- (67) Respass, W.; Tamborski, C. *J. Organomet. Chem.* **1970**, *22*, 251–263.
- (68) Burdon, J.; Hollyhead, W.; Tatlow, J. *J. Chem. Soc.* **1965**, 5152–5156.
- (69) Allen, J.; Burdon, J.; Tatlow, J. *J. Chem. Soc.* **1965**, 6329–6336.
- (70) Gerasimova, T. N.; Semikolenova, N. V.; Orlova, N. A.; Fomenko, T. V.; Fokin, E. P. *Izv. Sib. Otd. Akad. Nauk SSSR, Ser. Khim. Nauk* **1975**, *14*, 54.
- (71) Chaudhry, M. T.; Stephens, R. *J. Chem. Soc.* **1963**, 4281–4283.
- (72) Sigalov, A.; Petrov, E.; Beletskaya, I. *Russ. Chem. B.* **1984**, *33*, 2181–2183.
- (73) Birchall, J.; Hazard, R.; Haszeldine, R.; Wakalski, A. *J. Chem. Soc. C* **1967**, 47–50.
- (74) Miyaura, N.; Yamada, K.; Suzuki, A. *Tetrahedron Lett.* **1979**, *20*, 3437–3440.
- (75) Miyaura, N.; Suzuki, A. *Chem. Rev.* **1995**, *95*, 2457–2483.
- (76) Frohn, H.-J.; Adonin, N. Y.; Bardin, V. V.; Starichenko, V. F. *J. Fluorine Chem.* **2002**, *117*, 115–120.
- (77) Korenaga, T.; Kosaki, T.; Fukumura, R.; Ema, T.; Sakai, T. *Org. Lett.* **2005**, *7*, 4915–4917.
- (78) Thiemann, T.; Umeno, K.; Ohira, D.; Inohae, E.; Sawada, T.; Mataka, S. *New J. Chem.* **1999**, *23*, 1067–1070.
- (79) Havelková, M.; Hocek, M.; Dvoák, D. *Synlett* **1999**, *1999*, 1145–1147.
- (80) Chambers, R.; Chivers, T. *J. Chem. Soc.* **1965**, 3933–3939.
- (81) Frohn, H.-J.; Adonin, N. Y.; Bardin, V.; Starichenko, V. *Anorg. Allg. Chem.* **2002**, *628*, 2834–2838.
- (82) Kinzel, T.; Zhang, Y.; Buchwald, S. L. *J. Am. Chem. Soc.* **2010**, *132*, 14073–14075.
- (83) Korenaga, T.; Kosaki, T.; Kawauchi, Y.; Ema, T.; Sakai, T. *J. Fluorine Chem.* **2006**, *127*, 604–609.
- (84) Butters, M.; Harvey, J. N.; Jover, J.; Lennox, A. J.; Lloyd-Jones, G. C.; Murray, P. M. *Angew. Chem. Int. Ed. Engl.*, **2010**, *49*, 5156–5160.

- (85) Frohn, H.-J.; Adonin, N. Y.; Bardin, V.; Starichenko, V. *Tetrahedron Lett.* **2002**, *43*, 8111–8114.
- (86) Frohn, H.-J.; Adonin, N. Y.; Bardin, V. V.; Starichenko, V. F. *J. Fluorine Chem.* **2003**, *122*, 195–199.
- (87) Adonin, N. Y.; Babushkin, D. E.; Parmon, V. N.; Bardin, V. V.; Kostin, G. A.; Mashukov, V. I.; Frohn, H.-J. *Tetrahedron* **2008**, *64*, 5920–5924.
- (88) Thathagar, M. B.; Beckers, J.; Rothenberg, G. *J. Am. Chem. Soc.* **2002**, *124*, 11858–11859.
- (89) Thathagar, M. B.; Beckers, J.; Rothenberg, G. *Adv. Synth. Catal.* **2003**, *345*, 979–985.
- (90) Proch, S.; Mei, Y.; Villanueva, J.; Lu, Y.; Karpov, A.; Ballauff, M.; Kempe, R. *Adv. Synth. Catal.* **2008**, *350*, 493–500.
- (91) Bandari, R.; Höche, T.; Prager, A.; Dirnberger, K.; Buchmeiser, M. R. *Chem. Eur. J.* **2010**, *16*, 4650–4658.
- (92) Cano, R.; Ramón, D. J.; Yus, M. *Tetrahedron* **2011**, *67*, 5432–5436.
- (93) Smith, R. C.; Bodner, C. R.; Earl, M. J.; Sears, N. C.; Hill, N. E.; Bishop, L. M.; Sizemore, N.; Hehemann, D. T.; Bohn, J. J.; Protasiewicz, J. D. *J. Organomet. Chem.* **2005**, *690*, 477–481.
- (94) Altenhoff, G.; Goddard, R.; Lehmann, C. W.; Glorius, F. *J. Am. Chem. Soc.* **2004**, *126*, 15195–15201.
- (95) Organ, M. G.; Calimsiz, S.; Sayah, M.; Hoi, K. H.; Lough, A. J. *Angew. Chem. Int. Ed. Engl.*, **2009**, *121*, 2383–2387.
- (96) So, C. M.; Chow, W. K.; Choy, P. Y.; Lau, C. P.; Kwong, F. Y. *Chem. Eur. J.* **2010**, *16*, 7996–8001.
- (97) Zhao, Q.; Li, C.; Senanayake, C. H.; Tang, W. *Chem. Eur. J.* **2013**, *19*, 2261–2265.
- (98) Saeki, T.; Takashima, Y.; Tamao, K. *Synlett* **2005**, *2005*, 1771–1774.
- (99) Strawser, D.; Karton, A.; Zenkina, O. V.; Iron, M. A.; Shimon, L. J.; Martin, J. M.; van der Boom, M. E. *J. Am. Chem. Soc.* **2005**, *127*, 9322–9323.
- (100) Nakamura, Y.; Yoshikai, N.; Ilies, L.; Nakamura, E. *Org. Lett.* **2012**, *14*, 3316–3319.
- (101) Cargill, M. R.; Sandford, G.; Tadeusiak, A. J.; Yufit, D. S.; Howard, J. A.; Kilickiran, P.; Nelles, G. *J. Org. Chem.* **2010**, *75*, 5860–5866.

- (102) Johnson, S. A.; Huff, C. W.; Mustafa, F.; Saliba, M. *J. Am. Chem. Soc.* **2008**, *130*, 17278–17280.
- (103) Lafrance, M.; Rowley, C. N.; Woo, T. K.; Fagnou, K. *J. Am. Chem. Soc.* **2006**, *128*, 8754–8756.
- (104) Lafrance, M.; Shore, D.; Fagnou, K. *Org. Lett.* **2006**, *8*, 5097–5100.
- (105) Do, H.-Q.; Daugulis, O. *J. Am. Chem. Soc.* **2008**, *130*, 1128–1129.
- (106) Do, H.-Q.; Khan, R. M. K.; Daugulis, O. *J. Am. Chem. Soc.* **2008**, *130*, 15185–15192.
- (107) René, O.; Fagnou, K. *Org. Lett.* **2010**, *12*, 2116–2119.
- (108) Chen, F.; Min, Q.-Q.; Zhang, X. *J. Org. Chem.* **2012**, *77*, 2992–2998.
- (109) Wei, Y.; Kan, J.; Wang, M.; Su, W.; Hong, M. *Org. Lett.* **2009**, *11*, 3346–3349.
- (110) Fang, X.; Huang, Y.; Chen, X.; Lin, X.; Bai, Z.; Huang, K.-W.; Yuan, Y.; Weng, Z. *J. Fluorine Chem.* **2013**, *151*, 50–57.
- (111) Zhu, X.; Li, F.; Su, W. *Tetrahedron Lett.* **2013**, *54*, 1285–1289.
- (112) Chang, J. W. W.; Chia, E. Y.; Chai, C. L. L.; Seayad, J. *Org. Biomol. Chem.* **2012**, *10*, 2289–2299.
- (113) Wei, Y.; Su, W. *J. Am. Chem. Soc.* **2010**, *132*, 16377–16379.
- (114) Li, H.; Liu, J.; Sun, C.-L.; Li, B.-J.; Shi, Z.-J. *Org. Lett.* **2010**, *13*, 276–279.
- (115) Kalkhambkar, R. G.; Laali, K. K. *Tetrahedron Lett.* **2011**, *52*, 5525–5529.
- (116) Cambeiro, X. C.; Boorman, T. C.; Lu, P.; Larrosa, I. *Angew. Chem. Int. Ed. Engl.*, **2013**, *52*, 1781–1784.
- (117) He, C.-Y.; Fan, S.; Zhang, X. *J. Am. Chem. Soc.* **2010**, *132*, 12850–12852.
- (118) Becht, J.-M.; Drian, C. L. *Org. Lett.* **2008**, *10*, 3161–3164.
- (119) Shang, R.; Fu, Y.; Wang, Y.; Xu, Q.; Yu, H.-Z.; Liu, L. *Angew. Chem. Int. Ed. Engl.*, **2009**, *48*, 9350–9354.
- (120) Dai, J.-J.; Liu, J.-H.; Luo, D.-F.; Liu, L. *Chem. Commun.* **2011**, *47*, 677–679.
- (121) Luo, H.-Q.; Dong, W.; Loh, T.-P. *Tetrahedron Lett.* **2013**, 2833–2836.
- (122) Xie, K.; Yang, Z.; Zhou, X.; Li, X.; Wang, S.; Tan, Z.; An, X.; Guo, C.-C. *Org. Lett.* **2010**, *12*, 1564–1567.

Chapter 2

Synthesis of Fluorinated Biphenylphosphonic Acids

2.1 Introduction

The focus of this thesis is to synthesise a range of fluorinated donor-acceptor compounds for the modification of AlO_x surfaces for potential future applications in OLEDs and OTFTs, in collaboration with the SONY Corporation. Depending on the nature of their structures, fluorinated monolayers will provide a means to alter the physical and electronic properties of the metal substrate on which they are deposited. The primary aim will be the modification of the work function of aluminium oxide.

2.2 Aims and Objectives

For this project, the general molecular structure of the desired compounds is shown. [Figure 7]

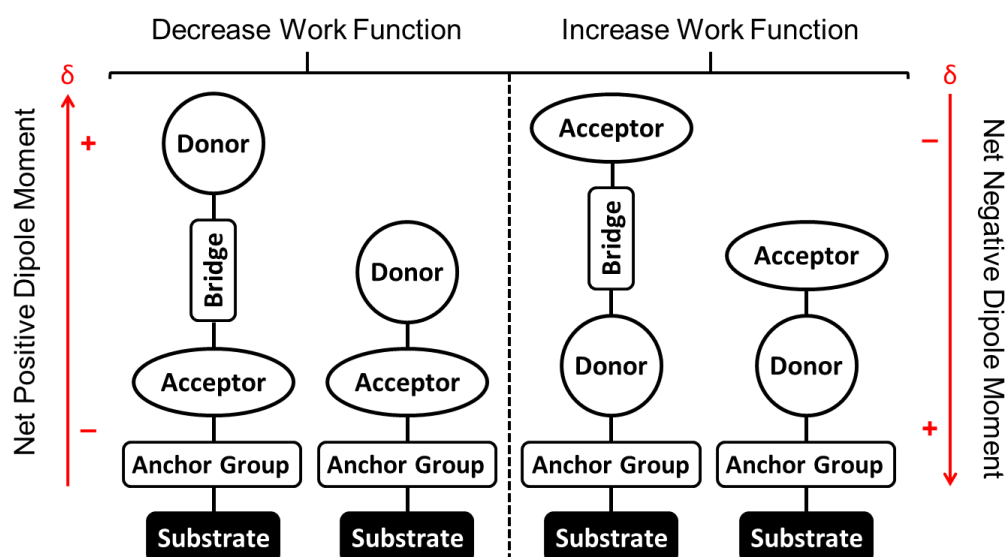


Figure 7. Schematic of various desired organic monolayer structures attached to a metal oxide substrate for work function modification.

Compounds targeted should comprise an electron-rich moiety (donor) which is directly, or via a conjugated bridge, bound to an electron-poor moiety (acceptor). The structures should also include an anchor group, allowing for covalent linkages to metal oxide surfaces. The design of these structures should allow for the synthesis of compounds with significant molecular dipoles. Depending on the orientation of the molecular dipoles, due to the arrangement of the donor and acceptor units, the monolayer formed has the potential to either raise or lower the work function of the bound metal oxide substrate. Both scenarios are of interest within this project. As described in chapter 1, those molecules exhibiting a net-positive dipole moment are expected to reduce the observed work function, whilst those exhibiting a net-negative dipole moment should increase the observed work function. [Figure 7]

We targeted the development of molecular donor-acceptor structures that sufficiently alter the chemical and electronic properties of an AlO_x surface without affecting the quality and structural properties of the resulting self-assembled monolayers. This involves an iterative process including molecular design, molecular modelling, synthesis and experimental verification of the surface modification.

For our initial studies, we were interested in developing monolayer surfaces capable of lowering the work function of an AlO_x substrate and as such targeted compounds with net-positive dipole moments. The known high affinity of phosphonic acid compounds to metal oxide surfaces makes them suitable anchor groups in the design of our structures. Highly fluorinated aromatics could act as the acceptor units in Figure 7 and the donor fragment of the SAM would be electron donating aromatic or aliphatic units, allowing for the synthesis of a range of polyfluoroaromatic systems.

SAMs displaying a highly dense packing motif are extremely desirable as, when employed within a variety of devices, such characteristics can result in improved device performance. It has been shown that π - π stacking between aryl end-groups in a SAM can lead to a more closely packed surface compared to the equivalent linearly terminated SAM.¹ For this reason, our initial targets consist of two aryl rings, one of which will be highly fluorinated to act as an acceptor group due to the F atoms, directly attached to a phosphonic acid group. Also included in this series will be the non-fluorinated biphenyl-4-ylphosphonic acid **18** and the bridged biphenyl **27**. [Figure 8]

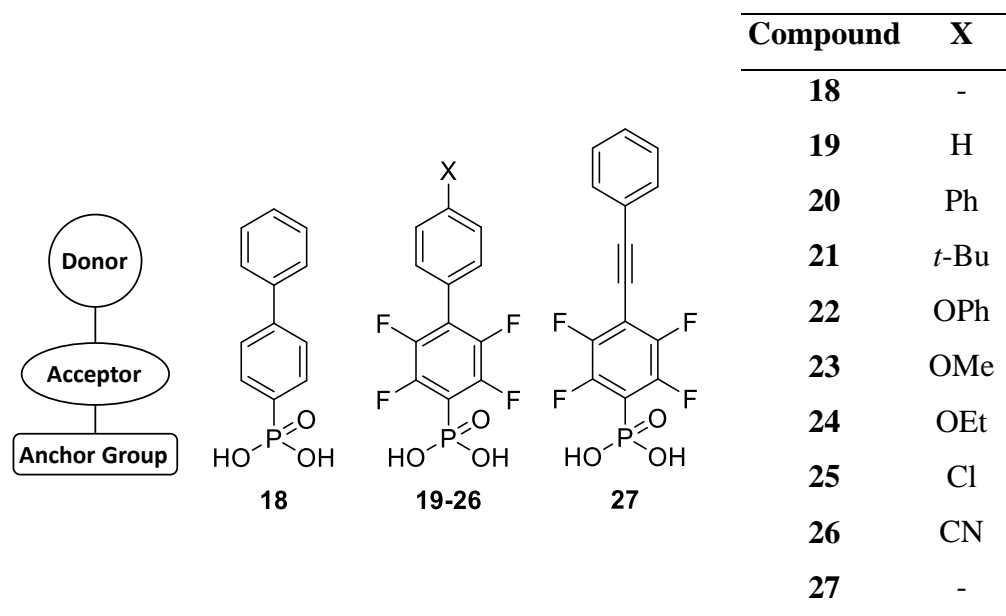


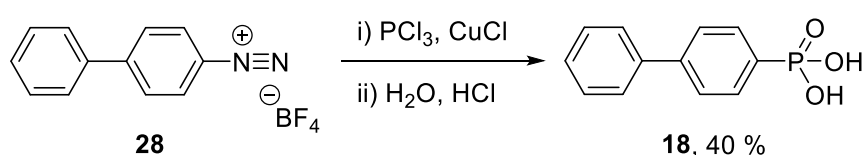
Figure 8. Targeted phosphonic acid derivatives.

The inclusion of electron-withdrawing fluorine substituents in **19** and **27** will induce a net-positive dipole moment compared to **18**, with the magnitude of the dipole of phosphonic acids **20-26** dependent upon substituent X. To achieve a greater positive molecular dipole, substituent X should consist of an electron-donating group attached to a donor aryl ring, however attempts would be made to vary substituent X to determine how much of an influence this has upon the monolayers' structural and electronic properties. The phosphonic acid anchor group should keep the molecules stably bound to the surface while enabling the self-assembly process for the formation of high-coverage, robust monolayers.

In this series, compound **18** will act as a 'standard' for our testing, allowing for the effect of fluorine substituents on the acceptor ring and substituents at the *para*- position of the donor ring to be evaluated. Targets **20-24** were designed to exhibit a greater net-positive dipole moment than **19**, through the inclusion of an electron-donating substituent on the donor ring. As such, monolayers of **19-24** may be expected to reduce the observed work function of the metal oxide substrate with which they are bound. Although electron-donating groups at the *para*- position of the donor ring were favoured for our initial studies, targets **25** and **26** were proposed to quantify the effect of the nature of substituents at this position on the observed work function of a metal substrate. Target **25** offers the potential to conduct further chemistry using the chlorine

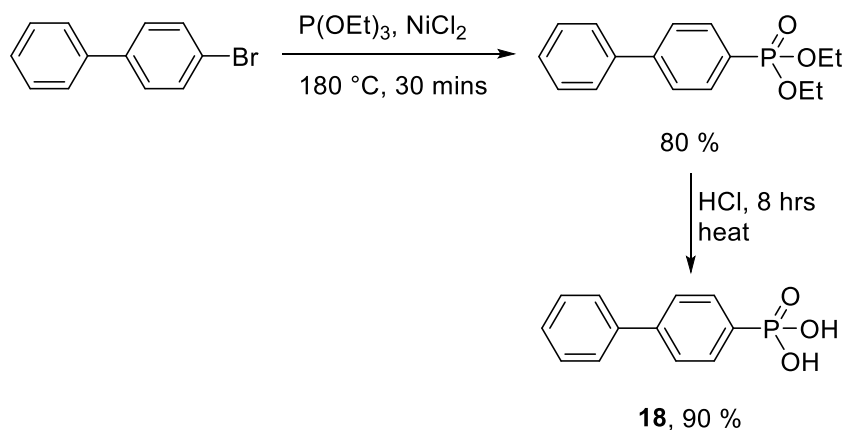
substituent as a functional group. Target **27** was included as a comparison to **19** to evaluate the effect of the inclusion of a conjugated bridge between the donor and acceptor ring systems.

Of these target systems, synthetic routes to non-fluorinated phosphonic acid **18** have already been described in the literature. Biphenyl-4-ylphosphonic acid **18** was first synthesised from the corresponding diazonium fluoroborate salt **28** with phosphorus trichloride and copper (I) chloride.² [Scheme 42]



Scheme 42. First documented synthesis of biphenyl-4-ylphosphonic acid **18**.²

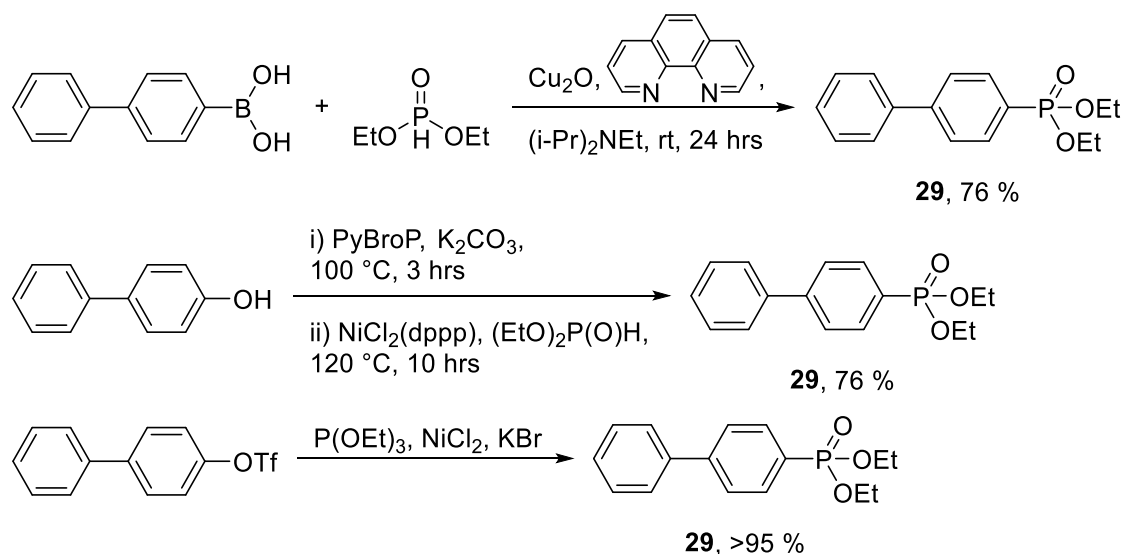
Many years later, Grabiak *et al.* reported the synthesis of **18**, in a far superior yield, through treatment of 4-bromobiphenyl with triethylphosphite and nickel (II) chloride.³ [Scheme 43]



Scheme 43. Alternative synthesis of biphenyl-4-ylphosphonic acid **18**.³

More recently, a number of procedures have emerged for the synthesis of diethyl biphenyl-4-ylphosphonate **29**, the precursor to biphenyl-4-ylphosphonic acid **18**.⁴⁻⁶ [Scheme 44] These methods include copper catalysed addition of diethyl phosphite to

an aryl boronic acid, nickel catalysed coupling of a phenol and diethyl phosphite, and nickel catalysed phosphorylation of an aryl triflate.

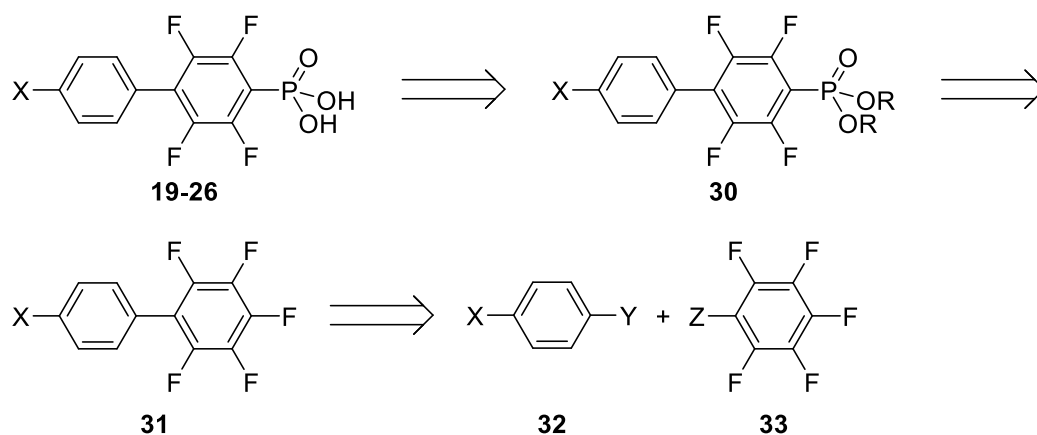


Scheme 44. Syntheses of diethyl biphenyl-4-ylphosphonate **29**.⁴⁻⁶

2.3 Synthetic Strategy

Although, as described, several routes to biphenyl-4-ylphosphonic acid **18** and its precursor phosphonate **29** have been reported, no syntheses, have yet, been described for the corresponding highly fluorinated biphenyl targets **19–27**.

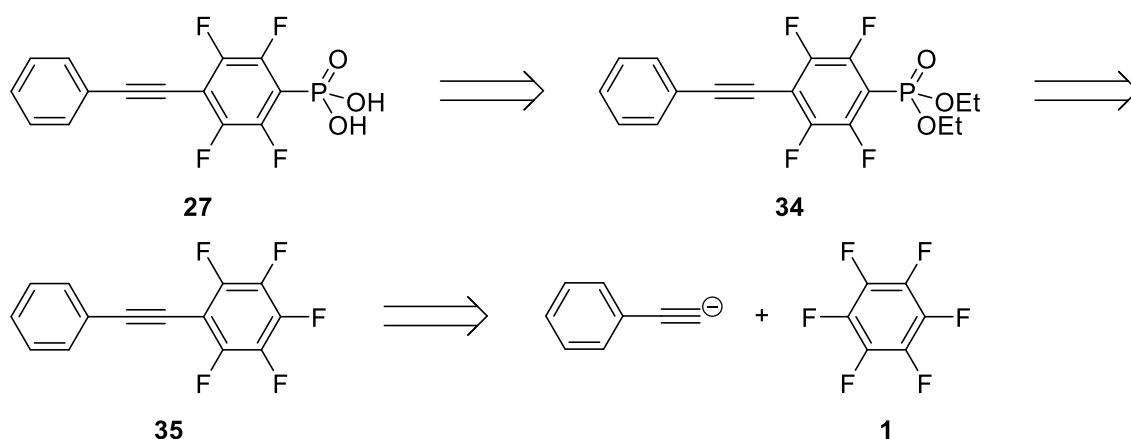
For targets **19–26** the following retrosynthetic analysis is proposed based on chemistry discussed in Chapter 1 for the key aryl-aryl coupling process. [Scheme 45]



Scheme 45. Retrosynthetic analysis of targets **19–26**.

The syntheses will begin with the establishment of a coupling reaction between compound type **32** and **33**, by a Suzuki-Miyaura cross-coupling process, to yield the core fluorinated biphenyl structures **31**. Reactions of **31** with appropriate phosphorus nucleophiles are expected to occur exclusively *para* to the unfluorinated aryl ring, yielding phosphonates **30**. The synthesis of targets **29-26** will then be completed via hydrolysis of these phosphonates.

For the synthesis of **27**, an alternative retrosynthetic pathway is proposed, involving two separate nucleophilic aromatic substitutions. [Scheme 46] Firstly, the reaction of hexafluorobenzene **1** with the anion of phenyl acetylene will be attempted to give the core fluorinated structure **35**. The attachment of the phosphonic acid moiety will then be implemented as for targets **19-26**.



Scheme 46. Retrosynthetic analysis of target **27**.

Whilst there exist a number of methods for the synthesis of sp^2 hybridised carbon-phosphorus bonds, attempts will be made to establish nucleophilic aromatic substitution (S_NAr) reactions involving phosphorus nucleophiles, for the synthesis of arylphosphonates **30** and **34**. As described in chapter 1, highly fluorinated aromatic systems are extremely reactive towards nucleophilic attack, with a wide range of experimental data concerning such reactions already reported.⁷

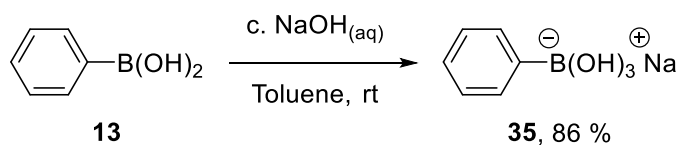
2.4 Results and Discussion

2.4.1 Synthesis of Fluorinated Phosphonic Acid Precursors

2.4.1.1 Palladium Catalysed Synthesis of Fluorinated Biphenyl Systems

As discussed in chapter 1, transition metal catalysed cross-coupling reactions of pentafluorobenzene derivatives have already been reported in the literature. However, many of these procedures make use of expensive additives and complex catalytic species. Previous collaborative work in the Durham group has shown that the synthesis of fluorinated biphenyls, analogous to **31** (Scheme 45), under standard Suzuki-Miyaura conditions can prove problematic due to the reactive nature of the fluorinated starting material.⁸ Under such conditions undesired S_NAr reactions have been observed between the fluorinated starting material and the nucleophilic species present for the *in situ* activation of boron.⁹ It has been shown that alkali-metal boronate salts can be used as pre-activated boron equivalents in Suzuki-Miyaura cross-coupling reactions¹⁰, negating the need for the addition of further basic or nucleophilic reagents. We utilised this method for the synthesis of the desired fluorinated biphenyls **31**.

Following a literature procedure,¹⁰ reaction of a concentrated solution of phenylboronic acid **13** in toluene with a saturated solution of aqueous sodium hydroxide resulted in the precipitation of sodium phenylborate **35**, which was filtered, washed and isolated in good yield. [Scheme 47]

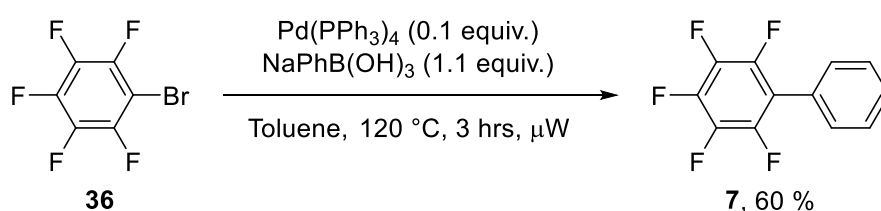


Scheme 47. Synthesis of sodium phenylborate **35**.

It was not possible to confirm the purity of **35** by NMR analysis as it rapidly dissociates back to phenylboronic acid and sodium hydroxide in D_2O . However, the melting point of the isolated product was in excess of $360\text{ }^\circ\text{C}$, significantly higher than that of phenylboronic acid **13** at $216 - 219\text{ }^\circ\text{C}$,¹¹ suggesting the formation of the boronate salt was successful. The solid product was thoroughly dried *in vacuo* to remove any residual

toluene and was ground to a fine powder for use in the subsequent cross-coupling reaction.

Reaction of sodium phenylborate with bromopentafluorobenzene **36**, in the presence of a catalytic quantity of $\text{Pd}(\text{PPh}_3)_4$, under microwave irradiation resulted in 77 % conversion of bromopentafluorobenzene by ^{19}F NMR, and isolation of 2,3,4,5,6-pentafluorobiphenyl **7** in good yield. [Scheme 48] The employment of a pre-formed sodium borate salt in this reaction allows for the omission of a boron-activating reagent, thereby avoiding any undesired side reactions at the reactive C–F bonds.

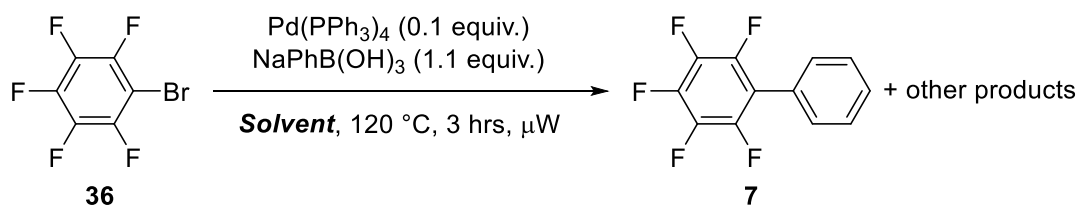


Scheme 48. Cross-coupling reaction of bromopentafluorobenzene with sodium phenylborate.

Microwave irradiation was employed for the synthesis of **7** in an attempt to decrease the timescale of the reaction. However, even with a high catalyst loading, the reaction still required prolonged heating at an elevated temperature to achieve reasonable conversion of starting material to the corresponding biphenyl **7**.

As toluene is a low absorber of microwave energy, due in part to its low polarity¹², a number of other solvents were screened under the conditions outlined in Scheme 48 in an attempt to achieve greater conversions. [Table 4]

None of the alternative solvents screened yielded biphenyl **7** in a greater yield than that achieved in toluene. It was also noted that, although not observed for the reaction in toluene, ^{19}F NMR resonances at -138.9 , -153.9 , and -162.3 ppm appeared in a 2:1:2 ratio in all other solvents, corresponding to pentafluorobenzene. The presence of pentafluorobenzene within the crude reaction solutions was further identified by comparison to that of a commercial sample.

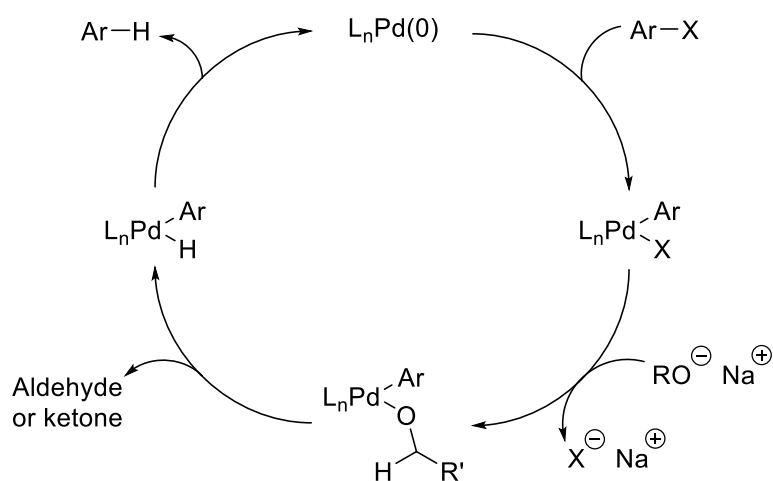
Table 4. Solvent screen.

Solvent	Yield 7 / % ^a	Solvent	Yield 7 / % ^a
Toluene	77	MeOH	37 ^b
THF	59 ^b	1,4-Dioxane	37 ^b
DMF	54 ^b	MeCN	27 ^b
EtOH	53 ^b		

^a¹⁹F NMR Yield determined by **36**.

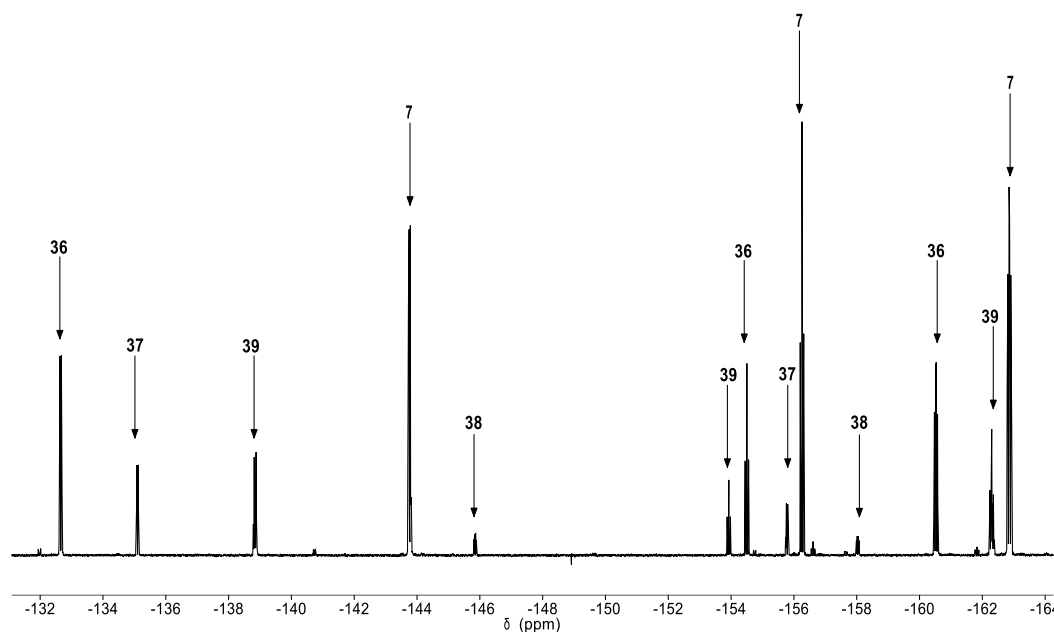
^bOther products observed, see text.

A reasonable possibility for the formation of pentafluorobenzene is via the catalytic dehalogenation of bromopentafluorobenzene **36**. Reduction of aryl halides by alcohols and base, catalysed by tetrakis(triphenylphosphine)palladium have been reported previously,¹³ with similar reactions also reported for alternative palladium catalysts.¹⁴ In all of these systems, oxidative addition of the aryl halide to the palladium catalyst followed by alkoxide attack at the metal centre, rearrangement and subsequent reductive elimination of the arene is suggested as a likely pathway. [Scheme 49]



Scheme 49. Proposed mechanism for the catalytic dehalogenation of aryl halides.¹⁴

For the Suzuki-Miyaura cross-coupling reactions conducted in methanol and ethanol (Table 4), yields of pentafluorobenzene by ^{19}F NMR spectroscopy were 21 and 52 % respectively. It is postulated that within these solvents, the borate salt **35** begins to dissociate back to the parent boronic acid and sodium hydroxide, allowing for the formation of sodium alkoxides capable of reacting in the manner shown in scheme 49. Further evidence for the degradation of the borate salt **35** within these solvents is observed with the presence of resonances due to alkoxy-substituted by-products in the ^{19}F NMR spectrum. For example, in the reaction conducted in ethanol, competing $\text{S}_{\text{N}}\text{Ar}$ reactions were observed between ethoxide and bromopentafluorobenzene **36**, and ethoxide and biphenyl **7** through the formation of **37** and **38** respectively, both displaying two resonances of equal intensity. [Figure 9]



Legend:

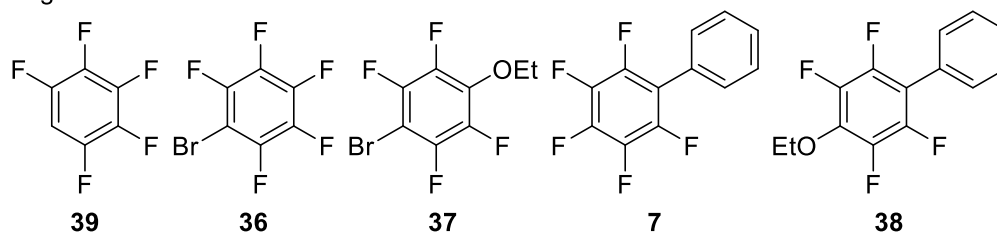


Figure 9. ^{19}F NMR spectrum of the crude reaction mixture in ethanol.

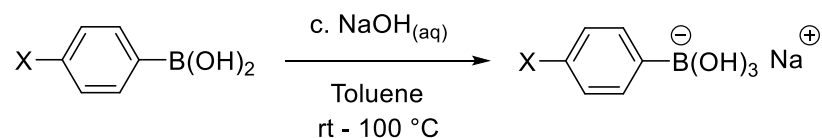
These by-products were observed alongside resonances due to pentafluorobenzene **39**, bromopentafluorobenzene **36**, and tetrafluorobiphenyl **7**. The presence of ethoxy-

substituted by-products **37** and **38** was further characterised by GC-MS analysis ($m/z = 272$ and 270 respectively), and were in accordance with literature data.^{15,16}

For the remaining reactions in the solvent screen (Table 4), pentafluorobenzene, bromopentafluorobenzene and pentafluorobiphenyl were the only fluorinated materials observed by ^{19}F NMR spectroscopy. In all of these cases, the nucleophilic solvent may attack the palladium intermediate and act as a source of hydride within the proposed catalytic dehydrogenation reaction. As toluene was found to afford the greatest yield of biphenyl **7**, and was the only solvent screened not to promote the formation of pentafluorobenzene, it was selected as the preferred solvent for further cross-coupling reactions of sodium borate salts.

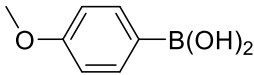
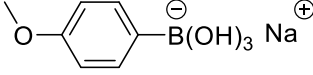
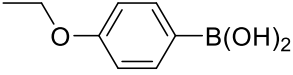
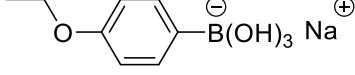
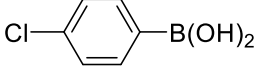
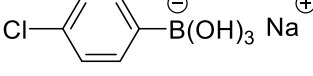
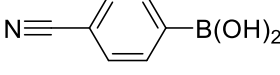
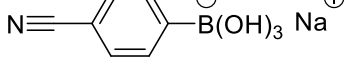
Following the successful cross-coupling reaction of the sodium borate salt **35** with bromopentafluorobenzene, the remaining required sodium arylborate salts were synthesised as precursors for the synthesis of targets **20-26**. [Table 5]

Table 5. Syntheses of sodium arylborate salts.



Boronic Acid	Boronic Acid Melting Point / °C	Product, (Yield / %)	Product Melting Point / °C
	232–234 ¹⁷	 40 , (95)	> 350
	191–196 ¹⁸	 41 , (77)	> 350
	134–135 ¹⁹	 42 , (84)	> 350

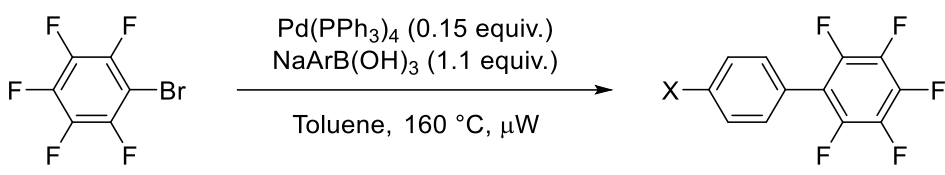
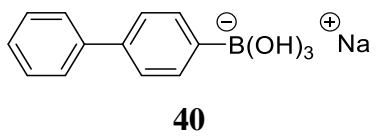
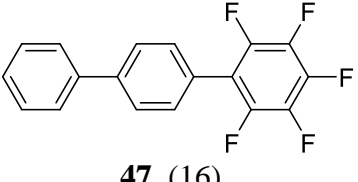
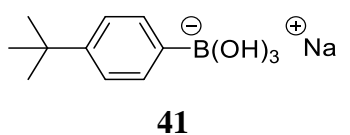
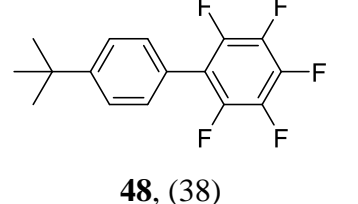
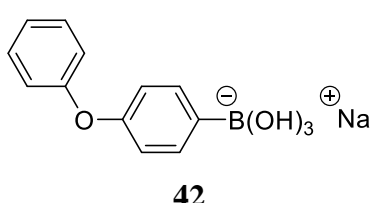
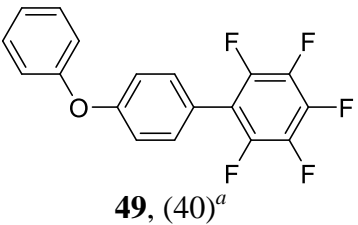
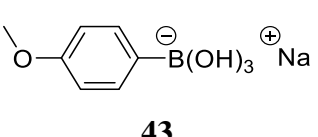
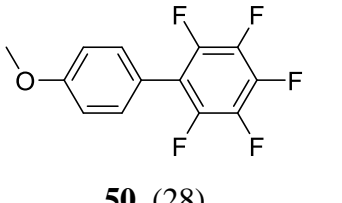
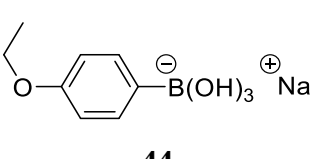
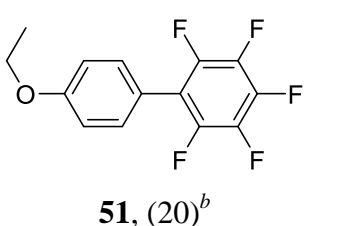
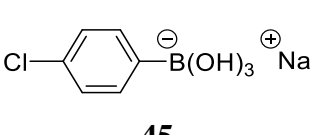
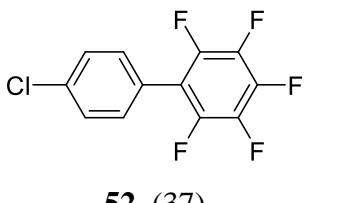
Table 5 (cont.). Syntheses of sodium arylborate salts.

Boronic Acid	Boronic Acid Melting Point / °C	Product, (Yield / %)	Product Melting Point / °C
	204–206 ²⁰	 43 , (82)	> 350
	150 ²¹	 44 , (81)	> 350
	306–307 ²¹	 45 , (85)	> 350
	> 350 ²²	 46 , (0)	-

In the case of 4-cyanophenylboronic acid, no sodium borate salt **46** was isolated. This was due to the inability to dissolve the precursor boronic acid in an excess of toluene, even with prolonged heating.

The isolated borate salts **40-45** were again thoroughly dried and ground to fine powders before use in subsequent cross-coupling reactions with bromopentafluorobenzene. [Table 6]

Table 6. Cross-coupling reactions of bromopentafluorobenzene with 4-substituted sodium phenylborate salts.

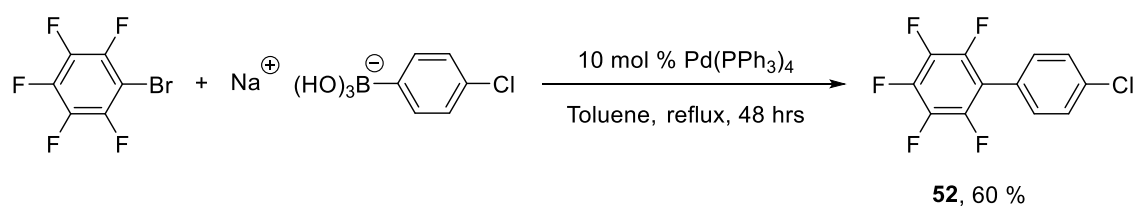
		
Sodium Aryl Borate	Time / hrs	Product (Yield / %)
 <p>40</p>	10	 <p>47, (16)</p>
 <p>41</p>	8	 <p>48, (38)</p>
 <p>42</p>	12	 <p>49, (40)^a</p>
 <p>43</p>	9	 <p>50, (28)</p>
 <p>44</p>	7	 <p>51, (20)^b</p>
 <p>45</p>	9	 <p>52, (37)</p>

^a74 % purity as determined by GC-MS, ^b80 % purity as determined by GC-MS.

As was necessary for the synthesis of 2,3,4,5,6-pentafluorobiphenyl **7**, prolonged heating at elevated temperatures with high catalyst loadings were required to achieve isolable quantities of products. Yields for the microwave assisted syntheses of **47-52** are all significantly lower than that of the unsubstituted fluorinated biphenyl **7**. Several factors could account for these observations. Similarly to the synthesis of **7**, 100 % conversion of starting material proved unachievable for the syntheses of **47-52**. For many of these reactions ^{19}F NMR analysis highlighted the presence of significant quantities of bromopentafluorobenzene remaining within the crude reaction solutions even after extended reaction times. Trace amounts of other, unknown, fluorinated material were also detected by ^{19}F NMR analyses, indicating the occurrence of unwanted side reactions. GC-MS analysis of the crude reaction solutions, before work-up, of **47-52** showed the presence of amounts of triphenylphosphine and triphenylphosphine oxide, evidence for the degradation of the catalytic palladium species used within the reactions.

Problems were also encountered during the purification of compounds **47-52**. Crude products were purified by column chromatography but many systems required several columns to obtain pure samples. In the case of biphenyls **49** and **51**, separation of the desired product from contaminants proved unsuccessful with the isolated sample of **49** containing deborylated boronic acid, and **51** containing traces of triphenylphosphine and triphenylphosphine oxide. It is probable that the overall poor yields observed for the syntheses of compounds **47-52** can be attributed to the exposure of reaction solutions to prolonged periods of microwave radiation, causing degradation of reaction components; as well as general lack of reactivity of the starting materials under these reaction conditions.

After the initial screening of biphenyl production using microwave irradiation, the synthesis of compound **52** was repeated using conventional laboratory techniques. [Scheme 50] The final product was isolated in a higher yield of 60 % compared to the alternative microwave synthesis conducted previously. Although this yield is still low in comparison to alternative syntheses reported for similar structures, this has been achieved with minimum reaction optimisations.

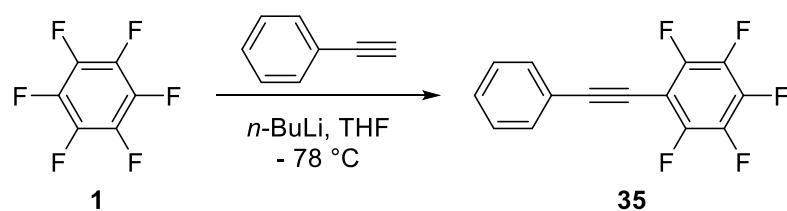


Scheme 50. Synthesis of **52** using standard laboratory apparatus.

Consequently, it has been shown that the synthesis of polyfluorinated biphenyls by Suzuki-Miyaura reactions is possible using pre-formed sodium borate salts and, more importantly, with the use of simple, commercially available and inexpensive Pd(PPh₃)₄ catalyst, rather than the designed literature systems discussed in Chapter 1. The use of microwave reaction conditions provide the desired products in low to moderate yields, which can be improved through the use of conventional laboratory equipment. This procedure provides a valid synthetic route for the first step of the retrosynthetic pathway for targets **19-26**. [Scheme 45]

2.4.1.2 Synthesis of an Acetylene Bridged Fluorinated Biphenyl

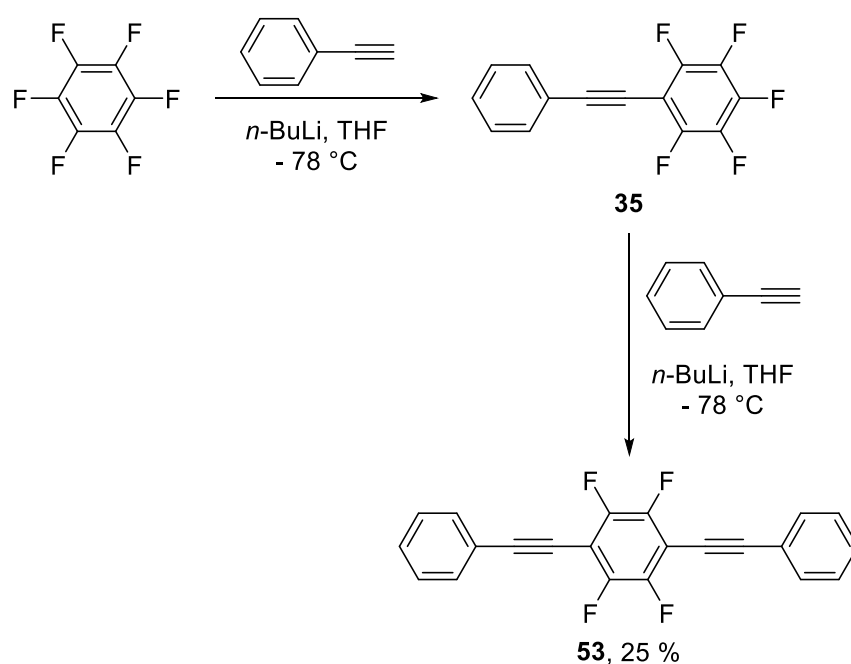
The synthesis of pentafluoro-(2-phenylethynyl)benzene **35** was attempted by S_NAr reaction of hexafluorobenzene **1** with lithium phenylacetylide, which was prepared through reaction of phenylacetylene with *n*-butyllithium. [Scheme 51]



Scheme 51. Attempted synthesis of pentafluoro-(2-phenylethynyl)benzene **35**.

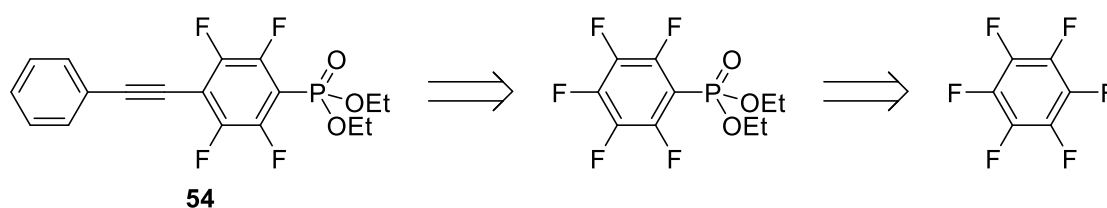
Analysis of the crude reaction solution by ¹⁹F NMR spectroscopy showed the presence of one resonance at -137.8 ppm alongside residual hexafluorobenzene **1** (-162.5 ppm), rather than three resonances that would be expected for the monosubstituted target **35**. It appears that, although the initial reactivity of hexafluorobenzene towards lithium phenylacetylide is relatively low, the monoacetylenic product **35** formed is more activated towards further nucleophilic attack. Subsequently, the resulting disubstituted

product **53** is obtained as the sole product of the reaction, confirmed by GC–MS analysis ($m/z = 350$) and the single resonance observed at -137.8 in the ^{19}F NMR spectrum. [Scheme 52] ^1H NMR analysis also confirms the structure of **53** by the observation of two complex multiplets in the aromatic region which have integrals in the ratio 2:3.



Scheme 52. Observed reaction between hexafluorobenzene and lithium phenylacetylide.

Since reaction of acetylene derivatives with hexafluorobenzene is unselective, other routes towards the synthesis of target phosphonic acid **27** were required. Initial attachment of the phosphonate moiety, to form a substituted pentafluorobenzene ring, followed by further reaction with lithium phenylacetylide could yield an alternative synthetic route towards the desired precursor phosphonate **54**. [Scheme 53]



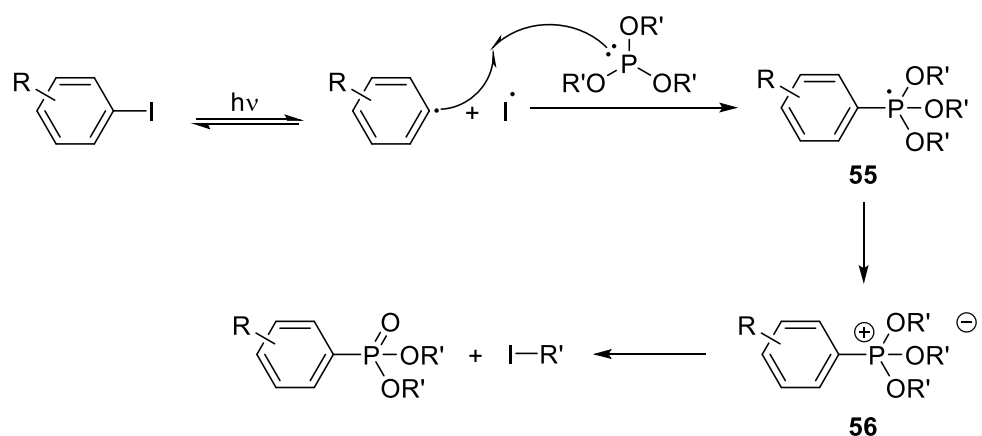
Scheme 53. Alternative retrosynthetic analysis of phosphonate target **54** from hexafluorobenzene **1**.

2.4.2 Attachment of a Phosphonic Acid Moiety by S_NAr

With methodology for C–C bond formation established, attention was turned to a model reaction for Ar–P bond formation.

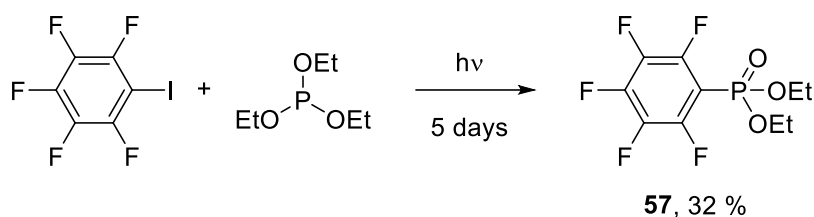
There exist a number of synthetic routes towards the production of phosphonic acids. Three key reactions for attachment of phosphonate groups to aryl rings are often utilised; the photo-initiated Arbuzov reaction, transition metal assisted Arbuzov reactions and a Friedel-Crafts type reaction.

Aryl-iodine bonds can undergo homolytic cleavage in the presence of UV light in photo-initiated Arbuzov reactions.²³ The radicals formed from exposure to UV light can be trapped by exposure to a trialkyl phosphite, yielding a phosphoranyl radical **55**. A single electron transfer from **55** to an iodine atom gives rise to the formation of a quasi-phosphonium salt **56** which can then collapse to the desired aryl phosphonate and the appropriate alkyl iodide.²⁴ [Scheme 54] Yields for the photo-initiated Arbuzov reaction are generally low to moderate due to the formation of side-products.



Scheme 54. Mechanism for the photo-initiated Arbuzov reaction.

Although limited by these factors, the photo-initiated Arbuzov reaction has been shown to be applicable to many aryl iodides, incorporating a number of substituents on the aryl ring.^{25,26} This includes the reported synthesis of the perfluorinated arylphosphonate **57**.²⁷ [Scheme 55]

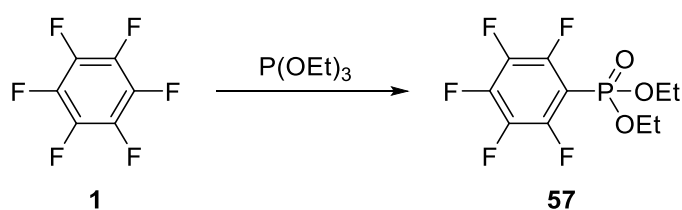


Scheme 55. Synthesis of diethyl pentafluorobenzenephosphonate **57** by the photo-initiated Arbuzov reaction.²⁷

The use of transition metal catalysts can also be a useful tool for the synthesis of aryl phosphonates, with many examples shown to be catalysed by nickel, copper and palladium.²⁸ Although these reactions require the use of temperatures in excess of 150 °C, the yields of arylphosphonates obtained are high.

Since many of the established methods for aryl C–P bond formation are time consuming and require the use of expensive reagents, attempts will be made to establish nucleophilic aromatic substitution (S_NAr) reactions for the synthesis of arylphosphonate precursors of targets **19-27**.

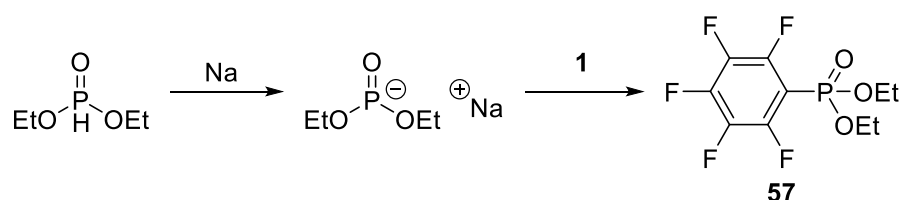
The synthesis of diethyl pentafluorobenzenephosphonate **57** was first attempted by the S_NAr reaction of triethyl phosphite with hexafluorobenzene **1**, following a modified literature procedure.^{25,29} [Scheme 56]



Scheme 56. Proposed S_NAr of hexafluorobenzene with triethyl phosphite.

However, no evidence of the desired reaction was observed by NMR analysis, with only starting materials shown to be present. It was noted that microwave irradiation was employed for similar S_NAr -Arbuzov reactions, shortening reaction times and increasing product yields.³⁰ The reaction was repeated under microwave conditions but again no reaction was observed.

A similar reaction was attempted, employing a different phosphorous reagent as the nucleophilic species. [Scheme 57] Diethyl phosphite was reacted with sodium metal to give the corresponding metal salt, and was subsequently reacted with hexafluorobenzene. This reaction has previously been reported in the literature although no experimental data was provided for the formation of **57**.³¹



Scheme 57. Proposed reaction of the sodium salt of diethyl phosphite with hexafluorobenzene.

After prolonged heating, ¹⁹F NMR analysis revealed the presence of **57**, as a minor side-product, through three separate resonances in a 2:1:2 ratio, corresponding to reported literature values.²⁵ However, as only trace amounts were observed along with a number of unidentified side-products, additional purification procedures were not attempted and this approach to highly fluorinated biphenyls bearing phosphonic acid anchor groups was not pursued further.

2.5 Conclusions

Pentafluorobromobenzene **36** was shown to be a suitable substrate for palladium catalysed Suzuki-Miyaura cross-coupling reactions with pre-activated borate salts and standard, inexpensive palladium catalysts. Cross-coupling syntheses involving highly fluorinated borate salts have not previously been reported and possess some experimental advantages. A range of fluorinated biphenyls were synthesised using this methodology. Employing microwave irradiation for these reactions has a detrimental effect on the overall product yields, with improved yields achieved in conventional glassware. The use of toluene as a solvent is crucial to limiting the formation of unwanted by-products.

The S_NAr reaction of hexafluorobenzene with lithium phenylacetylide proceeds to give the disubstituted compound **53** exclusively, making syntheses of initial biphenyl targets very difficult.

Attempts to synthesise and isolate diethyl pentafluorophenylphosphonate by S_NAr reactions proved unsuccessful. S_NAr reactions between hexafluorobenzene and triethyl phosphite resulted in no observable product formation. The corresponding reaction with the sodium salt of diethyl phosphite proved more successful with trace amounts of the desired product observable by ¹⁹F NMR spectroscopy. Difficulties regarding the extent of the reaction and product purification, however, meant no product was isolated.

No attempts were made to further develop methodology for highly fluorinated aryl derivatives bearing phosphorous containing groups whereby P bonded directly to the aryl ring. Consequently, new target systems were identified.

2.6 References to Chapter 2

- (1) Halik, M.; Klauk, H.; Zschieschang, U.; Schmid, G.; Dehm, C.; Schütz, M.; Maisch, S.; Effenberger, F.; Brunnbauer, M.; Stellacci, F. *Nature* **2004**, *431*, 963–966.
- (2) Jaffe, H.; Freedman, L. D.; Doak, G. *J. Am. Chem. Soc.* **1954**, *76*, 1548–1552.
- (3) Grabiak, R. C.; Miles, J. A.; Schwenzler, G. M. *Phosphorus, Sulfur Silicon Relat. Elem.* **1980**, *9*, 197–202.
- (4) Zhuang, R.; Xu, J.; Cai, Z.; Tang, G.; Fang, M.; Zhao, Y. *Org. Lett.* **2011**, *13*, 2110–2113.
- (5) Zhao, Y.-L.; Wu, G.-J.; Han, F.-S. *Chem. Commun.* **2012**, *48*, 5868–5870.
- (6) Yang, G.; Shen, C.; Zhang, L.; Zhang, W. *Tetrahedron Lett.* **2011**, *52*, 5032–5035.
- (7) Brooke, G. M. *J. Fluorine Chem.* **1997**, *86*, 1–76.
- (8) Cargill, M. R. *Durham University PhD Thesis*, **2010**.
- (9) Chen, J.; Cammers-Goodwin, A. *Tetrahedron Lett.* **2003**, *44*, 1503–1506.
- (10) Cammidge, A. N.; Goddard, V. H.; Gopee, H.; Harrison, N. L.; Hughes, D. L.; Schubert, C. J.; Sutton, B. M.; Watts, G. L.; Whitehead, A. J. *Org. Lett.* **2006**, *8*, 4071–4074.
- (11) Seaman, W.; Johnson, J. R. *J. Am. Chem. Soc.* **1931**, *53*, 711–723.
- (12) Lidström, P.; Tierney, J.; Wathey, B.; Westman, J. *Tetrahedron* **2001**, *57*, 9225–9283.
- (13) Zask, A.; Helquist, P. *J. Org. Chem.* **1978**, *43*, 1619–1620.
- (14) Viciu, M. S.; Grasa, G. A.; Nolan, S. P. *Organometallics* **2001**, *20*, 3607–3612.
- (15) Fang, X.; Huang, Y.; Chen, X.; Lin, X.; Bai, Z.; Huang, K.-W.; Yuan, Y.; Weng, Z. *J. Fluorine Chem.* **2013**, *151*, 50–57.
- (16) Vasilevskaya, T. N.; Badashkeeva, A. G.; Gerasimova, T. N. *Zh. Org. Khim.* **1970**, *6*, 126–132.
- (17) Yabroff, D. L.; Branch, G.; Bettman, B. *J. Am. Chem. Soc.* **1934**, *56*, 1850–1857.
- (18) Deng, Y.; Zhang, Y.; Jiang, H.; Xu, L.; Liu, H.; Li, S.; He, N. *J. Biomed. Nanotech.* **2009**, *5*, 551–556.
- (19) Bowie, R.; Musgrave, O. *J. Chem. Soc. C* **1970**, 485–488.
- (20) Staab, H. A.; Meissner, B. *Liebigs Ann. Chem.* **1971**, *753*, 80–91.
- (21) Branch, G.; Yabroff, D. L.; Bettman, B. *J. Am. Chem. Soc.* **1934**, *56*, 937–941.

- (22) Matsubara, H.; Seto, K.; Tahara, T.; Takahashi, S. *Bull. Chem. Soc. Jpn.* **1989**, *62*, 3896–3901.
- (23) Wolf, W.; Kharasch, N. *J. Org. Chem.* **1965**, *30*, 2493–2498.
- (24) Plumb, J.; Obrycki, R.; Griffin, C. *J. Org. Chem.* **1966**, *31*, 2455–2458.
- (25) Burton, D. J.; Flynn, R. M. *Synthesis* **1979**, *8*, 615–615.
- (26) Obrycki, R.; Griffin, C. E. *J. Org. Chem.* **1968**, *33*, 632–636.
- (27) Burton, D. J.; Flynn, R. M. *Synthesis* **1979**, *1979*, 615–615.
- (28) Beletskaya, I.; Kazankova, M. *Russ. J. Org. Chem.* **2002**, *38*, 1391–1430.
- (29) Dawson, N. D.; Burger, A. *J. Am. Chem. Soc.* **1952**, *74*, 5312.
- (30) Qu, G.-R.; Xia, R.; Yang, X.-N.; Li, J.-G.; Wang, D.-C.; Guo, H.-M. *J. Org. Chem.* **2008**, *73*, 2416–2419.
- (31) Markovskii, L.; Furin, G.; Shermolovich, Y. G.; Yakobson, G. *Russ. Chem. Bull.* **1981**, *30*, 646–648.

Chapter 3

Synthesis of Fluorinated Benzylphosphonic Acids

3.1 Introduction

Chapter 2 was concerned with the attempted syntheses of a range of fluorinated biphenylphosphonic acids, which were initially identified as promising candidate materials for the modification of metal oxide surfaces. Difficulties were encountered with the direct attachment of a phosphonic acid group to a fluorinated aryl ring and, consequently, a new series of target molecules for the modification of metal oxide surfaces were required. This chapter is concerned with the synthesis and isolation of a series of related fluorinated benzylphosphonic acid derivatives. Structural variations between a series of fluorobenzyl analogues will allow for a direct comparison between the number and positioning of fluorine substituents on the aryl ring and the effect on the resulting associated monolayer properties.

3.2 Aims and Objectives

Due to difficulties encountered during the attempted direct attachment of a phosphonic acid moiety to a fluorinated aryl ring, we proposed that new targets should contain a methylene bridge between the anchor group and the ring structure. A series of benzylphosphonic acids were envisaged which had varying degrees of fluorination upon the benzene ring. [Figure 10] Although differing from the original biphenylphosphonic acid targets in Chapter 2, fluorobenzyl structures conform to the general donor-acceptor structure required for work function modification outlined in chapter 2. Rather than possessing two aryl rings, however, the electron-donor functionality will be provided within these targets through the presence of a methoxy substituent at the 4-position of the benzyl ring. Phosphonic acid **66**, although not possessing a methoxy substituent, was included following a request from the SONY Corporation to allow for a comparison with the equivalent methoxylated phosphonic acid **62**.

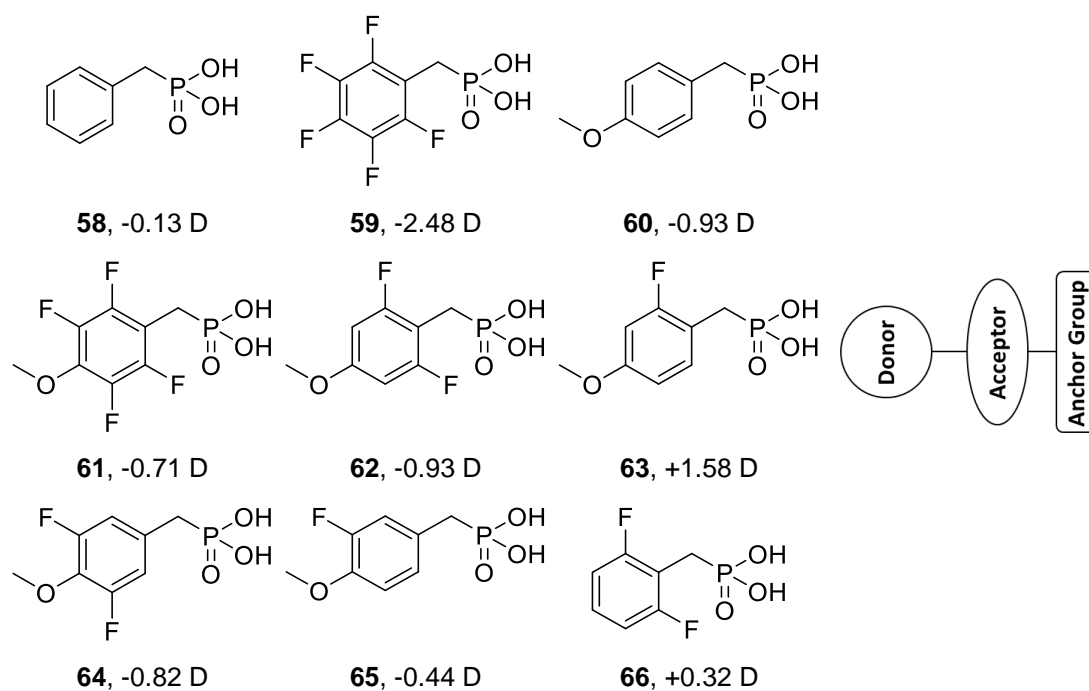


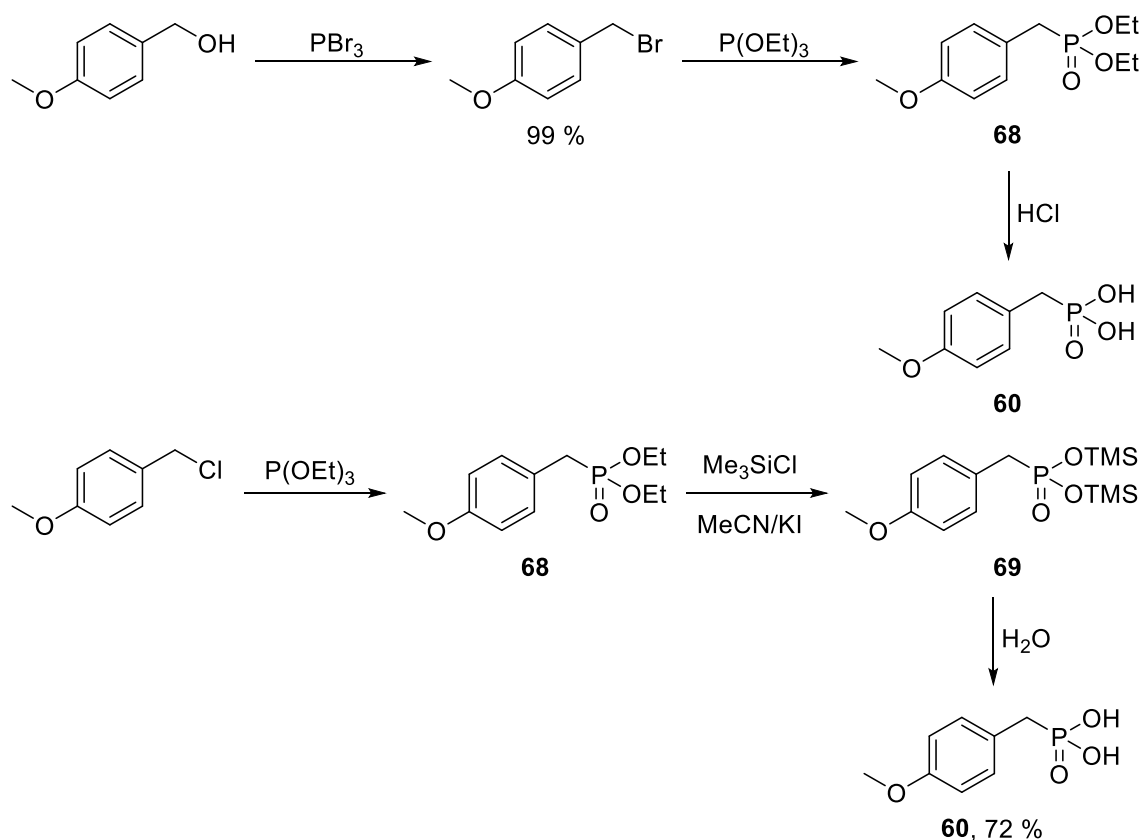
Figure 10. Targeted benzylphosphonic acids and their calculated relative dipole moments.

The research within this thesis is focused upon the synthesis of benzyl phosphonic acid derivatives, displaying a donor-acceptor structure through electron-donating and –withdrawing functionalities, for the modification of aluminium oxide (AlO_x). Aluminium is a cheap and robust material, and the ability to alter and control its chemical and physical properties, such as work function, will enhance the potential for its use within electronic devices applications.

Of the targets proposed for our research (Figure 10), benzylphosphonic acid **58** is available commercially and synthetic routes to 4-methoxybenzylphosphonic acid **60**, pentafluorobenzylphosphonic acid **59** and 2,6-difluorobenzylphosphonic acid **66** have already been described in the literature.

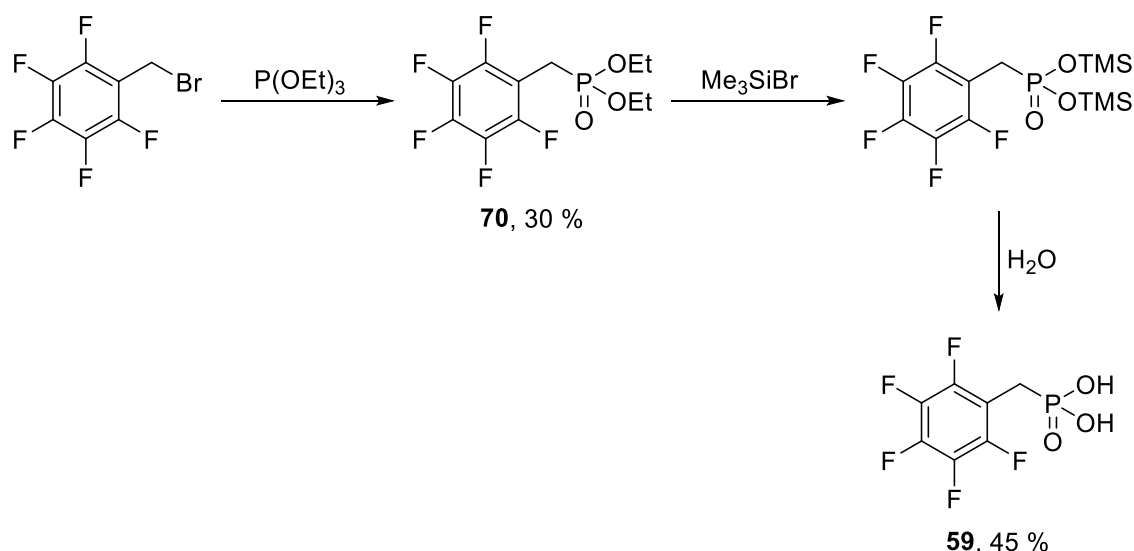
4-Methoxybenzylphosphonic acid **60** was first synthesised from the parent alcohol, via the corresponding benzyl bromide and a Michaelis-Arbuzov reaction, yielding the diethyl phosphonate **68** which was subsequently hydrolysed to the acid.¹ A similar synthesis was published a number of years later, again utilising a Michaelis-Arbuzov

reaction, with hydrolysis to the acid **60** via the *bis*-trimethylsilyl phosphonate **69**.² [Scheme 58]



Scheme 58. Documented syntheses of 4-methoxybenzylphosphonic acid **60**.^{1,2}

Using a similar synthetic procedure to that described previously, pentafluorobenzylphosphonic acid **59** was first synthesised from pentafluorobenzyl bromide, albeit in low yields.³ [Scheme 59] More recently pentafluorobenzylphosphonic acid was isolated using a similar synthesis, giving both the diethyl phosphonate **70** (96 %) and phosphonic acid **59** (77 %) in higher yields.⁴ 2,6-Difluorobenzylphosphonic acid **66**, has been synthesised in a similar manner, with the precursor phosphonate and acid isolated in an 86 and 76 % yield, respectively.⁴

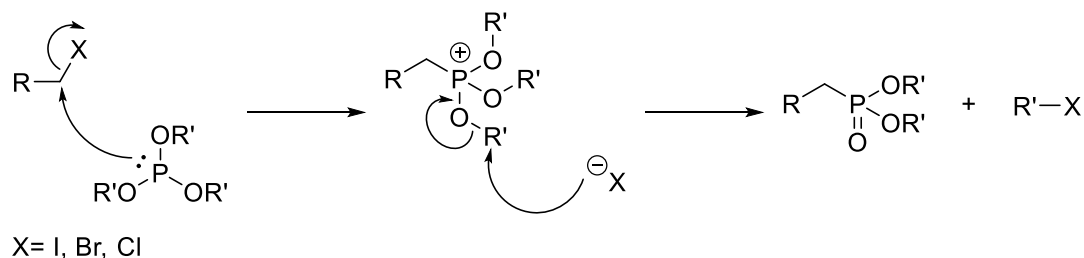


Scheme 59. Documented synthesis of pentafluorobenzylphosphonic acid **59**.³

No fluorinated methoxybenzylphosphonic acids have been reported in the literature or assessed for monolayer applications previously.

3.3 Synthetic Strategy

A Michaelis-Arbuzov reaction between the relevant benzyl bromides and triethylphosphite, is proposed for the synthesis of the precursors to targets **59-65**. This transformation is a two-step reaction of a trialkyl phosphite with a primary or secondary alkyl halide in which a trivalent phosphorous reagent is converted into a pentavalent phosphorous species. [Scheme 60] Hydrolysis of these phosphonates will yield the target phosphonic acids.

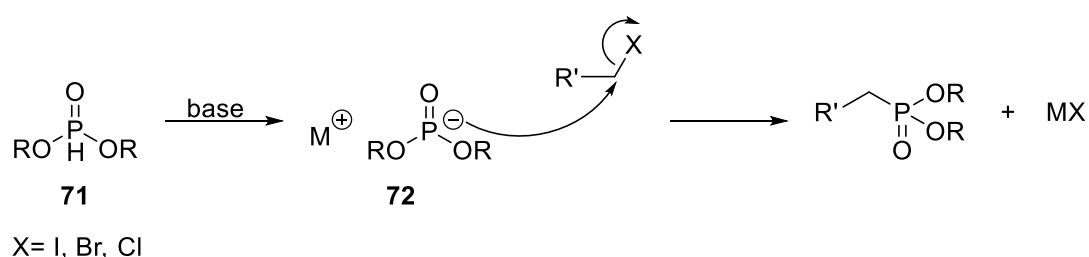


Scheme 60. Mechanism of the Michaelis-Arbuzov reaction.

Although the Michaelis-Arbuzov reaction is generally high yielding, one key side-reaction should be noted; the alkyl halide formed in the last step of the reaction can

itself undergo a Michaelis-Arbuzov reaction. To account for this, trimethyl- or triethylphosphite is often the reagent of choice as the resulting alkyl halides have relatively low boiling points and can easily evaporate out of the reaction flask. To further suppress any unwanted side-reactions the starting phosphite is often used in a large excess and, as such, acts as a solvent for the reaction.

In addition, the Michaelis Becker reaction also transforms primary and secondary halides to dialkylphosphonates by reaction of the anion of a dialkyl phosphite **71** with the alkyl halide. [Scheme 61]



Scheme 61. Mechanism of the Michaelis-Becker reaction.

Michaelis-Becker reactions do not require as forceful heating as the associated Michaelis-Arbuzov reactions and associated side-reactions are suppressed. However, the metal salts **72** formed during the reaction suffer from low-solubility in many solvents⁵ and so the Michael-Arbuzov reaction⁵ remains the most convenient method for the majority of systems and was the preferred synthetic route used in this work.

3.4 Results and Discussion

3.4.1 DFT Calculations of Benzylphosphonic Acids

DFT calculations were used to predict the relative surface dipole moments of target phosphonic acids **58-65** on an aluminium oxide surface and the calculated dipole moments are collated. [Figure 11] All calculations were performed by Dr. William Ford of the SONY Corporation using the Materials Studio package (Accelrys). All of the net dipole moments reported are given relative to that of an ethylphosphonic acid modified AlO_x surface.

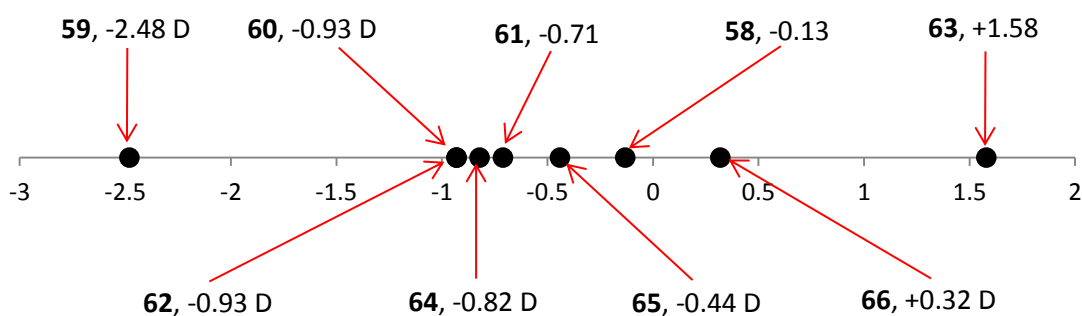


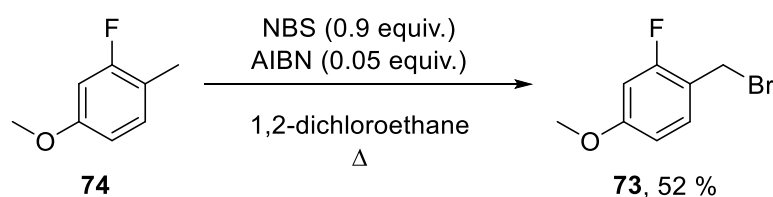
Figure 11. Relative surface dipole moments of phosphonic acids on a simulated AlO_x surface.

For the benzylphosphonic acids targeted (Figure 10), a range of 4 D is achieved depending on the degree and nature of the substituents attached to the aryl ring. The most negative surface dipole moment is calculated for a SAM of pentafluorobenzylphosphonic acid **59**. This result is unsurprising, **59** is the only modifier targeted possessing a terminal fluorine substituent creating a negative dipole pointing away from the surface. Replacement of fluorine *para* to the benzyl moiety with a methoxy group, to give target **61**, reduces the dipole moment by more than 1.5 D highlighting the key role of the terminal functional group. Although methoxy substituents have been targeted within this study as a source of electron donation through the lone pairs on oxygen, these calculations also highlight the effect of the relatively high electronegativity of oxygen. This is shown for the surface dipole obtained for methoxybenzylphosphonic acid **60**, which possessed a more negative dipole moment than the unsubstituted target **58**.

The most positive surface dipole achieved from the calculations was for target **63**. The presence of a *para* methoxy substituent as well as fluorine *ortho* to the benzyl functionality creates the desired donor–acceptor–anchor structure, and is accompanied by a positive dipole moment. It would be expected that *ortho* disubstitution, as for target **62**, would create a more positive dipole moment, however, a dipole identical to target **60** is predicted by calculation.

3.4.2 Synthesis of Benzylphosphonate Esters by Michaelis-Arbuzov Reactions

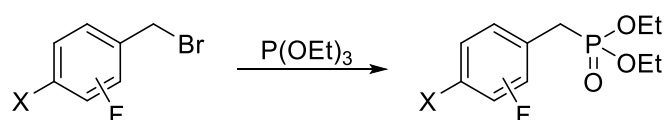
With the exception of 2-fluoro-4-methoxybenzyl bromide **73**, the precursor to target **63**, all of the parent benzyl bromides for the phosphonic acid targets are available commercially. In this case, **73** was synthesised by the free radical bromination of 3-fluoro-4-methylanisole **74** with *N*-bromosuccinimide (NBS), following a Wohl-Ziegler reaction procedure. [Scheme 62]



Scheme 62. Wohl-Ziegler radical bromination of 3-fluoro-4-methylanisole **74**.

After 3 hours of heating, the reaction of **74** with NBS afforded a mixture of desired product **73** and the analogous di-brominated product. ¹⁹F NMR analysis of the crude reaction solution possessed three resonances at - 114.8, - 114.9 and - 115.9 ppm corresponding to di-brominated product, desired product **73** and residual starting material respectively. GC-MS analysis of the crude reaction solution indicated the presence of two products, with m/z = 218 and 296 atomic mass units which are consistent with the mono- and di-brominated species, further confirming the dibromination of **74**. After distillation, **73** was obtained as a 95 % pure mixture with some residual di-brominated compound remaining. It was speculated that, due to steric restrictions, the di-brominated side-product would be unreactive during subsequent reactions with triethylphosphite and as such the remnants of this material could be removed during future purifications.

Following the synthesis of 2-fluoro-4-methoxybenzyl bromide **73**, Michaelis-Arbuzov reactions of all of the precursor benzyl bromides with neat triethylphosphite at high temperatures yielded the desired dialkyl phosphonates **68**, **70** and **75-80** in good yields, following evaporation of excess triethyl phosphite and purification. [Table 7]

Table 7. Synthesis of benzylphosphonates **68**, **70** and **75-80**.

X = F, OMe

Benzyl Bromide	Product, (Yield / %)	Benzyl Bromide	Product, (Yield / %)
	 70 , (70) ^a		 75 , (81) ^a
	 68 , (90) ^a		 76 , (74) ^a
	 77 , (87) ^b		 79 , (89) ^b
	 78 , (67) ^b		 80 , (76) ^b

Conditions: ^a160 °C, 4-6 hrs; ^b120 °C, 4 hrs.

³¹P NMR spectroscopy of the purified compounds show a single resonance in the region +20 to +26 ppm, consistent with literature data for benzyl phosphonate derivatives. These resonances display a large shift from the precursor triethyl phosphite at +139 ppm.

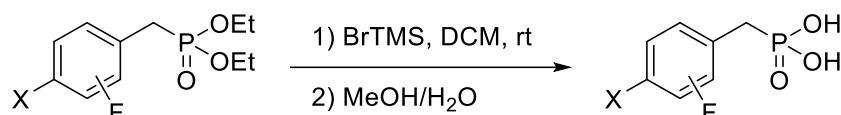
3.4.3 Hydrolysis to Benzylphosphonic Acids

Following the successful synthesis of benzylphosphonates **68**, **70** and **75-80**, subsequent hydrolysis, via corresponding bis(trimethylsilyl)phosphonate intermediates, to the

phosphonic acids **59-66** was achieved in moderate to good yields. [Table 8] The phosphonate esters were stirred, under a dry, inert atmosphere, with bromotrimethylsilane, before hydrolysing the resultant trimethylsilyl intermediates through reaction with methanol and water.

Although the conversion of phosphonate esters to their corresponding acids is more commonly achieved through reaction with a concentrated aqueous acid, this method is unsuitable for compounds containing acid sensitive functional groups. It has been shown that, upon contact with water and a low boiling alcohol at room temperature, bis(trimethylsilyl)phosphonate esters hydrolyse to their respective acids.⁶ For this reason, the milder approach employing bromotrimethylsilane⁷ was utilised for phosphonate esters **68**, **70** and **75-80**.

Table 8. Synthesis of benzylphosphonic acids **59-66**, **82** and **84**.



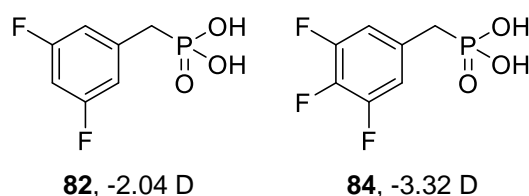
X = F, OMe

Phosphonate	Product, (Yield / %)	Phosphonate	Product, (Yield / %)
	59 , (80)		62 , (80)
	60 , (41)		63 , (69)
	61 , (76)		64 , (70)

Table 8 (cont.). Synthesis of benzylphosphonic acids **59-66**, **82** and **84**.

Phosphonate	Product, (Yield / %)	Phosphonate	Product, (Yield / %)
79	65, (91)	80	66, (78)
81, (81)	82, (81)	83, (87)	84, (62)

Phosphonic acids **59-66** were designed with specific structural variations to allow for a direct comparison between the number and position of fluorine substituents, the effect of a *para* positioned methoxy substituent, and the effect on work function modification in comparison to calculated data. Although not included in the original series, 3,5-difluorobenzylphosphonic acid **82** and 3,4,5-trifluorobenzylphosphonic acid **84** were suggested as interesting candidates for monolayer studies following initial testing by the SONY corporation on the structurally similar 3,5-difluoro-4-methoxybenzylphosphonic acid **64**. [Figure 12] The syntheses of **82** and **84** will allow for a direct comparison between the electronic nature of the substituent positioned *para* to the phosphonic acid moiety and its affects upon a SAM. The surface dipole moments calculated for phosphonic acids **82** and **84** are, along with the pentafluorinated target **59**, the most negative dipoles observed within this series, due to the fluorine substituents *meta* and *para* to the benzylphosphonic acid functionality.

**Figure 12.** Phosphonic acids **82** and **84** and their calculated relative dipole moments on a simulated AlO_x surface.

Phosphonic acids **82** and **84** were synthesised in good yields following the same synthetic protocols described for the synthesis of phosphonic acids **59-66**. [Table 8]

3.4.4 Synthesis of Benzylphosphonic Acids with Alternative Terminal Substituents

Alongside varying the electronic nature of the substituent positioned *para* to the benzylphosphonic acid moiety, we chose to synthesise phosphonic acids **85** and **86** in order to assess the effect of the chain length within an alkoxy-terminated SAM, upon SAM formation and subsequent properties. [Figure 13] The inclusion of a perfluorinated core will allow for direct comparisons with phosphonic acids **59** and **61**.

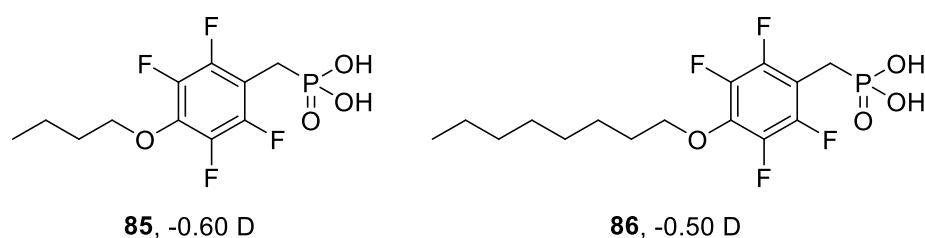
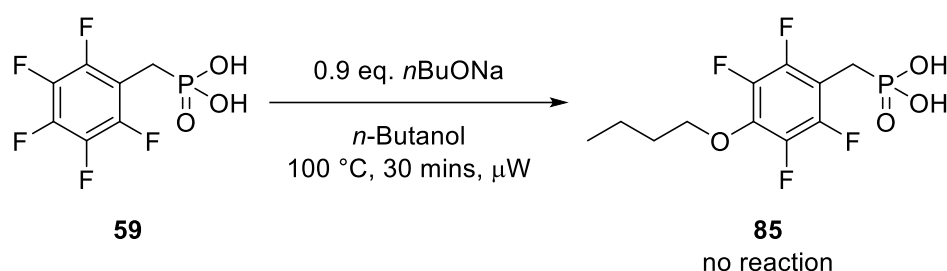


Figure 13. Phosphonic acid targets **85** and **86** and their calculated relative dipole moments on a simulated AlO_x surface.

The surface dipoles calculated for **85** and **86**, closely resemble that of the related methoxylated target **61**, with the calculated dipole moment becoming more positive as the alkyl chain length, and subsequent electron donating ability, increases. Although calculated to induce a similar surface dipole moment to **60**, varying the chain length of the alkoxy substituent in **85** and **86** may have a large impact on the properties of a SAM of these compounds. The presence of terminal, long-chain alkyl groups within a SAM are known to promote close-packing on the molecular level, with the formation of highly ordered layers capable of enhancing the wettability of a surface.⁸ The formation of SAMs containing highly ordered aliphatic chains have proven beneficial within organic thin film transistors, suppressing the migration of small molecules and lowering the supply voltage, with the potential to include such technology within low-power, portable electronic devices.^{9,10}

It was envisaged that the introduction of the desired butoxy- and octoxy- chains to a perfluorinated benzylphosphonic acid could be achieved via the S_NAr reactions of the appropriate sodium alkoxide and fluorinated precursors. To limit the number of synthetic steps required and potentially develop an efficient synthetic route towards a

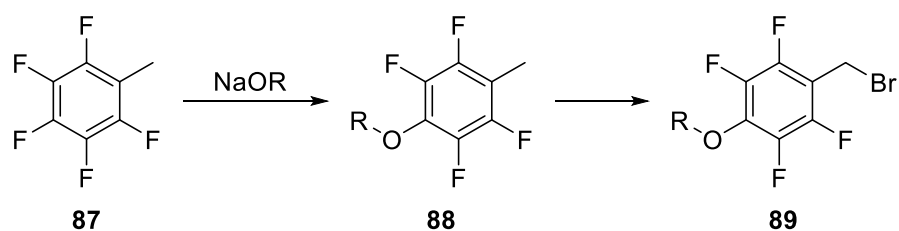
library of functionalised compounds, the first reaction attempted was with the pre-synthesised pentafluorobenzylphosphonic acid **59**. [Scheme 63]



Scheme 63. Attempted S_NAr reaction of sodium butoxide and **59**.

After 30 minutes of heating in a microwave reactor, no reaction was observed by either ^{19}F or ^{31}P NMR spectroscopy, with **59** the only observable compound by these means. It is likely that no reaction occurred due to the very low pK_a of phosphonic acids¹¹ ($pK_1 \sim 1-2$). The subsequent reaction between sodium butoxide and diethyl pentafluorobenzylphosphonate **70**, under the same reaction conditions, led to the production of a complex reaction mixture from which no target material could be isolated. Analysis of the GC-MS and NMR spectroscopy data obtained indicated multiple S_NAr reaction occurring on the ring as well as nucleophilic attack at the phosphorous centre.

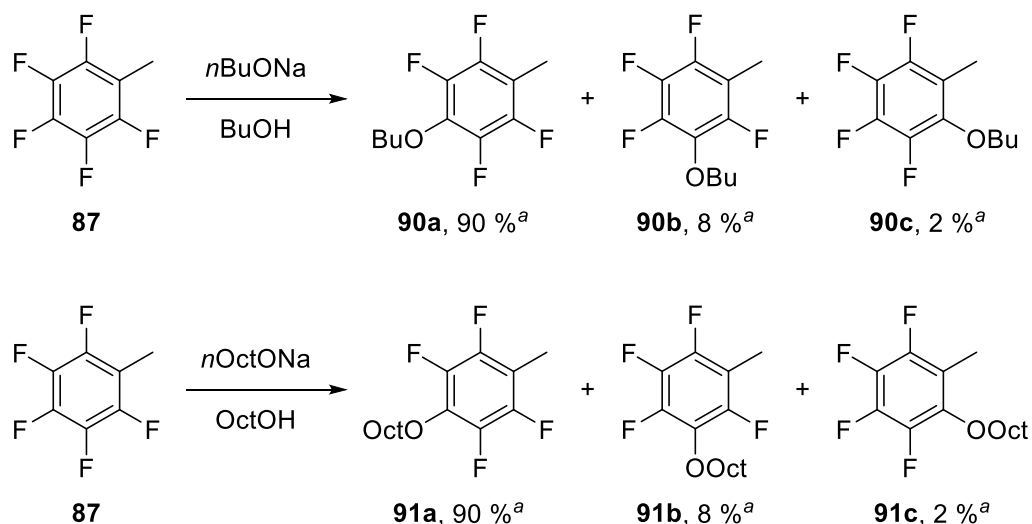
Since nucleophilic attack on pentafluorotoluene **87** is known to occur exclusively *para* to the methyl substituent,¹² a new synthetic strategy was proposed for the preparation of alkoxy-substituted derivatives **88**. Subsequent bromination of **88**, repeating methodology applied to the earlier bromination of the substituted toluene derivative **74**, would provide a synthetic route to the required benzyl bromide precursors **89**. [Scheme 64] Michealis-Arbuzov reactions with the bromides **89** and hydrolysis of the resulting phosphonates would complete the synthesis of phosphonic acids **85** and **86**.



R = C₄H₉ or C₈H₁₇

Scheme 64. Proposed synthesis for the benzyl bromide precursors to phosphonic acids **85** and **86**.

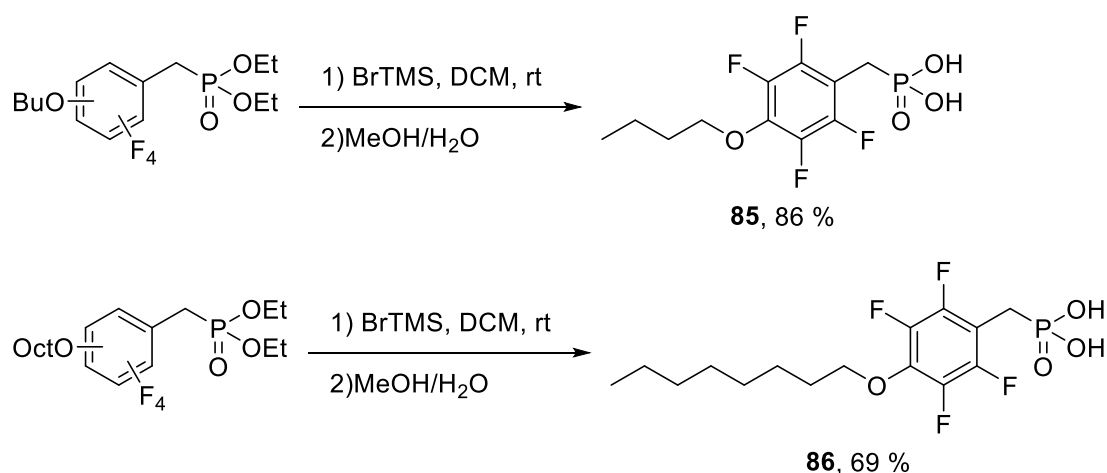
Reactions of pentafluorotoluene **87** with sodium butoxide and sodium octoxide yielded the desired reaction products **90a** and **91a**, along with a small proportion of other regioisomers, which could not be separated by column chromatography. [Scheme 65]



^aDetermined by ¹⁹F NMR spectroscopy.

Scheme 65. Synthesis of substituted fluorotoluenes **90** and **91** and ratios of product regioisomers.

The ratio of these regioisomers was maintained throughout the subsequent free radical brominations and Michaelis-Arbuzov reactions, with complete purification and isolation of the desired products occurring during the hydrolysis of the diethyl phosphonates to phosphonic acids **85** and **86**. [Scheme 66]



Scheme 66. Hydrolysis of diethyl phosphonates to yield phosphonic acids **85** and **86**.

3.5 Conclusions

A series of benzylphosphonic acids have been successfully synthesised from their parent benzyl bromides, displaying varying degrees of fluorination upon the benzyl ring. The incorporation of a methoxy substituent positioned *para* to the benzyl moiety enables these systems to potentially display the desired donor-acceptor type character outlined in chapter 2. For targets in which the precursor bromide is unavailable commercially, free radical bromination of the appropriate toluene derivatives provided a successful synthetic route to the benzyl bromide.

One-step $\text{S}_{\text{N}}\text{Ar}$ reactions between electrophilic pentafluorotoluene and sodium alkoxide nucleophiles yield the *para*-substituted products in high yields, along with small amounts of the *ortho*- and *meta*- regioisomers. Although difficulties were encountered with the separation of these isomers, this proved not to be essential and reactions through to the phosphonic acid were successful, with purification by recrystallisation of the desired targets achieved during the final step.

In summary, the following benzylphosphonic acids were successfully synthesised for assessment of work function properties. [Figure 14]

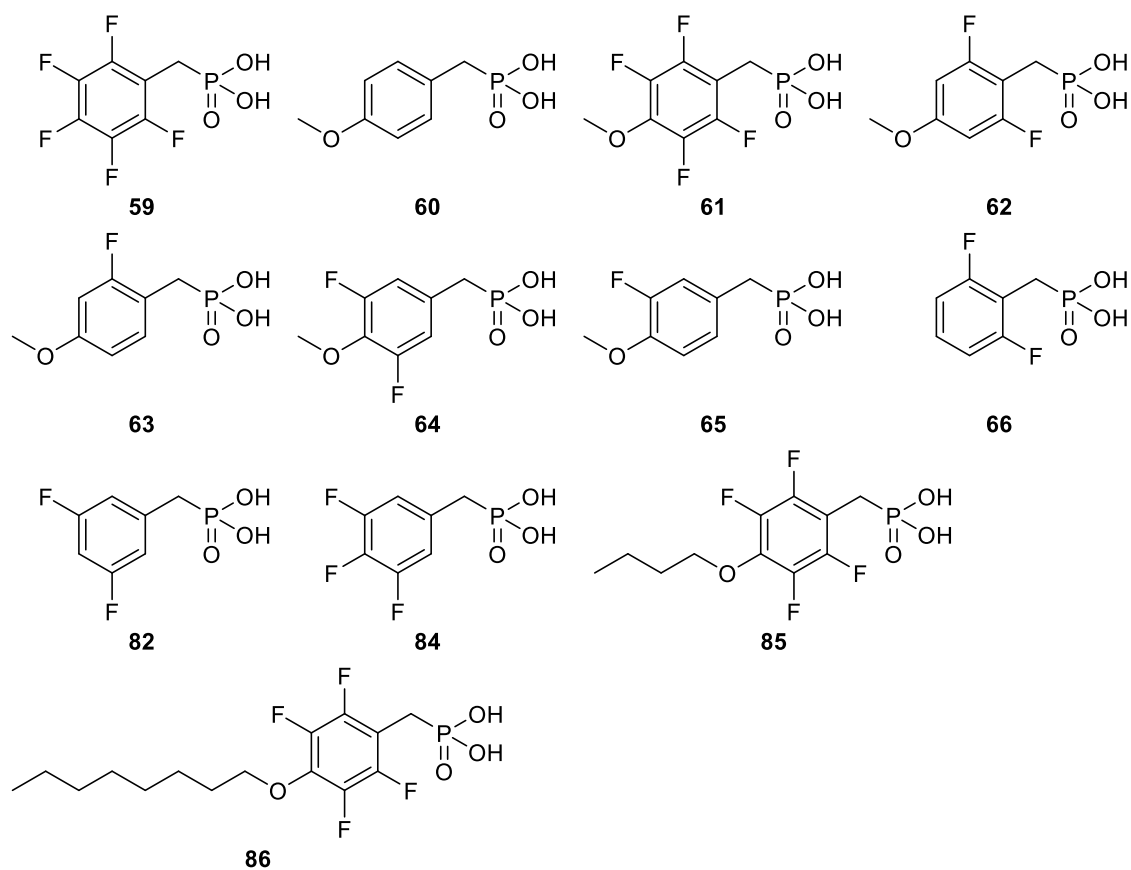


Figure 14. Series of benzylphosphonic acid derivatives successfully synthesised for work function studies.

3.6 References to Chapter 3

- (1) Williams, A.; Naylor, R. A.; Collyer, S. G. *J. Chem. Soc., Perkin Trans. 2* **1973**, 25–33.
- (2) Katritzky, A. R.; Pilarski, B.; Johnson, J. W. *Org. Prep. Proced. Int.* **1990**, 22, 209–213.
- (3) Rice, B. L.; Guo, C. Y.; Kirchmeier, R. L. *Inorg. Chem.* **1991**, 30, 4635–4638.
- (4) Kim, P.; Jones, S. C.; Hotchkiss, P. J.; Haddock, J. N.; Kippelen, B.; Marder, S. R.; Perry, J. W. *Adv. Mater.* **2007**, 19, 1001–1005.
- (5) Murphy, P. J. *Organophosphorus Reagents: A Practical Approach In Chemistry*; Oxford University Press, 2004.
- (6) Rabinowitz, R. *J. Org. Chem.* **1963**, 28, 2975–2978.
- (7) McKenna, C. E.; Higa, M. T.; Cheung, N. H.; McKenna, M.-C. *Tetrahedron Lett.* **1977**, 18, 155–158.
- (8) Strong, L.; Whitesides, G. M. *Langmuir* **1988**, 4, 546–558.
- (9) Boulas, C.; Davidovits, J.; Rondelez, F.; Vuillaume, D. *Phys. Rev. Lett.* **1996**, 76, 4797–4800.
- (10) Halik, M.; Klauk, H.; Zschieschang, U.; Schmid, G.; Dehm, C.; Schütz, M.; Maisch, S.; Effenberger, F.; Brunnbauer, M.; Stellacci, F. *Nature* **2004**, 431, 963–966.
- (11) Jaffe, H.; Freedman, L. D.; Doak, G. *J. Am. Chem. Soc.* **1953**, 75, 2209–2211.
- (12) Burdon, J.; Hollyhead, W.; Tatlow, J. *J. Chem. Soc.* **1965**, 5152–5156.

Chapter 4

Synthesis of Fluorinated Biaryl Benzylphosphonic Acids

4.1 Introduction

Chapter 3 described the syntheses of a range of fluorinated benzylphosphonic acids for SAM formation on AlO_x . Variations displayed amongst this series, including fluorination pattern and the inclusion of an alkoxy substituent on the aryl ring allowed for direct comparisons between molecular design and characteristics of the resultant SAMs (Chapter 5). This chapter is concerned with the design and synthesis of a series of analogous biaryl benzylphosphonic acids to provide further quantification of the effect that certain molecular features have upon SAM formation and properties (Chapter 5).

Although the additional phenyl ring is expected to have a minimal effect upon the resultant dipole of the molecule, the presence of a terminal non-fluorinated aryl ring may aid with π - π stacking interactions in future device fabrication. Aromatic terminal groups have already proven beneficial within thin film transistors incorporating SAMs of silanes on silicon¹, with the interaction between the SAM and pentacene providing a robust and well-defined interface which improves device performance.

4.2 Aims and Approach

The initial biphenyl benzylphosphonic acids targeted for SAM studies resemble the general donor-acceptor structure outlined within chapter 2, as well as complementing a number of the benzylphosphonic acids synthesised in chapter 3. [Figure 15]

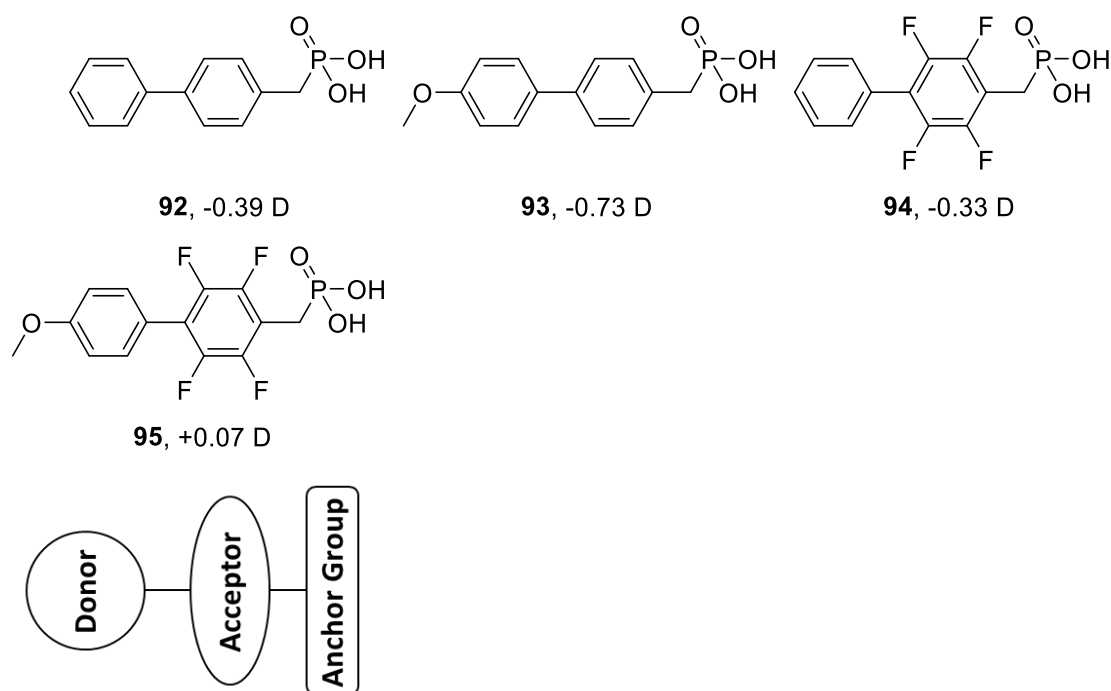
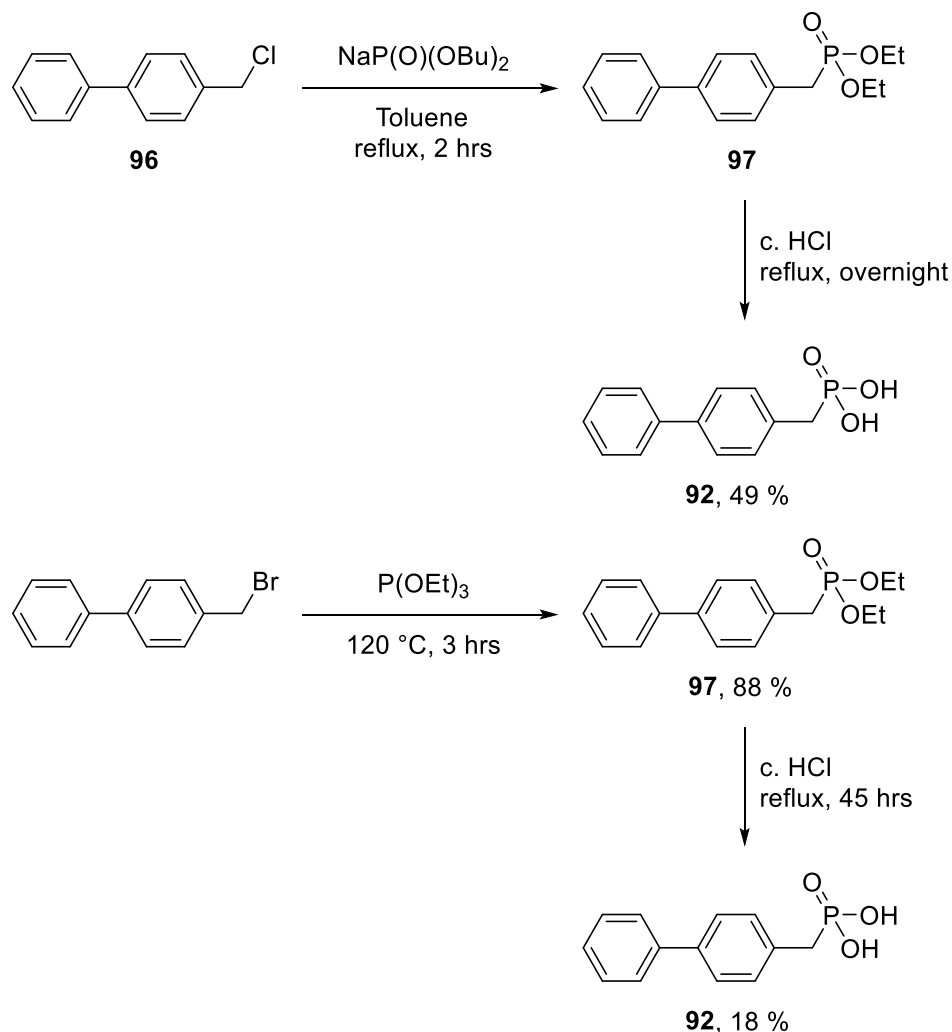


Figure 15. Targeted biphenyl benzylphosphonic acids and their calculated relative dipole moments.

The syntheses of non-fluorinated compounds **92** and **93** will provide control systems to assess the effect of fluorination within a resulting SAM as well as allowing a comparison for the incorporation of a methoxy substituent. Unlike structurally similar benzylphosphonic acids, the donor-acceptor functionality within compounds **92-95** will be provided by two separate ring moieties. Initially, only fluorinated compounds in which the fluorinated ring is directly attached to the benzyl linker, and contained no hydrogen substituents, were targeted (**94** and **95**). This will allow our initial investigations to concentrate on the properties of SAMs possessing the acceptor functionality in close proximity to the anchor group. Depending upon results gained from performance of these compounds in SAMs, further studies concerning systems with differing structural layouts, including systems with different functionalities is also possible.

Of the targeted biphenyl benzylphosphonic acids (Figure 15), the only literature syntheses reported are for the non-fluorinated phosphonic acid **92**. In 1945, Kosolapoff described the synthesis of **92** via the Michaelis-Becker reaction of *p*-chloromethylbiphenyl **96** and sodium dibutyl phosphite.² Hydrolysis of the resulting dibutyl phosphonate **97** with hydrochloric acid yielded **92** in an overall moderate yield.

More recently, the synthesis of **92** has been reported employing a Michaelis-Arbuzov reaction from the precursor benzyl bromide giving the diethyl phosphonate **97**.³ [Scheme 67]



Scheme 67. Syntheses of biphenyl-4-ylmethylphosphonic acid **92**.^{2,3}

No syntheses for the remaining targets **93-95** or their precursor phosphonates have been published so methodology, involving biphenyl formation and the introduction of a phosphonic acid moiety, will be developed.

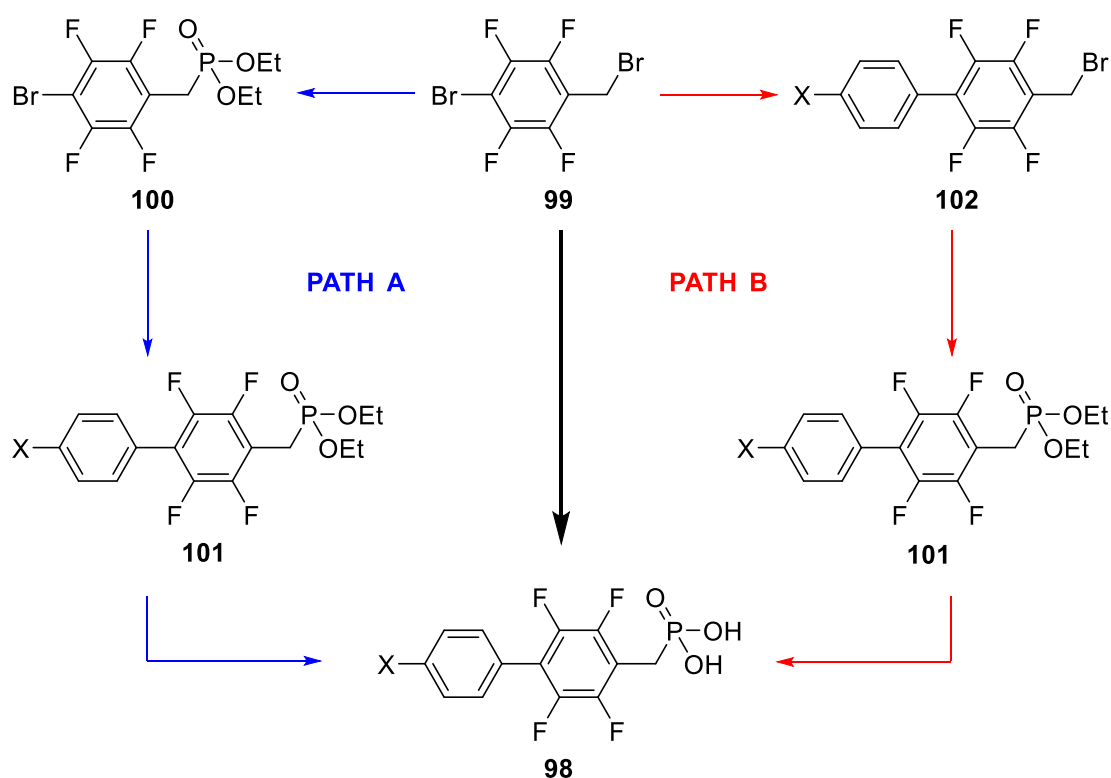
4.3 Synthetic Strategy

For non-fluorinated target **92**, the precursor benzyl bromide is available commercially and, consequently, synthesis of the acid would be undertaken using a Michaelis-

Arbuzov reaction of the bromide and subsequent hydrolysis, in an analogous reaction to the literature. [Scheme 67]

For the remaining non-fluorinated target **93**, a Suzuki-Miyaura cross-coupling reaction will be employed to synthesise the desired biphenyl scaffold. Subsequent bromination, phosphorylation and hydrolysis of this compound will be performed to yield the desired phosphonic acid.

To limit the number of synthetic steps incurred and to aid the potential production of a library of compounds from one common starting material, two potential synthetic pathways are proposed for the synthesis of substituted fluorobiphenyl benzylphosphonic acids **98** from 4-bromo-2,3,5,6-tetrafluorobenzyl bromide **99**. [Scheme 68]



Scheme 68. Proposed synthesis of fluorinated biphenyl benzylphosphonic acids.

The first synthetic route towards **98** may proceed via a Michaelis-Arbuzov reaction of benzyl bromide **99** to give phosphonate **100**. Coupling of phosphonate **100** with the appropriate sodium borate salt to produce biphenyl **101** may precede hydrolysis to the desired phosphonic acid **98**. [Scheme 68, Path A] Alternatively, initial cross-coupling of

benzyl bromide **99** to produce the biphenyl benzyl bromide **102** could be attempted, followed by phosphorylation and hydrolysis to the desired compounds **98**. [Scheme 68, Path B]

Developing a synthesis from the benzyl bromide **99**, will allow for the potential production of a series of phosphonic acids **98** in which substituent X may be varied during future investigations. The cross-coupling reactions to afford biphenyls **101** and **102** will be conducted in a manner similar to the reactions described in chapter 2 using pre-activated sodium borate salts.

4.4 Results and Discussion

4.4.1 DFT Calculations of Biphenyl Benzylphosphonic Acids

DFT calculations were used to predict the relative surface dipole moments of phosphonic acids **92-95** on an aluminium oxide surface and the calculated dipole moments are collated. [Figure 16] All calculations were performed by Dr. William Ford of the SONY Corporation using a previously discussed software package.

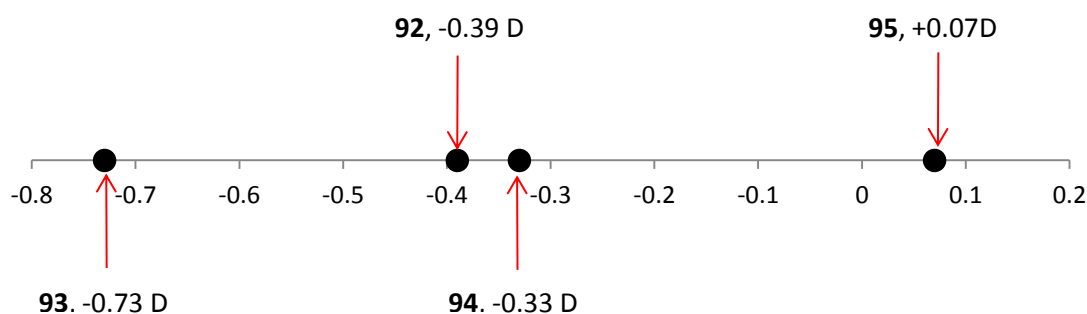


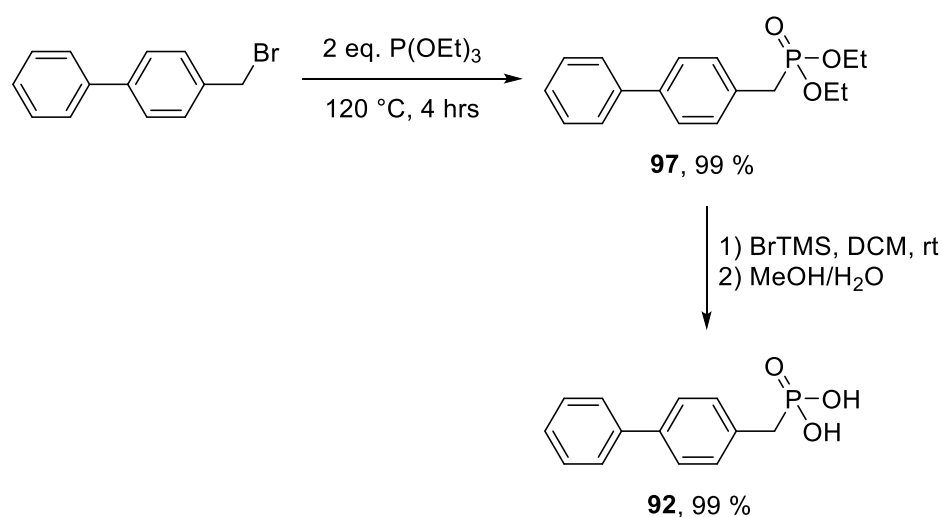
Figure 16. Relative surface dipole moments of biphenyl benzylphosphonic acids on a simulated AlO_x surface.

As is to be expected, phosphonic acid **95** displays the most positive dipole moment of the four target molecules (Figure 16). The presence of both an electron donating methoxy substituent and tetrafluorosubstituted aryl ring create a dipole with the positive 'end' directed away from the surface. Removal of the alkoxy functionality, to give target **94**, reduces the surface dipole, which further decreases with replacement of the fluorine substituents for hydrogen, as for **92**. As described for particular

benzylphosphonic acids in Chapter 3, a terminal methoxy group can also act as an acceptor within the structure due to the electronegativity of oxygen atom. This trend is observed for target **93**, for which there are no electron withdrawing fluorine substituents, creating a more negative dipole pointing away from the surface.

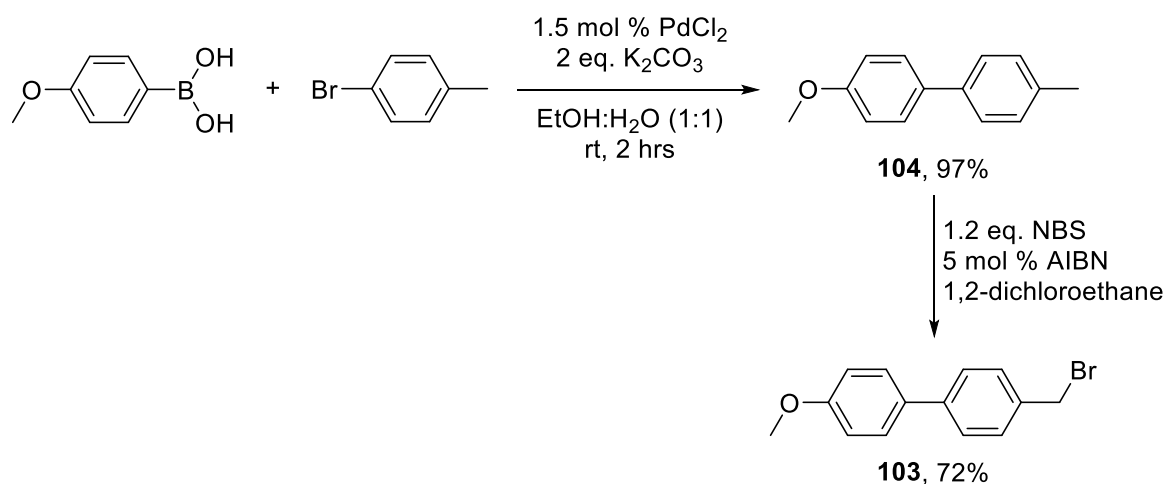
4.4.2 Synthesis of Non-Fluorinated Biphenyl Benzylphosphonic Acids

Biphenyl-4-ylmethylphosphonic acid **92** was synthesised from the precursor benzyl bromide, following a modified literature procedure.³ [Scheme 69] Both the diethyl phosphonate **97** and phosphonic acid **92** were obtained in excellent yield.



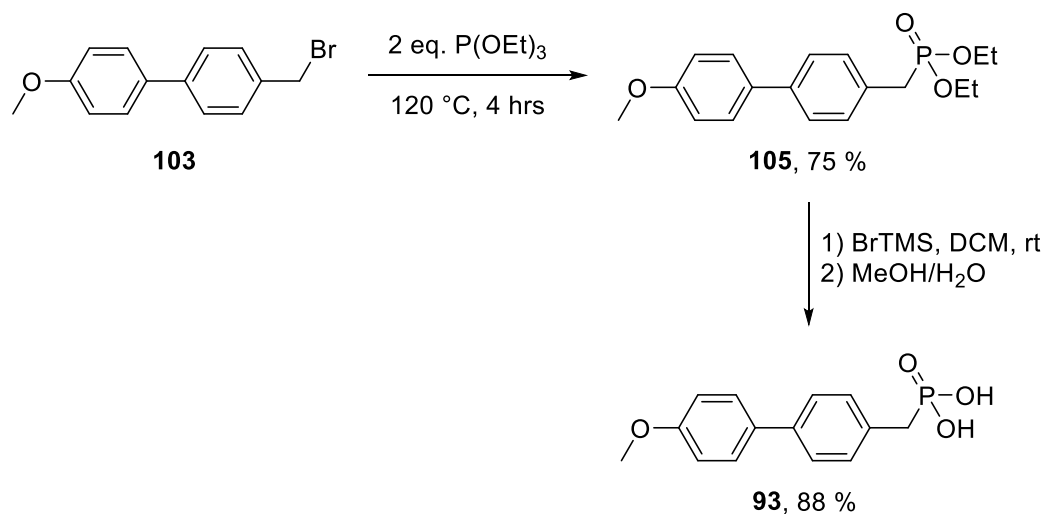
Scheme 69. Synthesis of biphenyl-4-ylmethylphosphonic acid **92**.

Benzyl bromide **103** is required for the synthesis of methoxy-substituted phosphonic acid **93** and was synthesised via a modified literature⁴ Suzuki-Miyaura reaction, and free radical bromination of the resultant biphenyl **104**. [Scheme 70]



Scheme 70. Synthesis of benzyl bromide **103**.

Synthesis of **93** was completed following reaction of the bromide **103** with triethyl phosphite and hydrolysis to the desired compound by analogous processes to the synthesis of **92**. [Scheme 71]



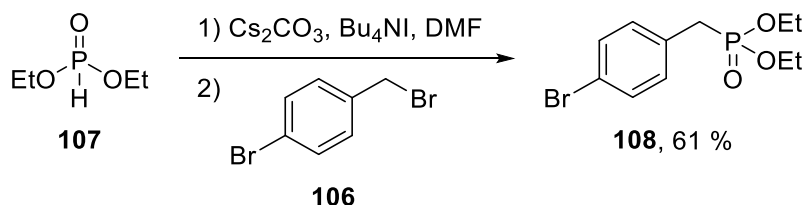
Scheme 71. Synthesis of phosphonic acid **93** from the benzyl bromide **103**.

4.4.3 Synthesis of Fluorinated Biphenyl Benzylphosphonic Acids

4.4.3.1 Reactions of 4-Bromobenzyl Bromide

To confirm proof-of-principle and validate the suggested syntheses outlined in scheme 68, all initial test reactions were conducted with 4-bromobenzylbromide **106** due to the

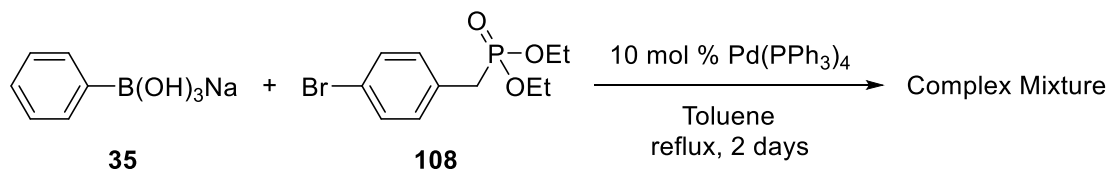
commercial availability of this reagent. Phosphonylation of **106** was attempted via a literature⁵ Michaelis-Becker reaction to assess and compare reaction conditions and yields to the Michaelis-Arbuzov processes we conducted previously (Chapter 3). [Scheme 72]



Scheme 72. Synthesis of diethyl 4-bromobenzylphosphonate **108**.

Although the synthesis of phosphonate **108** under these conditions was a success, and the reagents employed allowed the reaction to be conducted at room temperature, the overall reaction time was far longer than the corresponding Michaelis-Arbuzov processes, a more time consuming work-up and purification procedure was required, and isolation of the desired product occurred in a comparatively lower yield. Use of diethyl phosphite **107** also necessitates the use of various additional chemical reagents that are redundant under standard Michaelis-Arbuzov conditions. For these reasons, the Michaelis-Arbuzov reaction was employed as the method of choice for future syntheses of benzyl phosphonates.

The cross-coupling reaction, between phosphonate **108** and sodium trihydroxy(phenyl)borate **35** was then attempted. [Scheme 73]



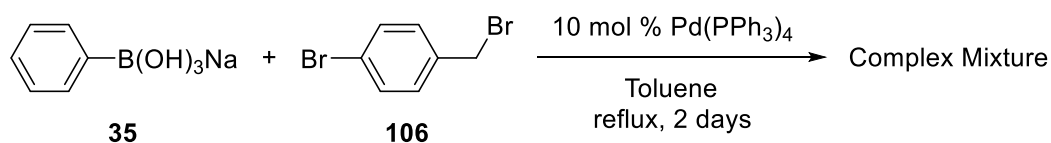
Scheme 73. Attempted Suzuki-Miyaura cross-coupling reaction of benzyl phosphonate **108**.

Analysis of the crude reaction solution by GC-MS showed the presence of the desired product **97** ($m/z = 306$) and the starting phosphonate **108** ($m/z = 304$) along with a number of other substances including biphenyl, from the homo-coupling of the borate

salt, and triphenylphosphine and triphenylphosphine oxide, from catalyst degradation. The presence of the product phosphonate **97** was further confirmed by comparison of GC-MS and ^{31}P NMR spectroscopy data obtained during the total synthesis of biphenylmethylphosphonic acid **92** described previously. A number of attempts to purify the crude product were undertaken but separation of the desired phosphonate **97** from the reaction mixture could not be achieved by either column chromatography or recrystallisation.

Following the failure to isolate phosphonate **97** via the cross-coupling reaction of a benzyl phosphonate and sodium borate species, attention was focused on the alternative, reverse reaction pathway proposed. [Scheme 68, Path B] It was hoped that conducting the cross-coupling reaction in the absence of a phosphonate moiety would aid the reaction purification procedure.

Reaction between 4-bromobenzylbromide **106** and sodium trihydroxy(phenyl)borate **35** was attempted (Scheme 74) and after two days of heating at reflux, a dark brown solution was obtained along with formation of a tarry substance coating the reaction vessel. Analysis of the crude reaction solution by ^1H NMR spectroscopy and GC-MS revealed the presence of a large number of side-products and, although evidence for the formation of the desired biphenyl **109** was observed by GC-MS analysis ($m/z = 246$), the relevant CH_2 peak in the ^1H NMR spectrum did not compare with literature data.⁶ After a number of purification procedures no product could be isolated, with mixtures of products obtained after all attempts.

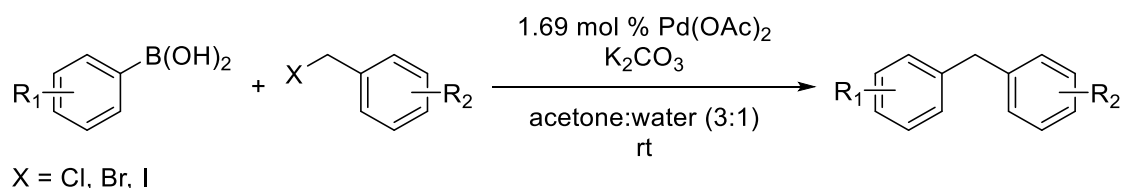


Scheme 74. Attempted Suzuki-Miyaura cross-coupling reaction of benzyl bromide **106**.

The observation of an appropriate mass peak, displaying a bromine isotope splitting pattern, within the GC-MS spectrum along with the lack of expected methylene peak within the ^1H NMR spectrum indicates that the reaction may occur at the benzylic bromine, thereby forming a structural isomer of the desired product. This claim is

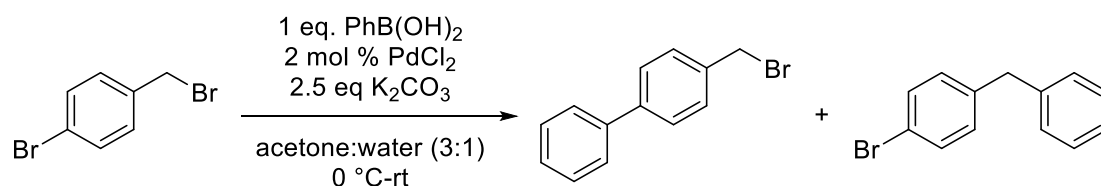
supported by the observation of a peak at 3.97 ppm, representative of the methylene bridged bromobiphenyl⁷, along with the appropriate peaks in the aromatic region of the ¹H NMR spectrum.

Indeed, palladium catalysed cross-coupling reactions of benzylic halides with aryl boronic acids have been reported.⁶ [Scheme 75]



Scheme 75. Palladium catalysed synthesis of diarylmethane derivatives.⁶

The authors claimed that, under the reaction conditions proposed, the use of 4-bromobenzyl bromide **106** exclusively yields the product from reaction at the aromatic bromide. It was postulated that if this procedure can provide an efficient method for the synthesis of biphenyl benzyl bromides then it could be adapted for fluorinated reagents. However, when the reaction was repeated it was found that the product was obtained as an impure mixture of isomers, which could not be separated by column chromatography. [Scheme 76]

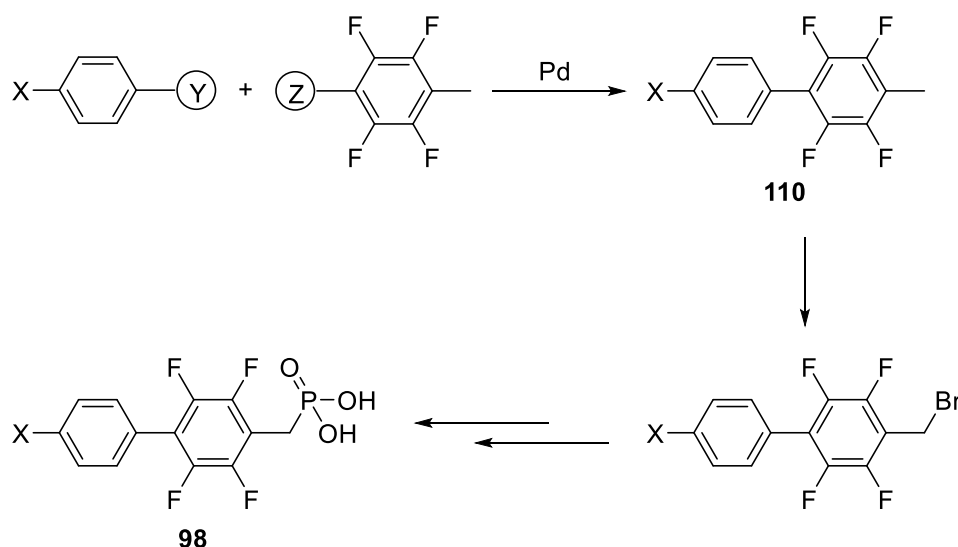


Scheme 76. Reaction between 4-bromobenzyl bromide and phenylboronic acid.

Due to problems regarding reactivity and purification encountered during these cross-coupling reactions, attempts to incorporate either a benzyl bromide or phosphonate moiety within a Suzuki-Miyaura cross-coupling reaction were abandoned.

4.4.3.2 C–H Bond Activation Reactions

Following the difficulties experienced with both synthetic routes originally proposed for the synthesis of biphenyl benzylphosphonic acids (Scheme 68), a new pathway was devised for the synthesis of fluorinated phosphonic acids **98**. [Scheme 77] Initial cross-coupling reactions will be conducted to produce biphenyl methyl derivatives **110**, which will then be converted to phosphonic acids **98** following previously described procedures. Although this route requires an additional synthetic step compared to our alternative suggested pathways, the lack of additional functional groups within the cross-coupling step will potentially overcome problems experienced previously.

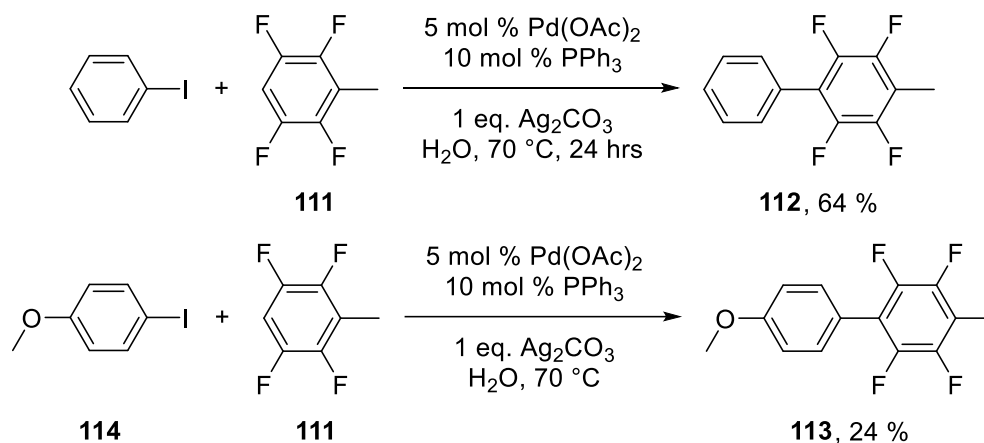


Scheme 77. Alternative, proposed synthesis of fluorinated biphenyl benzylphosphonic acids.

For the initial synthesis of biphenyls **110** we decided not to use sodium borate salts and highly fluorinated aryl halides in cross-coupling reactions due to problems encountered with the general reactivity of these systems, and additional purification difficulties. Due to the electron deficient nature of highly fluorinated aromatic compounds, we envisaged that C–H bond activation chemistry would be more appropriate for the synthesis of biphenyls **108** ahead of more traditional Suzuki-Miyaura cross-coupling reactions.

A recently published literature paper presented a procedure for the arylation of polyfluoroarenes in excellent yields via a C–H bond activation pathway.⁸ Reactions of

2,3,5,6-tetrafluorotoluene **111** were conducted yielding biphenyls **112** and **113** in good yield, following the literature procedure. [Scheme 78] The use of water as a reaction solvent and the low cost PPh₃ ligand make this synthetic route towards highly fluorinated biphenyls particularly attractive.



Scheme 78. Synthesis of biphenyls **112** and **113** by C–H bond activation reactions.

For both reactions, analysis of the crude reaction mixture was only achievable following filtration and extraction of the reaction solution due to the presence of a large amount of a black tarry substance. It should be noted that all reactions of this nature reported in the literature were conducted on a 0.9 mmol scale, significantly lower than 9 mmol scale conducted for these reactions, with no reports of difficulty during purification.

For biphenyl **112** a significant quantity of unreacted iodobenzene remained after the 24 hour reaction period time and proved difficult to separate completely from the product biphenyl. This observed lack of reactivity explains the lower than expected yield achieved.

Fluorinated biphenyl **113** was obtained in a far lower yield than the 78 % reported by Zhang *et al.* however several, unreported, side reactions were observed when we repeated the procedure. The initial attempted synthesis of **113** was conducted with 1.5 equivalents of the fluorinated starting material **111**, with a thick, dark green residue obtained after 24 hours. Purification by recrystallisation yielded a white powder, consisting of a number of separate products. GC-MS analysis identified these compounds as 4-iodoanisole **114** ($m/z = 235$), the desired biphenyl **113** ($m/z = 271$), and

4,4'-dimethoxybiphenyl ($m/z = 215$), the product of homo-coupling of the aryl iodide, as well as triphenylphosphine oxide ($m/z = 279$). The three methoxylated compounds were further identified by three separate methyl shifts within the ^1H NMR spectrum at 3.78, 3.86 and 3.84 ppm, respectively. Further purification of this mixture enabled the separation of triphenylphosphine oxide and 4,4'-dimethoxybiphenyl, however the product biphenyl **113** and aryl iodide **114** remained inseparable.

The reaction was repeated with an increased excess of the starting fluoroarene **111** in an attempt to achieve greater conversions of iodide to product. Again, large amounts of the starting iodo compound remained along with the desired biphenyl, and product arising from homocoupling of the 4-iodoanisole. The homocoupling product was separated by column chromatography, and the resultant reaction mixture combined with the impure product from the previous reaction, before re-reacting with 2,3,5,6-tetrafluorotoluene **111**. As observed with previous reactions, after 24 hours, a thick dark substance coated the reaction vessel with a dark solid obtained after work-up. GC-MS analysis of the crude reaction product showed the desired product constituted 82 % of the compounds present along with the side-products observed previously and 2,3,5,6-tetrafluoro-4-methylbiphenyl **112**. [Figure 17] It is possible that the formation of **112** occurs via an exchange reaction with triphenylphosphine in an intermediate palladium complex.

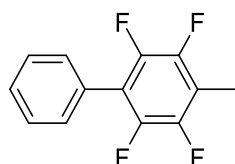


Figure 17. 2,3,5,6-Tetrafluoro-4-methylbiphenyl, **112**.

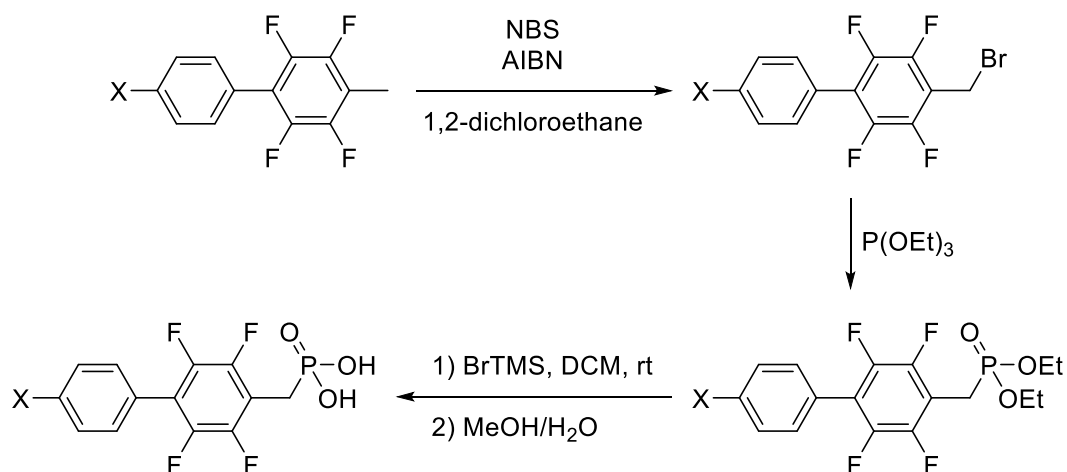
After several purification procedures, the desired biphenyl **113** was obtained in an overall 24 % yield. Although low, the isolated yield is representative of the difficulties faced during the synthesis of **113**, with low reactivity of 4-iodoanisole observed throughout and subsequent separation proving challenging, along with the formation of a number of side-products.

Similar low reactivities of aryl iodides have been observed during catalytic intermolecular direct arylation reactions reported by Fagnou.⁹ Under conditions

optimised for aryl bromides the related iodides displayed extremely poor reactivities within these transformations with conversions of no greater than 64 % achieved. Low reactivities of these reactions was attributed to catalyst poisoning by iodide ions which could be suppressed through the addition of a silver salt. However, it is possible that the low conversions of aryl iodides observed within C–H bond activation reactions reported within this chapter are due in part to similar issues occurring due to the increased scale of the reactions being conducted.

Following the successful syntheses of fluorinated biphenyl methyls **112** and **113**, the related phosphonic acids **94** and **95** were obtained following successive free radical bromination, phosphonylation, and hydrolysis reactions, following synthetic procedures described previously (Chapter 3), in moderate to excellent yields. [Table 9]

Table 9. Synthesis of fluorinated biphenyl benzylphosphonic acids from the precursor biphenyl methyl compounds.



X	Benzyl Bromide, (Yield / %)	Phosphonate, (Yield / %)	Phosphonic Acid, (Yield / %)
H	115 , (72)	116 , (92)	94 , (71)
OMe	117 , (94 ^a)	118 , (85)	95 , (56)

^a77 % purity as determined by GC-MS

¹H NMR spectroscopy provides a useful tool for monitoring reaction progress for the total syntheses of phosphonic acids **94** and **95**. The continually changing chemical environment of the methylene linker provides a useful reference point, as shown by the ¹H NMR spectra of the key intermediates in the synthesis of **94**. [Figure 18] Free radical

bromination of biphenyl **112** to benzyl bromide **115** is accompanied by the disappearance of the methyl peak at 2.3 ppm and the appearance of the methylene peak at 4.6 ppm, with the deshielding effect of the bromine increasing the chemical shift. The subsequent Michaelis-Arbuzov reaction for the synthesis of phosphonate **116** is accompanied by the observance of the relevant peaks due to the ethyl chains of the phosphonate ester, as well as a doublet at 3.3 ppm. This doublet displays a splitting of 21.5 Hz, indicative of a $^2J_{\text{HP}}$ coupling. Hydrolysis of phosphonate **116** to phosphonic acid **94** occurs with the disappearance of the ester ethyl peaks, whilst maintaining the doublet due to the methylene linker.

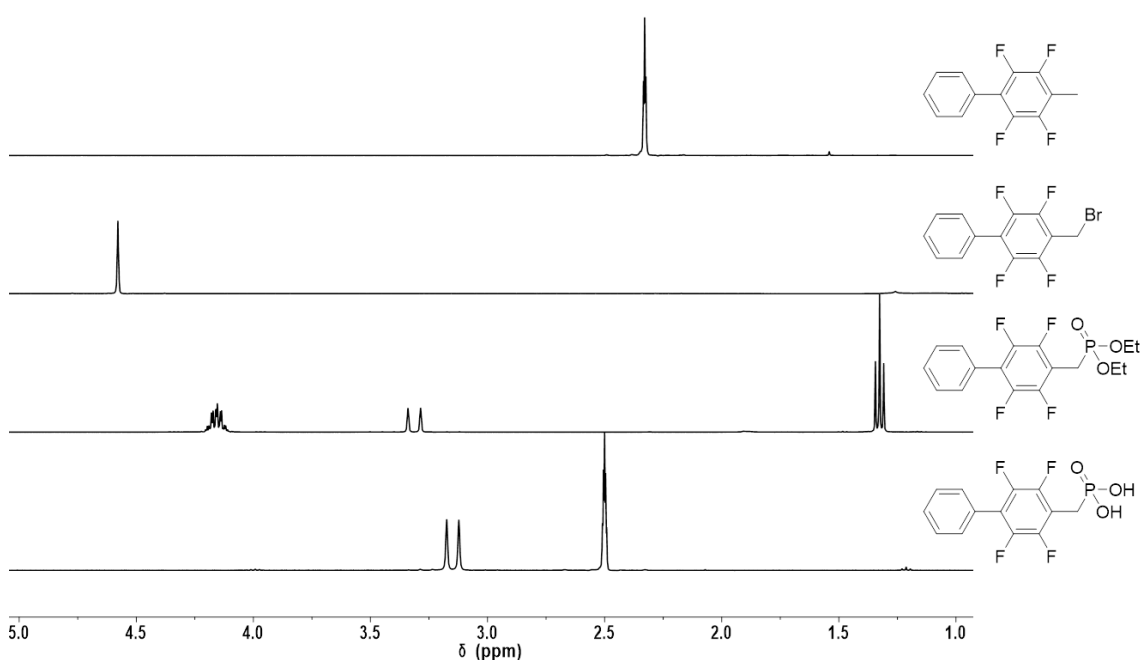


Figure 18. Comparison of the high field region of the ^1H NMR spectra for the key compounds in the total synthesis of phosphonic acid **94**.

In the case of biphenyl **113** a large excess of NBS was required for the synthesis of benzyl bromide **117**, and the reaction was allowed to run for 4 days until only trace amounts of the starting biphenyl could be observed by ^{19}F NMR spectroscopy. Unlike for previous brominations, no dibromination product was observed. Although difficulties arose regarding separation of **117** from the starting biphenyl and other side-products, these impurities were removed during later stage purifications. Similarly, for benzyl bromide **115** no dibromination was observed during the reaction but separation

of benzyl bromide **115** from biphenyl **112** proved more facile than for the similar methoxylated compound.

4.4.3.3 Synthesis of Alternative Fluorinated Benzylphosphonic Acids

Having synthesised fluorinated biphenyl benzylphosphonic acids **94** and **95** following a four-step reaction procedure, two structurally similar phosphonic acids **119** and **120** were identified as interesting candidates for SAM studies by the SONY Corporation.

[Figure 19]

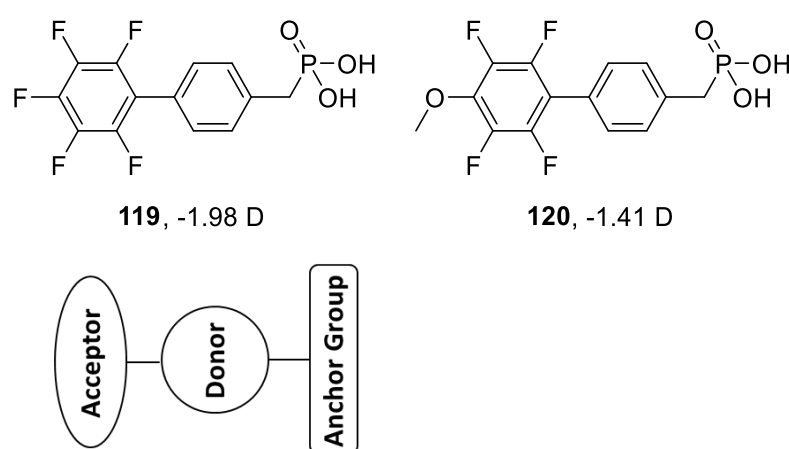


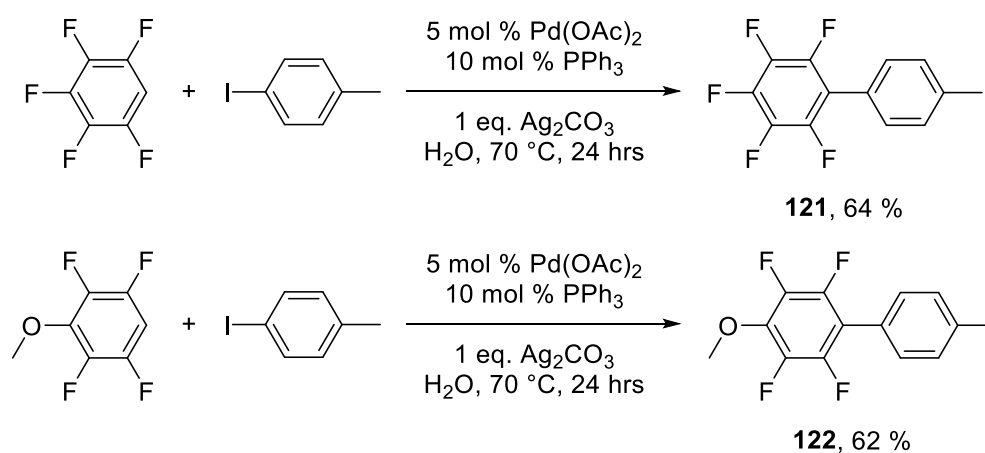
Figure 19. New fluorinated biphenyl benzylphosphonic acid targets and related dipole moments.

By displaying a ‘reverse’ fluorination pattern to the phosphonic acids described previously, the relative surface dipole moment calculated for phosphonic acids **119** and **120** are more negative. The presence of a terminal acceptor functionality creates a negative dipole pointing away from the surface for both **119** and **120**, with the more negative dipole calculated for phosphonic acid **119** due to the *para* fluorine substituent.

As well as affecting the net dipole moment of a SAM of these compounds, the inclusion of a highly fluorinated aryl terminal group has the potential to further enhance stacking interactions with many commonly employed aromatic organic layers within a device. Efficient stacking of such compounds may lead to increased π - π interactions, and consequently can improve the charge transport abilities between these layers.¹⁰

It is widely acknowledged that strong interactions exist between perfluoro- and hydroaromatics due to attractions between the electron-poor and electron-rich aromatic structures. The first example of this nature was reported almost 65 years ago with the observation of a crystalline white solid upon mixing benzene and hexafluorobenzene.¹¹ Individually, each compound possesses a melting point of lower than 6 °C and, when solidified, stacks in an edge-to-face fashion. However, upon mixing a solid with a melting point of 23.7 °C instantaneously forms which stacks in a face-to-face formation. This interaction has been attributed to the individual quadrupole moments of the two compounds, allowing the formation of benzene:hexafluorobenzene stacked columns, with neighbouring stacks exhibiting weak F...H-C interactions. These latter attractions further enhance the stability of such mixtures and although they behave in a manner similar to hydrogen bonds they are, in fact, much lower in energy.^{10,12} Interactions between perfluoroarenes and their hydrocarbon counterparts have an important effect upon the organisation of such compounds, with well controlled nano-structures obtained in the solid state. For these reasons, polyfluorinated and hydrocarbon aromatic compounds, in particular polyfluorinated biaryls, find multiple applications in electronic devices.¹³

As with the previous fluorinated biphenyl targets, no literature syntheses exist for phosphonic acids **119** and **120**. Consequently, in a similar manner to that described previously, biphenyl methyl compounds **121** and **122** were synthesised via a C-H bond activation reaction of a highly fluorinated benzene derivative. [Scheme 79]



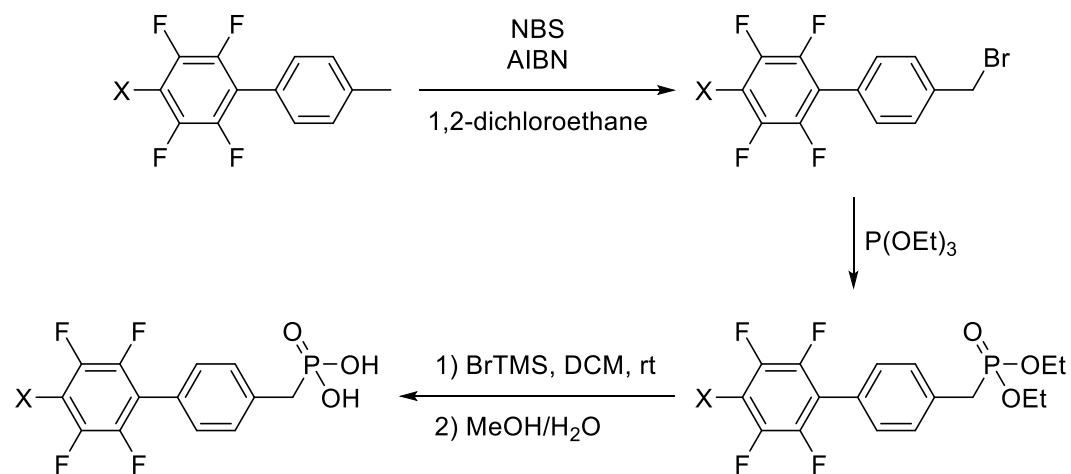
Scheme 79. Synthesis of biphenyls **121** and **122** by C-H bond activation reactions.

For the synthesis of methoxy substituted biphenyl **122**, analysis of the reaction solution by GC-MS indicated the presence of 4-iodotoluene and homo-coupled 4,4'-dimethylbiphenyl along with desired **122**, which was purified by column chromatography.

For polyfluorinated biphenyl **121**, the amount of pentafluorobenzene was increased to 4 equivalents in an attempt to drive the reaction to completion. Although fewer side products were observed within the reaction mixture, and only trace amounts of 4-iodotoluene were observable during analysis, the isolated yield of **121** remained similar to those obtained for similar compounds.

The synthesis of phosphonic acids **119** and **120** were completed following the standard bromination and phosphonylation procedure employed for previous biphenyl benzylphosphonic acids. [Table 10]

Table 10. Synthesis of alternative fluorinated biphenyl benzylphosphonic acids from the precursor biphenyl methyl compounds.



X	Benzyl Bromide, (Yield / %)	Phosphonate, (Yield / %)	Phosphonic Acid, (Yield / %)
F	123 , (88 ^a)	124 , (89)	116 , (77)
OMe	125 , (81 ^b)	126 , (97)	117 , (56)

^a86 % purity as determined by ¹⁹F NMR spectroscopy

^b78 % purity as determined by ¹⁹F NMR spectroscopy

In a similar manner as for phosphonic acids **93** and **94**, reaction progress of targets **119** and **120** could be followed by ^1H NMR spectroscopy. [Figure 20]

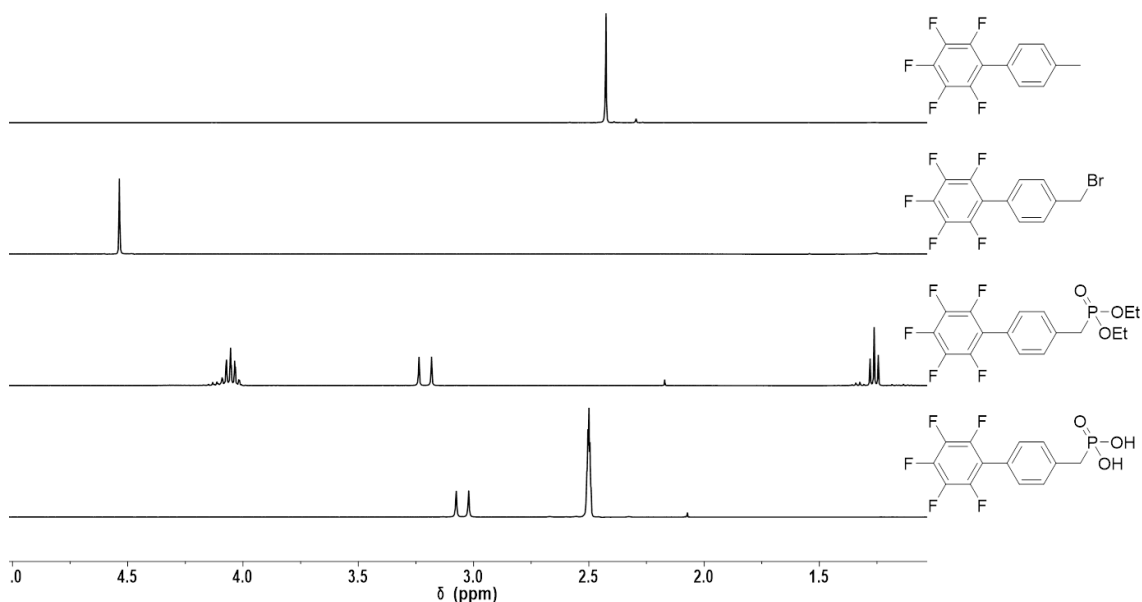


Figure 20. Comparison of the high field region of the ^1H NMR spectra for the key compounds in the total synthesis of phosphonic acid **119**.

Purification of benzyl bromides **123** and **125** from the di-brominated side-products by column-chromatography proved problematic, however any residual dibrominated species were removed during purification of the diethyl phosphonates **124** and **126**. The remaining reactions for the synthesis of **119** and **120** proceeded smoothly.

4.4.4 Incorporation of a Carboxylic Acid Anchor Group

Experimental results have proven that the inclusion of a methylene linker when comparing aryl- and benzylphosphonic acid SAMs appears to have very little effect upon the resultant properties of the SAM and the metal surface.¹⁴ Although true for monophenyl phosphonic acids, it is unclear whether these results hold true for the related biphenyl benzyl systems.

Having previously experienced difficulties regarding the direct attachment of a phosphonic acid moiety to a fluorinated aryl ring, synthesis of the related carboxylic acid **127** was pursued. [Figure 21] Although replacement of a phosphonic acid anchor

group for a carboxylic acid will have implications on certain properties of a SAM, the synthesis of **127** may allow for initial comparisons to be drawn.

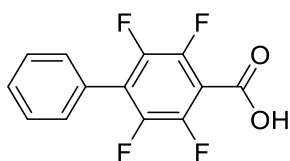
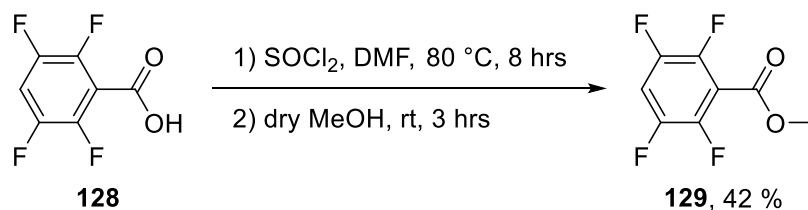


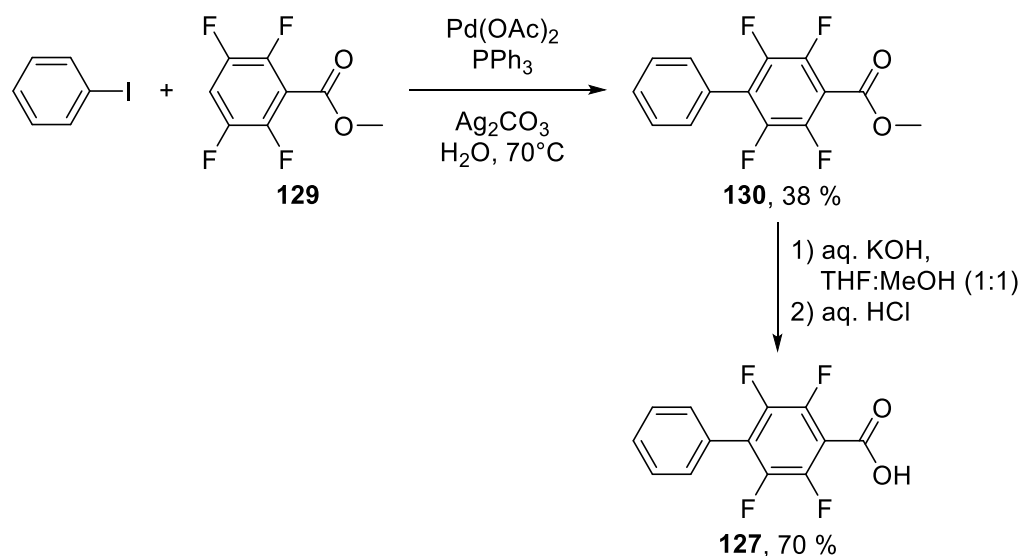
Figure 21. 2,3,5,6-Tetrafluorobiphenyl-4-carboxylic acid, **127**.

Unlike the related phosphonic acids, the commercial availability of 2,3,5,6-tetrafluorobenzoic acid and the compatibility of the methyl ester analogue in C–H bond activation reactions, negates the pre-synthesis of a non-carboxylated biphenyl core. For use in C–H bond activation reaction, methyl 2,3,5,6-tetrafluorobenzoate **129** was synthesised through protection of the partially fluorinated benzoic acid **128**. [Scheme 80]



Scheme 80. Synthesis of methyl tetrafluorobenzoate **129**.

Following the protocol outlined for biphenyl methyl derivatives, the synthesis of carboxylic acid **127** was completed via a C–H bond activation reaction with iodobenzene. [Scheme 81]



Scheme 81. Synthesis of biphenylcarboxylic acid **127** from the precursor benzoate **129**.

Unlike similar reactions of fluoroarenes, large amounts of the fluorobenzoate **129** remained in the reaction mixture and could not be separated from the intermediate biphenyl **130**. However, reaction with additional iodobenzene, and multiple tedious purification steps, allowed for the isolation of pure **130**. Conversion of **130** back to the free acid gave **127** in good yield.

The synthesis of **127** allows for direct comparison with the related phosphonic acid **94**. These studies may provide an insight into the effect of an additional methylene unit within a biphenyl SAM upon, amongst others, resultant surface energy and tilt angle of a SAM as well as work function of the metal substrate.

4.4.5 Synthesis of Alternative Biaryl Phosphonic Acids

Numerous fluorinated benzylphosphonic acid derivatives described within this thesis were initially designed to possess large net-dipole moments due to the inclusion of highly electronegative fluorine substituents. Another way to significantly alter the observed dipole moment is through modification of the structural nature of the core spacer groups.

The inclusion of a piperazine ring was highlighted by computational techniques as an extremely desirable feature within a biaryl SAM by the SONY Corporation, for specific

properties in device applications. To begin studies with compounds of this type, three aminomethylphosphonic acids **131-133** were proposed for synthesis. [Figure 22] Compounds possessing this particular structural design are of particular interest due to the associated dipole moments being as large, or larger, than the analogous phenyl compounds. To aid with quantitative comparisons, corresponding biphenyl benzylphosphonic acids **134-136** were also targeted.

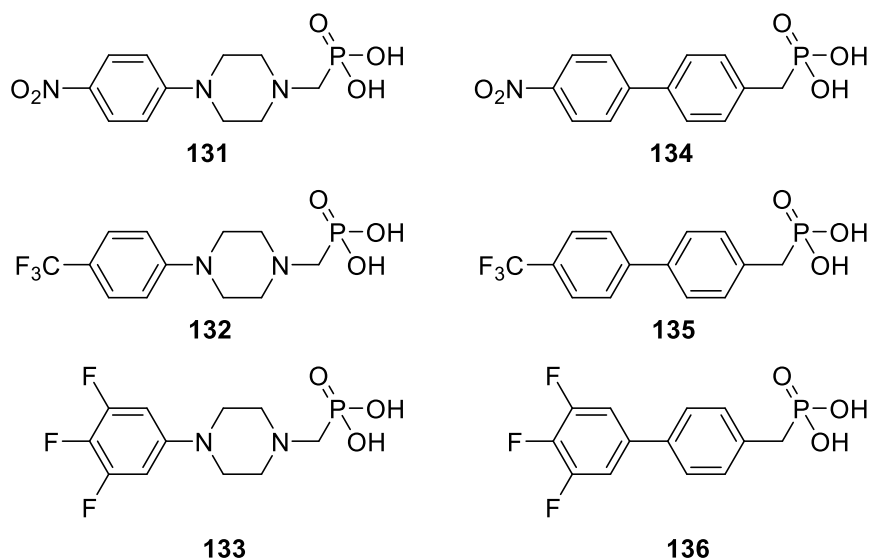
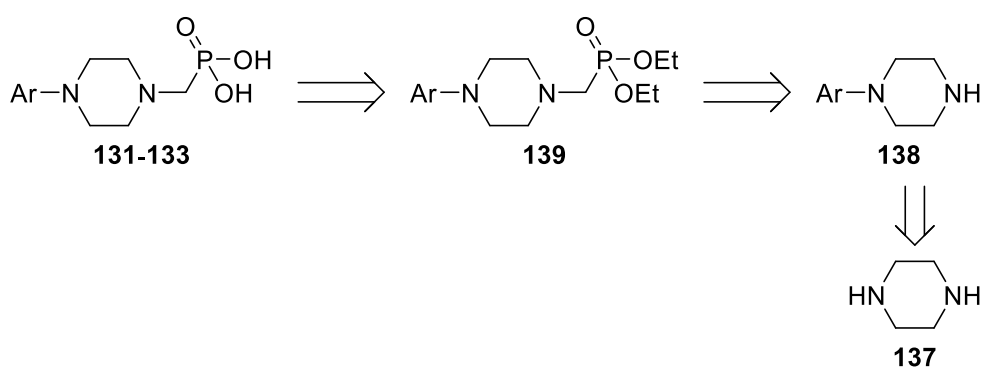


Figure 22. Targeted aminomethylphosphonic acids and analogous phenyl derivatives.

4.4.5.1 Synthesis of Aminomethylphosphonic Acids

A retrosynthetic analysis for phosphonic acids **131-133** from piperazine **137** was proposed. [Scheme 82]

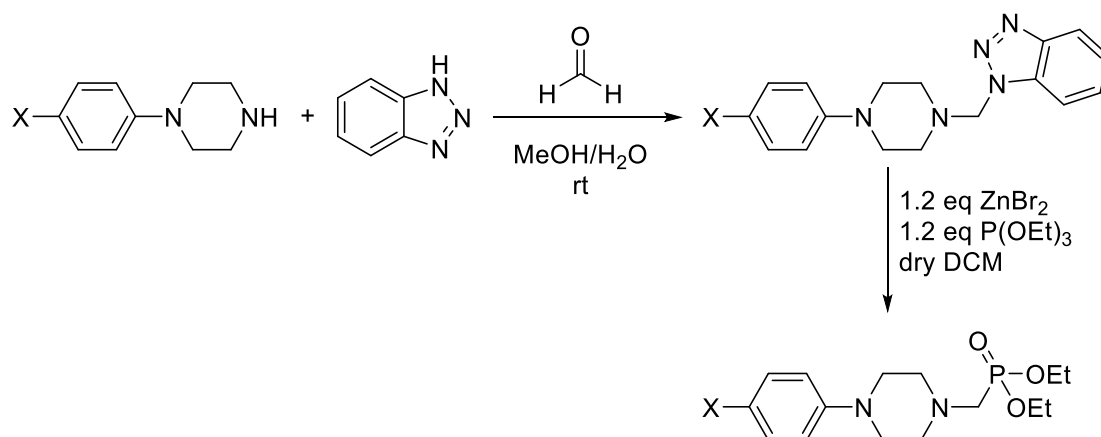


Scheme 82. Retrosynthetic analysis of aminomethylphosphonic acids **131-133**.

A Buchwald-Hartwig amination of **137** will provide a potential synthetic pathway to biaryls **138**, with phosphonates **139** obtained following a known, two-step procedure.¹⁵ Hydrolysis of **139** will yield the desired phosphonic acids **131-133**. For phosphonic acids **131** and **132** the precursor biaryls **138** are commercially available and therefore syntheses began from these reagents.

A literature synthesis presented an efficient method for the conversion of *N*-aryl substituted piperazines to aminomethyl phosphonates via benzotriazolyl derivatives¹⁵. Phosphonates **141** and **143** were synthesised in this manner in good to excellent yields. [Table 11]

Table 11. Synthesis of aminomethylphosphonate derivatives **141** and **143**.



X	Benzotriazolyl, (Yield / %)	Phosphonate, (Yield / %)
NO ₂	140 , (95)	141 , (98)
CF ₃	142 , (82)	143 , (91)

2-Substituted benzotriazolyl intermediates omitted for clarity.

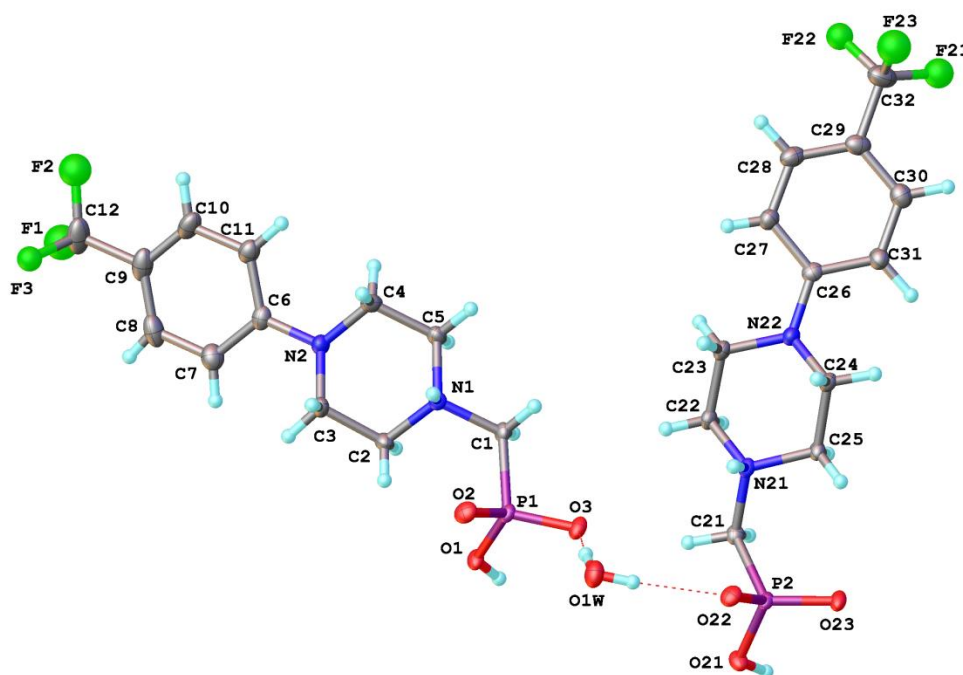
It was found that for benzotriazolyl intermediates **140** and **142** products were obtained as a mixture of the 1- and 2-substituted isomers in a ratio of 4:1 respectively, a common feature of (aminomethyl)benzotriazoles.¹⁶

Following the synthesis of phosphonates **141** and **143**, both compounds were hydrolysed to their respective phosphonic acids. [Table 12]

Table 12. Hydrolysis of aminomethylphosphonate derivatives to phosphonic acids.

X	Phosphonic Acid, (Yield / %)
NO ₂	131 , (58)
CF ₃	132 , (53)

Purification by recrystallization proved challenging for phosphonic acids **131** and **132** due to the high insolubility of these compounds in a number of solvents. Vigorous heating in a large quantity of solvent was required to solubilise both **131** and **132**, and for phosphonic acid **132** ¹³C NMR data was unattainable due to the low sample concentration obtained producing extremely weak signals. The structure of **132** was confirmed by X-ray crystallography, showing it to exist as a semi-hydrate containing two independent molecules with different conformations. [Figure 23]

**Figure 23.** X-ray structure of **132**.

Both independent molecules present in **132** exist in their zwitter-ionic form and are further connected by a series of hydrogen bonds within the crystal lattice. The intermolecular interactions shown may account for the poor solubility observed for **132**.

Similarly, phosphonic acid **131** exists as a zwitterion with the structure also confirmed by X-ray crystallography. [Figure 24]

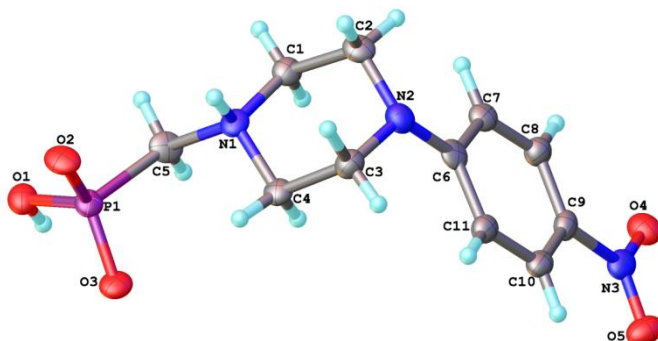


Figure 24. X-ray structure of **131**.

Pairs of hydrogen bonds existing between the zwitterions of **131** were also shown to intermolecularly link **131** into chains. [Figure 25]

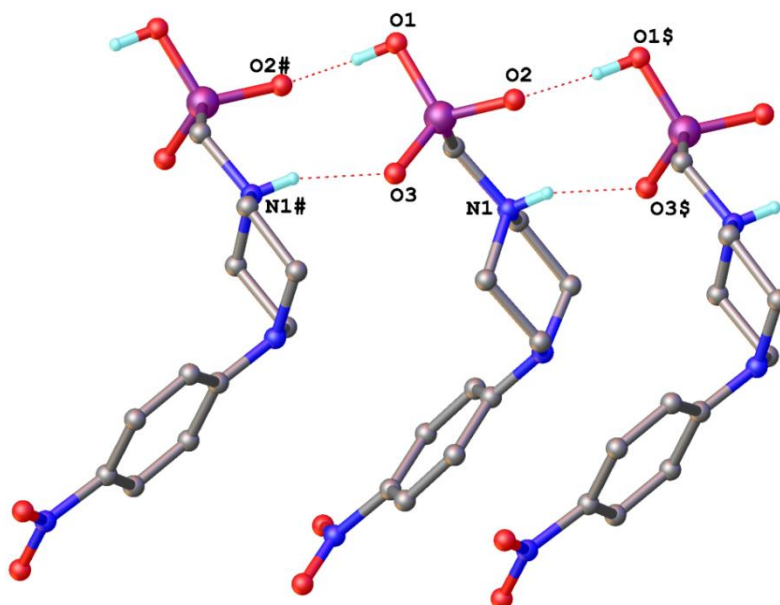
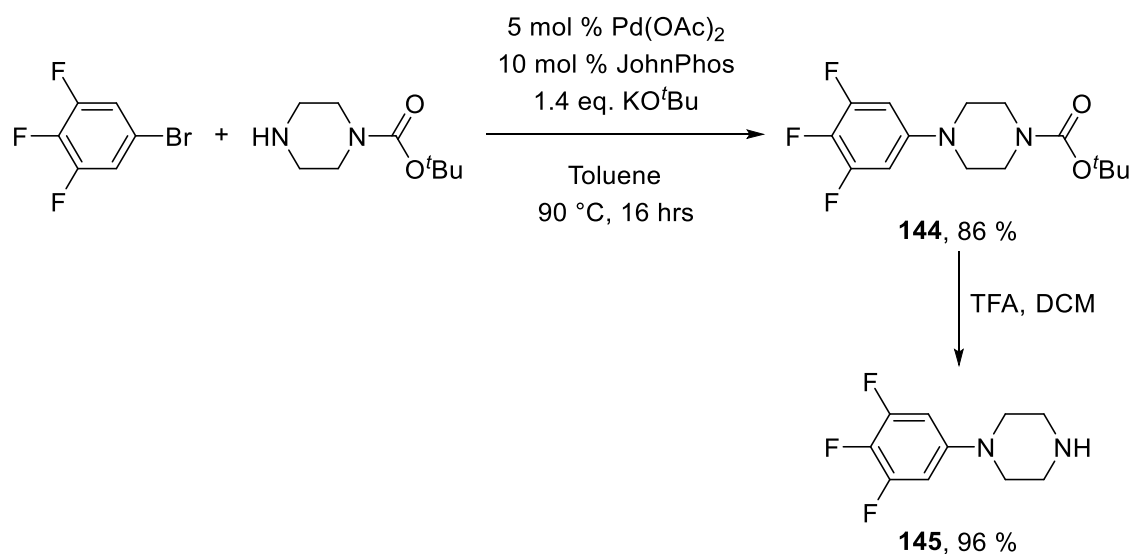


Figure 25. Intermolecular hydrogen bonding present within **131**.

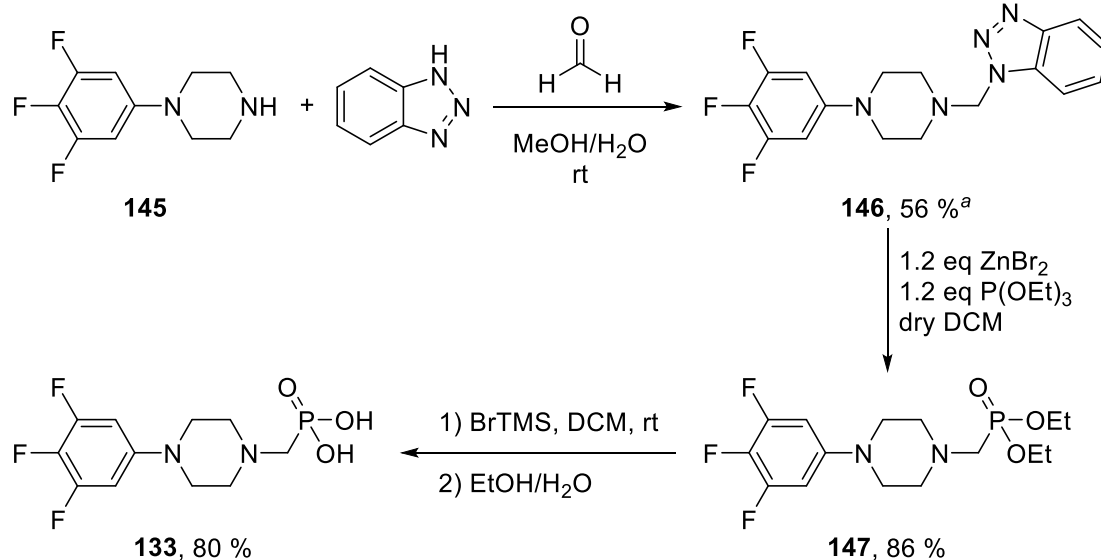
For the remaining piperazine phosphonic acid target **133** the precursor biaryl derivative is unavailable commercially. Although a literature patent procedure has been published for the synthesis of piperazine **145** from 3,4,5-trifluoroaniline¹⁷, in this instance **145** was successfully synthesised following an alternative, modified literature procedure.¹⁸

[Scheme 83] Amination of 3,4,5-trifluorobromobenzene gave *N*-Boc protected biaryl **144** with deprotection to the free amine achieved in excellent yield.



Scheme 83. Synthesis of 1-(3,4,5-trifluorophenyl)piperazine **145**.

The remaining synthesis of phosphonic acid **133** was completed as described for the structurally similar phosphonic acids **131** and **132**. [Scheme 84]



^a2-substituted benzotriazolyl intermediate omitted for clarity.

Scheme 84. Synthesis of phosphonic acid **133** from the precursor piperazine **145**.

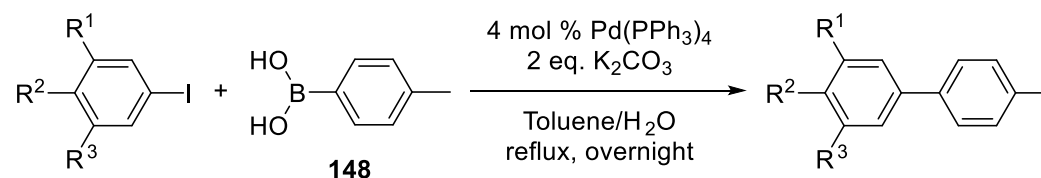
As was experienced in similar syntheses, the benzotriazolyl intermediate **146** was isolated as a mixture of the 1- and 2-isomers, and **133** was highly insoluble in many organic solvents.

4.4.5.2 Synthesis of Analogous Phenyl Derivatives

To complete the library of targeted phosphonic acids the remaining compounds synthesised consisted of the biphenyl systems **134-136**, the analogous counterparts of piperazine-derivatives **131-133**. Although there exists a number of literature syntheses for the precursor biphenyl methyl compounds and benzyl bromides of these targets, no reports have been published for the corresponding diethyl phosphonates or phosphonic acids.

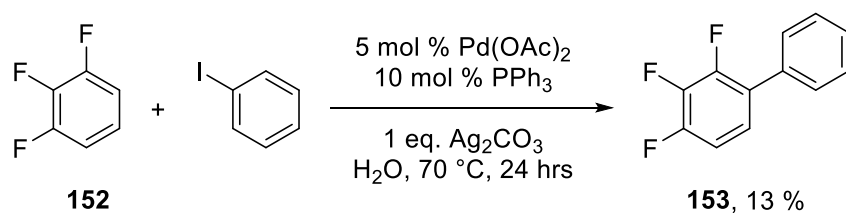
Suzuki-Miyaura cross-coupling reactions of *p*-tolylboronic acid **148** with the relevant iodides achieved biphenyls **149-151** in good yields. [Table 13]

Table 13. Palladium catalysed synthesis of biphenyls **149-151**.



Entry	R ¹	R ²	R ³	Biphenyl, (Yield / %)
1	H	NO ₂	H	149 , (88)
2	H	CF ₃	H	150 , (72)
3	F	F	F	151 , (94)

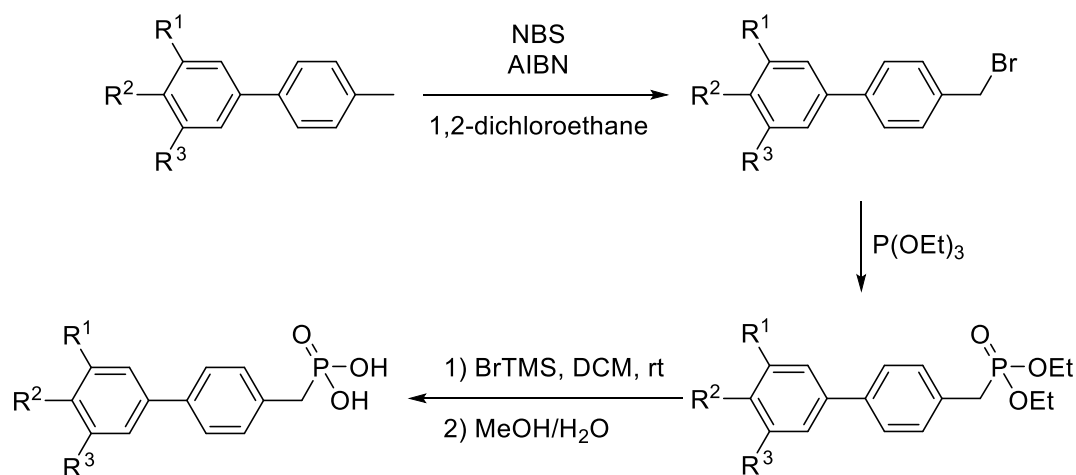
Unlike for previous fluorinated biphenyl systems, synthesis of **151** was not viable by C–H bond activation due to the low acidity, and subsequent reactivity, expected at the desired site of arylation in 1,2,3-trifluorobenzene **152**. Reaction of **152** with iodobenzene, under the reaction conditions employed previously, yielded 2,3,4-substituted biphenyl **153** in low yield; clarifying the predicted, undesired reactivity. [Scheme 85] Consequently, standard Suzuki-Miyaura conditions were employed. The reaction of 3,4,5-trifluoroiodobenzene proceeds cleanly, with isolation of the desired biphenyl **151** in excellent yield. [Table 13, entry 3]



Scheme 85. C–H bond activation reaction of 1,2,3-trifluorobenzene **152**.

The syntheses of phosphonic acids **134-136** were concluded following the same reaction sequence employed for previous syntheses of phosphonic acids from precursor biphenyl methyl derivatives. [Table 14]

Table 14. Synthesis of biphenyl benzylphosphonic acids from the precursor biphenyl methyl compounds.



R ¹	R ²	R ³	Benzyl Bromide, (Yield / %)	Phosphonate, (Yield / %)	Phosphonic Acid, (Yield / %)
H	NO ₂	H	154 , (70) ^a	157 , (70) ^b	134 , (60)
H	CF ₃	H	155 , (86) ^c	158 , (80)	135 , (54)
F	F	F	156 , (52) ^d	159 , (89)	136 , (57)

^a83 % pure by GC-MS, ^b67 % pure by GC-MS, ^c81 % pure by ¹⁹F NMR spectroscopy, ^d85 % pure by ¹⁹F NMR spectroscopy.

For benzyl bromides **154-156**, column chromatography was unable to fully separate the dibrominated side-product formed within the reactions. However, all dibrominated material was removed during the subsequent purification of phosphonates **157-159**. In the case of **157** the phosphonate was isolated as an impure mixture due to the inability

to separate the desired product from a number of unknown compounds. As before, these undesired substances were removed during purification of a product obtained in a later stage of the synthesis.

The successful syntheses of biphenyl methyl phosphonic acids **134-136** will allow for a direct comparison with the structurally similar piperazines **131-133** during SAM investigations.

4.5 Conclusions

Suzuki-Miyaura cross-coupling reactions of pre-formed boronate salts with benzylic halides containing a bromine or phosphonate moiety proved unsuccessful. Although the desired product could be observed in the coupling of aryl phosphonate **108**, isolation from the complex reaction mixture, containing a number of side-products, was unsuccessful.

Palladium catalysed C–H bond activation reactions were successfully employed for the synthesis of a library of fluorinated biphenyl methyl substrates. Moderate to good yields were observed for these reactions but it was noted that unsatisfactory conversions of aryl iodides were observed in all cases which subsequently complicated purification procedures. A range of fluorinated biphenyl methyl phosphonic acids were synthesised following an established bromination, phosphorylation and hydrolysis procedure, described in chapter 2, from the products of the C–H bond activations. Differing fluorination patterns upon the synthesised biphenyl methyl phosphonic acids will allow for the quantification of the effect of fluorine substituents on SAM formation and work function tuning as well as the subsequent interactions with an organic layer.

Due to difficulties experienced previously concerning direct attachment of a phosphonic acid functional group, biphenyl carboxylic acid **127** was synthesised following the same C–H bond activation procedure as for the previously mentioned phosphonic acids. The synthesis of **127** will give an insight into the effect of a methylene linker upon SAM formation and structure, and the resulting dipole upon a metal substrate.

Chapter 4: Synthesis of Fluorinated Biaryl Benzylphosphonic Acids

In an attempt to further increase the net-dipole moment of a SAM, a series of alternative biaryl phosphonic acids were synthesised containing a piperazine ring. Although the syntheses of the precursor phosphonates proceeded smoothly, difficulties were encountered during the purification of the final targeted aminomethyl phosphonic acids due to the insolubility of these compounds. X-ray crystallography showed these piperazine derivatives to exist in their zwitter-ionic form, with extensive H-bonding within the crystal lattice. The syntheses of these highly polar phosphonic acids, and their biphenyl analogues, will allow for SAM studies to begin on a completely new class of compound.

In summary, a range of biaryl benzylphosphonic acids were successfully synthesised for work function studies. [Figure 26]

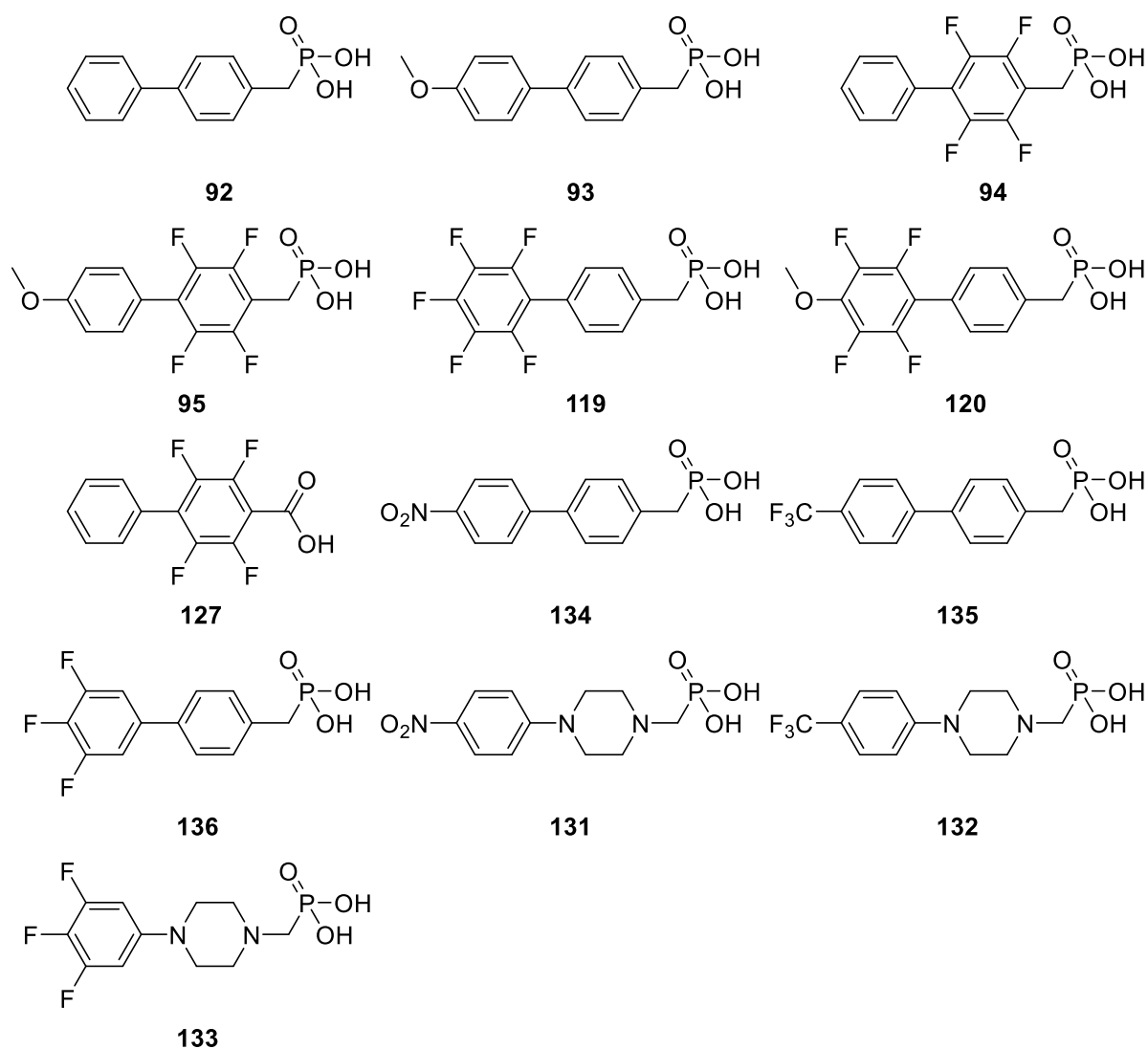


Figure 26. Biaryl derivatives synthesised for SAM studies.

4.6 References to Chapter 4

- (1) Halik, M.; Klauk, H.; Zschieschang, U.; Schmid, G.; Dehm, C.; Schütz, M.; Maisch, S.; Effenberger, F.; Brunnbauer, M.; Stellacci, F. *Nature* **2004**, *431*, 963–966.
- (2) Kosolapoff, G. M. *J. Am. Chem. Soc.* **1945**, *67*, 2259–2260.
- (3) Dow, R. L.; Goldstein, S. W. Benzylphosphonic Acid Tyrosine Kinase Inhibitors. U.S. Patent 5326905, July 5, **1994**.
- (4) Liu, C.; Ni, Q.; Hu, P.; Qiu, J. *Org. Biomol. Chem.* **2011**, *9*, 1054–1060.
- (5) Cohen, R. J.; Fox, D. L.; Eubank, J. F.; Salvatore, R. N. *Tetrahedron Lett.* **2003**, *44*, 8617–8621.
- (6) Bandgar, B.; Bettigeri, S. V.; Phopase, J. *Tetrahedron Lett.* **2004**, *45*, 6959–6962.
- (7) Bedford, R. B.; Gower, N. J.; Haddow, M. F.; Harvey, J. N.; Nunn, J.; Okopie, R. A.; Sankey, R. F. *Angew. Chem. Int. Ed.* **2012**, *51*, 5435–5438.
- (8) Chen, F.; Min, Q.-Q.; Zhang, X. *J. Org. Chem.* **2012**, *77*, 2992–2998.
- (9) Campeau, L.-C.; Parisien, M.; Jean, A.; Fagnou, K. *J. Am. Chem. Soc.* **2006**, *128*, 581–590.
- (10) Babudri, F.; Farinola, G. M.; Naso, F.; Ragni, R. *Chem. Commun.* **2007**, 1003–1022.
- (11) Patrick, C.; Prosser, G. *Nature* **1960**, *187*, 1021.
- (12) Meyer, E. A.; Castellano, R. K.; Diederich, F. *Angew. Chem. Int. Ed.* **2003**, *42*, 1210–1250.
- (13) Adonin, N. Y.; Babushkin, D. E.; Parmon, V. N.; Bardin, V. V.; Kostin, G. A.; Mashukov, V. I.; Frohn, H.-J. *Tetrahedron* **2008**, *64*, 5920–5924.
- (14) Hotchkiss, P. J.; Li, H.; Paramonov, P. B.; Paniagua, S. A.; Jones, S. C.; Armstrong, N. R.; Brédas, J.-L.; Marder, S. R. *Adv. Mater.* **2009**, *21*, 4496–4501.
- (15) Chaudhary, P.; Kumar, R.; Verma, A. K.; Singh, D.; Yadav, V.; Chhillar, A. K.; Sharma, G.; Chandra, R. *Bioorg. Med. Chem.* **2006**, *14*, 1819–1826.
- (16) Smith, J. R. L.; Sadd, J. S. *J. Chem. Soc., Perkin Trans. 1* **1975**, 1181–1184.
- (17) Ali, A.; Hunt, J.; Kowalchick, J.; Kim, D.; Smith, C.; Sinclair, P.; Sweis, R.; Taylor, G.; Thompson, C.; Chen, L. CETP Inhibitors. WO 070173, June 21, **2007**.

- (18) Bradley, D.; Branch, C.; Chan, W.; Coulton, S.; Dean, A.; Doyle, P.; Evans, B.; Gilpin, M.; Gough, S.; Macritchie, J. Acylated Piperidines as Glycine Transported Inhibitors. WO 094842, September 14, **2006**.

Chapter 5

Surface Modification of Aluminium Oxide by Fluorinated Phosphonic Acid Derivatives

5.1 Introduction

Chapters 3 and 4 were concerned with the syntheses of a range of polyfluorinated benzyl- and biphenyl benzylphosphonic acids, along with several non-fluorinated analogues, which were previously identified as promising candidate materials for the modification of AlO_x .

This chapter is concerned with the assembly, characterisation and analysis of a series of fluorinated benzyl- and biphenyl benzylphosphonic acids on AlO_x . The surface modification of AlO_x is assessed by a range of spectroscopic and other analytical techniques. Details regarding monolayer fabrication and the various experimental procedures that were used for monolayer analysis are collated in Chapter 6. All measurements were conducted by the author, unless otherwise stated, in the SONY Materials Science Laboratories in Stuttgart, in collaboration with scientists from the SONY Corporation. All DFT simulated IR spectra were obtained by Dr. Florian von Wrochem at the SONY Corporation.

5.2 Aims and Approach

Aluminium is an abundant, cheap and robust metal. These factors, along with the ease in which it can be handled, make aluminium a strong candidate for use in electronic devices of interest for propriety applications within SONY research and development programmes. The next phase of our studies was to assess the use of fluorinated benzyl- and biphenyl benzylphosphonic acids as self-assembled monolayers (SAMs) on AlO_x . For these purposes, a range of phosphonic acids were selected and synthesised, as described in Chapter 3 and 4. [Figure 27]

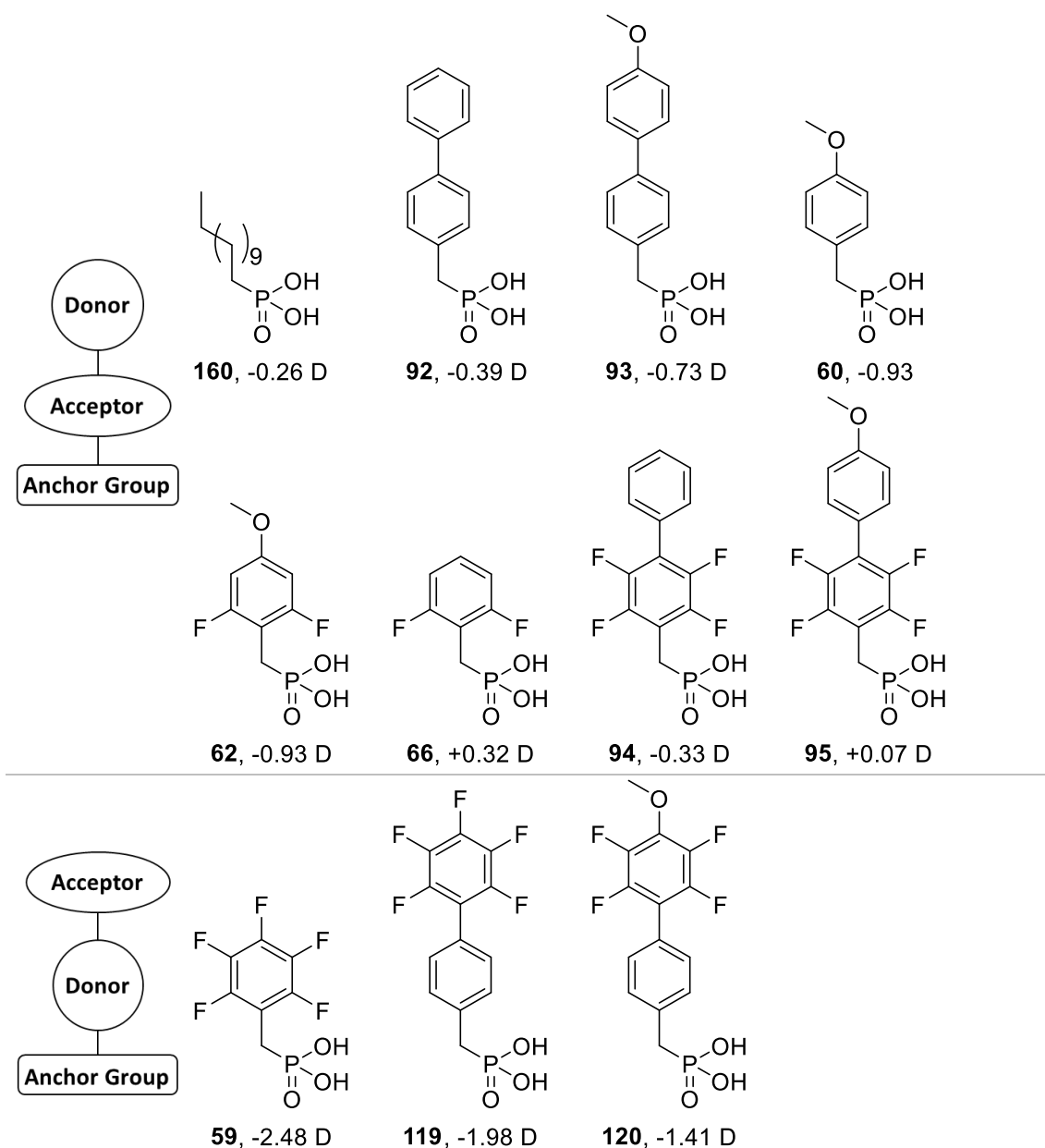


Figure 27. Chemical structures of the phosphonic acids used to study the modification of AlO_x and their calculated relative surface dipole moments.

Compounds conforming to both Acceptor–Donor–Anchor and Donor–Acceptor–Anchor structures, as described in Chapter 2, were targeted for studies. The set of phosphonic acid derivatives selected (Figure 27) were chosen to probe the relationships between level of fluorination and fluorine location and dipole moments of the monolayers, and the resultant properties of the surface to which they are adsorbed.

Although not part of the previously described syntheses, 1-dodecylphosphonic acid **160** was included in the series to provide a non-arylated comparison for the benzylic

phosphonic acids in the series. The inclusion of compounds with varying degrees of fluorination and substituent patterns will allow for an assessment of monolayer properties and structural characteristics of the fluorinated system. The compounds selected (Figure 27) display a broad range of calculated dipole moments on a model AlO_x surface, allowing for an investigation into the relationship between surface dipole moment and effective work function.

The properties of the monolayers formed with target phosphonic acids (Figure 27) were assessed using a range of spectroscopic and analytical techniques. Specifically, studies of surface characteristics and work function tuning of AlO_x were targeted using contact angle goniometry, polarisation modulation infrared reflectance absorption spectroscopy (PM-IRRAS) and X-ray Photoelectron Spectroscopy (XPS). The remainder of this chapter will provide brief explanations of each of these characterisation techniques and their uses along with the results of the testing conducted using fluorinated substrates (Figure 27).

5.3 Methods of Surface Characterisation for Monolayer Studies

5.3.1 Contact Angle Goniometry

The surface of a solid possesses energy, however, this energy is not directly observable and must be measured by indirect means.¹ The wetting method is an effective technique for the measurement of surface energy as the shape of a liquid droplet on a surface is dependent on the free energies of the liquid and the surface.² Young's equation relates the surface tension present when a liquid droplet comes into contact with a solid surface. [Equation 1]

$$\gamma_{SL} + \gamma_{LV}(\cos \theta_C) = \gamma_{SV} \quad (\text{Equation 1})$$

Here, γ_{SL} , γ_{LV} , and γ_{SV} are the surface tensions between the solid, the liquid and the vapour, and θ_C is the contact angle between the surface and the liquid. [Figure 28]

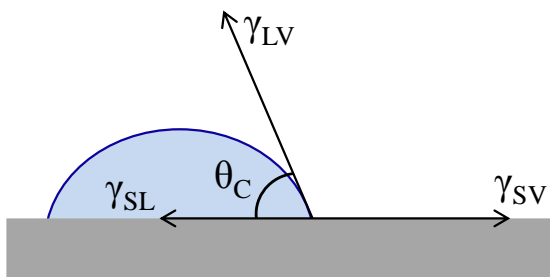


Figure 28. Contact angle and surface tensions of a liquid droplet on a solid surface.

Surface energy can be subdivided into polar and dispersion (nonpolar) components resulting from four individual Van der Waals interactions. The polar component is due to permanent and induced dipoles at the surface, and hydrogen bonding, whereas the dispersion component is due to instantaneous dipole moments.³ By knowing the surface tension components of two probing liquids and their contact angles, the total free surface energy of a surface can be calculated. In this work, two different probe liquids with different polarities were employed, water and diiodomethane (DIM).

The total surface free energy was calculated using the geometric-mean method, where γ represents the individual surface tensions, i refers to the probe liquid; s represents the surface in question; d is the dispersion component; and p is the polar component, following well established literature procedures. [Equation 2]⁴

$$(1 + \cos \theta_i)(\gamma_i^d + \gamma_i^p) = 2 \left(\sqrt{\gamma_i^d \gamma_s^d} + \sqrt{\gamma_i^p \gamma_s^p} \right) \quad (\text{Equation 2})$$

5.3.2 PM-IRRAS

Infrared (IR) spectroscopy is an extremely useful tool for the characterisation of compounds through identification of characteristic vibrational frequencies corresponding to specific functional groups. While the routinely employed transmission mode IR spectroscopy is used to examine compounds in the bulk, infrared reflection absorption spectroscopy (IRRAS) is a powerful and sensitive surface specific spectroscopy for the analysis of thin films on planar surfaces.⁵

During IRRAS, infrared radiation is polarised and then directed at the sample in question at near grazing incidence ($\sim 80^\circ$). The incoming radiation consists of two components, the vector of light perpendicular to the surface (p -polarized light) and the vector of light parallel to the surface (s -polarized light). At the grazing angle, different absorptions of p - and s -polarized light are observed at a surface, with maximum intensity achieved for p -polarized light, whilst the absorption of s -polarized light is virtually zero.⁶ In conventional IRRAS, the reflectivity of the p -polarized light is recorded and then normalised with respect to that of the bare metal surface, with any differences attributed to surface specific adsorptions.

Interpretation of data obtained from IRRAS relies on the ‘surface selection rule’ which states that, since only the p component of the incident light interacts with the surface, a vibrational mode can only be observed if it contains a component of the dynamic dipole moment perpendicular to the surface.⁷ Thus, IRRAS can provide an insight into the tilt angle and binding mode of a monolayer through the presence, or absence, of specific molecular vibrations.

Unfortunately, the use of IRRAS for ultrathin films, such as self-assembled monolayers, can be problematic due to insufficient detection of the surface. As such, measurement times are prolonged in order to achieve an acceptable signal-to-noise ratio. Any instability in the spectrometer is greatly amplified with this increase in acquisition time, and experiments cannot be carried out in an IR absorbing atmosphere as these signals dominate over those of the surface, both of which drastically affect the spectrum obtained.⁶ Modulation of the incoming polarised light is a technique used to enhance the sensitivity and eradicate the difficulties of IRRAS, leading to polarization modulation infrared reflection absorption spectroscopy (PM-IRRAS). A photoelastic modulator rapidly switches the polarisation of the incident beam between p and s states, allowing for the measurement of the two alternating signals by the same detector.⁷ By calculating the sum and the difference of these two signals, the “background” and “sample” spectra can be obtained simultaneously with elimination of signals from ambient contamination.⁸ PM-IRRAS allows for the measurement of high quality spectra and eliminates the need to prepare a blank substrate, which is often a complex procedure.

The use of PM-IRRAS as a characterisation technique provides an important insight into the nature and molecular orientation of a SAM, allowing for accurate determination of the conformation of the organic system at the surface.

5.3.3 XPS

X-ray photoelectron spectroscopy (XPS) is an extremely useful surface analytical technique used for the examination of SAMs. Part of the family of photoemission spectroscopy (PES), XPS can provide a wealth of information about a surface including elemental composition and work function.⁹ The principle behind PES is the photoelectric effect, in which electrons are emitted from a material after absorbing energy from electromagnetic radiation. XPS involves the photoemission of an electron from a core energy level of an atom by an X-ray photon.

If a solid is bombarded with sufficiently high energy X-rays, atoms absorb the energy of the photons and, if they absorb enough energy to overcome the materials' work function, an electron will escape. [Figure 29] Once the electron has overcome the work function of the material, any excess energy contributes to the kinetic energy of the electron.

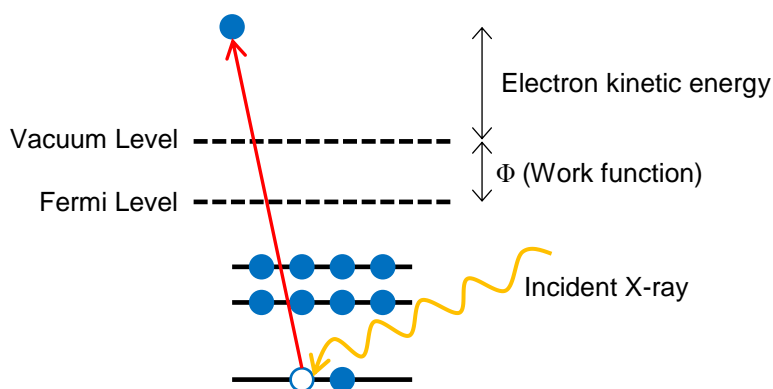


Figure 29. A schematic of photoemission in XPS.

The emitted (photo)electrons are detected, separated according to their kinetic energies and, subsequently, analysed. Since the kinetic energy of the emitted electron is dependent upon the energy of the X-ray used and the work function of the spectrometer, both of which are known, the binding energy of the ejected electron can be determined.

[Equation 3]¹⁰ Where E_B is the binding energy of the electron in the solid, $h\nu$ is the energy of the incident photon, E_K is the kinetic energy of the emitted electron and W is the work function of the spectrometer.

$$E_B = h\nu - E_K - W \quad (\text{Equation 3})$$

The binding energy of an electron is directly related to the electrons' original chemical environment, with each element exhibiting its own set of characteristic resonances within an X-ray photoelectron spectrum. Consequently, XPS can provide information regarding the elemental composition of a surface along with surface coverage. To minimise errors within the XPS data and to prevent contamination of the sample surface, ultra-high vacuum conditions are essential for XPS.

Low intensity XPS can directly yield the work function of a metal surface through measurement of the surfaces' secondary electron edge (SEE). Electrons emitted close to the SEE have almost no kinetic energy after leaving the surface due to a high binding energy. Comparison of this binding energy with the SEE of another clean metal surface with known work function yields the work function of the metal surface under observation.

5.4 Results and Discussion

5.4.1 Sample Preparation

Self-assembled monolayers (SAMs) of phosphonic acids (Figure 27) on AlO_x were prepared using a modified literature procedure following SONY protocol.¹¹ [Figure 30] The AlO_x substrates were placed within a sealed container after a pre-cleaning treatment, and left within the assembly solution overnight. Subsequent rinsing and drying of the substrates was conducted to complete the procedure.

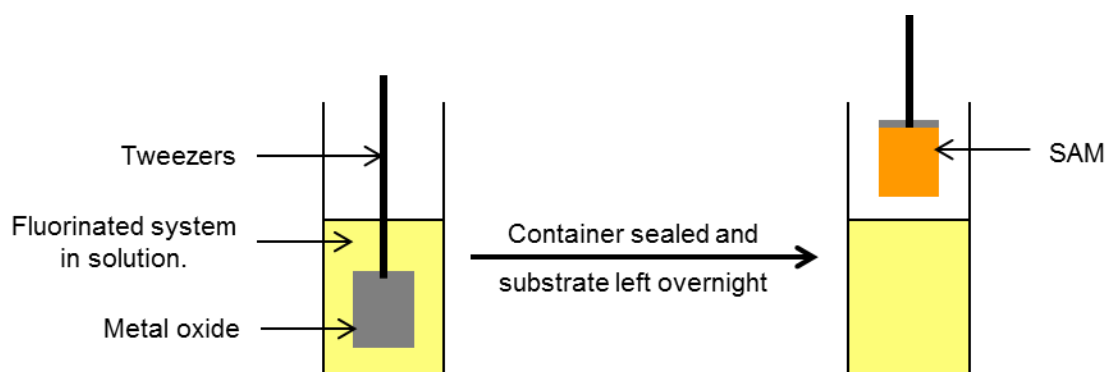


Figure 30. The assembly procedure used for the growth of self-assembled monolayers. Adapted from Hanson *et al.*¹¹

Cleaning of the substrates prior to the assembly procedure is particularly important to remove any residual hydrocarbon contaminants, as well as “activating” the surface. It is widely accepted that high surface hydroxyl content on a metal surface is necessary to obtain dense coverages of a SAM, thereby activating it towards monolayer growth. Three methods of pre-cleaning were examined during initial substrate preparation investigations; general solvent cleaning (SC), general solvent cleaning followed by UV-ozone treatment (SC/UVO), and general solvent cleaning followed by oxygen plasma treatment (SC/OP). UV-ozone (UVO) and oxygen plasma treatments both clean and activate metal surfaces through the generation of volatile oxygenated surface species which subsequently desorb, removing surface contamination and generating surface hydroxyl groups.¹²

Cleaning of a metal surface is often quantified by contact angle measurements, the higher the surface hydroxyl content and the lower the hydrocarbon contamination, the higher the surface energy should be. Therefore, if a surface has been adequately cleaned, water contact angle measurements should approach 0°. ³ Contact angle measurements for SC, SC/UVO and SC/OP cleaned AlO_x substrates were recorded. [Figure 31]

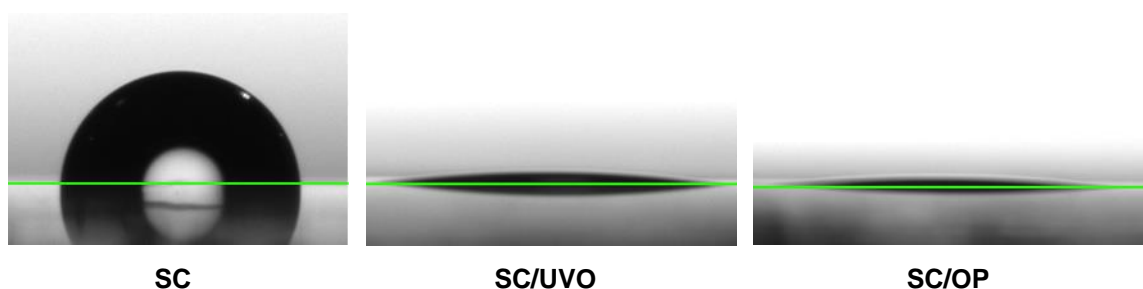


Figure 31. Images of water droplets on pre-cleaned AlO_x surfaces.

Both UVO and oxygen plasma treated samples produce an extremely small contact angle with water, indicating that these surfaces are highly polar and, therefore, very clean. In the instance of the SC/OP treated AlO_x surface, complete wetting¹³ is observed, with the camera software unable to detect a value for the angle. On the contrary, for the SC treated surface, a high contact angle with water is observed. These results show that a significant amount of contamination remains upon the surface of the SC treated AlO_x surface, compared to the alternative cleaning methods.

The same pre-cleaned metal AlO_x substrates show much smaller changes in their contact angles with DIM. [Figure 32] These results indicate that, for the different pre-cleaning treatments employed, the polar component of the AlO_x surface is affected significantly more than the dispersion component.

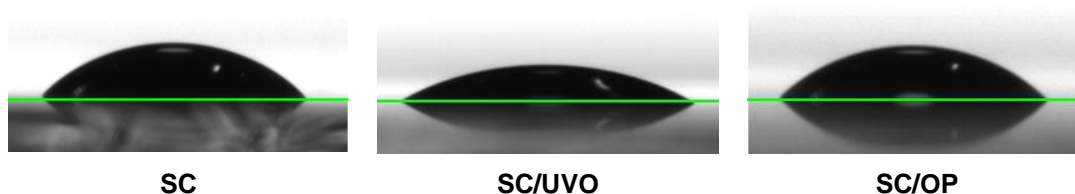


Figure 32. Images of DIM droplets on pre-cleaned AlO_x surfaces.

The results of the contact angle measurements for the three pre-cleaning treatments are collated. [Table 15] Surface energy and polarity of an oxygen-plasma treated AlO_x surface are unattainable due to the inability to computationally detect a contact angle for this surface with water.

Table 15. Contact angle measurements, Θ , surface energies, γ_s , with their dispersion, γ_s^d , and polar, γ_s^p , components, and polarities, χ_p , of pre-cleaned AlO_x surfaces.

AlO_x Treatment	$\Theta_{\text{water}} / ^\circ$	$\Theta_{\text{DIM}} / ^\circ$	γ_s^d / mJ/m^2	γ_s^p / mJ/m^2	$\gamma_s = \gamma_s^d + \gamma_s^p$ / mJ/m^2	χ_p (= γ_s^p / γ_s)
SC	91 ± 1	47 ± 1	35.9	1.2	37.1	0.03
SC/UVO	12 ± 2	34 ± 1	42.7	33.9	76.6	0.44
SC/OP	–	46 ± 2	–	–	–	–

The SC/UVO pre-treatment induces a higher surface polarity and surface energy than the SC treated AlO_x surface; it is presumed that the SC/OP treated sample would further increase these values had a contact angle with water been detected. The low surface energy and polarity observed for the SC treated AlO_x surface is due to a significant decrease in the polar component. The results obtained (Table 15) confirm that different pre-cleaning procedures can significantly alter the surface energy and characteristics of AlO_x .

Although results from the SC/OP pre-cleaning procedure showed the production of a highly polar AlO_x surface, the full effects of oxygen plasma treatment are unknown and often unpredictable. It is suggested that exposing a metal substrate to oxygen plasma can roughen and change the uniformity of the surface. For this reason, a SC/UVO pre-cleaning treatment was applied to all AlO_x metal surfaces before SAM deposition. UVO treatment is a mild and efficient method of cleaning, allowing for the production of near atomically clean surfaces without damaging the surface structure.

5.4.2 SAM studies

SONY protocol was used for the formation of monolayers of compounds (Figure 27) on UVO treated AlO_x substrates to modify surface energy and work function. XPS and PM-IRRAS spectra, and contact angles were recorded for each sample to probe the effects of the different SAMs. The following sections outline the results of the surface modifications of AlO_x by fluorinated SAMs.

5.4.2.1 Contact Angle Goniometry and Surface Coverage

As was discussed in chapter 1, the high surface energies of bare metal oxides can be extremely problematic from a device perspective.¹⁴ The ability to lower the surface energy of a metal oxide surface through the deposition of a SAM is highly desirable to improve subsequent wetting with an organic layer. Modification of metal oxide surfaces with SAMs also provides surfaces with reproducible properties, unlike bare metal oxides which are prone to alteration by various atmospheric contaminants. A clean AlO_x surface has already been shown to possess a high surface energy as a direct result of surface hydroxyl groups. [Table 15] The attachment of a phosphonic acid SAM that can decrease the surface energy of AlO_x is very attractive for device applications.

All of the phosphonic acids used for the modification of AlO_x (Figure 27) significantly decreased the overall surface energy of the SC/UVO cleaned AlO_x , with a particularly large effect on the polar component. [Figure 33] The adsorption of a SAM of any of the benzyl phosphonic acid derivatives decreases the surface energy of a SC/UVO treated AlO_x surface from 77 mJ/m^2 to $31\text{-}56 \text{ mJ/m}^2$. Lowering of the surface energy of AlO_x by modification with the phosphonic acids studied is to be expected due to the replacement of a highly polar hydroxylated surface by hydrocarbon and fluorocarbon species.

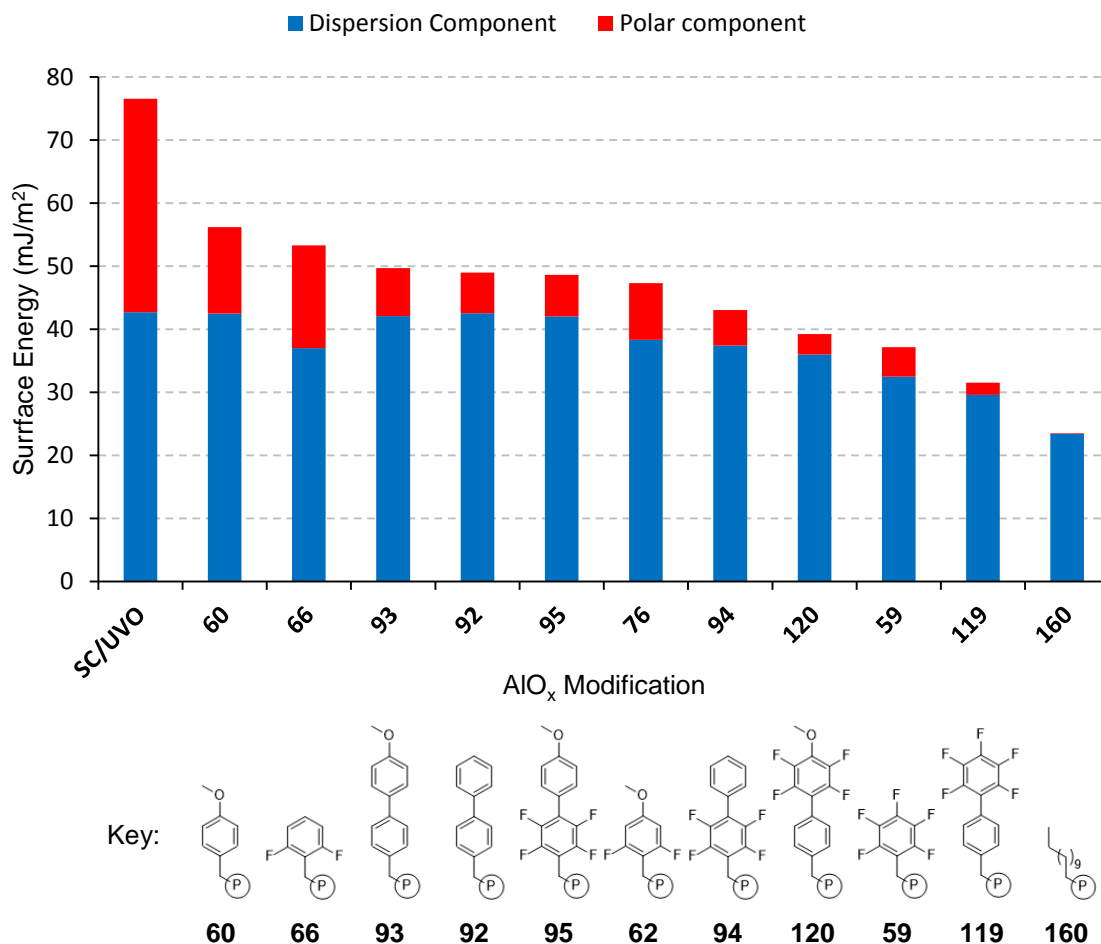


Figure 33. Surface energies comprising their polar and dispersion components for AlO_x samples after SC/UVO treatment and modification with phosphonic acids.

The extremely low surface energy observed by modification using **160** can be attributed to close packing of the long alkyl chains, resulting in a mostly hydrophobic surface. Apart from dodecylphosphonic acid **160**, the lowest surface energies were achieved with the pentafluorophenyl terminated phosphonic acids **59** and **119** due to the highly hydrophobic nature of the C–F bond.¹⁵ The hydrophobic nature of SAMs **160** and **119** can be seen by comparing their contact angles with water to that of the non-fluorinated, methoxylated phosphonic acid **60**. [Figure 34]

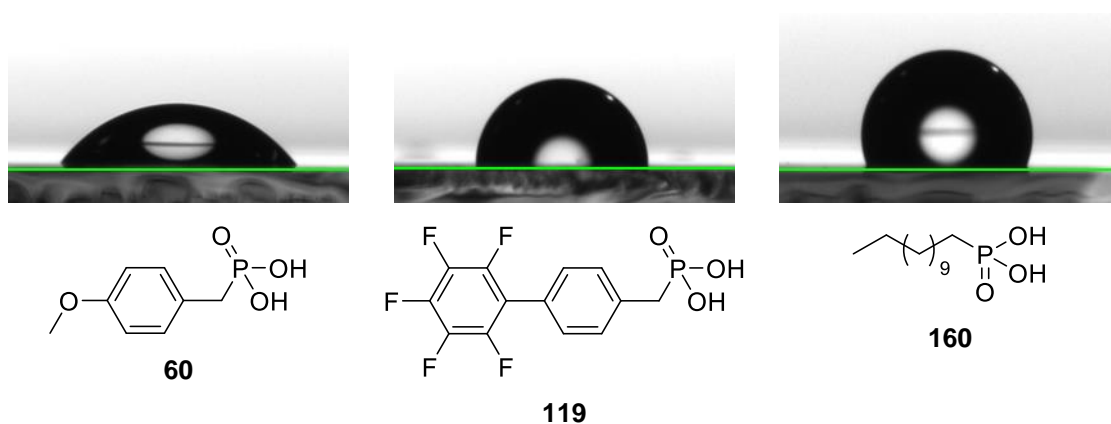


Figure 34. Images of water droplets on AlO_x surfaces modified with phosphonic acid SAMs.

The contact angle of water with a SAM of dodecylphosphonic acid **160** was measured at $109 \pm 1^\circ$, in accordance with a reported literature value of 110° .¹⁶ The reproducibility of this data provides evidence that the pre-cleaning method and assembly procedure employed during these studies are viable practices for SAM formation and consistent with literature reports.

The individual contact angles are presented along with relative surface coverages for all compounds studied. [Table 16] Relative coverages are calculated by comparison of the P2s peak in the XPS spectrum of the SAMs investigated with that of a substrate of known coverage, in this instance dodecanethiol on gold.¹⁷

Table 16. Contact angle measurements, θ , surface energies, γ_s , and relative surface coverages of SAMs of phosphonic acids on AlO_x .

SAM	$\theta_{\text{water}} / ^\circ$	$\theta_{\text{DIM}} / ^\circ$	Relative Coverage
160	109 ± 1	69 ± 1	0.90
60	56 ± 2	34 ± 1	0.91
66	55 ± 1	45 ± 1	0.93
62	68 ± 1	43 ± 1	0.56
59	81 ± 1	53 ± 1	0.49
92	70 ± 1	34 ± 1	1.22
93	68 ± 1	35 ± 1	0.73
119	92 ± 1	58 ± 1	0.81

Table 16 (cont.). Contact angle measurements, Θ , surface energies, γ_s , and relative surface coverages of SAMs of phosphonic acids on AlO_x .

SAM	$\Theta_{\text{water}} / ^\circ$	$\Theta_{\text{DIM}} / ^\circ$	Relative Coverage
120	83 ± 2	47 ± 1	0.67
94	76 ± 1	44 ± 2	0.51
95	70 ± 1	35 ± 1	0.77

As discussed above, phosphonic acids **59** and **119** possess the lowest surface energies of all the benzylic SAMs studied. Although small, the surface energy difference between the two SAMs ($\sim 5.6 \text{ mJ/m}^2$) can be explained by the difference in surface coverage, with the denser coverage providing the more hydrophobic surface. This can be further clarified by comparison of their individual water contact angles. [Figure 35]

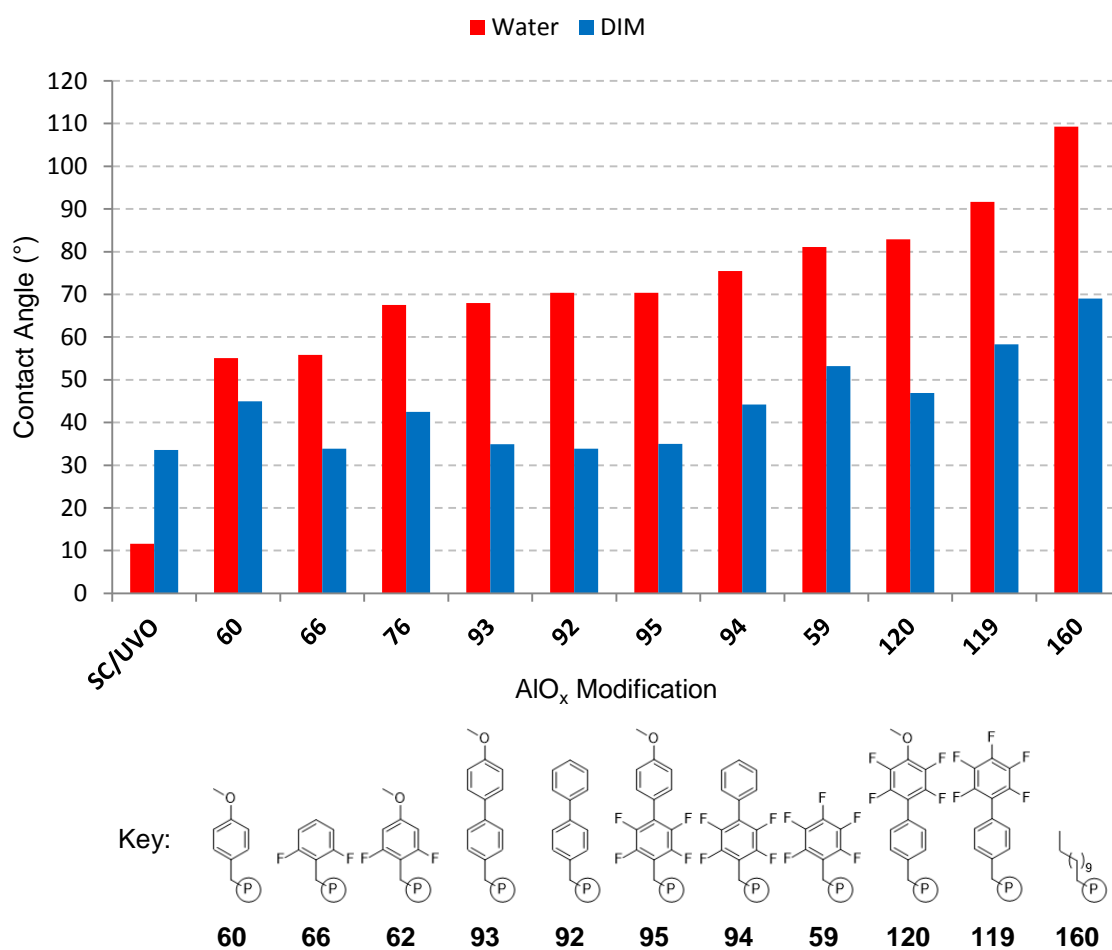


Figure 35. Water and diiodomethane contact angles for AlO_x after SC/UVO treatment and modification with phosphonic acids.

Through comparison of contact angles and structure, several trends can be observed for SAMs of the series of benzylphosphonic acids studied. Data that falls out of line with these trends can often be explained, in part, by consideration of relative surface coverages.

Of the five methoxy terminated SAMs, **93**, **95** and **62** all possess similar surface energies, with **60** and **120** the only examples to possess a surface energy of greater than 50 mJ/m^2 and less than 40 mJ/m^2 , respectively. A similar trend is observed for their recorded water contact angles. It is probable that the increased surface energy observed for **60** can be explained by the high relative surface coverage observed for this SAM compared to the other methoxyl terminated SAMs, creating a denser population of methoxy groups upon the surface. Of all of the methoxy substituted phosphonic acids, **120** is the only example to contain fluorine substituents *ortho* to the methoxy substituent. The close proximity of fluorine atoms to the terminal functional group in this SAM could be a factor in the observed reduced surface energy. It is also a possibility that the low surface coverage observed for **120** (0.67) allows for a slight molecular 'tilt' within the SAM. Any 'tilt' off vertical would expose the *ortho* fluorine substituents to the surface and this would account for the higher contact angle and lower surface energy recorded for **120**.

For the remaining SAMs studied, prepared from the C–H terminated phosphonic acids **66**, **92** and **94**, it is unclear from the results obtained whether the differences observed are due to variations in surface coverage, inclusion of fluorine substituents, or a combination of the two factors. The data obtained for the SAM of **66** are of particular interest due to the differing nature of the results recorded in this study and those of previously published results.¹⁸ Armstrong *et al.* reported that a SAM of **66** possessed a surface energy of 33 mJ/m^2 and a water contact angle of $81 \pm 1^\circ$, significantly different from the results obtained within this study.

5.4.2.2 PM-IRRAS Measurements

5.4.2.2.1 General Considerations for Measurements on AlO_x

It should be noted that, although PM-IRRAS provides a very useful and informative insight into the structural properties of monolayers on metal surfaces, there also exist drawbacks, especially in the case of studying modified AlO_x surfaces. The presence of a strong absorption band due to Al–O bond vibrations in the 800-1050 cm⁻¹ region of the infrared spectrum makes band assignments due to other commonly observed functional groups in this region impossible.

For a complete set of PM-IRRAS spectra of the SAMs studied within this investigation, along with IR spectra of the bulk compounds, the reader is referred to the appendices within this thesis. In the following discussion, key features of the PM-IRRAS spectra only are described.

5.4.2.2.2 PM-IRRAS Results

SAMs of phosphonic acids (Figure 27) on SC/UVO treated AlO_x surfaces were all probed using PM-IRRAS. Due to a number of publications concerning the same or structurally similar hydrocarbon compounds, the spectrum of a SAM of dodecylphosphonic acid **160** was the first to be analysed. The PM-IRRAS spectrum of **160** modified AlO_x was compared with the transmission FT-IR spectrum of **160** powder. [Figure 36] The intensities of the absorbances for the SAM of **160** were multiplied by a factor of 5 to allow for comparisons with the KBr spectrum.

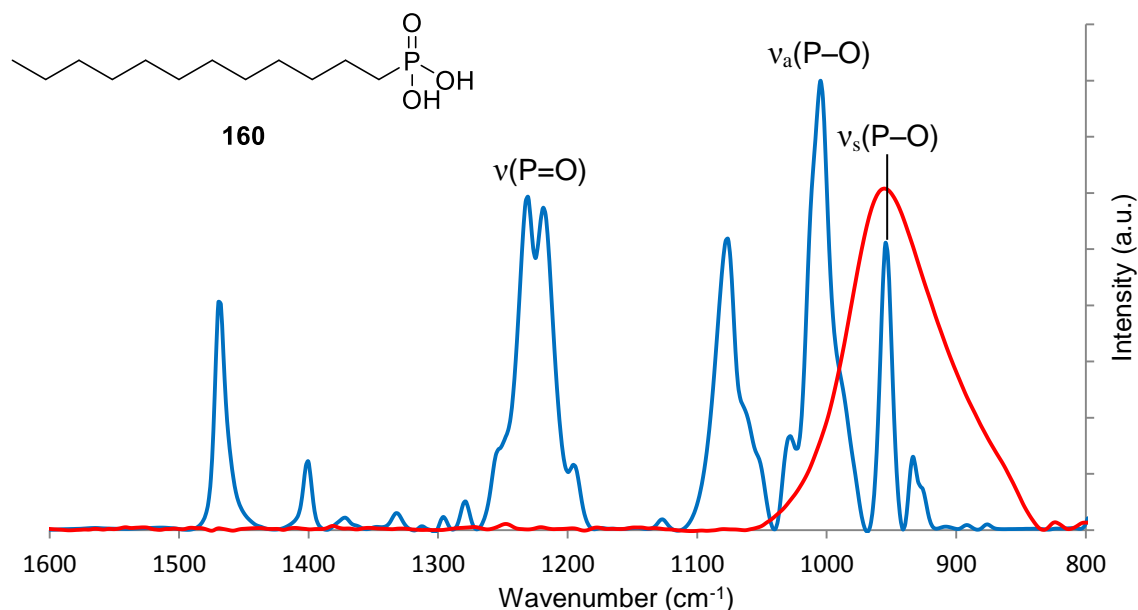


Figure 36. Comparison of the powder/KBr dodecylphosphonic acid transmission FT-IR spectrum (blue line) and the PM-IRRAS spectrum for a dodecylphosphonic acid modified SC/UVO treated AlO_x surface (red line).

As can be seen in figure 36, the two spectra acquired for the surface-bound and bulk dodecylphosphonic acid differ significantly. Using literature data, peaks corresponding to $\nu(\text{P}=\text{O})$, $\nu_a(\text{P}-\text{O})$ and $\nu_s(\text{P}-\text{O})$ stretching vibrations can be assigned for the bulk KBr powder spectrum at 1231, 1005 and 954 cm^{-1} respectively.^{19,20} As detailed previously, the large band due to Al-O bonds in the PM-IRRAS spectrum makes it impossible to observe the presence or absence of P-O stretching vibrations within this region, however, the disappearance of the band due to P=O is observed. The absence of a phosphoryl vibration has been reported previously for similar long chain alkyl phosphonic acid monolayers and has been provided as evidence of the phosphonic acid binding to the surface in a tridentate fashion.^{20,21} Although tridentate binding, involving all three of the available oxygen atoms of the phosphonic acid moiety (Figure 37, g), would be accompanied by the removal of the vibrational stretch due to the phosphoryl bond, we believe it is not possible to categorically state that the lack of such a stretching band equates to a particular binding mode. Firstly, there are a large number of potential binding configurations that are feasible with a phosphonic moiety. [Figure 37] If the phosphoryl bond is indeed involved in binding to the AlO_x surface it is not necessarily via the tridentate mode proposed by other groups.

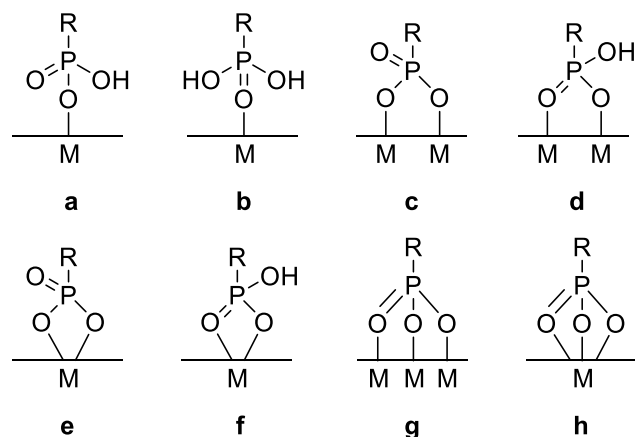


Figure 37. Schematic representation of some possible bridging and chelating binding modes of phosphonic acids to a metal oxide surface. Monodentate (a and b), bidentate (c-f) and tridentate (g and h). Adapted from Brodard-Severac *et al.*²²

The second, and potentially more significant consideration, involves the surface selection rule described earlier in the chapter. The absence of a band due to the phosphoryl group could also be indicative of a molecular orientation on the surface such that the dynamic dipole moment of the phosphoryl group lies parallel to the AlO_x surface and, therefore, will not be observed by this technique. This reasoning applies to all of the spectra for compounds studied in which there appears to be a lack of a band due to the phosphoryl bond.

Assignments of the bands at higher wavenumbers for the SAM of **160** were aided by data in the literature for dodecylphosphonic acid. [Figure 38] A previous study by Adler *et al.*²⁰ on a SAM of **160** on AlO_x recognised that the molecular orientation of the SAM was highly dependent upon the assembly time allowed for molecular adsorption, evidenced by the ratio of the methylene to methyl peaks in the PM-IRRAS spectrum.

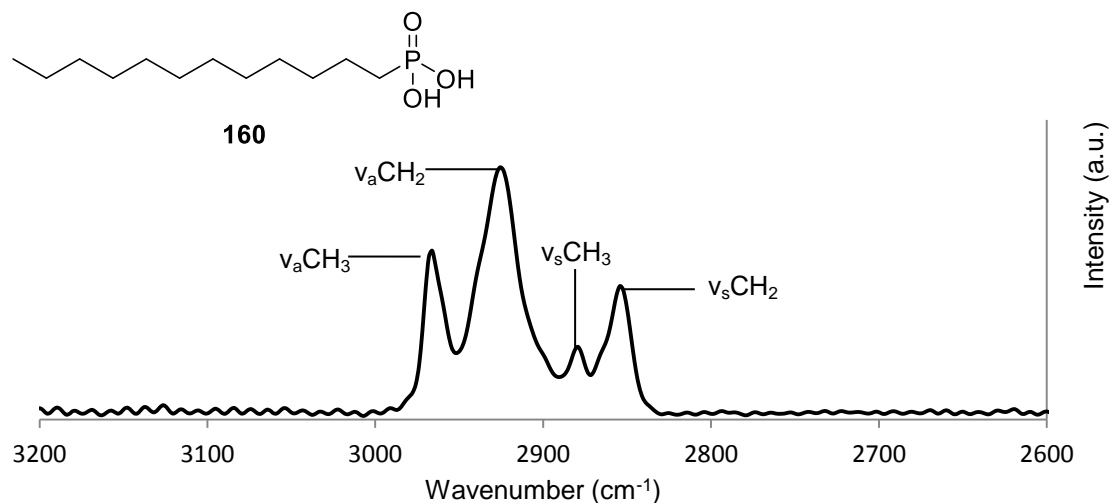


Figure 38. The high frequency PM-IRRAS spectrum for a dodecylphosphonic acid modified SC/UVO treated AlO_x surface.

Considering the amount of CH₂ groups compared to the lone CH₃ group in **160**, the ratio of bands within the PM-IRRAS spectrum (Figure 38) implies that the molecular orientation within the SAM is close to an optimal, perpendicularly adsorbed monolayer due to the surface selection rule. [Figure 39, Situation A] Should the molecular orientation lean further away from this ideal angle, the dipole moment due to the CH₂ groups in the direction normal to the surface would increase significantly, increasing the observable band in the PM-IRRAS. [Figure 39, Situation B] Our observation of a vertically aligned SAM of **160**, as well as the position of the ν_a(CH₂) band, is indicative of a dense monolayer,²³ mirroring the results of the contact angle and surface coverage data obtained for the same sample.

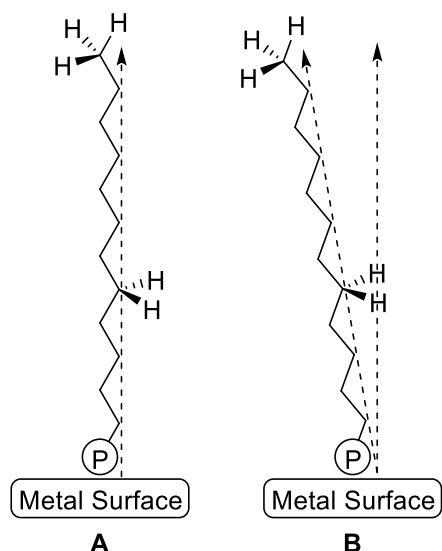


Figure 39. Effect of molecular geometry on bond dipole moment of the CH_2 groups in dodecylphosphonic acid.

Of the remaining compounds to be investigated (Figure 27), literature IR data exists for the equivalent thiols on gold of **60**, **92** and **93**.²⁴ As thiols are a relevant model of vibrations away from the surface for the equivalent phosphonic acids, assignments of the PM-IRRAS spectra of **60**, **92** and **93** were made using this literature data. [Figure 40]

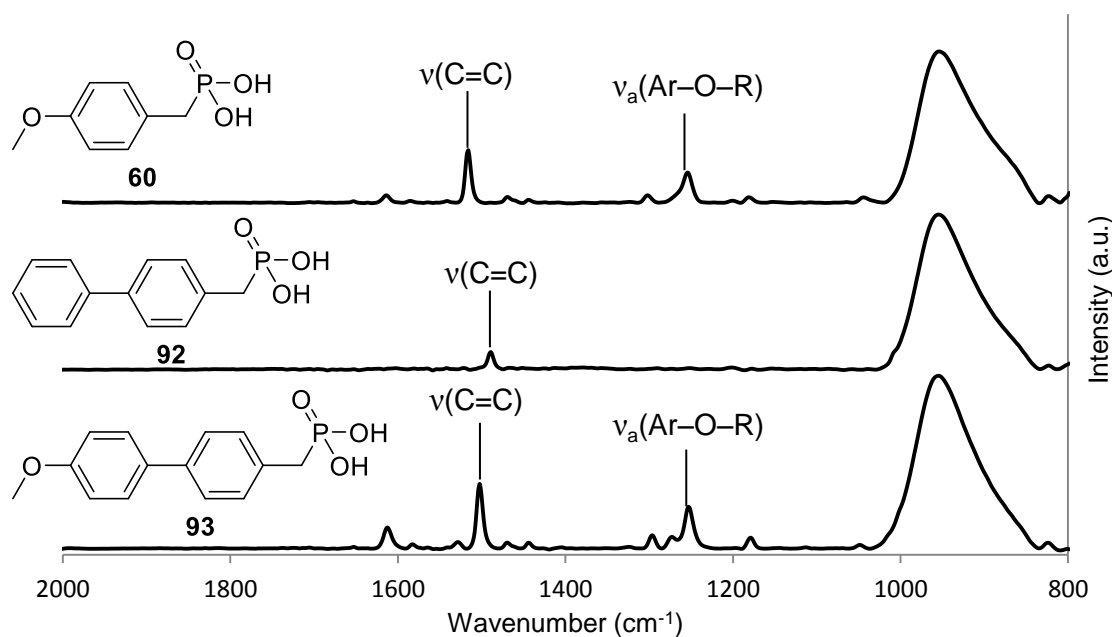


Figure 40. Comparison of the low frequency PM-IRRAS spectra for a **93** (bottom), **92** (middle) and **60** (top) modified SC/UVO treated AlO_x surface.

It is difficult to categorically assign the phosphoryl stretch within the powder KBr spectrum of **60** and, although there exists a peak at 1254 cm^{-1} in the PM-IRRAS spectrum of **60**, the area expected for a phosphoryl stretch,²⁵ the same peak is present for the related thiol on gold and, therefore, is assigned as the $\nu_a(\text{Ar-O-R})$ stretch of the methoxy group. The same stretch is assigned at 1253 cm^{-1} in the spectrum for **93** and, as expected, no such stretch exists for the SAM of **92**. It is possible that the related $\nu_s(\text{Ar-O-R})$ stretch for the methoxy group could correspond to the weak bands observable around 1045 cm^{-1} , however, they could be masked by the large, overlapping Al-O peak. The remaining methoxy substituted phosphonic acids studied also display similar stretches in this frequency region. For all three of the non-fluorinated SAMs, **60**, **92**, and **93**, the prominent peak at approximately 1500 cm^{-1} is assigned to C=C ring stretching and matches bands for the equivalent thiols on gold.

Assigning the higher frequency portion (Figure 41) of the PM-IRRAS spectrum for compounds **60**, **92**, and **93** proves slightly more problematic due to a number of overlapping bands, and weak spectral signals recorded for the corresponding thiols on gold described in the literature.

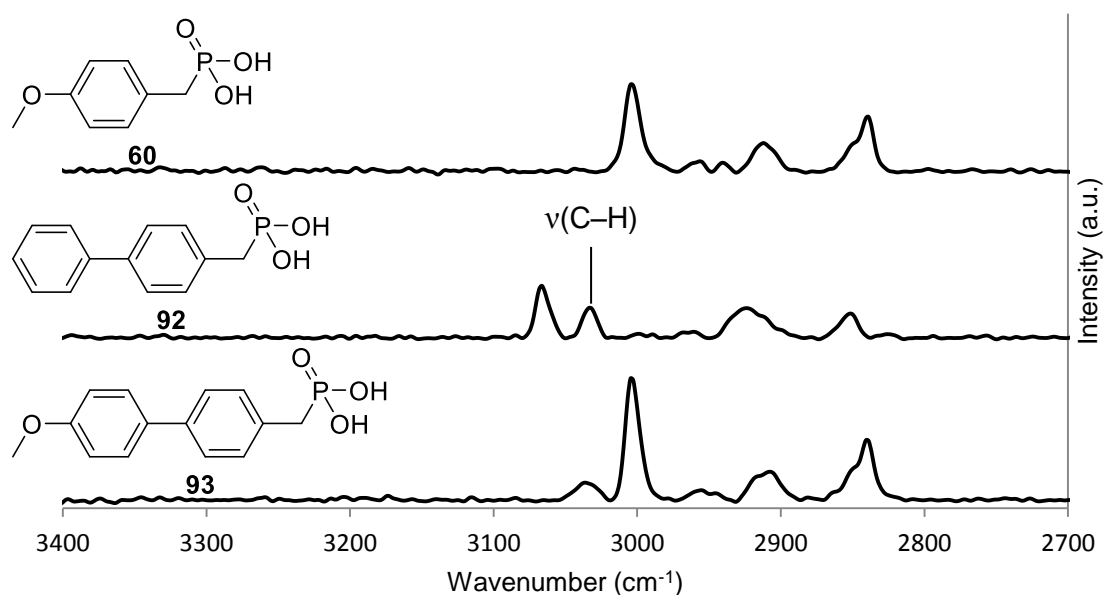


Figure 41. Comparison of the high frequency PM-IRRAS spectra for a **93** (bottom), **92** (middle) and **60** (top) modified SC/UVO treated AlO_x surface.

For **92**, a weak surface spectrum is obtained for the equivalent thiol with only one peak observable at 3062 cm^{-1} , assigned as an aromatic C–H stretch. An equivalent peak is observable at 3071 cm^{-1} in the PM-IRRAS spectrum for the SAM of phosphonic acid **94**, the only other phenyl terminated phosphonic acid. Peaks for the symmetric and asymmetric stretch of the methylene group of **92** are assigned at 2851 and 2924 cm^{-1} respectively, in line with data reported for the equivalent thiol on gold nanoparticles.²⁶

It was expected that for compounds **60** and **93**, a minimum of four bands would be observable at higher wavenumbers, corresponding to the symmetric and anti-symmetric stretch of both the methylene and methyl groups present within the SAM. Application of peak-fitting software to the PM-IRRAS spectra obtained for **60** and **93** allowed for a more accurate peak position determination. [Figure 42]

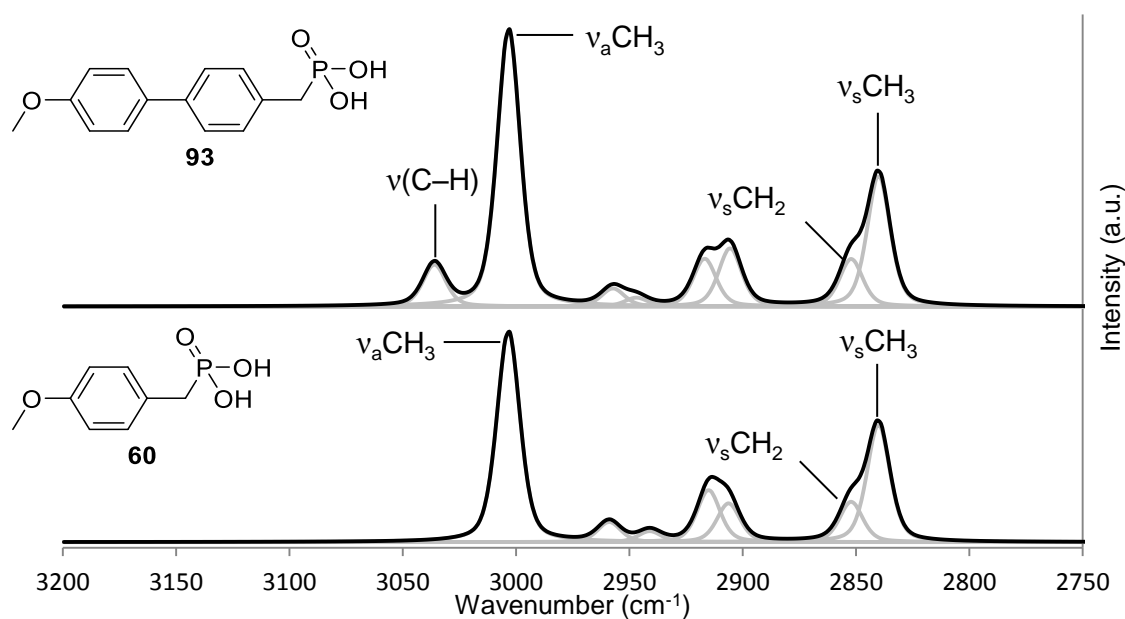


Figure 42. Peak fitting for the PM-IRRAS spectra for a **60** (bottom) and **93** (top) modified SC/UVO treated AlO_x surface.

Only two peaks are observed at high wavenumbers for the SAM of the thiol derivative of **60**, these are assigned as the $\nu_s(\text{C-H, CH}_3)$ at 2838 cm^{-1} and $\nu_a(\text{C-H, CH}_3)$ at 3000 cm^{-1} .²⁴ Using the band positions from peak fitting, two similar peaks are observed at 2840 and 3003 cm^{-1} , leaving three other prominent peaks at 2852 , 2906 , and 2915 cm^{-1} . If the data from the thiol on gold is accurate, this would leave a natural assignment of $\nu_s(\text{C-H, CH}_2)$ at 2852 cm^{-1} , with the $\nu_a(\text{C-H, CH}_2)$ band accounting for one of the

remaining peaks. It should be noted that in the powder KBr spectrum of **60**, no peak is observed at 3003 cm^{-1} , however, a strong peak can be seen at 2969 cm^{-1} . It is possible that the peak at 3003 cm^{-1} in the bulk sample correlates to the $\nu_a(\text{C-H, CH}_3)$ stretch, and is shifted to a higher frequency in the PM-IRRAS spectrum due to the absence of any hydrogen bonding.

Using these assignments for **60** as a guideline it follows that, considering the PM-IRRAS spectra shown are extremely similar (Figure 42), the bands observed for the SAM of **93** can be assigned identically. However, for the equivalent thiol on gold the $\nu_s(\text{C-H, CH}_3)$ and $\nu_a(\text{C-H, CH}_3)$ are assigned at 2850 and 3002 cm^{-1} respectively, a contradiction to the assignments made for **60**. Using the data from the SAM of **92**, along with other non-methoxylated compounds, the band observed at 2852 cm^{-1} is assigned as stretching of the methylene C-H, not the methoxy. The remaining, significant peak observable within the PM-IRRAS spectra of **93** at 3036 cm^{-1} is potentially due to either an aromatic C-H stretch or a ring vibration, both of which would be expected upwards of 3000 cm^{-1} .²⁵ The presence of a band due to aromatic C-H stretching within **93** would be indicative of a SAM that is leaning slightly away from the surface normal, due to the surface selection rule. Evidence for this observation is supported by the relevant contact angle and surface energy results, with the data for the SAM of **93** more closely resembling the SAM of **92** than that of **60**. [Figure 33, Table 16]

For the remaining phosphonic acids studied, to the best of our knowledge, there exists no data within the literature for the same or similar compounds. Several reports have described the use of phosphonic acids **66** and **59** for SAMs on metal oxide surfaces, although no IR or PM-IRRAS data has been presented.^{18,27,28}

For the SAM of **59** a clear band is observable at 1131 cm^{-1} , assigned to stretching of the terminal C-F bond, implying the vertically aligned nature of the SAM on the AlO_x surface. The alternative pentafluorophenyl terminated phosphonic acid within this series, **119**, also displays a similar sharp band at 1070 cm^{-1} . DFT simulated IR spectra, calculated by the SONY Corporation, of compounds **59** and **119** confirm the nature of these two stretching bands.²⁹ Although absolute DFT shifts cannot be compared directly to experimental values, as the values determined depend heavily on the DFT function used, the comparison of peak shifts can aid the identification of specific functionalities.

For example, in the DFT simulated IR spectrum of **59** there exist two neighbouring modes as 1479 and 1495 cm^{-1} ($\Delta 16 \text{ cm}^{-1}$) which are the strongest in the region, and correspond to aromatic C=C stretching. These modes can subsequently be related to the experimental modes observed at 1509 and 1527 cm^{-1} ($\Delta 16 \text{ cm}^{-1}$).

The PM-IRRAS spectrum of the SAM of phosphonic acid **120** displays two similar stretching bands within the same region in which a C–F stretch would be expected, at 1097 and 1212 cm^{-1} . The band at 1097 cm^{-1} has been assigned as stretching due to the ether functionality by comparison to a DFT simulated IR spectrum of **120**. This leaves the possibility that the band at 1212 cm^{-1} is due to a similar C–F bond stretch observed for **59** and **119**. The presence of a C–F bond with a transition dipole moment perpendicular to the AlO_x surface would further explain the contact angle and surface energy recorded for the SAM of **120**.

For both **59** and **119**, the high frequency PM-IRRAS are almost identical, with the symmetric and asymmetric stretches of the methylene linker appearing at 2850 and 2921 cm^{-1} respectively. For SAM **59**, the only C–H bonds present within the monolayer are due to the methylene group and, subsequently, the band assignments in the high frequency region are unambiguous. The lack of any other major bands for the SAM of **119** implies that the transition dipoles of the aromatic C–H bonds lie parallel to the AlO_x surface. [Figure 43]

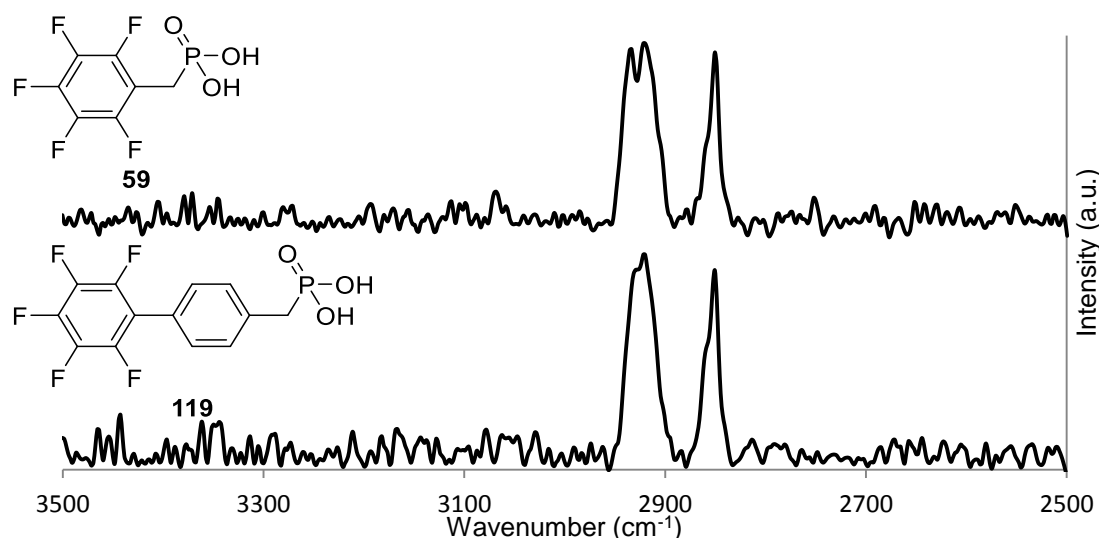


Figure 43. Comparison of the high frequency PM-IRRAS spectra for a **119** (bottom) and **59** (top) modified SC/UVO treated AlO_x surface.

For phosphonic acid **66**, the low frequency region of the PM-IRRAS spectrum of the resultant SAM possessed very weak band signals compared to the intense Al–O band, creating difficulties with subsequent baseline fitting and band assignments. Weak signals are observed at 1240 and 1276 cm^{-1} which, after comparison to a DFT simulated IR spectra, have tentatively been assigned as a combination of an aromatic C=C stretch and C–F stretch, and another combination of a C=C and P=O stretch. If a band due to the phosphoryl stretch is indeed observable, it remains difficult to assign a singular binding mode to this particular SAM due to the intensity of the band observed. It is possible that combination binding modes may exist within the SAM, a feature observed by other groups for phosphonic acids on metal oxide surfaces,³⁰ which would produce a weak phosphoryl stretch and could account for the unusual contact angle and surface energy data obtained for the same substrate. Analysis of the higher frequency PM-IRRAS spectrum obtained for the same SAM proved more facile, with the observed bands easily distinguishable from the baseline within this region. [Figure 44]

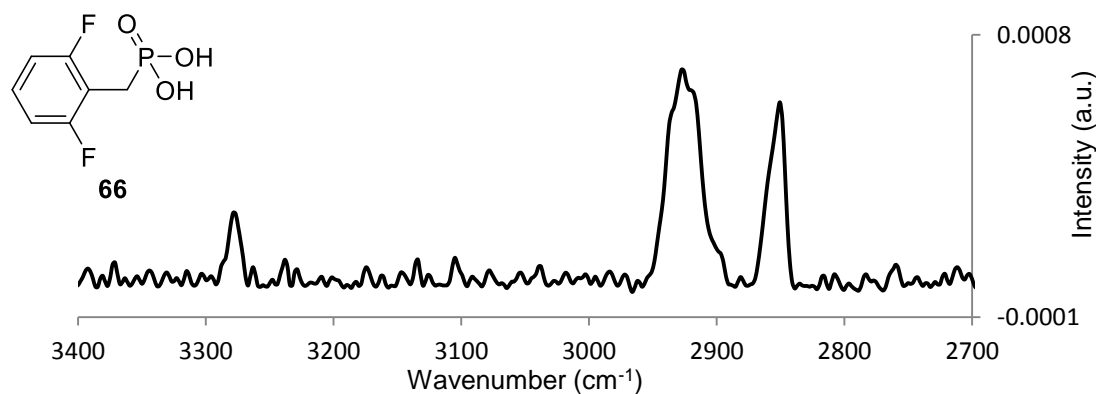


Figure 44. The high frequency PM-IRRAS spectrum for a **66** modified SC/UVO treated AlO_x surface.

The band at 2851 cm^{-1} is assigned as the $\nu_s(\text{C-H}, \text{CH}_2)$ with the corresponding asymmetric stretch overlapping with the broad peak at 2927 cm^{-1} . The weak signal at 3278 cm^{-1} , at first glance, posed several questions due to its high frequency positioning. However, examination of the IR spectrum of the bulk sample of **66**, along with a DFT simulated IR spectrum of the same compound, showed no analogous peak, with the band at 3278 cm^{-1} in the PM-IRRAS spectrum attributed to a contaminant. The lack of bands within the PM-IRRAS spectrum at 3030–3130 cm^{-1} , the characteristic region for aromatic C–H stretches,³¹ is surprising considering the other H terminated phosphonic

acids studied all possess such a band. The lack of C–H stretching in this region could be as a consequence of the surface selection rule, however, **66** is one of only two SAMs investigated containing a phenyl ring with both fluorine and hydrogen substituents. The close proximity of an electronegative fluorine atom to the aromatic hydrogens in **66** could weaken the C–H bond and shift its associated stretch to a lower frequency. As such, the expected stretching band may form part of the broad peak at 2927 cm^{-1} within the PM-IRRAS spectrum.

The high frequency PM-IRRAS spectrum of the monolayer of **62** was assigned by comparison with the PM-IRRAS spectra of the structurally similar **60** and **66**. [Figure 45]

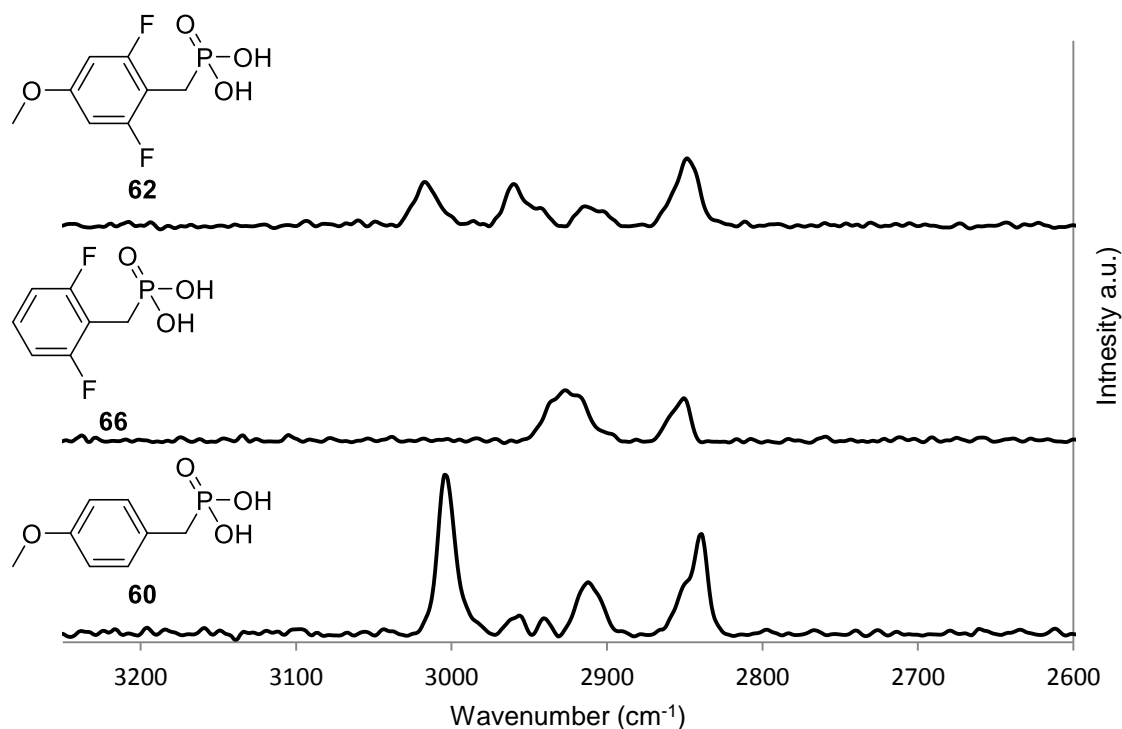


Figure 45. Comparison of the high frequency PM-IRRAS spectra for a **60** (bottom), **66** (middle) and **62** (top) modified SC/UVO treated AlO_x surface.

Although the presence of four main bands within the spectrum of **62** would appear to represent the four C–H stretching bands due to the methylene and methyl group, by comparing to the spectra of SAMs of **60** and **66**, the $\nu_s(\text{C-H})$ of the CH_2 and CH_3 have been assigned within the same band at 2849 cm^{-1} . This leaves assignments of the $\nu_a(\text{C-H})$ of the CH_2 and CH_3 at 2914 and 3017 cm^{-1} respectively. The remaining unassigned

bands may be due to generic ring vibrations or, as speculated with **66**, aromatic C–H stretching, with the latter dependent upon the tilt of the SAM.

The remaining SAMs studied concern phosphonic acids **120**, **94** and **95**. As mentioned previously, the low frequency PM-IRRAS spectrum of SAM **120** possesses bands potentially indicative of a C–F transition dipole moment normal to the surface, implying a slight tilt within the SAM away from the surface normal. Assignment of the high frequency PM-IRRAS spectrum of SAM **120** was aided by a DFT simulated IR spectrum. [Figure 46]

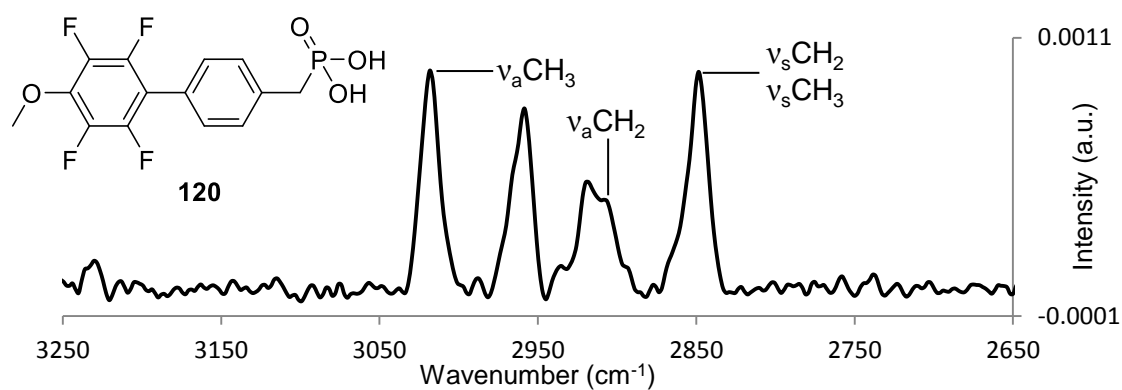


Figure 46. The high frequency PM-IRRAS spectrum for a **120** modified SC/UVO treated AlO_x surface.

As reported for SAMs discussed previously, both $\nu_s(C-H)$ stretches of the methylene and methyl group of **120** are assigned within the same band at 2849 cm^{-1} , with the corresponding asymmetric stretches occurring at 2912 and 3018 cm^{-1} respectively. From the corresponding DFT simulated IR spectrum, the prominent band at 2959 cm^{-1} is believed to be caused by another, unspecified, asymmetric vibration of the methoxy CH_3 group.

For the two structurally similar biphenyl phosphonic acids **94** and **95**, comparison of the high frequency PM-IRRAS spectra emphasises the effect of the exchange of a terminal hydrogen substituent for a methoxy group. [Figure 47]

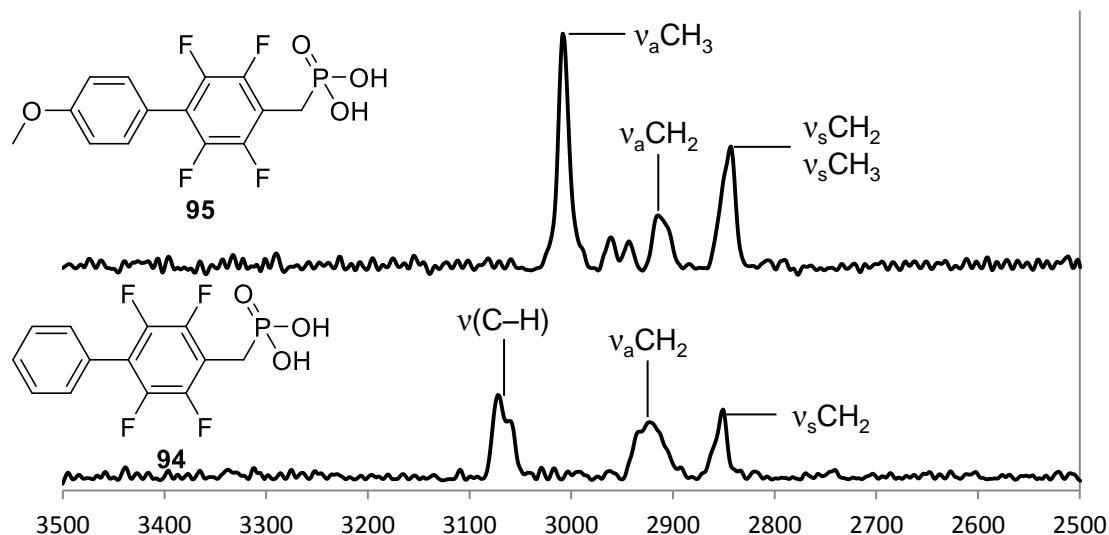


Figure 47. Comparison of the high frequency PM-IRRAS spectra for a **94** (bottom) and **95** (top) modified SC/UVO treated AlO_x surface.

The high frequency peak at 3071 cm^{-1} for **94**, discussed previously, is assigned to the stretch of the terminal C–H bond. This band is, of course, absent in the PM-IRRAS of **95** which instead possesses the $\nu_a(\text{C-H}, \text{CH}_3)$ in this high frequency region, at 3008 cm^{-1} . Both SAMs possess the symmetric and asymmetric stretch of the methylene group in the regions 2850 and 2920 cm^{-1} respectively, with the $\nu_s(\text{C-H}, \text{CH}_3)$ of the methoxy in **95** overlapping with the former of these bands.

All PM-IRRAS spectra of the phosphonic acids studied (Figure 27) are summarised for completeness. [Figure 48 and Figure 49]

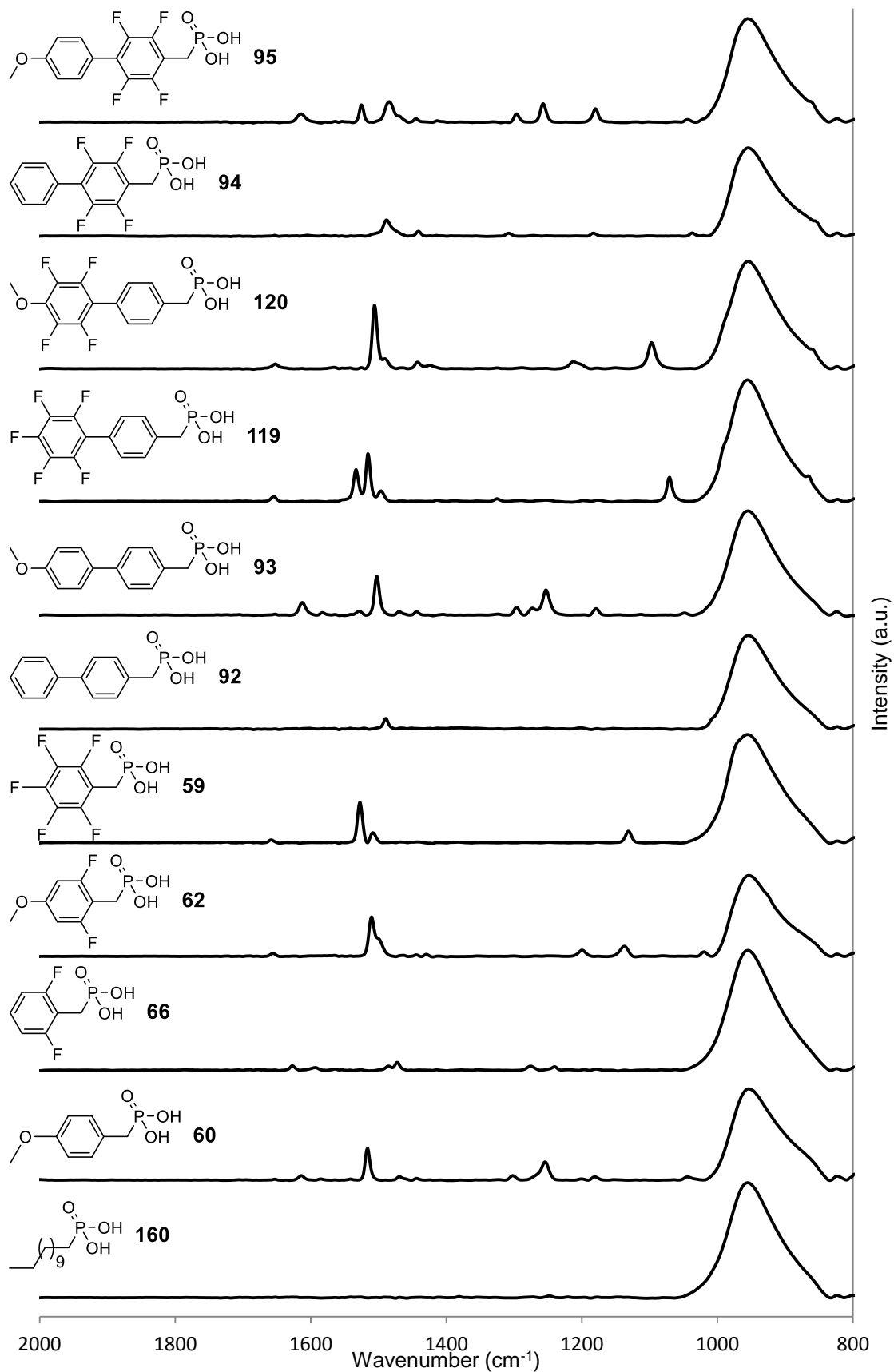


Figure 48. Comparison of the low frequency PM-IRRAS spectra for all phosphonic acid modified SC/UVO treated AlO_x surface.

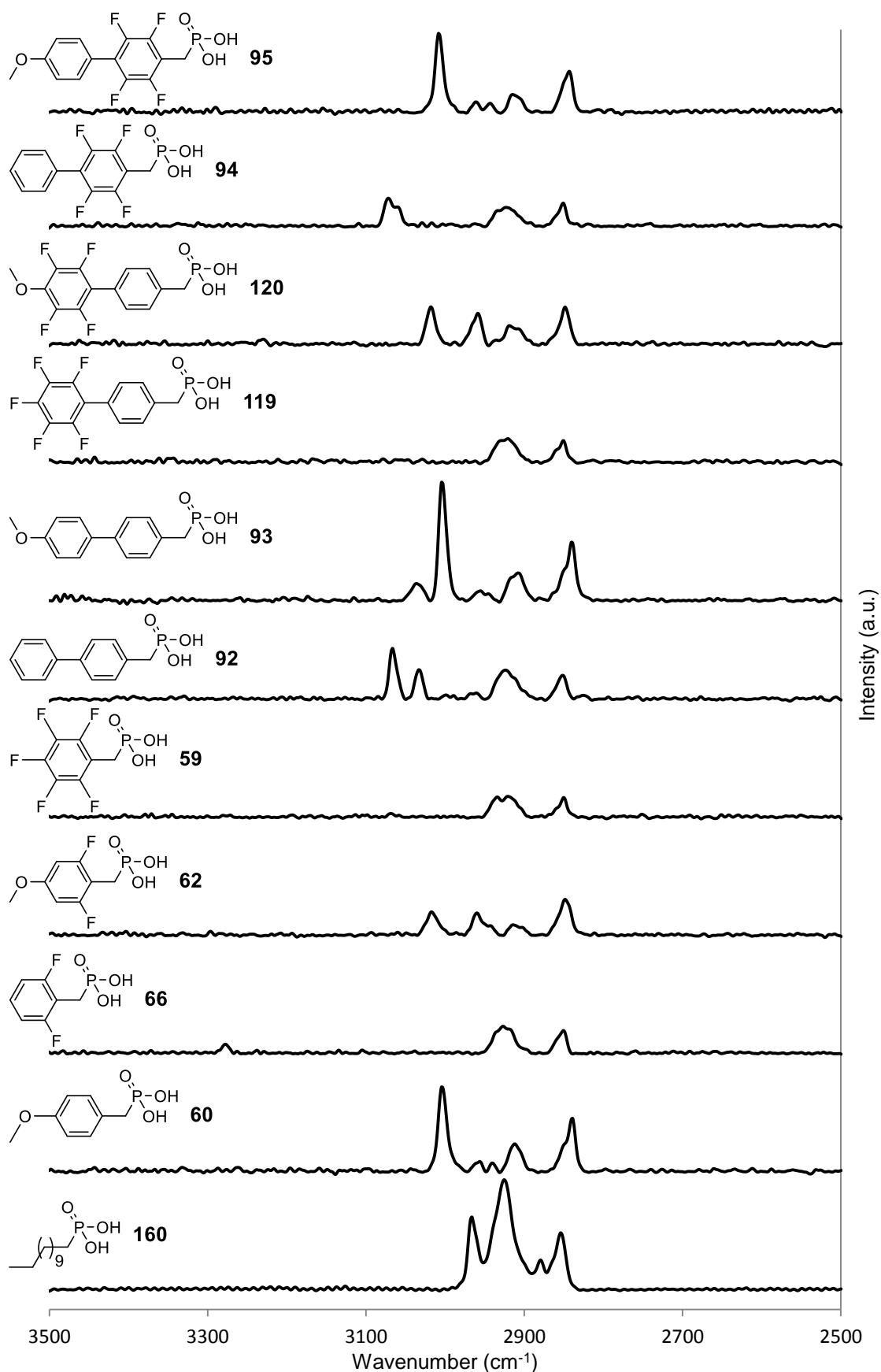


Figure 49. Comparison of the high frequency PM-IRRAS spectra for all phosphonic acid modified SC/UVO treated AlO_x surface.

5.4.2.3 Work Function Tuning

XPS is a powerful tool for assessing monolayers on metal oxide surfaces. For each of the SAMs studied, high resolution scans were conducted to confirm the modification of an AlO_x surface by attachment of phosphonic acids. [Figure 27] As discussed previously, XPS data was used to determine relative surface coverages of the monolayers studied, with a dense monolayer highly desirable for a robust surface. However, the primary XPS study conducted for this research focused upon quantification of the ability of phosphonic acids studied to modify the work function of AlO_x . All XPS data was collected by Dr. Frank Scholz at the SONY Corporation.

The work function of phosphonic acid modified SC/UVO treated AlO_x samples were probed using low intensity XPS, employing a sputtered gold sample as the reference metal. The SEE (secondary electron edge) for a selection of the substrates investigated is shown. [Figure 50] Since the work function of sputtered gold is a known value, work function values for phosphonic acid modified AlO_x samples were calculated by comparison of the relevant low intensity XPS spectra with that of the reference sample. For SAM modified AlO_x surfaces in which the SEE shifts to a lower binding energy than the blank substrate, there is an increase in the effective surface work function and *vice versa*. From these studies, we obtained an AlO_x work function value of 3.84 eV, which falls within the reported work function of aluminium with a native oxide layer of 3.45-3.9 eV.³² It should, however, be noted that the 'true' work function value of such an AlO_x surface is highly dependent upon the nature of the oxide, the cleaning of the substrate, and surface contamination.

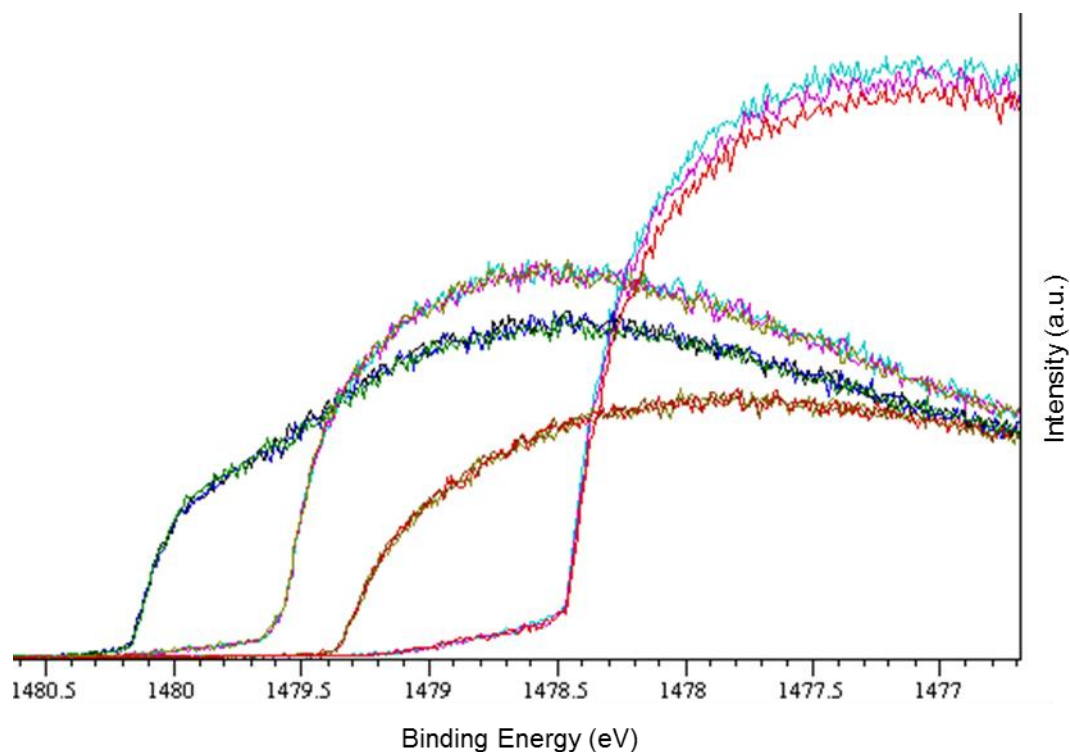


Figure 50. Low intensity XPS data for the secondary electron edge of SAMs (left to right) **60**, blank AlO_x substrate, **59** and sputtered gold. (Data collected by Frank Scholz)

As the dipole moment of the phosphonic acid adsorbed onto the AlO_x surface shifts from positive to negative, the SEE shifts to lower binding energy.

For all compounds studied (Figure 27) a total work function shift of 0.91 eV can be achieved for an AlO_x surface through adsorption of phosphonic acids **160** and **119**. [Figure 51] The lowest work function achieved was for that of AlO_x modified by **160**, surface however, as shown in earlier results, adsorption of a monolayer of the long chain alkylphosphonic acid **160** creates a surface that is extremely hydrophobic. [Figure 34] From a device perspective this is highly undesirable as subsequent coating of the modified AlO_x surface with an organic layer becomes very difficult. As such, the use of **160** for device applications is not a viable option. For the benzylic phosphonic acid derivatives tested, a total surface work function shift of 0.82 eV is observed between **66** and **119**.

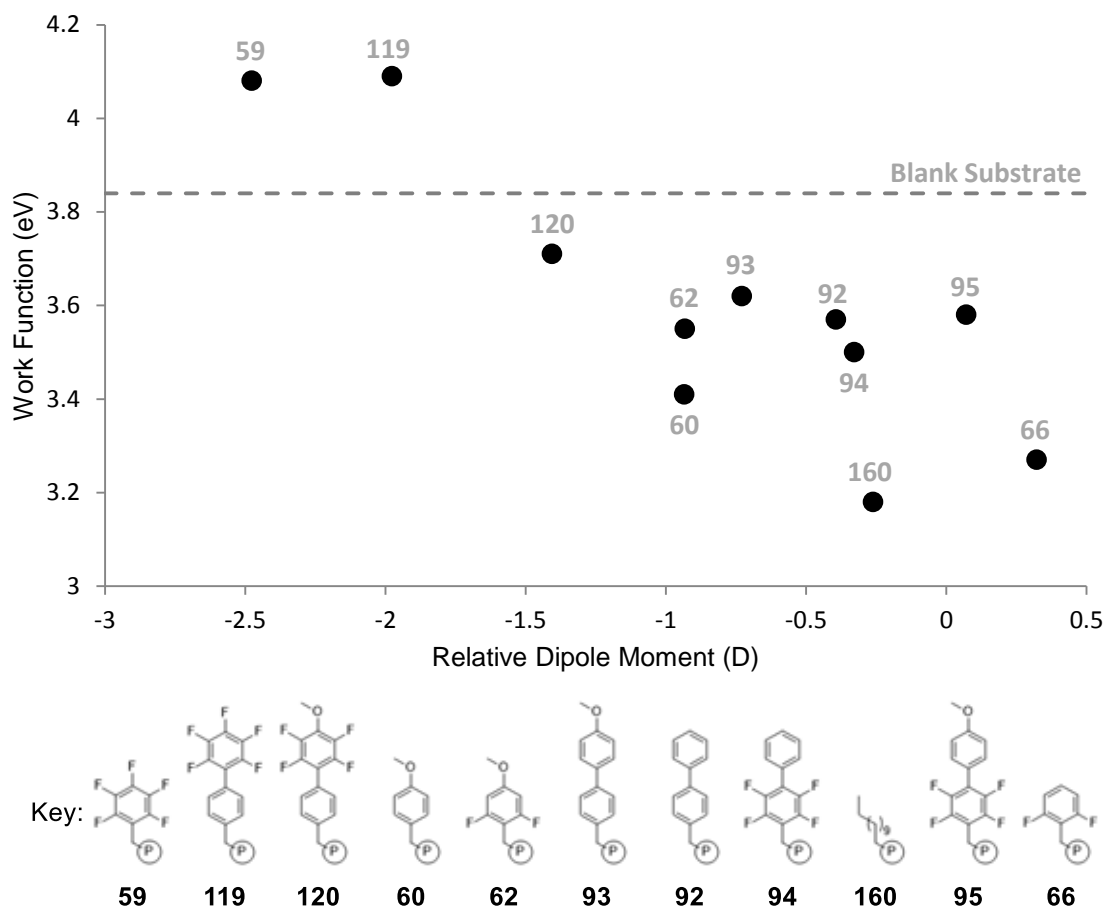


Figure 51. Comparisons of the changes in work function of phosphonic acid modified AlO_x surface with respect to relative dipole moments of the surface created by phosphonic acids (Figure 27).

The general trend observed for the phosphonic acids studied indicates that the change in work function of AlO_x is predominantly caused by a surface induced dipole moment.

The two pentafluorophenyl terminated phosphonic acids, **59** and **119**, both increase the work function of AlO_x , whereas the remaining phosphonic acids studied all decreased the work function relative to the blank AlO_x substrate. The terminal perfluoroaromatic ring of both **59** and **119** likely induce surface dipoles opposite to those of the other phosphonic acids studied, with the negative ‘end’ pointing away from the surface due to the highly electronegative fluorine atoms. The addition of a methoxy group to the pentafluoro- ring, as for **120**, seemingly offsets this effect and work function is correspondingly lowered. Due to the difference in relative dipole moment between a surface modified with **59** and **119**, one may expect the work function for the former to be increased further. However, as reported previously, the relative surface coverage of

59 (0.49) is significantly lower than for **119** (0.81) which could account for the lower than expected work function shift observed.

It is reported that for pentafluorobenzylphosphonic acid **59**, only one C–F group has a dipole which contributes towards the net molecular dipole, with the remaining C–F bonds cancelling one another out.⁴ This observation would explain the difference between **119** and **120**, with the latter having a molecular dipole with its negative end pointing towards the surface due to the electron-donating methoxy substituent.

Unlike for **119** and **120**, the work function shift between **92** and **94** and their methoxylated counterparts, **93** and **95**, respectively, is less pronounced with only a small difference observed (0.05 and 0.08 eV). It is possible that, with the negative end of the dipole already pointing towards the surface for SAMs of **92** and **94**, due to the polar phosphonic acid anchor group, the addition of a methoxy terminal group has a nominal effect on the total surface polarity.

The largest shift in work function observed with a benzylphosphonic acid SAM, compared to a blank AlO_x surface, is achieved for the partially fluorinated modifier **66** at 0.57 eV. This decrease in work function is to be expected with the two *ortho* fluorine substituents contributing towards the large negative dipole pointing towards the surface. Unlike for the other fluorinated phosphonic acids studied, the dipoles of the two C–F bonds are not counter balanced by any other substituent on the aryl ring.

Overall, modification of an AlO_x surface via SAMs of benzylphosphonic acid derivatives has been shown to either increase or decrease the work function of the metal surface depending on SAM composition. The observed shift is highly dependent upon the nature of the surface dipole following adsorption, with monolayers of **119** and **160** achieving the largest increase and decrease in work function, respectively.

5.5 Conclusions

A range of partially fluorinated benzyl phosphonic acid derivatives were synthesised (Figure 52) and an initial selection assessed for surface energy and work function modification.

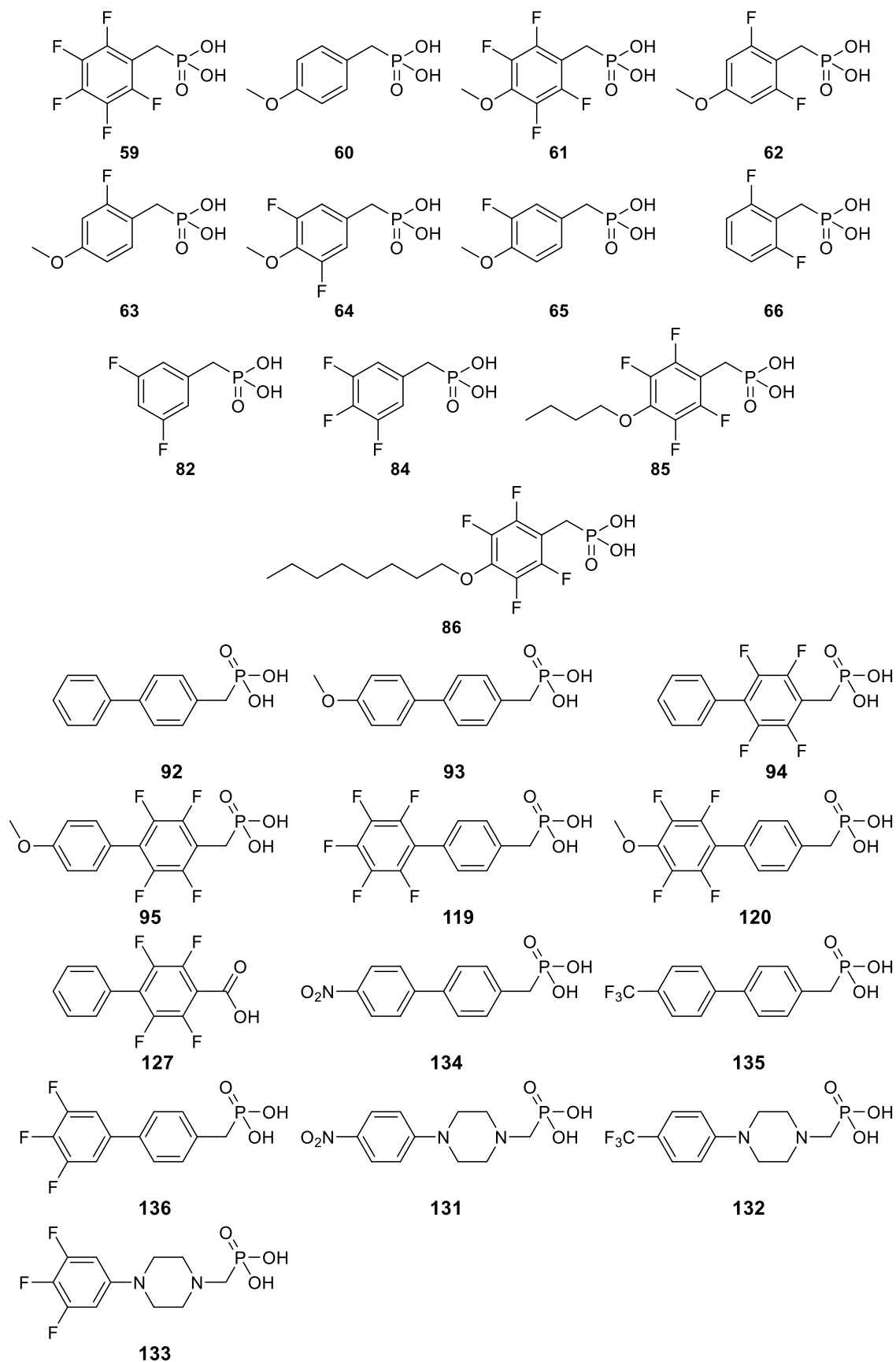


Figure 52. Benzyl phosphonic acid derivatives synthesised for the modification of AlO_x using self-assembled monolayers.

An investigation into pre-cleaning procedures was conducted, with either UVO or oxygen plasma treatment shown to be necessary in creating a highly polar, hydroxylated AlO_x surface. Following SONY protocol, SAMs of benzyl- and biphenyl benzylphosphonic acid derivatives (Figure 27) were successfully grown on SC/UVO pre-treated AlO_x substrates. Following SAM assembly, a number of surface sensitive analytical and characterisation techniques were employed to probe the nature of the resulting SAMs, with analysis of the acquired data discussed.

Modification of an AlO_x surface with each of the phosphonic acid derivatives investigated significantly reduced the surface energy compared to that of an unmodified cleaned substrate, a quality highly desirable for use in electronic devices. Of the aromatic phosphonic acid derivatives tested, the pentafluorophenyl terminated SAMs of compounds **59** and **119** provided the largest decrease in surface energy due to the hydrophobic nature of the highly fluorinated systems. The smallest decrease in surface energy was achieved by the non-fluorinated methoxylated phosphonic acid **60**. A lower than expected surface energy was recorded for a SAM of **120**, however, molecular tilt within the SAM would account for this. Further evidence for an angled molecular orientation for **120** was observed by PM-IRRAS with evidence of a C–F transition dipole moment perpendicular to the surface.

A dense packing motif is highly desirable for SAMs to enhance the quality and durability of devices. For the phosphonic acids investigated, a varied range of relative surface coverages were calculated. The reasons for the variation between monolayer coverages remains unclear, however, it is likely these results have a large influence on the data obtained from other characterisation methods. The highest relative coverages were observed for compounds **66** and **119**, with phosphonic acids **59**, **62** and **94** displaying significantly lower coverages. The differences observed in the surface coverages of pentafluorophenyl terminated derivatives **59** and **119** likely explains the preferential surface energy and work function values obtained for **119** over **59**, considering the difference in calculated surface dipole moment.

The use of PM-IRRAS allowed for an in-depth surface study of the planar SAMs, providing a large quantity of data for molecules that have previously been unreported in the literature. For certain compounds, analysis of spectra were aided by DFT simulated

IR spectra and computational peak fitting, both of which were provided by the SONY Corporation. Analysis of spectra obtained for the three non-fluorinated aromatic compounds **60**, **92** and **93** was supported by data from SAMs of the equivalent thiols on gold. However, the presence of a large absorption band in all spectra recorded at low frequency, due to Al–O bond vibrations, prevented a more thorough determination of binding modes between the phosphonic acid anchor groups and AlO_x surfaces.

Of all the phosphonic acids studied, reported literature studies of PM-IRRAS data exist only for dodecylphosphonic acid **160**. At low frequencies, no bands besides that due to Al–O vibrations were observed. Previous reports suggest that an absence of stretching due to the phosphoryl bond (P=O) is indicative of tridentate binding, however, we do not believe that the absence of a specific band in a PM-IRRAS spectrum can be used to categorically assign binding modes due to the surface selection rule. For phosphonic acid **66**, comparison with a DFT simulated IR spectrum led to the tentative assignment of a P=O stretch within the related PM-IRRAS spectrum of the SAM of **66**. This result implies the lack of binding to the AlO_x surface through the phosphoryl oxygen however, as for **160**, no definitive conclusions can be drawn due to the possibility of multiple binding modes being present within the SAM. A potential combination of binding modes for a SAM of **66** would clarify the unusual contact angle and surface energy data obtained for **66**.

Comparison of the PM-IRRAS spectra obtained for the phosphonic acids studied led to a number of general assignments for certain, common vibrations in both the low and high frequency spectra. For all targets, except the long chain hydrocarbon **160**, vibrations observed around 1500 cm⁻¹ are assigned as aromatic C=C ring stretches, with the number of bands observed dependent upon the nature of the carbon skeleton. For compounds possessing a methoxy substituent, symmetric stretching of the ether functionality was assigned in the region 1200-1250 cm⁻¹. Although many of the compounds studied possessed a fluorine substituent, C–F bond stretches were only observable for compounds **59**, **119** and **120**, with the positioning of this band variable. For **59** and **119**, this C–F transition dipole was assigned to the *para*-fluorine substituent, confirmed by DFT IR spectra. The C–F bond vibration observable for **120** rationalises the surface energy and contact angles recorded for this particular SAM.

Within the high frequency spectra acquired, a general assignment of the $\nu_s\text{CH}_2$ band for benzyl systems is made at $\sim 2850\text{ cm}^{-1}$, with the positioning of this band seemingly unaffected by the nature of the attached aromatic ring. The related asymmetric stretch for all benzylic compounds is assigned to be at $\sim 2920\text{ cm}^{-1}$. For those compounds with a terminal methoxyl group, the $\nu_a\text{CH}_3$ of the methyl group is assigned at $\sim 3000\text{ cm}^{-1}$ with the related $\nu_s\text{CH}_3$ band overlapping with the symmetric methylene stretch at 2850 cm^{-1} . Also observable for the majority of methoxylated targets is a band at $\sim 2950\text{ cm}^{-1}$ which, aided by the DFT simulated IR spectrum of **120**, has been assigned as an alternative asymmetric vibration of the methyl group. For phosphonic acids **92**, **93** and **94**, the prominent peak observed at a frequency greater than 3000 cm^{-1} is assigned to an aryl C–H stretch. For compound **93** in particular, like for **120**, this stretch is indicative of a molecular tilt within the SAM due to the surface selection rule.

Following PM-IRRAS studies, XPS was utilised to confirm SAM adsorption upon AlO_x surfaces, and to determine relative surface coverages of the phosphonic acids studied. The primary aim of this research was the use of fluorinated benzylphosphonic acid derivatives to modify the work function of AlO_x . Low intensity XPS provided the work function values for the modified AlO_x surfaces, with the phosphonic acids studied shown to modify the work function over a total range of 0.92 eV.

The general trend of the results obtained from the work function study clarified the prediction that a net-positive surface dipole would decrease the work function, with an increase observed for surfaces possessing a net-negative dipole moment. Of the compounds investigated, both **59** and **119** increased the work function of AlO_x due to a terminal pentafluorophenyl moiety creating a negative dipole pointing away from the surface. From the surface dipole calculated for **59** a larger increase may be expected, however, a low surface coverage was calculated for the SAM which could affect the true dipole created at the surface. In contrast to the terminal fluorine substituted phosphonic acids **59** and **119**, *ortho* disubstituted **66** induced the largest decrease in work function of the benzylphosphonic acid derivatives. Positioning the fluorine substituents close to the benzylic functionality directs the negative end of the dipole towards the surface creating a net positive dipole, and favouring a decrease in work function.

In summary, a range of fluorinated benzyl- and biphenyl benzylphosphonic acid derivatives have been shown to effectively alter the surface energy and work function of AlO_x , upon adsorption from solution to form a self-assembled monolayer. Phosphonic acids displaying both an Acceptor–Donor–Anchor and Donor–Acceptor–Anchor structure, with varying degrees of fluorination and a broad range of calculated surface dipoles, were investigated. The work function of AlO_x was successfully tuned over a broad range, with fluorinated phosphonic acids capable of both increasing and decreasing the work function depending on the degree and positioning of fluorination.

Applications of these systems (Figure 52) on AlO_x in OLEDs and OTFTs are ongoing within the SONY Corporation.

5.6 References to Chapter 5

- (1) Kim, J.; Friend, R.; Cacialli, F. *J. Appl. Phys.* **1999**, *86*, 2774–2778.
- (2) Aswal, D.; Lenfant, S.; Guerin, D.; Yakhmi, J.; Vuillaume, D. *Anal. Chim. Acta* **2006**, *568*, 84–108.
- (3) Kim, J.; Friend, R.; Cacialli, F. *Synth. Met.* **2000**, *111*, 369–372.
- (4) Paniagua, S. A.; Hotchkiss, P. J.; Jones, S. C.; Marder, S. R.; Mudalige, A.; Marrikar, F. S.; Pemberton, J. E.; Armstrong, N. R. *J. Phys. Chem. C* **2008**, *112*, 7809–7817.
- (5) Frey, B. L.; Corn, R. M.; Weibel, S. C. *Handbook of Vibrational Spectroscopy*; John Wiley & Son Inc., **2001**.
- (6) Buffeteau, T.; Desbat, B.; Turllet, J. *Appl. Spectrosc.* **1991**, *45*, 380–389.
- (7) Yates Jr, J. T.; Madey, T. E. **1987**.
- (8) Golden, W. G.; Saperstein, D. D.; Severson, M. W.; Overend, J. *J. Phys. Chem.* **1984**, *88*, 574–580.
- (9) Somasundaran, P. *Encyclopedia of Surface and Colloid Science, Volume 1*; CRC Press, 2006.
- (10) Rivière, J. C.; Myhra, S. *Handbook of Surface and Interface Analysis: Methods for Problem-solving*; CRC Press, 2010.
- (11) Hanson, E. L.; Schwartz, J.; Nickel, B.; Koch, N.; Danisman, M. F. *J. Am. Chem. Soc.* **2003**, *125*, 16074–16080.
- (12) Hattori, T.; Ruzyllo, J.; Novak, R.; Mertens, P.; Besson, P. *Cleaning and Surface Conditions Technology in Semiconductor Device Manufacturing 11: ECS Transactions: Volume 25*; 2009.
- (13) Complete wetting is defined as a contact angle with water of 10° or less.
- (14) Lee, J.; Jung, B.-J.; Lee, J.-I.; Chu, H. Y.; Do, L.-M.; Shim, H.-K. *J. Mater. Chem.* **2002**, *12*, 3494–3498.
- (15) O'Hagan, D. *Chem. Soc. Rev.* **2008**, *37*, 308–319.
- (16) Kraft, U.; Zschieschang, U.; Ante, F.; Kälblein, D.; Kamella, C.; Amsharov, K.; Jansen, M.; Kern, K.; Weber, E.; Klauk, H. *J. Mater. Chem.* **2010**, *20*, 6416–6418.
- (17) Strong, L.; Whitesides, G. M. *Langmuir* **1988**, *4*, 546–558.
- (18) Hotchkiss, P. J.; Li, H.; Paramonov, P. B.; Paniagua, S. A.; Jones, S. C.; Armstrong, N. R.; Brédas, J.-L.; Marder, S. R. *Adv. Mater.* **2009**, *21*, 4496–4501.

- (19) Feichtenschlager, B.; Pabisch, S.; Peterlik, H.; Kickelbick, G. *Langmuir* **2012**, *28*, 741–750.
- (20) Maege, I.; Jaehne, E.; Henke, A.; Adler, H.-J. P.; Bram, C.; Jung, C.; Stratmann, M. *Prog. Org. Coat.* **1998**, *34*, 1–12.
- (21) Gao, W.; Dickinson, L.; Grozinger, C.; Morin, F. G.; Reven, L. *Langmuir* **1996**, *12*, 6429–6435.
- (22) Brodard-Severac, F.; Guerrero, G.; Maquet, J.; Florian, P.; Gervais, C.; Mutin, P. H. *Chem. Mater.* **2008**, *20*, 5191–5196.
- (23) Spori, D. M.; Venkataraman, N. V.; Tosatti, S. G.; Durmaz, F.; Spencer, N. D.; Zürcher, S. *Langmuir* **2007**, *23*, 8053–8060.
- (24) Tao, Y.-T.; Wu, C.-C.; Eu, J.-Y.; Lin, W.-L.; Wu, K.-C.; Chen, C. *Langmuir* **1997**, *13*, 4018–4023.
- (25) Silverstein, R.; Webster, F. *Spectrometric Identification of Organic Compounds*; John Wiley & Son Inc., 2006.
- (26) Jang, S.; Park, J.; Shin, S.; Yoon, C.; Choi, B. K.; Gong, M.; Joo, S.-W. *Langmuir* **2004**, *20*, 1922–1927.
- (27) Hotchkiss, P. J.; Jones, S. C.; Paniagua, S. A.; Sharma, A.; Kippelen, B.; Armstrong, N. R.; Marder, S. R. *Acc. Chem. Res.* **2012**, *45*, 337–346.
- (28) Hotchkiss, P. J.; Malicki, M.; Giordano, A. J.; Armstrong, N. R.; Marder, S. R. *J. Mater. Chem.* **2011**, *21*, 3107–3112.
- (29) De La Pierre, M.; Orlando, R.; Maschio, L.; Doll, K.; Ugliengo, P.; Dovesi, R. *J. Comput. Chem.* **2011**, *32*, 1775–1784.
- (30) Holland, G. P.; Sharma, R.; Agola, J. O.; Amin, S.; Solomon, V. C.; Singh, P.; Buttry, D. A.; Yarger, J. L. *Chem. Mater.* **2007**, *19*, 2519–2526.
- (31) Coates, J. *Interpretation of Infrared Spectra, A Practical Approach*; John Wiley & Son Inc., 2000.
- (32) Braun, S.; Salaneck, W. R.; Fahlman, M. *Adv. Mater.* **2009**, *21*, 1450–1472.

Chapter 6

Experimental

6.1 General

NMR Spectroscopy: Proton, carbon, fluorine and phosphorous nuclear magnetic resonance spectra (^1H NMR, ^{13}C NMR, ^{19}F NMR and ^{31}P NMR) were recorded on a Varian Inova-600 (^1H NMR, 600 MHz; ^{13}C NMR, 151 MHz; ^{19}F NMR, 564 MHz; ^{31}P NMR 243 MHz), a Varian DD-700 (^1H NMR, 700 MHz; ^{13}C NMR, 176 MHz; ^{19}F NMR, 658 MHz; ^{31}P NMR, 283 MHz) or a Varian 400 (^1H NMR, 400 MHz; ^{19}F NMR, 376 MHz; ^{31}P NMR, 162 MHz) spectrometer with solvent resonance as the internal standard (^1H NMR, CHCl_3 at 7.26 ppm; ^{19}F NMR, CFCl_3 at 0.00 ppm). ^1H , ^{13}C , ^{19}F and ^{31}P spectroscopic data are reported as follows: chemical shift, integration, multiplicity (s = singlet, d = doublet, t = triplet, m = multiplet), coupling constant (Hz) and assignment.

Mass Spectrometry: GC-MS analysis was performed on a Trace GC-MS device (Thermo-Finnigan Corporation) operating in electron impact ionisation (EI^+) mode and accurate mass analysis was achieved with a Xevo QtoF mass spectrometer (Waters Ltd, UK) equipped with an accurate solids analysis probe (ASAP).

Elemental Analysis: C, H and N analyses were collected with an Exeter Analytical CE-440 Elemental Analyser.

Melting Points Analysis: Melting points were measured in open-ended capillaries using either a Gallenkamp melting point apparatus or a Stuart Scientific SMP3 melting point apparatus at a ramping rate of 5 °C/min. All melting points were recorded at atmospheric pressure and are uncorrected.

Microwave: All microwave irradiated reactions were heated in a Biotage InitiatorTM Sixty microwave.

Chemicals and Solvents: Unless otherwise stated, commercially available reagents were used without purification. An Innovative Technology Inc. Solvent Purification System fitted with a Metrohm 831 Karl Fischer Coulometric Titrator was used to dry MeCN, DMF, THF and toluene whilst anhydrous DMSO was purchased from Sigma Aldrich. Hexane and DCM were purchased from Fischer and used without further purification. Flash column chromatography was carried out using Fluorochem Silicagel LC60A (40-63 micron).

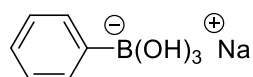
6.2 Experimental Data to Chapter 2

6.2.1 Synthesis of Sodium Phenyl Borate Salts

General Procedure for the Synthesis of Sodium Phenyl Borate Salts

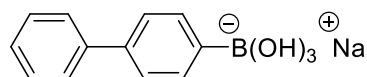
Sodium hydroxide was dissolved in the minimum amount of water and the resulting solution added drop-wise to a saturated solution of the aryl boronic acid in toluene, until the precipitation of the sodium borate salt was complete. The precipitate was filtered, washed with copious quantities of toluene, ground to a fine powder and thoroughly dried *in vacuo* to yield the sodium phenyl borate salt, which was used without further purification.

Sodium Trihydroxy(phenyl)borate, 35



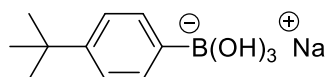
Phenylboronic acid (2.650 g, 21.7 mmol), toluene (500 mL) and NaOH (0.908 g, 22.7 mmol) at 35 °C gave *sodium trihydroxy(phenyl)borate* (3.01 g, 86 %) as a white solid which had a melting point in excess of 350 °C.

Sodium (4-Biphenyl)trihydroxyborate, 40



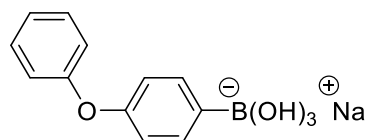
4-Biphenylboronic acid (0.500 g, 2.52 mmol), toluene (175 mL) and NaOH (0.101 g, 2.53 mmol) at 58 °C gave *sodium (4-biphenyl)trihydroxyborate* (0.57 g, 95 %) as a white solid which had a melting point in excess of 350 °C.

Sodium (4-Tert-butylphenyl)trihydroxyborate, 41



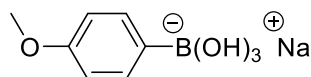
4-Tert-butylphenylboronic acid (0.500 g, 2.81 mmol), toluene (175 mL) and NaOH (0.112 g, 2.80 mmol) at 58 °C gave *sodium (4-tert-butylphenyl)trihydroxyborate* (0.47 g, 77 %) as a white solid which had a melting point in excess of 350 °C.

Sodium Trihydroxy(4-phenoxyphenyl)borate, 42

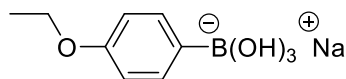


4-Phenoxyphenylboronic acid (0.400 g, 1.87 mmol), toluene (175 mL) and NaOH (0.075 g, 1.88 mmol) at 58 °C gave *sodium trihydroxy(4-phenoxyphenyl)borate* (0.40 g, 84 %) as a white solid which had a melting point in excess of 350 °C.

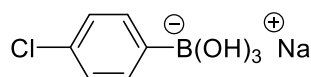
Sodium Trihydroxy(4-methoxyphenyl)borate, 43



4-Methoxyphenylboronic acid (0.500 g, 3.29 mmol), toluene (175 mL) and NaOH (0.132 g, 3.30 mmol) at 58 °C gave *sodium trihydroxy(4-methoxyphenyl)borate* (0.52 g, 82 %) as a white solid which had a melting point in excess of 350 °C.

Sodium (4-Ethoxyphenyl)trihydroxyborate, 44

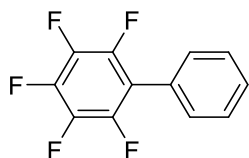
4-Ethoxyphenylboronic acid (0.500 g, 3.00 mmol), toluene (150 mL) and NaOH (0.120 g, 3.00 mmol) at 50 °C gave *sodium (4-ethoxyphenyl)trihydroxyborate* (0.50 g, 81 %) as a white solid which had a melting point in excess of 350 °C.

Sodium (4-Chlorophenyl)trihydroxyborate, 45

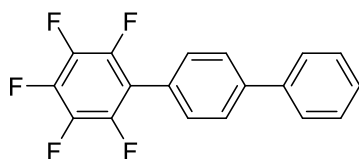
4-Chlorophenylboronic acid (5.00 g, 32.0 mmol), toluene (1000 mL) and NaOH (1.280 g, 32.0 mmol) at 58 °C gave *sodium (4-chlorophenyl)trihydroxyborate* (4.73 g, 71 %) as a white solid which had a melting point in excess of 350 °C.

6.2.2 Synthesis of Pentafluorobiphenyl Derivatives**General Cross-Coupling Procedure Using Sodium Phenyl Borate Salts**

$\text{Pd}(\text{PPh}_3)_4$ and the relevant sodium borate salt were charged into a flame dried microwave vial which was sealed, evacuated and back-filled with argon to create an inert atmosphere. Dry, degassed toluene and bromopentafluorobenzene were added in sequence to the microwave vial using a syringe and the reaction vessel heated to 120 °C under microwave irradiation. The reaction mixture was cooled and filtered through silica gel with acetone as the eluent to remove inorganic and particulate material. Volatile material was removed from the filtrate *in vacuo*, and the crude product extracted with NaOH solution and ethyl acetate, dried (MgSO_4) and purified by column chromatography on silica gel to give the biphenyl derivative.

2,3,4,5,6-Pentafluorobiphenyl, 7

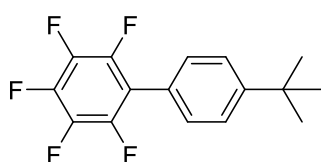
Pd(PPh₃)₄ (0.231 g, 0.20 mmol), sodium trihydroxy(phenyl)borate (0.356 g, 2.20 mmol), bromopentafluorobenzene (0.25 mL, 2.00 mmol) and dry, degassed toluene (3 mL), after 3 hours and column chromatography on silica gel using hexane as the eluent, afforded 2,3,4,5,6-pentafluorobiphenyl (0.29 g, 60 %) as a white solid; mp 106-108 °C [lit¹ 110-112 °C]; Anal. Calcd for C₁₂H₅F₅: C, 59.03; H, 2.06. Found: C, 58.75; H, 2.18; HRMS-ASAP *m/z*: [M⁺] calcd for C₁₂H₅F₅ 244.0311; found 244.0306; GC-MS *m/z* (% relative intensity, ion): 244 (100, [M]⁺), 224 (29), 28 (26); IR (cm⁻¹): 1527, 1485; ¹H NMR (600 MHz, CDCl₃): δ 7.40-7.44 (2H, m, Ar-*H*), 7.44-7.53 (3H, m, Ar-*H*); ¹³C NMR (176 MHz, CDCl₃): δ 116.3 (td, ²J_{CF} 17.3, ⁴J_{CF} 3.8, 1-*C*), 126.8 (s, 1'-*C*), 129.1 (s, Ar-CH), 129.6 (s, Ar-CH), 130.5 (s, Ar-CH), 138.2 (dm, ¹J_{CF} 250.8, Ar-CF), 140.7 (dt, ¹J_{CF} 250.8, ²J_{CF} 13.3, ³J_{CF} 4.9, 4-*C*), 144.5 (dm, ¹J_{CF} 247.6, Ar-CF); ¹⁹F NMR (564 MHz, CDCl₃/CFCl₃): δ -143.7- -143.9 (2F, m, 2-*F*, 6-*F*), -156.2 (1F, t, ³J_{FF} 21.0, 4-*F*), -162.7- -162.9 (2F, m, 3-*F*, 5-*F*); data in agreement with literature.¹

4'-Phenyl-2,3,4,5,6-pentafluorobiphenyl, 47

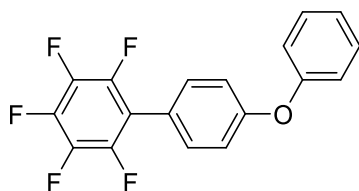
Pd(PPh₃)₄ (0.132 g, 0.11 mmol), sodium (4-biphenyl)trihydroxyborate (0.200 g, 0.84 mmol), bromopentafluorobenzene (0.10 mL, 0.80 mmol) and dry, degassed toluene (1.5 mL), after 10 hours and column chromatography on silica gel using hexane as the eluent, afforded 4'-phenyl-2,3,4,5,6-pentafluorobiphenyl (0.038 g, 16 %) as a white solid; mp 182-184 °C [lit² 193-194 °C]; HRMS-ASAP *m/z*: [M⁺] calcd for C₁₈H₉F₅ 320.0624; found 320.0631; GC-MS *m/z* (% relative intensity, ion): 320 (100, [M]⁺), 160 (23); IR (cm⁻¹): 1513, 1485; ¹H NMR (600 MHz, CDCl₃): δ 7.37-7.42 (1H, m, 4''-*H*),

7.45-7.54 (4H, m, Ar-H), 7.62-7.66 (2H, m, Ar-H), 7.70-7.74 (2H, m, Ar-H); ^{13}C NMR (176 MHz, CDCl_3): δ 116.0 (td, $^2J_{\text{CF}}$ 16.8, $^4J_{\text{CF}}$ 3.4, 1-C), 125.6 (s, Ar-C), 127.5 (s, Ar-CH), 127.8 (s, Ar-CH), 128.2 (s, Ar-CH), 129.3 (s, Ar-CH), 130.9 (s, Ar-CH), 138.3 (dm, $^1J_{\text{CF}}$ 251.9, Ar-CF), 140.5 (s, Ar-C), 140.7 (dm, $^1J_{\text{CF}}$ 254.0, Ar-CF), 142.6 (s, Ar-C), 144.6 (dm, $^1J_{\text{CF}}$ 247.5, Ar-CF); ^{19}F NMR (564 MHz, $\text{CDCl}_3/\text{CFCl}_3$): δ -143.6- -143.7 (2F, m, 2-F, 6-F), -156.1 (1F, t, $^3J_{\text{FF}}$ 21.0, 4-F), -162.6- -162.8 (2F, m, 3-F, 5-F); data in agreement with literature.²

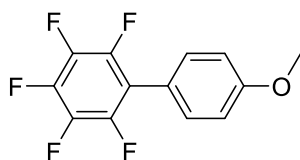
4'-*Tert*-butyl-2,3,4,5,6-pentafluorobiphenyl, 48



$\text{Pd}(\text{PPh}_3)_4$ (0.145 g, 0.13 mmol), sodium (4-*tert*-butylphenyl)trihydroxyborate (0.200 g, 0.92 mmol), bromopentafluorobenzene (0.10 mL, 0.83 mmol) and dry, degassed toluene (1.5 mL), after 8 hours and column chromatography on silica gel using hexane as the eluent, afforded 4'-*tert*-butyl-2,3,4,5,6-pentafluorobiphenyl (0.095 g, 38 %) as a white solid; mp 80-82 °C; HRMS-ASAP m/z : $[\text{M}^+]$ calcd for $\text{C}_{16}\text{H}_{13}\text{F}_5$ 300.0937; found 300.0928; GC-MS m/z (% relative intensity, ion): 300 (45, $[\text{M}]^+$), 285 (100), 257 (60), 129 (51), 41 (53); IR (cm^{-1}): 2970, 1488; ^1H NMR (600 MHz, CDCl_3): δ 1.37 (9H, s, CH_3), 7.35-7.38 (2H, m, Ar-H), 7.48-7.54 (2H, m, Ar-H); ^{13}C NMR (176 MHz, CDCl_3): δ 31.6 (s, C-(CH_3)₃), 35.2 (s, C-(CH_3)₃), 116.3 (td, $^2J_{\text{CF}}$ 17.1, $^4J_{\text{CF}}$ 3.6, 1-C), 123.8 (s, 1'-C), 126.1 (s, Ar-CH), 130.2 (s, Ar-CH), 138.2 (dm, $^1J_{\text{CF}}$ 250.5, Ar-CF), 140.5 (dm, $^1J_{\text{CF}}$ 253.2, Ar-CF), 144.6 (dm, $^1J_{\text{CF}}$ 247.2, Ar-CF), 152.8 (s, 4'-C); ^{19}F NMR (564 MHz, $\text{CDCl}_3/\text{CFCl}_3$): δ -143.8- -144.0 (2F, m, 2-F, 6-F), -156.7 (1F, t, $^3J_{\text{FF}}$ 21.0, 4-F), -162.9- -163.1 (2F, m, 3-F, 5-F).

2,3,4,5,6-Pentafluoro-4'-phenoxybiphenyl, 49

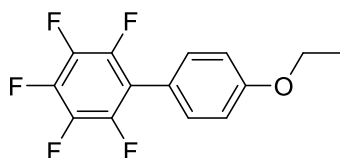
Pd(PPh₃)₄ (0.124 g, 0.11 mmol), sodium trihydroxy(4-phenoxyphenyl)borate (0.200 g, 0.79 mmol), bromopentafluorobenzene (0.09 mL, 0.72 mmol) and dry, degassed toluene (1.5 mL), after 12 hours and column chromatography on silica gel using hexane and DCM (9:1) as the eluent, afforded a white solid. GC-MS analysis of the acquired solid revealed an inseparable mixture of the desired product *2,3,4,5,6-pentafluoro-4'-phenoxybiphenyl*; ¹⁹F NMR (564 MHz, CDCl₃/CFCl₃): δ -143.8- -144.0 (2F, m, 2-*F*, 6-*F*), -156.4 (1F, t, ³J_{FF} 21.0, 4-*F*), -162.6- -162.9 (2F, m, 3-*F*, 5-*F*); and deborylated boronic acid.

2,3,4,5,6-Pentafluoro-4'-methoxybiphenyl, 50

Pd(PPh₃)₄ (0.164 g, 0.14 mmol), sodium trihydroxy(4-methoxyphenyl)borate (0.200 g, 1.04 mmol), bromopentafluorobenzene (0.12 mL, 0.95 mmol) and dry, degassed toluene (1.5 mL), after 9 hours and column chromatography on silica gel using hexane and ethyl acetate (4:1) as the eluent, afforded *2,3,4,5,6-pentafluoro-4'-methoxybiphenyl* (0.075 g, 28 %) as a white solid; mp 117-119 °C [lit³ 116-118 °C]; HRMS-ASAP *m/z*: [M⁺] calcd for C₁₃H₇F₅O 274.0417; found 274.0419; GC-MS *m/z* (% relative intensity, ion): 274 (98, [M]⁺), 259 (73), 231 (100), 205 (86); IR (cm⁻¹): 1607, 1484; ¹H NMR (600 MHz, CDCl₃): δ 3.87 (3H, s, CH₃), 6.98-7.06 (2H, m, 3'-*H*, 5'-*H*), 7.32-7.40 (2H, m, 2'-*H*, 6'-*H*); ¹³C NMR (176 MHz, CDCl₃): δ 55.7 (s, CH₃), 114.6 (s, Ar-CH), 116.1 (td, ²J_{CF} 17.0, ⁴J_{CF} 3.7, 1-C), 118.7 (s, 1'-C), 131.8 (s, Ar-CH), 138.2 (dm, ¹J_{CF} 250.1, Ar-CF), 140.4 (dt, ¹J_{CF} 253.1, ²J_{CF} 13.6, ³J_{CF} 5.3, 4-C), 144.5 (dm, ¹J_{CF} 246.7, Ar-CF), 160.6 (s,

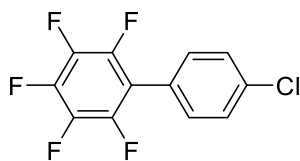
4'-C) ; ^{19}F NMR (564 MHz, $\text{CDCl}_3/\text{CFCl}_3$): δ -144.1- -144.3 (2F, m, 2-F, 6-F), -157.0 (1F, t, $^3J_{\text{FF}}$ 21.0, 4-F), -163.0- -163.2 (2F, m, 3-F, 5-F); data in agreement with literature.³

4'-Ethoxy-2,3,4,5,6-pentafluorobiphenyl, 51



$\text{Pd}(\text{PPh}_3)_4$ (0.153 g, 0.13 mmol), sodium (4-ethoxyphenyl)trihydroxyborate (0.200 g, 0.97 mmol), bromopentafluorobenzene (0.11 mL, 0.88 mmol) and dry, degassed toluene (1.5 mL), after 6.5 hours and column chromatography on silica gel using hexane and ethyl acetate (9:1) as the eluent, afforded a white solid. GC-MS analysis of the acquired solid revealed an inseparable mixture of the desired product *4'-ethoxy-2,3,4,5,6-pentafluorobiphenyl*; ^1H NMR (600 MHz, CDCl_3): δ 1.45 (3H, t, $^3J_{\text{HH}}$ 7.0, CH_3), 4.09 (2H, q, $^3J_{\text{HH}}$ 7.0, CH_2), 6.97-7.05 (2H, m, Ar-H), 7.32-7.38 (2H, m, Ar-H); ^{19}F NMR (564 MHz, $\text{CDCl}_3/\text{CFCl}_3$): δ -144.1- -144.3 (2F, m, 2-F, 6-F), -157.2 (1F, t, $^3J_{\text{FF}}$ 21.0, 4-F), -163.0- -163.2 (2F, m, 3-F, 5-F); and triphenylphosphine and triphenylphosphine oxide.

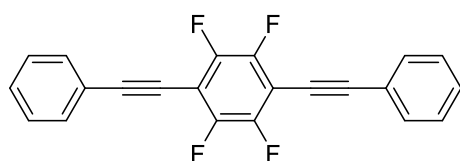
4'-Chloro-2,3,4,5,6-pentafluorobiphenyl, 52



$\text{Pd}(\text{PPh}_3)_4$ (0.160 g, 0.14 mmol), sodium (4-chlorophenyl)trihydroxyborate (0.200 g, 1.02 mmol), bromopentafluorobenzene (0.12 mL, 0.93 mmol) and dry, degassed toluene (2 mL), after 6 hours and column chromatography on silica gel using hexane as the eluent, afforded *4'-tert-butyl-2,3,4,5,6-pentafluorobiphenyl* (0.096 g, 37 %) as a white solid.

Method B: In a flame dried flask, under an inert atmosphere, sodium (4-chlorophenyl)trihydroxyborate (4.19 g, 21.3 mmol) and Pd(PPh₃)₄ (2.24 g, 1.94 mmol) were added to dry, degassed toluene (30 mL). Bromopentafluorobenzene (2.42 mL, 19.4 mmol) was added and the resulting solution was heated to reflux for 48 hours. The reaction mixture was cooled and filtered through a silica plug with toluene as the eluent to remove inorganic and particulate material. Volatile material was removed *in vacuo* and the crude organic products extracted with NaOH solution (2M, 100 mL) and DCM (3 × 50 mL). The combined extracts were washed with water (100 mL) and dried (MgSO₄). The mixture was filtered and the solvent removed *in vacuo*. Column chromatography using silica gel with hexane and DCM (4:1) as the eluent afforded 4'-chloro-2,3,4,5,6-pentafluorobiphenyl (3.24 g, 60 %) as a white solid; mp 85-87 °C [lit⁴ 83-84 °C]; HRMS-ASAP *m/z*: [M⁺] calcd for C₁₂H₄F₅Cl 277.9922; found 277.9924; GC-MS *m/z* (% relative intensity, ion): 278 (99, [M]⁺), 242 (97), 223 (100), 192 (91), 139 (49); IR (cm⁻¹): 1657, 1527, 1485; ¹H NMR (600 MHz, CDCl₃): δ 7.34-7.39 (2H, m, Ar-H), 7.46-7.50 (2H, m, Ar-H); ¹³C NMR (151 MHz, CDCl₃): δ 115.2 (td, ²J_{CF} 16.9, ⁴J_{CF} 3.9, 1-C), 125.1 (s, 1'-C), 129.4 (s, Ar-CH), 131.8 (s, Ar-CH), 136.0 (s, 4'-C), 138.3 (dm, ¹J_{CF} 253.2, Ar-CF), 141.0 (dt, ¹J_{CF} 256.6, ²J_{CF} 13.5, ³J_{CF} 5.1, 4-C), 144.4 (dm, ¹J_{CF} 252.0, Ar-CF); ¹⁹F NMR (564 MHz, CDCl₃/CFCl₃): δ -143.5- -143.8 (2F, m, 2-F, 6-F), -155.3 (1F, t, ³J_{FF} 21.0, 4-F), -162.2- -162.4 (2F, m, 3-F, 5-F); data in agreement with literature.⁵

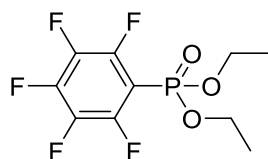
1,2,4,5-Tetrafluoro-3,6-bis(phenylethynyl)benzene, 53



In a flame dried flask, under an inert atmosphere, phenylacetylene (0.30 mL, 2.69 mmol) was added to dry, degassed THF (~ 30 mL) and cooled to - 78 °C. A 1.6 M solution of *n*-BuLi in hexanes (1.68 mL, 2.69 mmol) was then added drop-wise and the solution left stirring for 20 minutes. This solution was then added drop-wise to hexafluorobenzene (0.62 mL, 5.37 mmol), under an inert atmosphere, at - 78 °C and stirred for 17 hours whilst warming to room temperature. Volatile material was removed

in vacuo and the remaining solution poured on to water (100 mL) and extracted with DCM (3 × 50 mL). The combined extracts were washed with water (100 mL) and dried (MgSO₄). The mixture was filtered and the solvent removed *in vacuo*. Column chromatography using silica gel and hexane as the eluent afforded *1,2,4,5-tetrafluoro-3,6-bis(phenylethynyl)benzene* (0.12 g, 25 %) as a yellow solid; mp 179-181 °C [lit⁴ 181-183 °C]; Anal. Calcd for C₂₂H₁₀F₄: C, 75.43; H, 2.88. Found: C, 75.25; H, 2.91; HRMS-ASAP *m/z*: [M⁺] calcd for C₂₂H₁₀F₄ 350.0719; found 350.0710; GC-MS *m/z* (% relative intensity, ion): 350 (100, [M]⁺), 175 (70); IR (cm⁻¹): 2226, 1484; ¹H NMR (600 MHz, CDCl₃): δ 7.37-7.45 (6H, m, 3'-H, 4'-H, 5'-H), 7.61 (4H, dd, ³J_{HH} 8.0, ⁴J_{HH} 1.6, 2'-H, 6'-H); ¹³C NMR (176 MHz, CDCl₃): δ 75.0 (s, C≡CPh), 103.4 (s, C≡CPh), 104.9-105.4 (m, 3-C, 6-C), 122.0 (s, 1'-C), 128.9 (s, Ar-CH), 130.0 (s, Ar-CH), 132.3 (s, Ar-CH), 146.9 (dm, ¹J_{CF} 252.2, 1-C, 2-C, 4-C, 5-C); ¹⁹F NMR (564 MHz, CDCl₃/CFCl₃): δ -137.8 (s); data in agreement with literature.⁶

Diethyl Perfluorophenylphosphonate, 57



Method A: Triethyl phosphite (3.00 mL, 17.5 mmol) was added dropwise to hexafluorobenzene (2.00 mL, 17.5 mmol) in dry, degassed toluene (15 mL) under an inert atmosphere of dry argon. The reaction mixture was heated and stirred at 100 °C for 45 minutes, then cooled to room temperature. ¹⁹F and ³¹P NMR spectroscopy of the crude reaction mixture showed the presence of only starting materials.

Method B: Sodium metal (0.240 g, 10.5 mmol) was charged to a 10–20 mL microwave vial which was sealed, evacuated and back-filled with argon to create an inert atmosphere. Dry, degassed THF (15 mL) and diethyl phosphite (1.50 mL, 11.7 mmol) were added in sequence to the microwave vial using a syringe and the solution was stirred for 2 hours. Once the evolution of hydrogen gas had stopped, hexafluorobenzene (1.10 mL, 9.45 mmol) was added to the microwave vial using a syringe and the reaction vessel heated to 130 °C for 30 minutes under microwave irradiation. The reaction mixture was cooled, poured on to water (20 mL) and extracted with diethyl ether (3 × 15

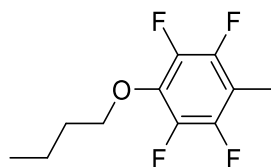
mL). The combined extracts were washed with water (20 mL) and dried (MgSO_4). The mixture was filtered and the solvent removed *in vacuo*. Distillation of the remaining residue gave a colourless oil, b.p. 93-95 °C / 7.2 mbar.

Method C: 60 % (w/w) sodium hydride in mineral oil (0.93 g, 23.3 mmol) was washed with dry hexane (50 mL) under an inert atmosphere of argon. The hexane/oil solution was removed using a syringe and dry, degassed toluene (20 mL) was added to the clean sodium hydride. Diethyl phosphite (3.00 mL, 23.3 mmol) was carefully added to the sodium hydride solution, with stirring, and allowed to stir for a further 2 hours at room temperature. This solution was then cooled to -78 °C. Hexafluorobenzene (2.20 mL, 23.3 mmol) was added to the reaction vessel and stirred at -78 °C for 4 hours before slowly warming to room temperature. ^{19}F and ^{31}P NMR spectroscopy of the crude reaction mixture showed the presence of only starting materials.

6.3 Experimental Data to Chapter 3

6.3.1 Synthesis of Tetrafluorotoluene Derivatives

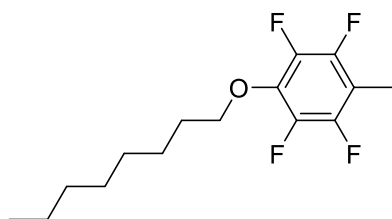
1-Butoxy-2,3,5,6-tetrafluoro-4-methylbenzene, 90



Sodium metal (0.115 g, 5.00 mmol) was added to *n*-Butanol (10 mL) in a 10-20 mL microwave vial and, once the evolution of hydrogen gas had stopped, the vial sealed and purged with argon. Pentafluorotoluene (0.70 mL, 5.50 mmol) was added to the vial using a syringe and the reaction vessel heated to 100 °C for 2 hours under microwave irradiation. The mixture was left to cool, poured on to water (30 ml) and extracted with DCM (3×50 ml). The combined extracts were washed with water (100 ml) and dried (MgSO_4). The mixture was filtered and the solvent removed *in vacuo*. Column chromatography using silica gel with hexane as the eluent afforded *1-butoxy-2,3,5,6-tetrafluoro-4-methylbenzene* (0.87 g) as a colourless oil. The purity of the product was shown to be 83 % by GC-MS; GC-MS *m/z* (% relative intensity, ion): 237 (3, $[\text{M} +$

H]⁺), 236 (21, [M]⁺), 180 (100), 41 (45); ¹H NMR (400 MHz, CDCl₃): δ 0.97 (3H, t, ³J_{HH} 7.4, CH₂CH₃), 1.41-1.55 (2H, m, CH₂), 1.68-1.77 (2H, m, CH₂), 2.20 (3H, t, ⁵J_{HF} 2.1, 4-CH₃), 4.16 (2H, tt, ³J_{HH} 6.6, ⁴J_{HH} 0.9, O-CH₂); ¹⁹F NMR (376 MHz, CDCl₃/CFCl₃): δ -145.3 (2F, dd, ³J_{FF} 21.6, ⁵J_{FF} 9.2, Ar-F), -158.6 (2F, dd, ³J_{FF} 21.6, ⁵J_{FF} 9.2, Ar-F); and was used without further purification.

1-Octoxy-2,3,5,6-tetrafluoro-4-methylbenzene, 91



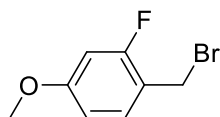
Sodium metal (0.115 g, 5.00 mmol) was added to *n*-Octanol (15 mL) in a 10-20 mL microwave vial and, once the evolution of hydrogen gas had stopped, the vial sealed and purged with argon. Pentafluorotoluene (0.70 mL, 5.50 mmol) was added to the vial using a syringe and the reaction vessel heated to 110 °C for 3 hours under microwave irradiation. The mixture was left to cool, poured on to water (30 ml) and extracted with DCM (3 × 50 ml). The combined extracts were washed with water (100 ml) and dried (MgSO₄). The mixture was filtered and the solvent removed *in vacuo*. Column chromatography using silica gel with hexane as the eluent afforded *1-octoxy-2,3,5,6-tetrafluoro-4-methylbenzene* (1.12 g) as a colourless oil. The purity of the product was shown to be 89 % by ¹⁹F NMR spectroscopy; GC-MS *m/z* (% relative intensity, ion): 293 (3, [M+ H]⁺), 292 (18, [M]⁺), 180 (83), 112 (80), 83 (49), 71 (69), 70 (65), 57 (80), 55 (41), 43 (100), 41 (88); ¹H NMR (400 MHz, CDCl₃): δ 0.84-0.93 (3H, m, CH₂CH₃), 1.20-1.38 (8H, m, CH₂), 1.38-1.51 (2H, m, CH₂), 1.69-1.83 (2H, m, CH₂), 2.20 (3H, t, ⁵J_{HF} 2.1, 4-CH₃), 4.15 (2H, t, ³J_{HH} 6.6, O-CH₂); ¹⁹F NMR (376 MHz, CDCl₃/CFCl₃): δ -145.8 (2F, dd, ³J_{FF} 21.7, ⁵J_{FF} 9.3, Ar-F), -159.1 (2F, dd, ³J_{FF} 21.7, ⁵J_{FF} 9.3, Ar-F); and was used without further purification.

6.3.2 Synthesis of Benzyl Bromide Derivatives

General Wohl-Ziegler Reaction Procedure

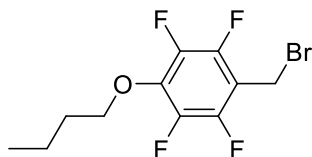
The toluene derivative and AIBN were dissolved in 1,2-dichloroethane, and the mixture heated to reflux. NBS was added slowly and the mixture heated at reflux, with the reaction being monitored by TLC and NMR spectroscopy, before cooling to room temperature. The precipitate was filtered off, washed with 1,2-dichloroethane, and the combined filtrates evaporated *in vacuo*. The crude bromide was purified by either vacuum distillation or column chromatography on silica gel.

2-Fluoro-4-methoxybenzyl Bromide, 73



3-Fluoro-4-methylanisole (4.50 mL, 33.6 mmol), AIBN (0.276 g, 1.68 mmol), NBS (5.30 g, 29.8 mmol) and 1,2-dichloroethane (100 mL), after 3 hours and vacuum distillation, afforded *2-fluoro-4-methoxybenzyl bromide* (3.39g, 52 %) as a light yellow liquid; bp 86-88 °C / 6.6 mbar; GC-MS *m/z* (% relative intensity, ion): 220 (26, [M]⁺), 218 (24, [M]⁺), 139 (100), 95 (84); ¹H NMR (400 MHz, CDCl₃): δ 3.77 (3H, s, O-CH₃), 4.49 (2H, s, CH₂), 6.48-6.68 (2H, m, Ar-H), 7.18-7.31 (1H, m, Ar-H); ¹⁹F NMR (376 MHz, CDCl₃/CFCl₃): δ -114.8- -115.0 (m); data in agreement with literature.⁷

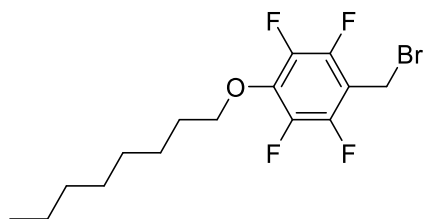
1-(Bromomethyl)-4-butoxy-2,3,5,6-tetrafluorobenzene



1-Butoxy-2,3,5,6-tetrafluoro-4-methylbenzene (0.614 g, 2.60 mmol), AIBN (52 mg, 0.32 mmol), NBS (1.34 g, 7.53 mmol) and 1,2-dichloroethane (25 mL), after 5 hours and column chromatography on silica gel using hexane as the eluent, afforded *1-(bromomethyl)-4-butoxy-2,3,5,6-tetrafluorobenzene* (0.77 g) as a colourless liquid. The

purity of the product was shown to be 79 % by ^{19}F NMR spectroscopy; GC-MS m/z (% relative intensity, ion): 316 (2, $[\text{M}]^+$), 314 (1, $[\text{M}]^+$), 179 (100); ^1H NMR (400 MHz, CDCl_3): δ 0.97 (3H, t, $^3J_{\text{HH}}$ 7.4, CH_3), 1.43-1.57 (2H, m, CH_2CH_2), 1.69-1.81 (2H, m, CH_2CH_2), 4.21-4.27 (2H, m, $\text{O}-\text{CH}_2$), 4.46-4.52 (2H, m, $\text{Ar}-\text{CH}_2$); ^{19}F NMR (376 MHz, $\text{CDCl}_3/\text{CFCl}_3$): δ -144.8- -145.0 (2F, m, $\text{Ar}-\text{F}$), -157.3- -157.5 (2F, m, $\text{Ar}-\text{F}$); and was used without further purification.

1-(Bromomethyl)-4-octoxy-2,3,5,6-tetrafluorobenzene

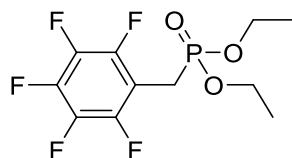


1-Octoxy-2,3,5,6-tetrafluoro-4-methylbenzene (0.943 g, 3.23 mmol), AIBN (0.060 g, 0.37 mmol), NBS (1.55 g, 8.70 mmol) and 1,2-dichloroethane (25 mL), after 5 hours and column chromatography on silica gel using hexane as the eluent, afforded 1-(bromomethyl)-4-octoxy-2,3,5,6-tetrafluorobenzene (0.90 g) as a colourless liquid. The purity of the product was shown to be 84 % by GC-MS; GC-MS m/z (% relative intensity, ion): 372 (2, $[\text{M}]^+$), 370 (2, $[\text{M}]^+$), 179 (100), 71 (7), 57 (84), 43 (86), 74 (70); ^1H NMR (400 MHz, CDCl_3): δ 0.85-0.92 (3H, m, CH_3), 1.22-1.36 (8H, m, CH_2CH_2), 1.40-1.50 (2H, m, CH_2CH_2), 1.72-1.84 (2H, m, CH_2CH_2), 4.24 (2H, t, $^3J_{\text{HH}}$ 6.6, $\text{O}-\text{CH}_2$), 4.50 (2H, t, $^5J_{\text{HF}}$ 1.4, $\text{Ar}-\text{CH}_2$); ^{19}F NMR (376 MHz, $\text{CDCl}_3/\text{CFCl}_3$): δ -144.3- -144.5 (2F, m, $\text{Ar}-\text{F}$), -156.8- -156.9 (2F, m, $\text{Ar}-\text{F}$); and was used without further purification.

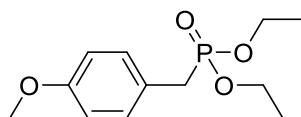
6.3.3 Synthesis of Benzylphosphonate Derivatives

General Michaelis-Arbuzov Procedure

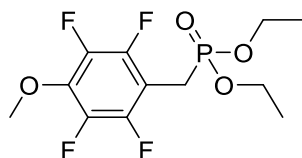
The benzyl bromide was combined with triethylphosphite and the mixture heated and stirred. Excess triethylphosphite and other side products were removed under vacuum, with heating and, where necessary, the desired phosphonate was purified by column chromatography on silica gel.

Diethyl Pentafluorobenzylphosphonate, 70

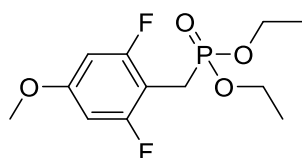
2,3,4,5,6-Pentafluorobenzyl bromide (1.74 mL, 11.5 mmol) and triethylphosphite (1.97 mL, 11.5 mmol), after 4 hours at 160 °C and column chromatography on silica gel using hexane as the eluent, afforded *diethyl pentafluorobenzylphosphonate* (2.56 g, 70 %) as an orange oil; GC-MS m/z (% relative intensity, ion): 318 (54, $[M]^+$), 270 (46), 181 (84), 161 (45), 137 (75), 109 (100), 91 (65), 81 (75), 29 (40); ^1H NMR (400 MHz, CDCl_3): δ 1.25 (6H, t, $^3J_{\text{HH}}$ 7.1, CH_2CH_3), 3.17 (2H, d, $^2J_{\text{HP}}$ 21.2, P- CH_2), 3.99-4.13 (4H, m, CH_2CH_3); ^{19}F NMR (376 MHz, $\text{CDCl}_3/\text{CFCl}_3$): δ -141.8 (2F, m, 2-*F*, 6-*F*), -156.3 (1F, m, 4-*F*), -162.8 (2F, m, 3-*F*, 5-*F*); ^{31}P NMR (162 MHz, CDCl_3): δ 20.4-20.9 (m); data in agreement with literature.⁸

Diethyl 4-Methoxybenzylphosphonate, 68

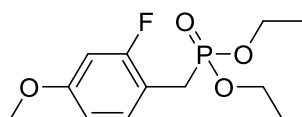
4-Methoxybenzyl bromide (0.36 mL, 2.50 mmol) and triethylphosphite (1.28 mL, 7.46 mmol), after 5 hours at 160 °C and column chromatography on silica gel using ethyl acetate as the eluent, afforded *diethyl 4-methoxybenzylphosphonate* (0.58 g, 90 %) as a clear, light-yellow oil; GC-MS m/z (% relative intensity, ion): 259 ($[M + H]^+$, 100), 258 ($[M]^+$, 94), 231 (96), 230 (52), 203 (70), 121 (100); ^1H NMR (400 MHz, CDCl_3): δ 1.22 (6H, t, $^3J_{\text{HH}}$ 7.1, CH_2CH_3), 3.06 (2H, d, $^2J_{\text{HP}}$ 21.1, P- CH_2), 3.76 (3H, s, O- CH_3), 3.90-4.06 (4H, m, CH_2CH_3), 6.77-6.87 (2H, m, 3-*H*, 5-*H*), 7.15-7.23 (2H, m, 2-*H*, 6-*H*); ^{31}P NMR (162 MHz, CDCl_3): δ 25.9 (s); data in agreement with literature.⁹

Diethyl 2,3,5,6-Tetrafluoro-4-methoxybenzylphosphonate, 75

4-Methoxy-2,3,5,6-tetrafluorobenzyl bromide (0.24 mL, 1.50 mmol) and triethylphosphite (0.45 mL, 2.62 mmol), after 6 hours at 160 °C, afforded *diethyl 2,3,5,6-tetrafluoro-4-methoxybenzylphosphonate* (0.40 g, 81 %) as a yellow oil; ^1H NMR (400 MHz, CDCl_3): δ 1.27 (6H, t, $^3J_{\text{HH}}$ 7.1, CH_2CH_3), 3.16 (2H, d, $^2J_{\text{HP}}$ 21.1, P- CH_2), 4.03 (3H, s, O- CH_3), 4.04-4.14 (4H, m, CH_2CH_3); ^{19}F NMR (376 MHz, $\text{CDCl}_3/\text{CFCl}_3$): δ -143.6- -144.0 (2F, m, Ar- F), -158.4- -158.9 (2F, m, Ar- F); ^{31}P NMR (162 MHz, CDCl_3): δ 21.3-21.6 (m); which was used without further purification.

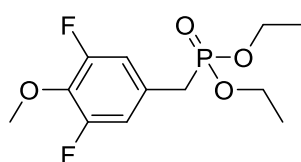
Diethyl 2,6-Difluoro-4-methoxybenzylphosphonate, 76

2,6-Difluoro-4-methoxybenzyl bromide (0.730 g, 3.08 mmol) and triethylphosphite (1.58 mL, 9.21 mmol), after 5 hours at 160 °C, afforded *diethyl 2,6-difluoro-4-methoxybenzylphosphonate* (0.67 g, 74 %) as a yellow oil; ^1H NMR (400 MHz, CDCl_3): δ 1.18-1.10 (6H, m, CH_2CH_3), 3.01 (2H, d, $^2J_{\text{HP}}$ 20.7, P- CH_2), 3.60-3.70 (3H, m, O- CH_3), 3.96-4.07 (4H, m, CH_2CH_3), 6.34 (2H, d, $^3J_{\text{HF}}$ 9.3, 3- H , 5- H); ^{19}F NMR (376 MHz, $\text{CDCl}_3/\text{CFCl}_3$): δ -112.9- -113.4 (m, 2- F , 6- F); ^{31}P NMR (162 MHz, CDCl_3): δ 23.1-23.5 (m); which was used without further purification.

Diethyl 2-Fluoro-4-methoxybenzylphosphonate, 77

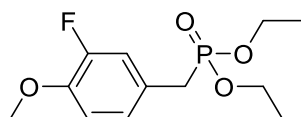
2-Fluoro-4-methoxybenzyl bromide (3.39 g, 15.5 mmol) and triethylphosphite (2.92 mL, 17.0 mmol), after 4 hours at 120 °C, afforded *diethyl 2-fluoro-4-methoxybenzylphosphonate* (3.72 g, 87 %) as a yellow oil; ^1H NMR (400 MHz, CDCl_3): δ 1.16 (6H, t, $^3J_{\text{HH}}$ 7.1, CH_2CH_3), 3.02 (2H, d, $^2J_{\text{HP}}$ 21.0, $\text{P}-\text{CH}_2$), 3.67 (3H, s, $\text{O}-\text{CH}_3$), 3.95 (4H, m, CH_2CH_3), 6.45-6.62 (2H, m, $\text{Ar}-\text{H}$), 7.12-7.21 (1H, m, $\text{Ar}-\text{H}$); ^{19}F NMR (376 MHz, $\text{CDCl}_3/\text{CFCl}_3$): δ -115.4- -115.9 (m); ^{31}P NMR (162 MHz, CDCl_3): δ 24.7 (d, $^4J_{\text{PF}}$ 4.5); which was used without further purification.

Diethyl 3,5-Difluoro-4-methoxybenzylphosphonate, 78



3,5-Difluoro-4-methoxybenzyl bromide (0.450 g, 1.90 mmol) and triethylphosphite (0.36 mL, 2.10 mmol), after 4 hours at 120 °C, afforded *diethyl 3,5-difluoro-4-methoxybenzylphosphonate* (0.37 g, 67 %) as a light yellow oil; ^1H NMR (400 MHz, CDCl_3): δ 1.26 (6H, t, $^3J_{\text{HH}}$ 7.1, CH_2CH_3), 3.02 (2H, d, $^2J_{\text{HP}}$ 21.6, $\text{P}-\text{CH}_2$), 3.95 (3H, s, $\text{O}-\text{CH}_3$), 3.99-4.10 (4H, m, CH_2CH_3), 6.76-6.91 (2H, m, 2-*H*, 6-*H*); ^{19}F NMR (376 MHz, $\text{CDCl}_3/\text{CFCl}_3$): δ -129.1 (d, $^3J_{\text{FH}}$ 8.3, 3-*F*, 5-*F*); ^{31}P NMR (162 MHz, CDCl_3): δ 23.9-24.2 (m); which was used without further purification.

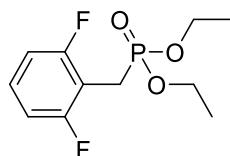
Diethyl 3-Fluoro-4-methoxybenzylphosphonate, 79



3-Fluoro-4-methoxybenzyl bromide (1.00 g, 4.57 mmol) and triethylphosphite (0.86 mL, 5.02 mmol), after 4 hours at 120 °C, afforded *diethyl 3-fluoro-4-methoxybenzylphosphonate* (1.12 g, 89 %) as a yellow oil; ^1H NMR (400 MHz, CDCl_3): δ 1.23 (6H, t, $^3J_{\text{HH}}$ 7.1, CH_2CH_3), 3.04 (2H, d, $^2J_{\text{HP}}$ 21.3, $\text{P}-\text{CH}_2$), 3.84 (3H, s, $\text{O}-\text{CH}_3$), 3.92-4.06 (4H, m, CH_2CH_3), 6.83-6.93 (1H, m, $\text{Ar}-\text{H}$), 6.94-7.07 (2H, m, $\text{Ar}-\text{H}$); ^{19}F

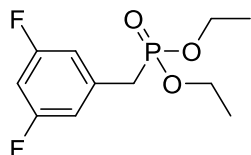
NMR (376 MHz, $\text{CDCl}_3/\text{CFCl}_3$): δ -135.7 (bt, $^3J_{\text{FH}}$ 10.3); ^{31}P NMR (162 MHz, CDCl_3): δ 25.0-25.2 (m); which was used without further purification.

Diethyl 2,6-Difluorobenzylphosphonate, 80

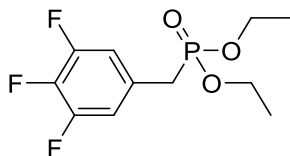


2,6-Difluorobenzyl bromide (6.81 g, 32.9 mmol) and triethylphosphite (6.20 mL, 36.2 mmol), after 4 hours at 120 °C, afforded *diethyl 2,6-difluorobenzylphosphonate* (6.61 g, 76 %) as a yellow oil; ^1H NMR (400 MHz, CDCl_3): δ 1.23 (6H, t, $^3J_{\text{HH}}$ 7.6, CH_2CH_3), 3.19 (2H, d, $^2J_{\text{HP}}$ 21.5, P- CH_2), 3.94-4.18 (4H, m, CH_2CH_3), 6.80-6.92 (2H, m, 3-*H*, 5-*H*), 7.09-7.22 (1H, m, 4-*H*); ^{19}F NMR (376 MHz, $\text{CDCl}_3/\text{CFCl}_3$): δ -114.3- -114.6 (m, 2-*F*, 6-*F*); ^{31}P NMR (162 MHz, CDCl_3): δ 22.8 (t, $^4J_{\text{PF}}$ 4.6); which was used without further purification. Data in agreement with literature.¹⁰

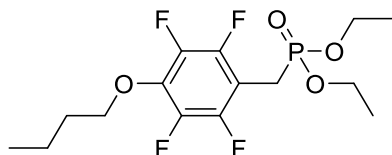
Diethyl 3,5-Difluorobenzylphosphonate, 81



3,5-Difluorobenzyl bromide (1.50 mL, 11.6 mmol) and triethylphosphite (3.98 mL, 23.2 mmol), after 4 hours at 120 °C, afforded *diethyl 3,5-difluorobenzylphosphonate* (2.48 g, 81 %) as a colourless oil; GC-MS m/z (% relative intensity, ion): 264 (62, $[\text{M}]^+$), 236 (40), 208 (61), 154 (74), 128 (55), 127 (100), 124 (55), 109 (81), 107 (54) 101 (60), 97 (55), 96 (65), 93 (56), 91 (62), 81 (80), 65 (49) 29 (49); ^1H NMR (400 MHz, CDCl_3): δ 1.26 (6H, t, $^3J_{\text{HH}}$ 7.1, CH_2CH_3), 3.10 (2H, d, $^2J_{\text{HP}}$ 21.9, P- CH_2), 3.99-4.09 (4H, m, CH_2CH_3), 6.68 (1H, td, $^3J_{\text{HF}}$ 9.0, $^4J_{\text{HH}}$ 2.2, 4-*H*), 6.77-6.86 (2H, m, 2-*H*, 6-*H*); ^{19}F NMR (376 MHz, $\text{CDCl}_3/\text{CFCl}_3$): δ -110.3- -110.6 (m, 3-*F*, 5-*F*); ^{31}P NMR (162 MHz, CDCl_3): δ 23.7 (s); which was used without further purification. Data in agreement with literature.¹⁰

Diethyl 3,4,5-Trifluorobenzylphosphonate, 83

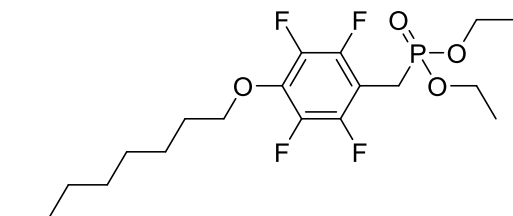
3,4,5-Trifluorobenzyl bromide (1.50 mL, 11.3 mmol) and triethylphosphite (3.86 mL, 22.5 mmol), after 4 hours at 120 °C, afforded *diethyl 3,4,5-trifluorobenzylphosphonate* (2.76 g, 87 %) as a colourless oil; GC-MS m/z (% relative intensity, ion): 282 (64, $[M]^+$), 254 (33), 226 (63), 172 (50), 146 (50), 145 (100), 137 (43), 124 (63), 109 (90), 97 (55), 96 (52), 93 (43), 91 (69), 81 (87), 65 (42), 29 (52); ^1H NMR (400 MHz, CDCl_3): δ 1.24 (6H, t, $^3J_{\text{HH}}$ 7.1, CH_2CH_3), 3.02 (2H, d, $^2J_{\text{HP}}$ 21.7, $\text{P}-\text{CH}_2$), 3.96-4.09 (4H, m, CH_2CH_3), 6.84-6.95 (2H, m, 2-*H*, 6-*H*); ^{19}F NMR (376 MHz, $\text{CDCl}_3/\text{CFCl}_3$): δ -134.8- -135.1 (2F, m, 3-*F*, 5-*F*), -163.2- -163.5 (1F, m, 4-*F*); ^{31}P NMR (162 MHz, CDCl_3): δ 23.3-23.5 (m); which was used without further purification. Data in agreement with literature.¹⁰

Diethyl (4-Butoxy-2,3,5,6-tetrafluorobenzyl)phosphonate

1-(Bromomethyl)-4-butoxy-2,3,5,6-tetrafluorobenzene (0.569 g, 1.81 mmol) and triethylphosphite (0.78 mL, 4.55 mmol), after 4 hours at 120 °C and column chromatography on silica gel using hexane and ethyl acetate (4:1) as the eluent, afforded *diethyl (4-butoxy-2,3,5,6-tetrafluorobenzyl)phosphonate* (0.74 g) as a yellow oil. The purity of the product was shown to be 73 % by GC-MS; GC-MS m/z (% relative intensity, ion): 373 (34, $[M + \text{H}]^+$), 372 (24, $[M]^+$), 316 (50), 268 (58), 260 (52), 179 (80), 137 (43), 109 (100); ^1H NMR (400 MHz, CDCl_3): δ 0.94 (3H, t, $^3J_{\text{HH}}$ 7.4, $\text{CH}_2\text{CH}_2\text{CH}_3$), 1.27 (6H, td, $^3J_{\text{HH}}$ 7.1, $^4J_{\text{HP}}$ 0.5, $\text{P}-\text{CH}_2\text{CH}_3$), 1.40-1.54 (2H, m, CH_2CH_2), 1.66-1.79 (2H, m, CH_2CH_2), 3.17 (2H, dt, $^2J_{\text{HP}}$ 21.1, $^5J_{\text{HF}}$ 1.5, $\text{Ar}-\text{CH}_2$), 4.04-4.13 (4H, m, $\text{P}-\text{CH}_2\text{CH}_3$), 4.18 (2H, t, $^3J_{\text{HH}}$ 6.5, $\text{O}-\text{CH}_2$); ^{19}F NMR (376 MHz,

$\text{CDCl}_3/\text{CFCl}_3$): δ -144.0 (2F, dm, $^3J_{\text{FF}}$ 20.3, Ar-F), -158.0 (2F, dm, $^3J_{\text{FF}}$ 21.7, Ar-F); ^{31}P NMR (162 MHz, CDCl_3): δ 22.3-22.7 (m).

Diethyl (4-Octoxy-2,3,5,6-tetrafluorobenzyl)phosphonate

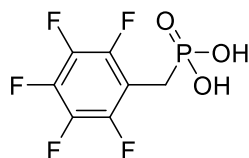


1-(Bromomethyl)-4-octoxy-2,3,5,6-tetrafluorobenzene (0.595 g, 1.60 mmol) and triethylphosphite (0.65 mL, 3.79 mmol), after 4 hours at 120 °C and column chromatography on silica gel using hexane and ethyl acetate (1:1) as the eluent, afforded *diethyl (4-octoxy-2,3,5,6-tetrafluorobenzyl)phosphonate* (0.79 g) as a colourless oil. The purity of the product was shown to be 74 % by GC-MS; GC-MS m/z (% relative intensity, ion): 429 (10, $[\text{M} + \text{H}]^+$), 428 (13, $[\text{M}]^+$), 317 (100), 316 (82), 268 (41), 260 (64), 179 (41), 109 (43), 43 (50); ^1H NMR (400 MHz, CDCl_3): δ 0.86 (3H, t, $^3J_{\text{HH}}$ 7.0, $\text{CH}_2\text{CH}_2\text{CH}_3$), 1.20-1.36 (14H, m, $\text{P}-\text{CH}_2\text{CH}_3$, CH_2CH_2), 1.38-1.49 (2H, m, CH_2CH_2), 1.69-1.81 (2H, m, CH_2CH_2), 3.19 (2H, dt, $^2J_{\text{HP}}$ 21.1, $^5J_{\text{HF}}$ 1.5, $\text{P}-\text{CH}_2$), 4.06-4.15 (4H, m, $\text{O}-\text{CH}_2\text{CH}_3$), 4.18 (2H, t, $^3J_{\text{HH}}$ 6.6, $\text{O}-\text{CH}_2$); ^{19}F NMR (376 MHz, $\text{CDCl}_3/\text{CFCl}_3$): δ -144.0 (2F, dm, $^3J_{\text{FF}}$ 19.2, Ar-F), -157.9- -158.0 (2F, m, Ar-F); ^{31}P NMR (162 MHz, CDCl_3): δ 22.2-22.7 (m).

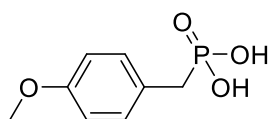
6.3.4 Synthesis of Benzylphosphonic Acid Derivatives

General Procedure for the Hydrolysis of Phosphonates to Phosphonic Acids

In a flame dried flask, under an inert atmosphere, the phosphonate was dissolved in dry DCM. Bromotrimethylsilane was added via syringe and the reaction stirred at room temperature. Volatile materials were removed under reduced pressure and the resulting product dissolved in an excess of 10:1 methanol:water and stirred overnight. Volatile materials were removed under reduced pressure and the crude product was purified by recrystallisation to yield the benzylphosphonic acid.

Pentafluorobenzylphosphonic Acid, 59

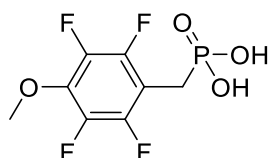
Diethyl perfluorobenzylphosphonate (2.12 g, 6.66 mmol), dry DCM (25 mL) and bromotrimethylsilane (2.81 mL, 21.3 mmol), after 5 hours and recrystallisation from acetonitrile, yielded *pentafluorobenzylphosphonic acid* (1.40 g, 80 %) as a white solid; mp 231-234 °C [lit⁸ 223 °C]; Anal. Calcd for C₇H₄F₅O₃P: C, 32.08; H, 1.54. Found: C, 32.19; H, 1.52; HRMS-ASAP *m/z*: [M + H⁺] calcd for C₇H₅O₃F₅P 262.9896; found 262.9888; ASAP *m/z* (% relative intensity, ion): 263 (100, [M + H]⁺), 242 (66), 224 (22), 178 (21); IR (cm⁻¹): 2334, 1658, 1525, 1501, 1407; ¹H NMR (700 MHz, *d*₆-DMSO): δ 3.06 (2H, d, ²J_{HP} 20.4, P-CH₂), 4.07 (bs, P-OH); ¹³C NMR (176 MHz, *d*₆-DMSO): δ 23.2 (d, ¹J_{CP} 133.0, P-CH₂), 109.5 (tdm, ²J_{CF} 19.1, ²J_{CP} 9.8, 1-C), 136.8 (dm, ¹J_{CF} 247.0, Ar-CF), 138.9 (dm, ¹J_{CF} 249.0, Ar-CF), 144.7 (dm, ¹J_{CF} 247.0, Ar-CF); ¹⁹F NMR (564 MHz, *d*₆-DMSO): δ -141.2- -141.4 (2F, m, 2-F, 6-F), -158.2 (1F, td, ³J_{FF} 22.2, ⁶J_{FP} 6.3, 4-F), -163.8- -164.0 (2F, m, 3-F, 5-F); ³¹P NMR (243 MHz, *d*₆-DMSO): δ 16.1-16.3 (m); data in agreement with literature.⁸

4-Methoxybenzylphosphonic Acid, 60

Diethyl 4-methoxybenzylphosphonate (0.580 g, 2.25 mmol), dry DCM (10 mL) and bromotrimethylsilane (0.95 mL, 7.20 mmol), after 5 hours and recrystallisation from acetonitrile, yielded *4-methoxybenzylphosphonic acid* (0.18 g, 41 %) as a white solid; mp 203-205 °C [lit¹¹ 204-206 °C]; Anal. Calcd for C₈H₁₁O₄P: C, 47.53; H, 5.48. Found: C, 47.60; H, 5.43; HRMS-ASAP *m/z*: [M + H⁺] calcd for C₈H₁₂O₄P 203.0473; found 203.0472; ASAP *m/z* (% relative intensity, ion): 202 (12, [M]⁺), 187 (2), 122 (6), 121 (100); IR (cm⁻¹): 2208, 1610, 1584, 1514, 1442; ¹H NMR (700 MHz, *d*₆-DMSO): δ 2.87 (2H, d, ²J_{HP} 21.0, P-CH₂), 3.71 (3H, s, O-CH₃), 6.82-6.86 (2H, m, 3-H, 5-H), 7.13-7.17

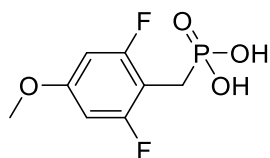
(2H, m, 2-*H*, 6-*H*); ^{13}C NMR (176 MHz, d_6 -DMSO): δ 34.3 (d, $^1J_{\text{CP}}$ 133.2, P-CH₂), 55.0 (s, O-CH₃), 113.5 (s, 3-*C*, 5-*C*), 126.0 (d, $^2J_{\text{CP}}$ 8.8, 1-*C*), 130.6 (d, $^3J_{\text{CP}}$ 6.3, 2-*C*, 6-*C*), 157.6 (d, $^5J_{\text{CP}}$ 3.1, 4-*C*); ^{31}P NMR (283 MHz, d_6 -DMSO): δ 21.7 (s); data in agreement with literature.¹¹

2,3,5,6-Tetrafluoro-4-methoxybenzylphosphonic Acid, 61



Diethyl 2,3,5,6-tetrafluoro-4-methoxybenzylphosphonate (0.390 g, 1.18 mmol), dry DCM (15 mL) and bromotrimethylsilane (0.49 mL, 3.75 mmol), after stirring overnight and recrystallisation from acetonitrile, yielded 2,3,5,6-tetrafluoro-4-methoxybenzylphosphonic acid (0.24 g, 76 %) as a white solid; mp 227-229 °C; Anal. Calcd for C₈H₇F₄O₄P: C, 35.13; H, 2.54. Found: C, 35.05; H, 2.57; HRMS-ASAP m/z : [M + H⁺] calcd for C₈H₈O₄F₄P 275.0096; found 275.0098; ASAP m/z (% relative intensity, ion): 275 (58, [M + H]⁺), 193 (100); IR (cm⁻¹): 2280, 1658, 1491, 1447, 1428; ^1H NMR (700 MHz, d_6 -DMSO): δ 3.01 (2H, d, $^2J_{\text{HP}}$ 20.4, P-CH₂), 4.02 (3H, s, O-CH₃), 10.4 (2H, bs, P-OH); ^{13}C NMR (151 MHz, d_6 -DMSO): δ 23.1 (d, $^1J_{\text{CP}}$ 133.5, P-CH₂), 62.4 (bs, O-CH₃), 107.4 (td, $^2J_{\text{CF}}$ 18.9, $^2J_{\text{CP}}$ 9.8, 1-*C*), 135.8-136.1 (m, 4-*C*), 140.4 (dm, $^1J_{\text{CF}}$ 243.8, Ar-CF), 144.8 (dm, $^1J_{\text{CF}}$ 247.1, Ar-CF); ^{19}F NMR (564 MHz, d_6 -DMSO): δ -142.8- -143.1 (2F, m, Ar-*F*), -159.0- -159.3 (2F, m, Ar-*F*); ^{31}P NMR (243 MHz, d_6 -DMSO): δ 16.7-17.1 (m).

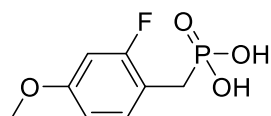
2,6-Difluoro-4-methoxybenzylphosphonic Acid, 62



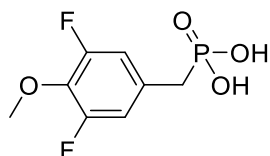
Diethyl 2,6-difluoro-4-methoxybenzylphosphonate (0.678 g, 2.30 mmol), dry DCM (15 mL) and bromotrimethylsilane (0.97 mL, 7.35 mmol), after stirring overnight and

recrystallisation from acetonitrile, yielded *2,6-difluoro-4-methoxybenzylphosphonic acid* (0.44 g, 80 %) as a white solid; mp 177-180 °C; Anal. Calcd for C₈H₉F₂O₄P: C, 40.35; H, 3.81. Found: C, 40.10; H, 3.85; HRMS-ASAP *m/z*: [M + H⁺] calcd for C₈H₁₀O₄F₂P 239.0285; found 239.0286; ASAP *m/z* (% relative intensity, ion): 239 (52, [M + H]⁺), 238 (11, [M]⁺), 157 (100); IR (cm⁻¹): 2845, 2358, 1638, 1594, 1504, 1470, 1448; ¹H NMR (700 MHz, *d*₆-DMSO): δ 2.87 (2H, d, ²*J*_{HP} 20.4, P-CH₂), 3.76 (3H, s, O-CH₃), 6.69 (2H, d, ³*J*_{HF} 9.2, 3-*H*, 5-*H*), 10.1 (2H, bs, P-OH); ¹³C NMR (176 MHz, *d*₆-DMSO): δ 22.5 (d, ¹*J*_{CP} 136.4, P-CH₂), 56.0 (s, O-CH₃), 97.9 (dm, ²*J*_{CF} 27.1, 3-*C*, 5-*C*), 102.3 (td, ²*J*_{CF} 21.2, ²*J*_{CP} 9.7, 1-*C*), 159.1 (td, ³*J*_{CF} 14.1, ⁵*J*_{CP} 3.0, 4-*C*), 161.2 (ddd, ¹*J*_{CF} 245.3, ³*J*_{CF} 11.8, ³*J*_{CP} 5.5, 2-*C*, 6-*C*); ¹⁹F NMR (564 MHz, *d*₆-DMSO): δ -112.3 (dd, ³*J*_{FH} 9.3, ⁴*J*_{FP} 3.4, 2-*F*, 6-*F*); ³¹P NMR (283 MHz, *d*₆-DMSO): δ 19.0 (t, ⁴*J*_{PF} 3.4).

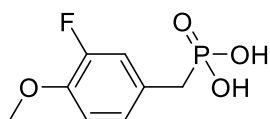
2-Fluoro-4-methoxybenzylphosphonic Acid, 63



Diethyl 2-fluoro-4-methoxybenzylphosphonate (3.71 g, 13.4 mmol), dry DCM (50 mL) and bromotrimethylsilane (5.67 mL, 43.0 mmol), after 6 hours and recrystallisation from acetonitrile, yielded *2-fluoro-4-methoxybenzylphosphonic acid* (2.04 g, 69 %) as a white solid; mp 185-188 °C; Anal. Calcd for C₈H₁₀FO₄P: C, 43.65; H, 4.58. Found: C, 43.61; H, 4.56; HRMS-ASAP *m/z*: [M + H⁺] calcd for C₈H₁₁O₄FP 221.0379; found 221.0383; ASAP *m/z* (% relative intensity, ion): 221 (33, [M + H]⁺), 220 (5, [M]⁺), 139 (100); IR (cm⁻¹): 2719, 2310, 1625, 1587, 1512, 1445; ¹H NMR (600 MHz, *d*₆-DMSO): δ 2.88 (2H, d, ²*J*_{HP} 20.8, P-CH₂), 3.74 (3H, s, O-CH₃), 6.70-6.79 (2H, m, 3-*H*, 5-*H*), 7.24 (1H, ddd, ³*J*_{HH} 8.8, ⁴*J*_{HF} 8.8, ⁴*J*_{HP} 2.4, 6-*H*), 9.89 (2H, bs, P-OH); ¹³C NMR (151 MHz, *d*₆-DMSO): δ 27.3 (d, ¹*J*_{CP} 135.4, P-CH₂), 55.5 (s, O-CH₃), 101.2 (dd, ²*J*_{CF} 26.0, ⁴*J*_{CP} 2.6, 3-*C*), 110.0 (dd, ⁴*J*_{CF} 2.8, ⁴*J*_{CP} 2.8, 5-*C*), 112.8 (dd, ²*J*_{CF} 16.3, ²*J*_{CP} 8.9, 1-*C*), 132.1 (dd, ³*J*_{CF} 5.5, ³*J*_{CP} 5.5, 6-*C*), 159.0 (dd, ³*J*_{CF} 10.9, ⁵*J*_{CP} 3.1, 4-*C*), 160.8 (dd, ¹*J*_{CF} 244.1, ³*J*_{CP} 7.0, 2-*C*); ¹⁹F NMR (564 MHz, *d*₆-DMSO): δ -114.9- -115.1 (m); ³¹P NMR (243 MHz, *d*₆-DMSO): δ 20.6 (d, ⁴*J*_{PF} 3.9).

3,5-Difluoro-4-methoxybenzylphosphonic Acid, 64

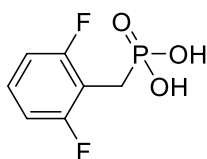
Diethyl 3,5-difluoro-4-methoxybenzylphosphonate (0.353 g, 1.20 mmol), dry DCM (10 mL) and bromotrimethylsilane (0.51 mL, 3.84 mmol), after stirring overnight and recrystallisation from acetonitrile, yielded *3,5-difluoro-4-methoxybenzylphosphonic acid* (0.20 g, 70 %) as a white solid; mp 179-181 °C; Anal. Calcd for $C_8H_9F_2O_4P$: C, 40.35; H, 3.81. Found: C, 40.32; H, 3.81; HRMS-ASAP m/z : $[M^+]$ calcd for $C_8H_9O_4F_2P$ 238.0207; found 238.0223; ASAP m/z (% relative intensity, ion): 239 (21, $[M + H]^+$), 157 (100); IR (cm^{-1}): 2923, 2360, 1582, 1520, 1442; 1H NMR (600 MHz, d_6 -DMSO): δ 2.95 (2H, d, $^2J_{HP}$ 21.3, P- CH_2), 3.88 (3H, s, O- CH_3), 6.95-7.06 (2H, m, 2- H , 6- H), 10.1 (2H, bs, P- OH); ^{13}C NMR (151 MHz, d_6 -DMSO): δ 34.4 (d, $^1J_{CP}$ 131.9, P- CH_2), 61.8 (bs, O- CH_3), 113.7 (dm, $^2J_{CF}$ 17.9, 2- C , 6- C), 130.7 (dt, $^2J_{CP}$ 9.3, $^3J_{CF}$ 9.3, 1- C), 133.9 (td, $^2J_{CF}$ 14.4, $^5J_{CP}$ 3.5, 4- C), 154.6 (ddd, $^1J_{CF}$ 245.3, $^3J_{CF}$ 6.4, $^4J_{CP}$ 3.2, 3- C , 5- C); ^{19}F NMR (564 MHz, d_6 -DMSO): δ -130.1 (d, $^3J_{FH}$ 9.1, 3- F , 5- F); ^{31}P NMR (243 MHz, d_6 -DMSO): δ 19.7-19.8 (m).

3-Fluoro-4-methoxybenzylphosphonic Acid, 65

Diethyl 3-fluoro-4-methoxybenzylphosphonate (1.10 g, 3.98 mmol), dry DCM (20 mL) and bromotrimethylsilane (1.68 mL, 12.7 mmol), after 5 hours and recrystallisation from acetonitrile, yielded *3-fluoro-4-methoxybenzylphosphonic acid* (0.80 g, 91 %) as a white solid; mp 186-188 °C; Anal. Calcd for $C_8H_{10}FO_4P$: C, 43.65; H, 4.58. Found: C, 43.60; H, 4.59; HRMS-ASAP m/z : $[M^+]$ calcd for $C_8H_{10}O_4FP$ 220.0301; found 220.0285; ASAP m/z (% relative intensity, ion): 220 (3, $[M]^+$), 139 (100); IR (cm^{-1}): 2846, 2269, 1622, 1586, 1515, 1459; 1H NMR (600 MHz, d_6 -DMSO): δ 2.90 (2H, d, $^2J_{HP}$ 21.1, P- CH_2), 3.80 (3H, s, O- CH_3), 6.96-7.02 (1H, m, Ar- H), 7.03-7.12 (2H, m,

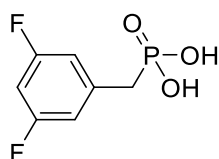
Ar-H), 9.82 (2H, bs, P-OH); ^{13}C NMR (151 MHz, d_6 -DMSO): δ 34.1 (d, $^1J_{\text{CP}}$ 132.8, P-CH₂), 56.0 (s, O-CH₃), 113.6 (bs, 5-C), 117.0 (dd, $^2J_{\text{CF}}$ 18.2, $^3J_{\text{CP}}$ 5.9, 2-C), 125.8 (dd, $^3J_{\text{CP}}$ 6.9, $^4J_{\text{CF}}$ 3.3, 6-C), 127.1 (dd, $^2J_{\text{CP}}$ 8.6, $^3J_{\text{CF}}$ 7.0, 1-C), 145.4 (dd, $^2J_{\text{CF}}$ 10.5, $^5J_{\text{CP}}$ 3.1, 4-C), 151.0 (dd, $^1J_{\text{CF}}$ 242.6, $^4J_{\text{CP}}$ 3.1, 3-C); ^{19}F NMR (564 MHz, d_6 -DMSO): δ -136.3- -136.6 (m); ^{31}P NMR (243 MHz, d_6 -DMSO): δ 21.0-21.2 (m).

2,6-Difluorobenzylphosphonic Acid, 66



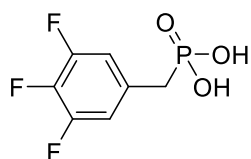
Diethyl 2,6-difluorobenzylphosphonate (6.60 g, 25.0 mmol), dry DCM (100 mL) and bromotrimethylsilane (10.5 mL, 79.9 mmol), after 6 hours and recrystallisation from acetonitrile, yielded 2,6-difluorobenzylphosphonic acid (4.04 g, 78 %) as a white solid; mp 226-228 °C; Anal. Calcd for C₇H₇F₂O₃P: C, 40.40; H, 3.39. Found: C, 40.36; H, 3.37; HRMS-ASAP m/z : [M + H⁺] calcd for C₇H₈O₃F₂P 209.0179; found 209.0177; ASAP m/z (% relative intensity, ion): 209 (100, [M + H]⁺), 188 (8), 127 (32); IR (cm⁻¹): 2750, 2320, 1626, 1594, 1570, 1472; ^1H NMR (600 MHz, d_6 -DMSO): δ 2.98 (2H, d, $^2J_{\text{HP}}$ 21.0, P-CH₂), 7.01-7.08 (2H, m, 3-H, 5-H), 7.23-7.41 (1H, m, 4-H), 10.2 (2H, bs, P-OH); ^{13}C NMR (176 MHz, d_6 -DMSO): δ 23.1 (d, $^1J_{\text{CP}}$ 134.8, P-CH₂), 110.6 (td, $^2J_{\text{CF}}$ 20.3, $^2J_{\text{CP}}$ 9.7, 1-C), 111.0-111.5 (m, 3-C, 5-C), 128.3 (td, $^3J_{\text{CF}}$ 10.2, $^5J_{\text{CP}}$ 3.6, 4-C), 160.8 (ddd, $^1J_{\text{CF}}$ 247.2, $^3J_{\text{CF}}$ 8.3, $^3J_{\text{CP}}$ 5.8, 2-C, 6-C); ^{19}F NMR (564 MHz, d_6 -DMSO): δ -113.0- -113.3 (m, 2-F, 6-F); ^{31}P NMR (243 MHz, d_6 -DMSO): δ 18.6 (t, $^4J_{\text{PF}}$ 4.0); data in agreement with literature.¹⁰

3,5-Difluorobenzylphosphonic Acid, 82

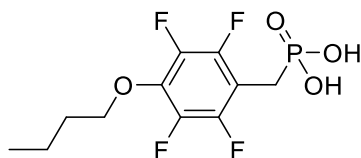


Diethyl 3,5-difluorobenzylphosphonate (2.45 g, 9.27 mmol), dry DCM (60 mL) and bromotrimethylsilane (3.90 mL, 29.6 mmol), after 24 hours and recrystallisation from acetonitrile, yielded 3,5-difluorobenzylphosphonic acid (1.01 g, 52 %) as a white solid; mp 178-181 °C; HRMS-ASAP m/z : $[M + H]^+$ calcd for $C_7H_8O_3F_2P$ 209.0179; found 209.0175; ASAP m/z (% relative intensity, ion): 209 (100, $[M + H]^+$); IR (cm^{-1}): 2750, 2362, 2110, 1619, 1599, 1465, 1439; 1H NMR (600 MHz, d_6 -DMSO): δ 3.04 (2H, d, $^2J_{HP}$ 21.6, P- CH_2), 6.93-6.99 (2H, m, 2- H , 6- H), 7.04 (1H, tm, $^3J_{HF}$ 9.4, 4- H), 9.92 (2H, s, P- OH); ^{13}C NMR (176 MHz, d_6 -DMSO): δ 35.0 (d, $^1J_{CP}$ 131.2, P- CH_2), 101.6 (td, $^2J_{CF}$ 25.7, $^5J_{CP}$ 3.1, 4- C), 112.9 (ddd, $^2J_{CF}$ 20.5, $^3J_{CP}$ 6.2, $^4J_{CF}$ 4.5, 2- C , 6- C), 138.8-139.1 (m, 1- C), 162.1 (ddd, $^1J_{CF}$ 244.9, $^3J_{CF}$ 13.5, $^4J_{CP}$ 3.1, 3- C , 5- C); ^{19}F NMR (564 MHz, d_6 -DMSO): δ -111.1- -111.2 (m, 3- F , 5- F); ^{31}P NMR (243 MHz, d_6 -DMSO): δ 19.9 (s); data in agreement with literature.¹⁰

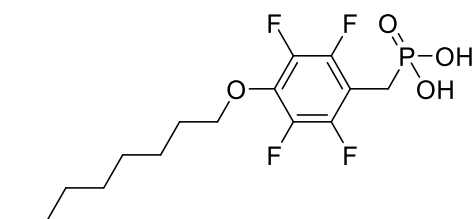
3,4,5-Trifluorobenzylphosphonic Acid, 84



Diethyl 3,4,5-trifluorobenzylphosphonate (2.70 g, 9.57 mmol), dry DCM (60 mL) and bromotrimethylsilane (4.10 mL, 31.1 mmol), after 5 hours and recrystallisation from acetonitrile, yielded 3,4,5-trifluorobenzylphosphonic acid (1.85 g, 86 %) as a white solid; mp 207-210 °C; HRMS-ASAP m/z : $[M + H]^+$ calcd for $C_7H_7O_3F_3P$ 227.0085; found 227.0070; ASAP m/z (% relative intensity, ion): 227 (100, $[M + H]^+$), 226 (4), 145 (16); IR (cm^{-1}): 2580, 2260, 2120, 2018, 1622, 1523, 1448, 1416; 1H NMR (600 MHz, d_6 -DMSO): δ 3.01 (2H, d, $^2J_{HP}$ 21.4, P- CH_2), 7.12-7.21 (2H, m, 2- H , 6- H), 9.69 (2H, bs, P- OH); ^{13}C NMR (126 MHz, d_6 -DMSO): δ 34.4 (d, $^1J_{CP}$ 131.5, P- CH_2), 114.2 (dm, $^2J_{CF}$ 15.8, 2- C , 6- C), 131.8-132.3 (m, 1- C), 137.4 (dtd, $^1J_{CF}$ 246.6, $^2J_{CF}$ 15.5, $^5J_{CP}$ 3.5, 4- C), 149.8 (dm, $^1J_{CF}$ 246.0, 3- C , 5- C); ^{19}F NMR (564 MHz, d_6 -DMSO): δ -136.5- -136.9 (2F, m, 3- F , 5- F), -165.6- -165.8 (1F, m, 4- F); ^{31}P NMR (243 MHz, d_6 -DMSO): δ 19.4-19.5 (m); data in agreement with literature.¹⁰

(4-Butoxy-2,3,5,6-tetrafluorobenzyl)phosphonic Acid, 85

Diethyl (4-butoxy-2,3,5,6-tetrafluorobenzyl)phosphonate (0.68 g, 1.83 mmol), dry DCM (20 mL) and bromotrimethylsilane (0.77 mL, 5.83 mmol), after 19 hours and recrystallisation from acetonitrile, yielded (*4-butoxy-2,3,5,6-tetrafluorobenzyl*)phosphonic acid (0.36 g, 86 %) as a white solid; mp 194-196 °C; HRMS-ASAP m/z : $[M + H]^+$ calcd for $C_{11}H_{14}O_4F_4P$ 317.0566; found 317.0572; ASAP m/z (% relative intensity, ion): 317 (100, $[M + H]^+$), 316 (6, $[M]^+$), 261 (78), 179 (45); IR (cm^{-1}): 2959, 2283, 2119, 1655, 1493, 1430; 1H NMR (700 MHz, d_6 -DMSO): δ 0.92 (3H, t, $^3J_{HH}$ 7.4, CH_3), 1.39-1.49 (2H, m, CH_2CH_2), 1.65-1.72 (2H, m, CH_2CH_2), 3.01 (d, $^2J_{HP}$ 20.4, $P-CH_2$), 4.20 (2H, t, $^3J_{HH}$ 6.4, $O-CH_2$); ^{13}C NMR (176 MHz, d_6 -DMSO): δ 13.5 (s, CH_2CH_3), 18.3 (s, $O-CH_2CH_2CH_2$), 23.2 (d, $^1J_{CP}$ 133.6, $P-CH_2$), 31.3 (s, $O-CH_2CH_2$), 74.9 (s, $O-CH_2$), 107.6 (td, $^2J_{CF}$ 19.0, $^2J_{CP}$ 9.6, 1-C), 135.2 (td, $^2J_{CF}$ 13.0, $^5J_{CP}$ 3.5, 4-C), 140.7 (ddm, $^1J_{CF}$ 243.9, $^2J_{CF}$ 11.4, Ar-CF), 144.8 (dm, $^1J_{CF}$ 248.7, Ar-CF); ^{19}F NMR (376 MHz, d_6 -DMSO): δ -143.0- -143.5 (2F, m, Ar-F), -159.0 (2F, dd, $^3J_{FF}$ 23.3, $^5J_{FF}$ 8.4, Ar-F); ^{31}P NMR (283 MHz, d_6 -DMSO): δ 16.5-17.0 (m).

(4-Octoxy-2,3,5,6-tetrafluorobenzyl)phosphonic Acid, 86

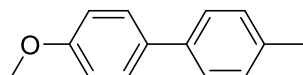
Diethyl (4-octoxy-2,3,5,6-tetrafluorobenzyl)phosphonate (0.479 g, 1.12 mmol), dry DCM (20 mL) and bromotrimethylsilane (0.64 mL, 4.85 mmol), after 19 hours and recrystallisation from acetonitrile, yielded (*4-octoxy-2,3,5,6-tetrafluorobenzyl*)phosphonic acid (0.29 g, 69 %) as a white solid; mp 171-173 °C; HRMS-ASAP m/z : $[M + H]^+$ calcd for $C_{15}H_{22}O_4F_4P$ 373.1192; found 373.1184; ASAP

m/z (% relative intensity, ion): 273 (100, $[M + H]^+$), 261 (40); IR (cm^{-1}): 2926, 2854, 2359, 2124, 1656, 1493; ^1H NMR (700 MHz, d_6 -DMSO): δ 0.80-0.90 (3H, m, CH_3), 1.18-1.34 (8H, m, CH_2CH_2), 1.37-1.46 (2H, m, CH_2CH_2), 1.65-1.74 (2H, m, CH_2CH_2), 3.01 (2H, d, $^2J_{\text{HP}}$ 20.4, $\text{P}-\text{CH}_2$), 4.19 (2H, t, $^3J_{\text{HH}}$ 6.4, $\text{O}-\text{CH}_2$); ^{13}C NMR (176 MHz, d_6 -DMSO): δ 13.9 (s, CH_2CH_3), 22.1 (s, $\text{O}-\text{CH}_2\text{CH}_2\text{CH}_2\text{CH}_2\text{CH}_2\text{CH}_2$), 23.1 (d, $^1J_{\text{CP}}$ 133.7, $\text{P}-\text{CH}_2$), 25.0 (s, $\text{O}-\text{CH}_2\text{CH}_2\text{CH}_2\text{CH}_2\text{CH}_2\text{CH}_2$), 28.5 (s, $\text{O}-\text{CH}_2\text{CH}_2\text{CH}_2\text{CH}_2\text{CH}_2$), 28.6 (s, $\text{O}-\text{CH}_2\text{CH}_2\text{CH}_2\text{CH}_2$), 29.3 (s, $\text{O}-\text{CH}_2\text{CH}_2\text{CH}_2$), 31.2 (s, $\text{O}-\text{CH}_2\text{CH}_2$), 75.2 (s, $\text{O}-\text{CH}_2$), 107.6 (td, $^2J_{\text{CF}}$ 18.9, $^2J_{\text{CP}}$ 9.5, 1-C), 134.9-135.3 (m, 4-C), 140.6 (dm, $^1J_{\text{CF}}$ 247.6, Ar-CF), 144.8 (dm, $^1J_{\text{CF}}$ 247.1, Ar-CF); ^{19}F NMR (376 MHz, d_6 -DMSO): δ -143.3 (2F, dm, $^3J_{\text{FF}}$ 21.5, Ar-F), -159.0 (2F, dd, $^3J_{\text{FF}}$ 23.1, $^5J_{\text{FF}}$ 8.4, Ar-F); ^{31}P NMR (283 MHz, d_6 -DMSO): δ 16.8 (s).

6.4 Experimental Data to Chapter 4

6.4.1 Synthesis of Biphenyl Derivatives by Suzuki-Miyaura Cross-Couplings

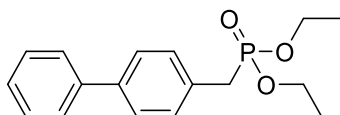
4-Methoxy-4'-methylbiphenyl, 104



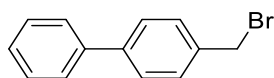
A mixture of 4-bromotoluene (1.00 g, 5.85 mmol), 4-methoxyphenylboronic acid (1.33 g, 8.75 mmol), PdCl_2 (0.016 g, 0.09 mmol), K_2CO_3 (1.62 g, 11.7 mmol), distilled water (25 mL) and ethanol (25 mL) was stirred at room temperature under air for 2 hours. The reaction mixture was added to brine and extracted with diethyl ether (3×50 mL). The combined extracts were washed with water (250 mL), dried (MgSO_4), filtered and concentrated. Column chromatography using silica gel with hexane and DCM (3:2) as the eluent afforded 4-methoxy-4'-methylbiphenyl (1.13 g, 97 %) as a white solid; GC-MS m/z (% relative intensity, ion): 198 (100, $[M]^+$), 184 (39), 183 (88), 155 (71), 154 (32), 153 (50), 152 (53), 128 (42), 115 (35); ^1H NMR (400 MHz, CDCl_3): δ 2.39 (3H, s, Ar- CH_3), 3.85 (3H, s, O- CH_3), 6.94-7.01 (2H, m, Ar- H), 7.23 (2H, d, $^3J_{\text{HH}}$ 7.9, Ar- H), 7.41-7.48 (2H, m, Ar- H), 7.49-7.56 (2H, m, Ar- H); data in agreement with literature.¹²

General Cross-Coupling Procedure Using Sodium Phenyl Borate Salts

$\text{Pd}(\text{PPh}_3)_4$ and the relevant sodium borate salt were charged into a flame dried microwave vial which was sealed, evacuated and back-filled with argon to create an inert atmosphere. Dry, degassed toluene and bromopentafluorobenzene were added in sequence to the microwave vial using a syringe and the reaction vessel heated to 120 °C under microwave irradiation. The reaction mixture was cooled and filtered through silica gel with acetone as the eluent to remove inorganic and particulate material. Volatile material was removed from the filtrate *in vacuo*, and the crude product extracted with NaOH solution and ethyl acetate, dried (MgSO_4) and purified by column chromatography on silica gel to give the biphenyl derivative.

Diethyl Biphenyl-4-ylmethylphosphonate, 97

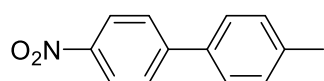
$\text{Pd}(\text{PPh}_3)_4$ (0.104 g, 0.09 mmol), sodium trihydroxy(phenyl)borate (0.146 g, 0.90 mmol), diethyl 4-bromobenzylphosphonate (0.304 g, 0.99 mmol) and dry, degassed toluene (10 mL), after 48 hours, afforded a complex mixture which was inseparable by column chromatography.

4-(Bromomethyl)biphenyl, 109

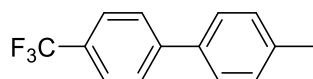
$\text{Pd}(\text{PPh}_3)_4$ (0.411 g, 0.36 mmol), sodium trihydroxy(phenyl)borate (0.970 g, 3.55 mmol), 4-bromobenzyl bromide (0.977 g, 3.90 mmol) and dry, degassed toluene (20 mL), after 48 hours, afforded a complex mixture which was inseparable by column chromatography.

General Cross-Coupling Procedure Using Aryl Boronic Acids

In a flame dried flask, under an inert atmosphere the aryl iodide, aryl boronic acid, Pd(PPh₃)₄ and potassium carbonate were added, before purging the flask with argon. Dry, degassed toluene and water were added in sequence and the reaction heated to reflux. The reaction was cooled to room temperature, added to toluene and filtered through Celite[®]. After extraction with water, the crude biphenyl was purified by column chromatography on silica gel to yield the biphenyl derivative.

4-Methyl-4'-nitrobiphenyl, 149

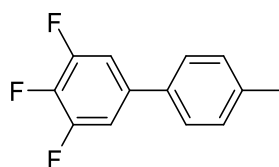
4-Iodonitrobenzene (1.25 g, 5.00 mmol), 4-methylbenzeneboronic acid (0.748 g, 5.50 mmol), Pd(PPh₃)₄ (0.231 g, 0.20 mmol), potassium carbonate (1.38 g, 10.0 mmol), toluene (25 mL) and deionised water (0.5 mL), after 16 hours and column chromatography on silica gel using a gradient of 0 to 10 % ethyl acetate in hexane as the eluent, afforded *4-methyl-4'-nitrobiphenyl* (0.94 g, 88 %) as a light yellow solid; GC-MS *m/z* (% relative intensity, ion): 214 (14, [M + H]⁺), 213 (100, [M]⁺), 165 (46), 152 (71); ¹H NMR (400 MHz, CDCl₃): δ 2.43 (3H, s, CH₃), 7.31 (2H, d, ³J_{HH} 8.1, 3-*H*, 5-*H*), 7.53 (2H, d, ³J_{HH} 8.1, 2-*H*, 6-*H*), 7.68-7.76 (2H, m, 2'-*H*, 6'-*H*), 8.24-8.33 (3'-*H*, 4'-*H*); data in agreement with literature.¹³

4-Methyl-4'-(trifluoromethyl)biphenyl, 150

4-Iodobenzotrifluoride (1.36 g, 5.00 mmol), 4-methylbenzeneboronic acid (0.748 g, 5.50 mmol), Pd(PPh₃)₄ (0.231 g, 0.20 mmol), potassium carbonate (1.38 g, 10.0 mmol), toluene (25 mL) and deionised water (0.5 mL), after 16 hours and column chromatography using silica gel and hexane as the eluent, afforded *4-methyl-4'-(trifluoromethyl)biphenyl* (0.85 g, 72 %) as a white solid; GC-MS *m/z* (% relative intensity, ion): 237 (15, [M + H]⁺), 236 (100, [M]⁺), 167 (48); ¹H NMR (400 MHz,

CDCl₃): δ 2.41 (3H, s, CH₃), 7.28 (2H, d, ³J_{HH} 8.1, Ar-H), 7.50 (2H, d, ³J_{HH} 8.1, Ar-H), 7.67 (4H, s, Ar-H); ¹⁹F NMR (376 MHz, CDCl₃/CFCl₃): δ -62.9 (s); data in agreement with literature.¹⁴

3,4,5-Trifluoro-4'-methylbiphenyl, 151

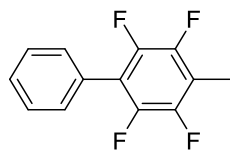


3,4,5-Trifluoriodobenzene (0.518 g, 2.01 mmol), 4-methylbenzeneboronic acid (0.523 g, 3.82 mmol), Pd(PPh₃)₄ (0.162 g, 0.14 mmol), potassium carbonate (0.967 g, 7.02 mmol), toluene (20 mL) and deionised water (0.5 mL), after 16 hours and column chromatography on silica gel using hexane as the eluent, afforded 3,4,5-trifluoro-4'-methylbiphenyl (0.42 g, 94 %) as a colourless oil; GC-MS *m/z* (% relative intensity, ion): 223 (30, [M + H]⁺), 222 (100, [M]⁺), 221 (61), 201 (79); ¹H NMR (400 MHz, CDCl₃): δ 2.45 (3H, s, CH₃), 7.15-7.24 (2H, m, 2-H, 6-H), 7.30 (2H, d, ³J_{HH} 8.0, Ar-H), 7.43 (2H, d, ³J_{HH} 8.0, Ar-H); ¹⁹F NMR (376 MHz, CDCl₃/CFCl₃): δ -134.9- -135.0 (2F, m, 3-F, 5-F), -163.8 (1F, tt, ³J_{FF} 20.5, ⁴J_{FH} 6.4, 4-F); data in agreement with literature.¹⁵

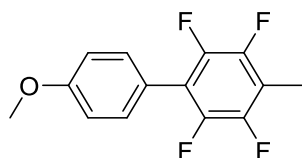
6.4.2 Synthesis of Biphenyl Derivatives by C–H Bond Activation

General C–H Bond Activation Procedure

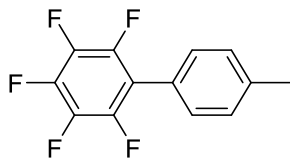
In a flame dried flask, under an inert atmosphere the aryl iodide was added to Pd(OAc)₂, PPh₃ and silver carbonate, followed by the aryl fluoride. After stirring for 1 minute, deionised water was added, and the resulting solution was heated to 70 °C and stirred for 24 h. The reaction was cooled to room temperature, added to ethyl acetate and filtered through Celite[®]. After extraction with brine, the crude biphenyl was purified by column chromatography on silica gel to yield the biphenyl derivative.

2,3,5,6-Tetrafluoro-4-methylbiphenyl, 112

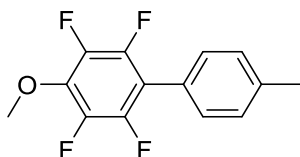
Iodobenzene (1.01 mL, 9.00 mmol), Pd(OAc)₂ (0.101 g, 0.45 mmol), PPh₃ (0.236 g, 0.90 mmol), silver carbonate (2.48 g, 9.00 mmol), 2,3,5,6-tetrafluorotoluene (2.19 mL, 18.0 mmol) and deionised water (30 mL), after column chromatography on silica gel using hexane and DCM (7:3) as the eluent, afforded 2,3,5,6-tetrafluoro-4-methylbiphenyl (1.39 g) as a white solid. The purity of the product was shown to be 96 % by GC-MS; GC-MS *m/z* (% relative intensity, ion): 240 (100, [M]⁺), 219 (87), 201 (31); ¹H NMR (400 MHz, CDCl₃): δ 2.33 (3H, t, ⁵J_{HF} 2.1, CH₃), 7.41-7.54 (5H, m, Ar-H); ¹⁹F NMR (376 MHz, CDCl₃/CFCl₃): δ -144.7 (2F, ddm, ³J_{FF} 14.8, ⁵J_{FF} 12.5, Ar-F), -146.1- -146.3 (2F, m, Ar-F); and was used without further purification. Data in agreement with literature.²

2,3,5,6-Tetrafluoro-4'-methoxy-4-methylbiphenyl, 113

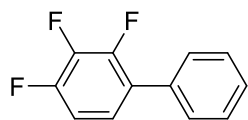
4-Iodoanisole (3.51 g, 15.0 mmol), Pd(OAc)₂ (0.240 g, 1.07 mmol), PPh₃ (0.580 g, 2.21 mmol), silver carbonate (5.61 g, 20.3 mmol), 2,3,5,6-tetrafluorotoluene (4.97 mL, 40.8 mmol) and deionised water (80 mL), after 48 hours and column chromatography on silica gel using hexane and DCM (3:2) as the eluent, afforded 2,3,5,6-tetrafluoro-4'-methoxy-4-methylbiphenyl (0.98 g, 24 %) as a white solid; GC-MS *m/z* (% relative intensity, ion): 270 (100, [M]⁺), 227 (74); ¹H NMR (400 MHz, CDCl₃): δ 2.31 (3H, t, ⁵J_{HF} 2.1, Ar-CH₃), 3.86 (3H, s, O-CH₃), 6.96-7.06 (2H, m, Ar-H), 7.36-7.43 (2H, m, Ar-H); ¹⁹F NMR (376 MHz, CDCl₃/CFCl₃): δ -144.9 (2F, dd, ³J_{FF} 22.5, ⁵J_{FF} 12.5, Ar-F), -146.5 (2F, dd, ³J_{FF} 22.5, ⁵J_{FF} 12.5, Ar-F); data in agreement with literature.³

2,3,4,5,6-Pentafluoro-4'-methylbiphenyl, 121

4-Iodotoluene (1.96 g, 9.00 mmol), Pd(OAc)₂ (0.101 g, 0.45 mmol), PPh₃ (0.236 g, 0.90 mmol), silver carbonate (2.48 g, 9.00 mmol), pentafluorobenzene (4.00 mL, 36.0 mmol) and deionised water (30 mL), after column chromatography on silica gel using hexane and ethyl acetate (9:1) as the eluent, afforded 2,3,4,5,6-pentafluoro-4'-methylbiphenyl (1.49 g, 64 %) as a white solid; GC-MS *m/z* (% relative intensity, ion): 258 (100, [M]⁺), 239 (35), 237 (76), 219 (45), 188 (33), 91 (32); ¹H NMR (400 MHz, CDCl₃): δ 2.43 (3H, s, CH₃), 7.31 (4H, s, Ar-H); ¹⁹F NMR (376 MHz, CDCl₃/CFC₃): δ -143.9 (2F, dd, ³J_{FF} 23.0, ⁵J_{FF} 8.2, Ar-F), -156.6 (1F, t, ³J_{FF} 21.0, Ar-F), -163.0 (2F, td, ³J_{FF} 23.0, ⁵J_{FF} 8.3, Ar-F); data in agreement with literature.²

2,3,5,6-Tetrafluoro-4-methoxy-4'-methylbiphenyl, 122

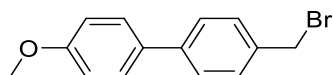
4-Iodotoluene (1.96 g, 9.00 mmol), Pd(OAc)₂ (0.101 g, 0.45 mmol), PPh₃ (0.236 g, 0.90 mmol), silver carbonate (2.48 g, 9.00 mmol), 2,3,5,6-tetrafluoroanisole (2.51 mL, 18.0 mmol) and deionised water (25 mL), after column chromatography on silica gel using hexane and DCM (9:1) as the eluent, afforded 2,3,5,6-tetrafluoro-4-methoxy-4'-methylbiphenyl (1.51 g, 62 %) as a white solid; GC-MS *m/z* (% relative intensity, ion): 271 (55, [M + H]⁺), 270 (99, [M]⁺), 256 (52), 255 (100), 227 (68), 224 (30), 207 (37), 206 (78), 187 (30), 177 (35); ¹H NMR (400 MHz, CDCl₃): δ 2.41 (3H, s, Ar-CH₃), 4.11 (3H, t, ⁵J_{HF} 1.3, O-CH₃), 7.27-7.35 (4H, m, Ar-H); ¹⁹F NMR (376 MHz, CDCl₃/CFC₃): δ -145.8 (2F, dd, ³J_{FF} 22.2, ⁵J_{FF} 8.7, Ar-F), -158.9 (2F, dd, ³J_{FF} 22.1, ⁵J_{FF} 8.8, Ar-F); data in agreement with literature.¹⁶

2,3,4-Trifluorobiphenyl, 153

4-Iodobenzene (1.00 mL, 9.00 mmol), Pd(OAc)₂ (0.101 g, 0.45 mmol), PPh₃ (0.236 g, 0.90 mmol), silver carbonate (2.48 g, 9.00 mmol), 2,3,5,6-trifluorobenzene (2.79 mL, 27.0 mmol) and deionised water (30 mL), after column chromatography on silica gel using hexane as the eluent, afforded 2,3,4-trifluorobiphenyl (0.24 g, 13 %) as a white solid; GC-MS *m/z* (% relative intensity, ion): 209 (13, [M + H]⁺), 208 (100, [M]⁺); ¹H NMR (400 MHz, CDCl₃): δ 7.30-7.40 (m, Ar-CH), 7.41-7.48 (m, Ar-CH), 7.57-7.65 (m, Ar-CH); ¹⁹F NMR (376 MHz, CDCl₃/CFCl₃): δ -136.2- -136.4 (1F, m, 4-F), -139.0- -139.7 (1F, m, 2-F), -160.4- -160.8 (1F, m, 3-F); data in agreement with literature.¹⁷

6.4.3 Synthesis of Biphenyl Benzyl Bromides**General Wohl-Ziegler Reaction Procedure**

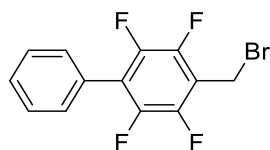
The toluene derivative and AIBN were dissolved in 1,2-dichloroethane, and the mixture heated to reflux. NBS was added slowly and the mixture heated at reflux, with the reaction being monitored by TLC and NMR spectroscopy, before cooling to room temperature. The precipitate was filtered off, washed with 1,2-dichloroethane, and the combined filtrates evaporated *in vacuo*. The crude bromide was purified by either vacuum distillation or column chromatography on silica gel.

4-(Bromomethyl)-4'-methoxybiphenyl, 103

4-Methoxy-4'-methylbiphenyl (0.964 g, 4.86 mmol), AIBN (0.040 g, 0.24 mmol), NBS (1.04 g, 5.84 mmol) and 1,3-dichloroethane (40 mL), after 90 minutes and column chromatography on silica gel using hexane and ethyl acetate (9:1) as the eluent, afforded

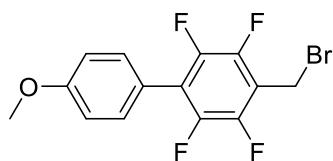
4-(bromomethyl)-4'-methoxybiphenyl (0.97 g, 72 %) as a white solid; GC-MS m/z (% relative intensity, ion): 278 (15, $[M]^+$), 276 (16, $[M]^+$), 198 (48), 197 (100), 181 (39), 154 (49), 99 (31); ^1H NMR (400 MHz, CDCl_3): δ 3.85 (3H, s, O- CH_3), 4.55 (2H, s, CH_2), 6.96-7.01 (2H, m, Ar- H), 7.40-7.47 (2H, m, Ar- H), 7.49-7.54 (4H, m, Ar- H). Data in agreement with literature.¹⁸

4-(Bromomethyl)-2,3,5,6-tetrafluorobiphenyl, 115



2,3,5,6-Tetrafluoro-4-methylbiphenyl (1.31 g, 5.45 mmol), AIBN (0.094 g, 0.56 mmol), NBS (2.22 g, 12.5 mmol) and 1,2-dichloroethane (30 mL), after 45 hours and column chromatography on silica gel using hexane as the eluent, afforded *4-(bromomethyl)-2,3,5,6-tetrafluorobiphenyl* (1.26 g, 72 %) as a white solid; GC-MS m/z (% relative intensity, ion): 320 (30, $[M]^+$), 318 (31, $[M]^+$), 240 (56), 239 (100), 219 (69), 119 (53); ^1H NMR (400 MHz, CDCl_3): δ 4.58 (2H, s, CH_2), 7.42-7.56 (5H, m, Ar- H); ^{19}F NMR (376 MHz, $\text{CDCl}_3/\text{CFCl}_3$): δ -143.7- -143.9 (2F, m, Ar- F), -143.9- -144.1 (2F, m, Ar- F).

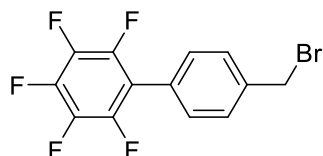
4-(Bromomethyl)-2,3,5,6-tetrafluoro-4'-methoxybiphenyl, 117



2,3,5,6-Tetrafluoro-4'-methoxy-4-methylbiphenyl (0.931 g, 3.45 mmol), AIBN (0.084 g, 0.51 mmol), NBS (2.15 g, 12.1 mmol) and 1,2-dichloroethane (20 mL), after 4 days and column chromatography on silica gel using hexane and ethyl acetate (9:1) as the eluent, afforded *4-(bromomethyl)-2,3,5,6-tetrafluoro-4'-methoxybiphenyl* (1.47 g) as an orange solid. The purity of the product was shown to be 77 % by GC-MS; GC-MS m/z (% relative intensity, ion): 350 (25, $[M]^+$), 348 (26, $[M]^+$), 270 (48), 269 (100), 226

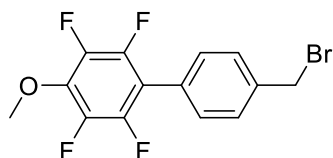
(80); ^1H NMR (400 MHz, CDCl_3): δ 3.87 (3H, s, $\text{O}-\text{CH}_3$), 4.57 (2H, s, CH_2) 6.98-7.06 (2H, m, $\text{Ar}-\text{H}$), 7.37-7.44 (2H, m, $\text{Ar}-\text{H}$); ^{19}F NMR (376 MHz, $\text{CDCl}_3/\text{CFCl}_3$): δ -143.9- -144.1 (2F, m, $\text{Ar}-\text{F}$), -144.3- -144.5 (2F, m, $\text{Ar}-\text{F}$); and was used without further purification.

4'-(Bromomethyl)-2,3,4,5,6-pentafluorobiphenyl, 123



2,3,4,5,6-Pentafluoro-4'-methylbiphenyl (1.30 g, 5.04 mmol), AIBN (0.042 g, 0.26 mmol), NBS (1.08 g, 6.58 mmol) and 1,2-dichloroethane (40 mL), after 2.5 hours and column chromatography on silica gel using hexane as the eluent, afforded 4'-(bromomethyl)-2,3,4,5,6-pentafluorobiphenyl (1.73 g) as a white solid. The purity of the product was shown to be 86 % by ^{19}F NMR spectroscopy; GC-MS m/z (% relative intensity, ion): 338 (5, $[\text{M}]^+$), 336 (5, $[\text{M}]^+$), 257 (100), 237 (51); ^1H NMR (400 MHz, CDCl_3): δ 4.54 (2H, s, CH_2) 7.38-7.43 (2H, m, $\text{Ar}-\text{H}$), 7.50-7.55 (2H, m, $\text{Ar}-\text{H}$); ^{19}F NMR (376 MHz, $\text{CDCl}_3/\text{CFCl}_3$): δ -143.6 (2F, dd, $^3J_{\text{FF}}$ 22.9, $^5J_{\text{FF}}$ 8.1, $\text{Ar}-\text{F}$), -155.5 (1F, t, $^3J_{\text{FF}}$ 21.0, 4-F), -162.3- -162.5 (2F, m, $\text{Ar}-\text{F}$); and was used without further purification.

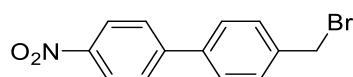
4'-(Bromomethyl)-2,3,5,6-tetrafluoro-4-methoxybiphenyl, 125



2,3,5,6-Tetrafluoro-4-methoxy-4'-methylbiphenyl (1.46 g, 5.40 mmol), AIBN (0.044 g, 0.27 mmol), NBS (1.15 g, 6.46 mmol) and 1,2-dichloroethane (50 mL), after 2.5 hours and column chromatography on silica gel using hexane and ethyl acetate (24:1) as the eluent, afforded 4'-(bromomethyl)-2,3,5,6-tetrafluoro-4-methoxybiphenyl (1.96 g) as a white solid. The purity of the product was shown to be 78 % by ^{19}F NMR spectroscopy;

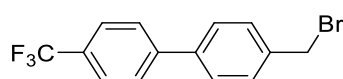
GC-MS m/z (% relative intensity, ion): 350 (24, $[M]^+$), 348 (25, $[M]^+$), 269 (100), 254 (66), 226 (56), 206 (48); ^1H NMR (400 MHz, CDCl_3): δ 4.13 (3H, t, $^5J_{\text{HF}}$ 1.4, O- CH_3), 4.54 (2H, s, CH_2) 7.39-7.44 (2H, m, Ar- H), 7.48-7.54 (2H, m, Ar- H); ^{19}F NMR (376 MHz, $\text{CDCl}_3/\text{CFCl}_3$): δ -145.6 (2F, dd, $^3J_{\text{FF}}$ 21.9, $^5J_{\text{FF}}$ 8.7, Ar- F), -158.5 (2F, dd, $^3J_{\text{FF}}$ 21.9, $^5J_{\text{FF}}$ 8.7, Ar- F); which was used without further purification.

4-(Bromomethyl)-4'-nitrobiphenyl, 154

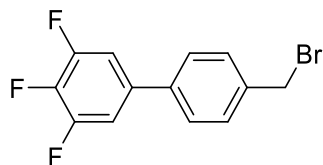


4-Methyl-4'-nitrobiphenyl (0.940 g, 4.41 mmol), AIBN (0.036 g, 0.20 mmol), NBS (0.941 g, 5.29 mmol) and 1,2-dichloroethane (30 mL), after 3 hours and column chromatography on silica gel using hexane and ethyl acetate (4:1) as the eluent, afforded 4-(bromomethyl)-4'-nitrobiphenyl (1.08 g) as a light orange solid. The purity of the product was shown to be 83 % by GC-MS; GC-MS m/z (% relative intensity, ion): 293 (6, $[M]^+$), 291 (6, $[M]^+$), 212 (100), 165 (48); ^1H NMR (400 MHz, CDCl_3): δ 4.58 (2H, s, CH_2) 7.52-7.58 (2H, m, Ar- H), 7.59-7.65 (2H, m, Ar- H), 7.73-7.81 (2H, m, Ar- H), 8.29-8.35 (2H, m, 3'- H , 5'- H); which was used without further purification.

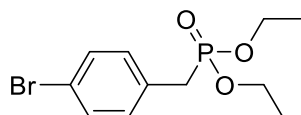
4-(Bromomethyl)-4'-(trifluoromethyl)biphenyl, 155



4-Methyl-4'-(trifluoromethyl)biphenyl (0.830 g, 3.51 mmol), AIBN (0.029 g, 0.18 mmol), NBS (0.750 g, 4.21 mmol) and 1,2-dichloroethane (35 mL), after 2 hours and column chromatography on silica gel using hexane and ethyl acetate (9:1) as the eluent, afforded 4-(bromomethyl)-4'-(trifluoromethyl)biphenyl (1.18 g) as a yellow solid. The purity of the product was shown to be 81 % by ^{19}F NMR spectroscopy; GC-MS m/z (% relative intensity, ion): 316 (4, $[M]^+$), 314 (5, $[M]^+$), 235 (100); ^1H NMR (400 MHz, CDCl_3): δ 4.56 (2H, s, CH_2) 7.47-7.53 (2H, m, Ar- H), 7.55-7.60 (2H, m, Ar- H), 7.65-7.72 (4H, m, Ar- H); ^{19}F NMR (376 MHz, $\text{CDCl}_3/\text{CFCl}_3$): δ -63.0 (s); which was used without further purification; data in agreement with literature.¹⁹

4'-(Bromomethyl)-3,4,5-trifluorobiphenyl, 156

3,4,5-Trifluoro-4'-methylbiphenyl (0.353 g, 1.58 mmol), AIBN (0.013 g, 0.08 mmol), NBS (0.339 g, 1.91 mmol) and 1,2-dichloroethane (20 mL), after 3 hours and column chromatography on silica gel using hexane and ethyl acetate (9:1) as the eluent, afforded 4'-(bromomethyl)-3,4,5-trifluorobiphenyl (0.29 g) as a white solid. The purity of the product was shown to be 85 % by ^{19}F NMR spectroscopy; GC-MS m/z (% relative intensity, ion): 302 (5, $[\text{M}]^+$), 300 (6, $[\text{M}]^+$), 221 (100); ^1H NMR (400 MHz, CDCl_3): δ 4.53 (2H, m, CH_2) 7.15-7.21 (2H, m, 2-*H*, 6-*H*), 7.46-7.48 (4H, m, Ar-*H*); ^{19}F NMR (376 MHz, $\text{CDCl}_3/\text{CFCl}_3$): δ -134.4 (2F, dd, $^3J_{\text{FF}}$ 20.5, $^3J_{\text{FH}}$ 8.6, 3-*F*, 5-*F*), -162.6 (1F, tt, $^3J_{\text{FF}}$ 20.5, $^4J_{\text{FH}}$ 6.4, 4-*F*); which was used without further purification.

6.4.4 Synthesis of Benzylphosphonates Derivatives**Diethyl 4-bromobenzylphosphonate, 108**

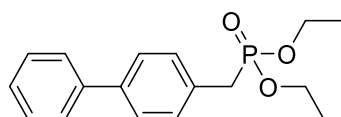
Diethyl phosphite (0.58 mL, 4.50 mmol) was added dropwise to a solution of cesium carbonate (4.41 g, 13.5 mmol) and tetrabutylammonium iodide (5.00 g, 13.5 mmol) in dry DMF (50 mL) and the resulting solution stirred vigorously at room temperature, under argon, for 1 h. 4-Bromobenzyl bromide (3.38 g, 13.5 mmol) was added dropwise to the solution and stirred at room temperature for an additional 24 h. The resulting suspension was then poured into water (50 mL) and extracted with ethyl acetate (3×50 mL). The combined extracts were washed with water (100 mL) and dried (MgSO_4). The mixture was filtered and the solvent removed *in vacuo*. Column chromatography using silica gel with hexane and ethyl acetate (4:1) afforded diethyl 4-bromobenzylphosphonate (0.81 g, 61 %) as a yellow oil; HRMS-ASAP m/z : $[\text{M} + \text{H}^+]$

calcd for $C_{11}H_{17}^{79}BrO_3P$ 307.0099; found 307.0097; GC-MS m/z (% relative intensity, ion): 308 (50, $[M]^+$), 306 (72, $[M]^+$), 278 (67), 250 (66), 199 (80), 168 (98), 124 (88), 108 (100), 96 (85), 88 (95), 80 (92), 63 (99); IR (cm^{-1}): 2983, 1488; 1H NMR (600 MHz, $CDCl_3$): δ 1.22 (6H, t, $^3J_{HH}$ 7.1, CH_3), 3.06 (2H, d, $^2J_{HP}$ 21.7, P- CH_2), 3.94-4.04 (4H, m, CH_2CH_3), 7.14 (2H, dd, $^3J_{HH}$ 8.4, $^4J_{HP}$ 2.5, 2- H , 6- H), 7.40 (2H, d, $^3J_{HH}$ 8.4, 3- H , 5- H); ^{13}C NMR (151 MHz, $CDCl_3$): δ 16.6 (d, $^3J_{CP}$ 6.0, CH_3), 33.5 (d, $^1J_{CP}$ 138.7, P- CH_2), 62.5 (d, $^2J_{CP}$ 6.8, CH_2CH_3), 121.1 (d, $^5J_{CP}$ 4.6, 4- C), 131.0 (d, $^2J_{CP}$ 9.2, 1- C), 131.7 (d, $^3J_{CP}$ 6.6, 2- C , 6- C), 131.9 (d, $^4J_{CP}$ 3.1, 3- C , 5- C); ^{31}P NMR ($CDCl_3$, 243 MHz): δ 25.4 (s); data in agreement with literature.²⁰

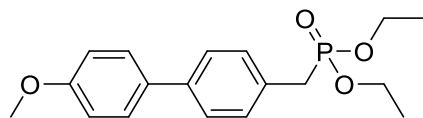
General Michaelis-Arbuzov Procedure

The benzyl bromide was combined with triethylphosphite and the mixture heated and stirred. Excess triethylphosphite and other side products were removed under vacuum, with heating and, where necessary, the desired phosphonate was purified by column chromatography on silica gel.

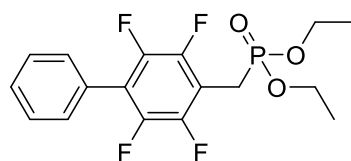
Diethyl Biphenyl-4-ylmethylphosphonate, 97



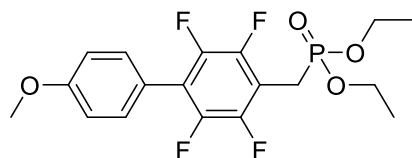
4-(Bromomethyl)biphenyl (1.02 g, 4.13 mmol) and triethylphosphite (1.42 mL, 8.28 mmol), after 4 hours at 120 °C, afforded *diethyl biphenyl-4-ylmethylphosphonate* (1.24 g, 99 %) as a yellow solid; 1H NMR (400 MHz, $CDCl_3$): δ 1.26 (6H, t, $^3J_{HH}$ 7.1, CH_2CH_3), 3.19 (2H, d, $^2J_{HP}$ 21.6, P- CH_2), 3.98-4.11 (4H, m, CH_2CH_3), 7.30-7.40 (3H, m, Ar- H), 7.40-7.47 (2H, m, Ar- H), 7.49-7.63 (4H, m, Ar- H); ^{31}P NMR (162 MHz, $CDCl_3$): δ 25.5 (s); which was used without further purification. Data in agreement with the literature.²¹

Diethyl (4'-Methoxybiphenyl-4-yl)methylphosphonate, 105

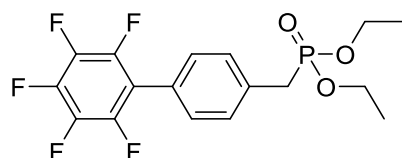
4-(Bromomethyl)-4'-methoxybiphenyl (0.972 g, 3.51 mmol) and triethylphosphite (1.20 mL, 7.00 mmol), after 4 hours at 120 °C, afforded *diethyl (4'-methoxybiphenyl-4-yl)methylphosphonate* (0.88 g, 75 %) as a white solid; GC-MS m/z (% relative intensity, ion): 334 (69, $[M]^+$), 197 (100), 182 (44), 154 (52); ^1H NMR (400 MHz, CDCl_3): δ 1.26 (6H, t, $^3J_{\text{HH}}$ 7.1, CH_2CH_3), 3.18 (2H, d, $^2J_{\text{HP}}$ 21.6, $\text{P}-\text{CH}_2$), 3.84 (3H, s, $\text{O}-\text{CH}_3$), 3.99-4.08 (4H, m, CH_2CH_3), 6.93-7.00 (2H, m, $\text{Ar}-\text{H}$), 7.31-7.38 (2H, m, $\text{Ar}-\text{H}$), 7.45-7.56 (4H, m, $\text{Ar}-\text{H}$); ^{31}P NMR (162 MHz, CDCl_3): δ 25.6 (s); which was used without further purification.

Diethyl (2,3,5,6-Tetrafluorobiphenyl-4-yl)methylphosphonate, 116

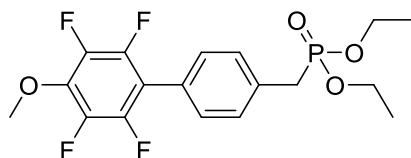
4-(Bromomethyl)-2,3,5,6-tetrafluorobiphenyl (1.14 g, 3.57 mmol) and triethylphosphite (1.23 mL, 7.17 mmol), after 4 hours at 120 °C, afforded *diethyl (2,3,5,6-tetrafluorobiphenyl-4-yl)methylphosphonate* (1.24 g, 92 %) as a yellow oil; ^1H NMR (400 MHz, CDCl_3): δ 1.33 (6H, t, $^3J_{\text{HH}}$ 7.1, CH_2CH_3), 3.31 (2H, d, $^2J_{\text{HP}}$ 21.5, $\text{P}-\text{CH}_2$), 4.08-4.23 (4H, m, CH_2CH_3), 7.40-7.53 (5H, m, $\text{Ar}-\text{H}$); ^{19}F NMR (376 MHz, $\text{CDCl}_3/\text{CFCl}_3$): δ -142.8- -143.0 (2F, m, $\text{Ar}-\text{F}$), -144.6- -145.0 (2F, m, $\text{Ar}-\text{F}$). ^{31}P NMR (162 MHz, CDCl_3): δ 21.2 (s); which was used without further purification.

Diethyl (2,3,5,6-Tetrafluoro-4'-methoxybiphenyl-4-yl)methylphosphonate, 118

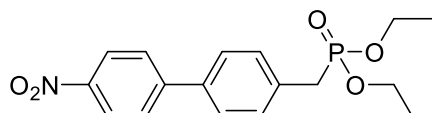
4-(Bromomethyl)-2,3,5,6-tetrafluoro-4'-methoxybiphenyl (1.13 g, 3.24 mmol) and triethylphosphite (1.44 mL, 8.40 mmol), after 4 hours at 120 °C and column chromatography on silica gel using hexane and ethyl acetate (2:3) as the eluent, afforded *diethyl (2,3,5,6-tetrafluoro-4'-methoxybiphenyl-4-yl)methylphosphonate* (1.12 g, 85 %) as a yellow oil; GC-MS *m/z* (% relative intensity, ion): 406 (86, [M]⁺), 270 (36), 269 (96), 226 (80), 109 (100), 91 (49), 81 (71); ¹H NMR (400 MHz, CDCl₃): δ 1.28 (6H, t, ³J_{HH} 7.0, CH₂CH₃), 3.26 (2H, d, ²J_{HP} 21.4, P-CH₂), 3.80 (3H, s, O-CH₃), 4.07-4.17 (4H, m, CH₂CH₃), 6.91-7.00 (2H, m, Ar-H), 7.30-7.40 (2H, m, Ar-H); ¹⁹F NMR (376 MHz, CDCl₃/CFCl₃): δ -142.3- -142.9 (2F, m, Ar-F), -145.1- -145.4 (2F, m, Ar-F); ³¹P NMR (162 MHz, CDCl₃): δ 21.3 (s).

Diethyl (2',3',4',5',6'-Pentafluorobiphenyl-4-yl)methylphosphonate, 124

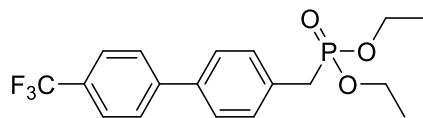
4'-(Bromomethyl)-2,3,4,5,6-pentafluorobiphenyl (1.39 g, 4.12 mmol) and triethylphosphite (1.65 mL, 9.62 mmol), after 4 hours at 120 °C and column chromatography on silica gel using DCM as the eluent, afforded *diethyl (2',3',4',5',6'-pentafluorobiphenyl-4-yl)methylphosphonate* (1.45 g, 89 %) as a white solid; GC-MS *m/z* (% relative intensity, ion): 394 (59, [M]⁺), 337 (36), 284 (35), 271 (43), 258 (41), 257 (100), 237 (80), 124 (70), 109 (83), 97 (47), 91 (33), 81 (67); ¹H NMR (400 MHz, CDCl₃): δ 1.26 (6H, t, ³J_{HH} 7.1, CH₂CH₃), 3.21 (2H, d, ²J_{HP} 21.9, P-CH₂), 4.01-4.10 (4H, m, CH₂CH₃), 7.35-7.40 (2H, m, Ar-H), 7.41-7.47 (2H, m, Ar-H); ¹⁹F NMR (376 MHz, CDCl₃/CFCl₃): δ -143.7 (2F, dd, ³J_{FF} 23.0, ⁵J_{FF} 8.1, Ar-F), -156.0 (1F, t, ³J_{FF} 21.0, 4'-F), -162.6- -162.8 (2F, m, Ar-F); ³¹P NMR (162 MHz, CDCl₃): δ 24.8 (s).

Diethyl (2',3',5',6'-Tetrafluoro-4'-methoxybiphenyl-4-yl)methylphosphonate, 126

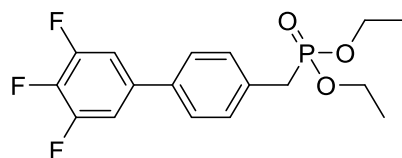
4'-(Bromomethyl)-2,3,5,6-tetrafluoro-4-methoxybiphenyl (1.90 g, 5.44 mmol) and triethylphosphite (1.87 mL, 10.9 mmol), after 4 hours at 120 °C and column chromatography on silica gel using DCM as the eluent, afforded *diethyl (2',3',5',6'-tetrafluoro-4'-methoxybiphenyl-4-yl)methylphosphonate* (2.15 g, 97 %) as a white solid; GC-MS m/z (% relative intensity, ion): 406 (60, $[M]^+$), 378 (46), 350 (34), 296 (44), 283 (52), 269 (100), 254 (60), 226 (53), 206 (37), 124 (32), 109 (55), 97 (34), 81 (50); ^1H NMR (400 MHz, CDCl_3): δ 1.25 (6H, t, $^3J_{\text{HH}}$ 7.0, CH_2CH_3), 3.20 (2H, d, $^2J_{\text{HP}}$ 21.8, $\text{P}-\text{CH}_2$), 3.99-4.09 (4H, m, CH_2CH_3), 4.11 (3H, t, $^5J_{\text{HF}}$ 1.3, $\text{O}-\text{CH}_3$), 7.34-7.43 (4H, m, $\text{Ar}-\text{H}$); ^{19}F NMR (376 MHz, $\text{CDCl}_3/\text{CFCl}_3$): δ -145.6 (2F, dd, $^3J_{\text{FF}}$ 22.1, $^5J_{\text{FF}}$ 8.6, $\text{Ar}-\text{F}$), -156.0 (2F, dd, $^3J_{\text{FF}}$ 22.1, $^5J_{\text{FF}}$ 8.6, $\text{Ar}-\text{F}$); ^{31}P NMR (162 MHz, CDCl_3): δ 25.0 (s).

Diethyl (4'-Nitrobiphenyl-4-yl)methylphosphonate, 157

4-(Bromomethyl)-4'-nitrobiphenyl (0.845 g, 2.89 mmol) and triethylphosphite (1.20 mL, 7.00 mmol), after 4 hours at 120 °C and column chromatography on silica gel using a gradient of 20 to 100 % DCM in hexane as the eluent, afforded *diethyl (4'-nitrobiphenyl-4-yl)methylphosphonate* (1.05 g) as a dark orange oil. The product was shown to be 67 % pure by GC-MS; GC-MS m/z (% relative intensity, ion): 350 (17, $[M + \text{H}]^+$), 349 (75, $[M]^+$), 226 (45), 212 (94), 166 (75), 165 (100); ^1H NMR (400 MHz, CDCl_3): δ 1.26 (6H, t, $^3J_{\text{HH}}$ 7.1, CH_2CH_3), 3.19 (2H, d, $^2J_{\text{HP}}$ 21.8, CH_2), 3.99-4.07 (4H, m, CH_2CH_3), 7.42 (2H, d, $^3J_{\text{HH}}$ 8.3, $\text{Ar}-\text{H}$), 7.55-7.59 (2H, m, $\text{Ar}-\text{H}$), 7.71 (2H, d, $^3J_{\text{HH}}$ 8.8, $\text{Ar}-\text{H}$), 8.23-8.30 (2H, m, 3'- H , 5'- H); ^{31}P NMR (162 MHz, CDCl_3): δ 25.8 (s).

Diethyl (4'-(Trifluoromethyl)biphenyl-4-yl)methylphosphonate, 158

4-(Bromomethyl)-4'-(trifluoromethyl)biphenyl (0.820 g, 2.60 mmol) and triethylphosphite (1.10 mL, 6.41 mmol), after 4 hours at 120 °C and column chromatography on silica gel using a gradient of 40 to 60 % ethyl acetate in hexane as the eluent, afforded *diethyl (4'-(trifluoromethyl)biphenyl-4-yl)methylphosphonate* (0.77 g, 80 %) as a light yellow solid; GC-MS m/z (% relative intensity, ion): 373 (12, [M + H]⁺), 372 (47, [M]⁺), 235 (100); ¹H NMR (400 MHz, CDCl₃): δ 1.27 (6H, t, ³J_{HH} 7.0, CH₂CH₃), 3.20 (2H, d, ²J_{HP} 21.7, P-CH₂), 4.00-4.10 (4H, m, CH₂CH₃), 7.41 (2H, dd, ³J_{HH} 8.3, ⁴J_{HH} 2.5, Ar-H), 7.52-7.59 (2H, m, Ar-H), 7.68 (4H, s, Ar-H); ¹⁹F NMR (376 MHz, CDCl₃/CFCl₃): δ -62.9 (s); ³¹P NMR (162 MHz, CDCl₃): δ 26.1 (s).

Diethyl (3',4',5'-Trifluorobiphenyl-4-yl)methylphosphonate, 159

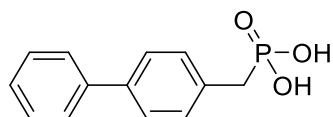
4'-(Bromomethyl)-3,4,5-trifluorobiphenyl (0.227 g, 0.75 mmol) and triethylphosphite (0.30 mL, 1.77 mmol), after 4 hours at 120 °C and column chromatography on silica gel using a gradient of 40 to 60 % ethyl acetate in hexane as the eluent, afforded *diethyl (3',4',5'-trifluorobiphenyl-4-yl)methylphosphonate* (0.24 g, 89 %) as a light yellow solid; GC-MS m/z (% relative intensity, ion): 359 (13, [M + H]⁺), 358 (55, [M]⁺), 221 (100); ¹H NMR (400 MHz, CDCl₃): δ 1.26 (6H, t, ³J_{HH} 7.1, CH₂CH₃), 3.18 (2H, d, ²J_{HP} 21.8, P-CH₂), 3.99-4.09 (4H, m, CH₂CH₃), 7.10-7.22 (2H, m, 2'-H, 6'-H), 7.37 (2H, d, ³J_{HH} 8.2, Ar-H), 7.44 (2H, d, ³J_{HH} 8.2, Ar-H); ¹⁹F NMR (376 MHz, CDCl₃/CFCl₃): δ -134.7 (2F, dd, ³J_{FF} 20.5, ³J_{FH} 9.0, 3'-F, 5'-F), -163.1- -163.3 (1F, m, 4'-F); ³¹P NMR (162 MHz, CDCl₃): δ 25.9 (s).

6.4.5 Synthesis of Biphenyl Benzylphosphonic Acids

General Procedure for the Hydrolysis of Phosponates to Phosphonic Acids

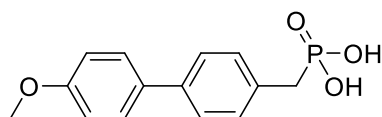
In a flame dried flask, under an inert atmosphere, the phosphonate was dissolved in dry DCM. Bromotrimethylsilane was added via syringe and the reaction stirred at room temperature. Volatile materials were removed under reduced pressure and the resulting product dissolved in an excess of 10:1 methanol:water and stirred overnight. Volatile materials were removed under reduced pressure and the crude product was purified by recrystallisation to yield to yield the benzylphosphonic acid.

Biphenyl-4-ylmethylphosphonic Acid, 92



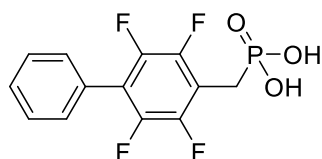
Diethyl biphenyl-4-ylmethylphosphonate (1.24 g, 4.07 mmol), dry DCM (20 mL) and bromotrimethylsilane (1.72 mL, 13.0 mmol), after 6 hours and recrystallisation from hexane, yielded *biphenyl-4-ylmethylphosphonic acid* (1.00 g, 99 %) as a white solid; mp 247-249 °C [lit²² 250 °C]; Anal. Calcd for C₁₃H₁₃O₃P: C, 62.90; H, 5.28. Found: C, 62.69; H, 5.18; HRMS-ASAP *m/z*: [M + H⁺] calcd for C₁₃H₁₄O₃P 249.0681; found 249.0698; ASAP *m/z* (% relative intensity, ion): 249 (100, [M + H]⁺), 248 (46, [M]⁺), 167 (48), 165 (31), 152 (16); IR (cm⁻¹): 2935, 2268, 1634, 1518, 1485; ¹H NMR (600 MHz, *d*₆-DMSO): δ 3.00 (2H, d, ²J_{HP} 21.4, P-CH₂), 7.31-7.37 (3H, m, Ar-H), 7.42-7.47 (2H, m, Ar-H), 7.55-7.59 (2H, m, Ar-H), 7.60-7.68 (2H, m, Ar-H); ¹³C NMR (151 MHz, *d*₆-DMSO): δ 35.1 (d, ¹J_{CP} 131.7, P-CH₂), 126.3 (d, ⁴J_{CP} 2.9, 2-C, 6-C), 126.5 (s, Ar-CH), 127.2 (s, Ar-CH), 128.9 (s, Ar-CH), 130.3 (d, ³J_{CP} 6.3, 3-C, 5-C), 133.6 (d, ²J_{CP} 8.8, 4-C), 137.9 (d, ⁵J_{CP} 3.6, 1-C), 140.1 (s, 1'-C); ³¹P NMR (243 MHz, *d*₆-DMSO): δ 21.0 (s).

(4'-Methoxybiphenyl-4-yl)methylphosphonic Acid, 93

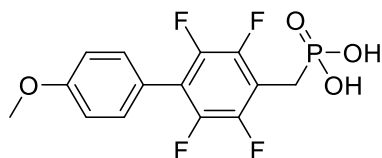


Diethyl (4'-methoxybiphenyl-4-yl)methylphosphonate (0.876 g, 2.62 mmol), dry DCM (25 mL) and bromotrimethylsilane (1.11 mL, 8.41 mmol), after 5 hours and recrystallisation from hexane, yielded (4'-methoxybiphenyl-4-yl)methylphosphonic acid (0.64 g, 88 %) as a white solid; mp 254-256 °C; HRMS-ASAP m/z : $[M^+]$ calcd for $C_{14}H_{15}O_4P$ 278.0708; found 278.0709; ASAP m/z (% relative intensity, ion): 279 (100, $[M + H]^+$), 278 (43, $[M]^+$), 198 (11), 197 (76); IR (cm^{-1}): 2840, 2346, 2018, 1607, 1498; 1H NMR (700 MHz, d_6 -DMSO): δ 2.98 (2H, d, $^2J_{HP}$ 21.3, P-CH₂), 3.79 (3H, s, O-CH₃), 7.01 (2H, d, $^3J_{HH}$ 8.8, Ar-H), 7.27-7.32 (2H, m, Ar-H), 7.52 (2H, d, $^3J_{HH}$ 8.0, Ar-H), 7.55-7.60 (2H, m, Ar-H); ^{13}C NMR (176 MHz, d_6 -DMSO): δ 35.0 (d, $^1J_{CP}$ 131.8, P-CH₂), 55.2 (s, O-CH₃), 114.3 (s, Ar-CH), 125.8 (d, $^4J_{CP}$ 2.8, 2-C, 6-C), 127.5 (s, Ar-CH), 130.2 (d, $^3J_{CP}$ 6.3, 3-C, 5-C), 132.5 (s, 1'-C), 132.8 (d, $^2J_{CP}$ 8.9, 4-C), 137.6 (d, $^5J_{CP}$ 3.5, 1-C), 158.7 (s, 4'-C); ^{31}P NMR (283 MHz, d_6 -DMSO): δ 21.0 (s).

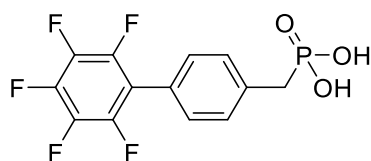
(2,3,5,6-Tetrafluorobiphenyl-4-yl)methylphosphonic Acid, 94



Diethyl (2,3,5,6-tetrafluorobiphenyl-4-yl)methylphosphonate (1.20 g, 3.19 mmol), dry DCM (30 mL) and bromotrimethylsilane (1.35 mL, 10.2 mmol), after 5 hours and recrystallisation from acetonitrile, yielded (2,3,5,6-tetrafluorobiphenyl-4-yl)methylphosphonic acid (0.72 g, 71 %) as a white solid; mp 257-260 °C; HRMS-ASAP m/z : $[M^+]$ calcd for $C_{13}H_{10}O_3F_4P$ 321.0304; found 321.0313; ASAP m/z (% relative intensity, ion): 321 (100, $[M + H]^+$), 300 (19); IR (cm^{-1}): 2955, 2361, 1577, 1482, 1436; 1H NMR (700 MHz, d_6 -DMSO): δ 3.15 (2H, d, $^2J_{HP}$ 20.8, P-CH₂), 7.47-7.53 (3H, m, Ar-H), 7.53-7.58 (2H, m, Ar-H), 10.7 (2H, bs, P(OH)₂); ^{13}C NMR (176 MHz, d_6 -DMSO): δ 23.9 (d, $^1J_{CP}$ 132.3, P-CH₂), 113.5 (td, $^2J_{CF}$ 18.7, $^2J_{CP}$ 9.6, 4-C), 118.0 (td, $^2J_{CF}$ 17.3, $^5J_{CP}$ 3.6, 1-C), 126.8 (s, 1'-C), 128.8 (s, Ar-CH), 129.3 (s, Ar-CH), 130.0 (s, Ar-CH), 143.0 (dm, $^1J_{CF}$ 243.0, Ar-CF), 144.7 (dm, $^1J_{CF}$ 247.0, Ar-CF); ^{19}F NMR (188 MHz, d_6 -DMSO): δ -142.3 (2F, ddd, $^3J_{FF}$ 23.7, $^5J_{FF}$ 12.1, $^4J_{FF}$ 4.5, Ar-F), -146.1 (2F, ddm, $^3J_{FF}$ 23.7, $^5J_{FF}$ 12.1, Ar-F); ^{31}P NMR (283 MHz, d_6 -DMSO): δ 16.6 (s).

(2,3,5,6-Tetrafluoro-4'-methoxybiphenyl-4-yl)methylphosphonic Acid, 95

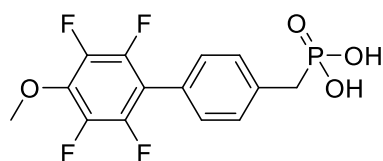
Diethyl (2,3,5,6-tetrafluoro-4'-methoxybiphenyl-4-yl)methylphosphonate (1.12 g, 2.76 mmol), dry DCM (20 mL) and bromotrimethylsilane (1.17 mL, 8.87 mmol), after 6 hours and recrystallisation from acetonitrile, yielded (2,3,5,6-tetrafluoro-4'-methoxybiphenyl-4-yl)methylphosphonic acid (0.54 g, 56 %) as a white solid; mp 258-259 °C; Anal. Calcd for C₁₄H₁₁F₄O₄P: C, 48.02; H, 3.17. Found: C, 47.99; H, 3.11; HRMS-ASAP *m/z*: [M⁺] calcd for C₁₄H₁₁O₄F₄P 350.0331; found 350.0323; ASAP *m/z* (% relative intensity, ion): 351 (100, [M + H]⁺); IR (cm⁻¹): 2162, 1612, 1520, 1481, 1444, 1411; ¹H NMR (600 MHz, *d*₆-DMSO): δ 3.13 (2H, d, ²J_{HP} 20.7, P-CH₂), 3.82 (3H, s, O-CH₃), 7.08-7.12 (2H, m, Ar-H), 7.45 (2H, d, ³J_{HH} 8.5, Ar-H); ¹³C NMR (176 MHz, *d*₆-DMSO): δ 23.8 (d, ¹J_{CP} 132.6, P-CH₂), 55.3 (s, O-CH₃), 112.8 (td, ²J_{CF} 18.7, ²J_{CP} 9.7, 4-C), 114.4 (s, Ar-CH), 117.8 (td, ²J_{CF} 17.0, ⁵J_{CP} 3.3, 1-C), 118.7 (s, 1'-C), 131.4 (s, Ar-CH), 143.1 (dm, ¹J_{CF} 242.4, Ar-CF), 144.7 (dm, ¹J_{CF} 242.9, Ar-CF), 159.9 (s, 4'-C); ¹⁹F NMR (564 MHz, *d*₆-DMSO): δ -142.1- -142.3 (2F, m, Ar-F), -145.8- -146.0 (2F, m, Ar-F); ³¹P NMR (243 MHz, *d*₆-DMSO): δ 16.6 (s).

(2',3',4',5',6'-Pentafluorobiphenyl-4-yl)methylphosphonic Acid, 119

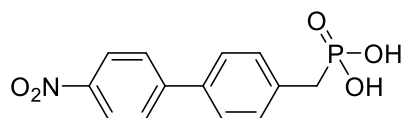
Diethyl (2',3',4',5',6'-pentafluorobiphenyl-4-yl)methylphosphonate (1.41 g, 3.58 mmol), dry DCM (35 mL) and bromotrimethylsilane (1.51 mL, 11.4 mmol), after 5 hours and recrystallisation from acetonitrile, yielded (2',3',4',5',6'-pentafluorobiphenyl-4-yl)methylphosphonic acid (0.93 g, 77 %) as a white solid; mp 235-237 °C; HRMS-ASAP *m/z*: [M⁺] calcd for C₁₃H₈O₃F₅P 338.0131; found 338.0135; ASAP *m/z* (% relative intensity, ion): 339 (100, [M + H]⁺), 338 (14, [M]⁺), 258 (4), 257

(32); IR (cm⁻¹): 2600, 2164, 1654, 1511, 1489, 1411; ¹H NMR (600 MHz, *d*₆-DMSO): δ 3.05 (2H, d, ²J_{HP} 21.6, P-CH₂), 7.37-7.46 (4H, m, Ar-H), 8.70 (2H, bs, P-OH); ¹³C NMR (151 MHz, *d*₆-DMSO): δ 35.3 (d, ¹J_{CP} 131.2, P-CH₂), 115.5 (t, ²J_{CF} 17.7, 1'-C), 123.4 (s, 4-C), 129.7 (s, 3-C, 5-C), 130.3 (d, ³J_{CP} 6.1, 2-C, 6-C), 136.1 (d, ²J_{CP} 8.8, 1-C), 137.3 (dtm, ¹J_{CF} 247.6, ²J_{CF} 15.4, 4'-C), 139.7 (dm, ¹J_{CF} 250.7, Ar-CF), 143.7 (dm, ¹J_{CF} 244.5, Ar-CF); ¹⁹F NMR (564 MHz, *d*₆-DMSO): δ -143.5- -143.8 (2F, m, Ar-F), -156.5 (1F, t, ³J_{FF} 22.3, 4'-F), -162.6- -162.9 (2F, m, Ar-F); ³¹P NMR (243 MHz, *d*₆-DMSO): δ 20.4 (s).

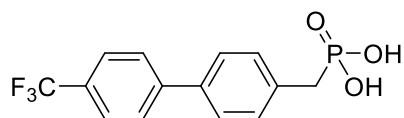
(2',3',5',6'-Tetrafluoro-4'-methoxybiphenyl-4-yl)methylphosphonic Acid, 120



Diethyl (2',3',5',6'-tetrafluoro-4'-methoxybiphenyl-4-yl)methylphosphonate (2.10 g, 5.17 mmol), dry DCM (55 mL) and bromotrimethylsilane (2.18 mL, 16.5 mmol), after 5 hours and recrystallisation from methanol:water (1:1), yielded (2',3',5',6'-tetrafluoro-4'-methoxybiphenyl-4-yl)methylphosphonic acid (1.00 g, 56 %) as a white solid; mp 259-262 °C; HRMS-ASAP *m/z*: [M + H⁺] calcd for C₁₄H₁₂O₄F₄P 351.0409; found 351.0419; ASAP *m/z* (% relative intensity, ion): 351 (100, [M + H]⁺), 350 (16, [M]⁺); IR (cm⁻¹): 2958, 2334, 1652, 1482, 1413; ¹H NMR (600 MHz, *d*₆-DMSO): δ 3.04 (2H, d, ²J_{HP} 21.5, P-CH₂), 4.09 (3H, s, O-CH₃), 7.35-7.45 (4H, m, Ar-H), 9.59 (bs, P-OH); ¹³C NMR (151 MHz, *d*₆-DMSO): δ 35.3 (d, ¹J_{CP} 131.1, P-CH₂), 62.3 (t, ⁴J_{CF} 3.3, O-CH₃), 113.6 (t, ²J_{CF} 18.1, 1'-C), 124.1 (bs, 4-C), 129.7 (bs, 3-C, 5-C), 130.1 (d, ³J_{CP} 6.1, 2-C, 6-C), 135.6 (d, ²J_{CP} 8.7, 1-C), 136.8-137.1 (m, 4'-C), 140.7 (dm, ¹J_{CF} 245.3, Ar-CF), 143.8 (dm, ¹J_{CF} 243.4, Ar-CF); ¹⁹F NMR (564 MHz, *d*₆-DMSO): δ -145.4 (2F, dd, ³J_{FF} 23.6, ⁵J_{FF} 8.2, Ar-F), -158.1 (2F, dd, ³J_{FF} 23.6, ⁵J_{FF} 8.2, Ar-F); ³¹P NMR (243 MHz, *d*₆-DMSO): δ 20.5 (s).

(4'-Nitrobiphenyl-4-yl)methylphosphonic Acid, 134

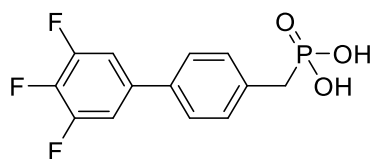
Diethyl (4'-nitrobiphenyl-4-yl)methylphosphonate (0.690 g, 1.98 mmol), dry DCM (40 mL) and bromotrimethylsilane (1.25 mL, 9.47 mmol), after 16 hours and recrystallisation from acetonitrile, yielded (4'-nitrobiphenyl-4-yl)methylphosphonic acid (0.35 g, 60 %) as a brown solid; mp 199-201 °C; HRMS-ASAP m/z : $[M^+]$ calcd for $C_{13}H_{12}NO_5P$ 293.0453; found 293.0447; ASAP m/z (% relative intensity, ion): 294 (100, $[M + H]^+$) 293 (33, $[M]^+$); IR (cm^{-1}): 2362, 2084, 2016, 1742, 1605, 1521, 1486; 1H NMR (700 MHz, d_6 -DMSO): δ 3.04 (2H, d, $^2J_{HP}$ 21.5, CH_2), 7.41 (2H, dd, $^3J_{HH}$ 8.2, $^4J_{HP}$ 2.3, 3-*H*, 5-*H*), 7.72 (2H, d, $^3J_{HH}$ 8.2, 2-*H*, 6-*H*), 7.95 (2H, d, $^3J_{HH}$ 8.8, 2'-*H*, 6'-*H*), 8.29 (2H, d, $^3J_{HH}$ 8.8, 3'-*H*, 5'-*H*); ^{13}C NMR (176 MHz, d_6 -DMSO): δ 35.2 (d, $^1J_{CP}$ 131.2, P- CH_2), 124.1 (s, Ar- CH), 126.9 (d, $^4J_{CP}$ 2.9, 2-*C*, 6-*C*), 127.5 (s, Ar- CH), 130.6 (d, $^3J_{CP}$ 6.2, 3-*C*, 5-*C*), 135.4 (d, $^5J_{CP}$ 3.5, 1-*C*), 135.6 (d, $^2J_{CP}$ 8.8, 4-*C*), 146.5 (s, 4'-*C*), 146.6 (d, $^6J_{CP}$ 1.4, 1'-*C*); ^{31}P NMR (283 MHz, d_6 -DMSO): δ 20.5 (s).

(4'-(Trifluoromethyl)biphenyl-4-yl)methylphosphonic Acid, 135

Diethyl (4'-(trifluoromethyl)biphenyl-4-yl)methylphosphonate (0.752 g, 2.02 mmol), dry DCM (25 mL) and bromotrimethylsilane (0.85 mL, 6.46 mmol), after 19 hours and recrystallisation from acetonitrile, yielded (4'-(trifluoromethyl)biphenyl-4-yl)methylphosphonic acid (0.35 g, 54 %) as a white solid; mp 232-235 °C; HRMS-ASAP m/z : $[M^+]$ calcd for $C_{14}H_{12}O_3F_3P$ 316.0476; found 316.0472; ASAP m/z (% relative intensity, ion): 317 (100, $[M + H]^+$) 316 (74, $[M]^+$); IR (cm^{-1}): 2604, 2288, 2178, 2102, 1615, 1532, 1499, 1400; 1H NMR (700 MHz, d_6 -DMSO): δ 3.03 (2H, d, $^2J_{HP}$ 21.5, P- CH_2), 7.38 (2H, dd, $^3J_{HH}$ 8.2, $^4J_{HP}$ 2.3, 3-*H*, 5-*H*), 7.66 (2H, dd, $^3J_{HH}$ 8.2, 2-*H*, 6-*H*), 7.80 (2H, d, $^3J_{HH}$ 8.1, Ar-*H*), 7.88 (2H, d, $^3J_{HH}$ 8.1, Ar-*H*); ^{13}C NMR (176

MHz, d_6 -DMSO): δ 35.1 (d, $^1J_{CP}$ 131.3, P-CH₂), 124.4 (d, $^1J_{CF}$ 271.8, CF₃), 125.7 (d, $^4J_{CF}$ 3.8, 2'-C, 6'-C), 126.6 (d, $^4J_{CP}$ 2.9, 2-C, 6-C), 127.2 (s, 3'-C, 5'-C), 127.6 (d, $^2J_{CF}$ 31.7, 4'-C), 130.5 (d, $^3J_{CP}$ 6.2, 3-C, 5-C), 134.9 (d, $^2J_{CP}$ 8.8, 4-C), 136.2 (d, $^5J_{CP}$ 3.4, 1-C), 144.1 (s, 1'-C); ^{19}F NMR (376 MHz, d_6 -DMSO): δ -60.8 (s); ^{31}P NMR (283 MHz, d_6 -DMSO): δ 20.6 (s).

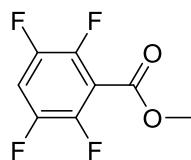
(3',4',5'-Trifluorobiphenyl-4-yl)methylphosphonic Acid, 136



Diethyl (3',4',5'-trifluorobiphenyl-4-yl)methylphosphonate (0.215 g, 0.60 mmol), dry DCM (10 mL) and bromotrimethylsilane (0.25 mL, 1.92 mmol), after 19 hours and recrystallisation from acetonitrile, yielded (3',4',5'-trifluorobiphenyl-4-yl)methylphosphonic acid (0.10 g, 57 %) as a white solid; mp 209-212 °C; HRMS-ASAP m/z : [M + H⁺] calcd for C₁₃H₁₁O₃F₃P 303.0398; found 303.0404; ASAP m/z (% relative intensity, ion): 303 (100, [M + H]⁺), 302 (70, [M]⁺); IR (cm⁻¹): 2732, 2272, 2159, 1964, 1617, 1573, 1540, 1509, 1446, 1402; ^1H NMR (700 MHz, d_6 -DMSO): δ 3.01 (2H, d, $^2J_{HP}$ 21.5, P-CH₂), 7.34 (2H, dd, $^3J_{HH}$ 8.2, $^4J_{HP}$ 2.3, 3-H, 5-H), 7.65 (2H, d, $^3J_{HH}$ 8.2, 2-H, 6-H), 7.67 (2H, $^3J_{HF}$ 9.5, $^4J_{HP}$ 6.6, 2'-H, 6'-H); ^{13}C NMR (176 MHz, d_6 -DMSO): δ 35.1 (d, $^1J_{CP}$ 131.3, P-CH₂), 110.9 (dd, $^2J_{CF}$ 17.5, $^3J_{CF}$ 3.7, 1'-C), 126.4 (d, $^4J_{CP}$ 2.9, 2-C, 6-C), 130.4 (d, $^3J_{CP}$ 6.2, 3-C, 5-C), 134.4-134.6 (m, Ar-C), 135.0 (d, $^2J_{CF}$ 8.8, 2'-C, 6'-C), 136.6-137.0 (m, Ar-C), 138.1 (dm, $^1J_{CF}$ 249.0, 4'-C), 150.6 (ddd, $^1J_{CF}$ 246.3, $^2J_{CF}$ 9.7, $^3J_{CF}$ 4.0, 3'-H, 5'-C); ^{19}F NMR (564 MHz, d_6 -DMSO): δ -135.4 (2F, dd, $^3J_{FF}$ 21.9, $^3J_{FH}$ 9.7, 3'-F, 5'-F), -164.3 (1F, tt, $^3J_{FF}$ 21.9, $^4J_{FH}$ 6.8, 4'-F); ^{31}P NMR (283 MHz, d_6 -DMSO): δ 20.6 (s).

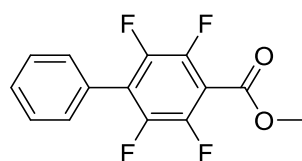
6.4.6 Synthesis of a Biphenyl Carboxylic Acid Derivative

Methyl 2,3,5,6-Tetrafluorobenzoate, 129



A mixture of 2,3,5,6-tetrafluorobenzoic acid (4.00 g, 20.6 mmol), thionyl chloride (16 mL, 0.22 mol) and DMF (0.50 mL) was heated at 80 °C for 8 h after which the excess thionyl chloride was removed by evaporation under reduced pressure to leave a residue of 1-chlorocarbonyl-2,3,5,6-tetrafluorobenzene. To this was added 40 mL of dry methanol and the mixture stirred for 3 hours at room temperature. Removal of excess methanol *in vacuo* afforded *methyl 2,3,5,6-tetrafluorobenzoate* (1.80 g, 42 %) as a yellow liquid; GC-MS *m/z* (% relative intensity, ion): 208 (83, [M]⁺), 189 (43), 178 (48), 177 (100), 149 (92), 130 (35), 99 (95), 80 (44), 59 (37); ¹H NMR (400 MHz, CDCl₃): δ 3.99 (3H, s, O-CH₃), 7.20 (1H, tt, ³J_{HF} 9.5, ⁴J_{HF} 7.2, Ar-H); ¹⁹F NMR (376 MHz, CDCl₃/CFCl₃): δ -137.8- -138.0 (2F, m, Ar-F), -139.8- -140.0 (2F, m, Ar-F); data in agreement with literature.

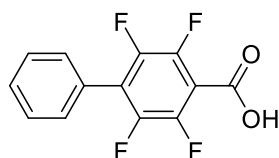
Methyl 2,3,5,6-Tetrafluorobiphenyl-4-carboxylate, 130



In a flame dried flask, under an inert atmosphere, iodobenzene (0.39 mL, 3.50 mmol), Pd(OAc)₂ (0.039 g, 0.18 mmol), PPh₃ (0.092 g, 0.35 mmol), silver carbonate (0.960 g, 3.50 mmol) and methyl 2,3,5,6-tetrafluorobenzoate (1.00 mL, 7.00 mmol) were stirred for 1 minute before the addition of deionised water (15 mL). The resulting solution was heated to 70 °C and stirred for 24 h. The reaction was cooled to room temperature, added to ethyl acetate, filtered through Celite[®] and extracted with brine. Column chromatography using silica gel with hexane and DCM (2:3) as the eluent afforded a

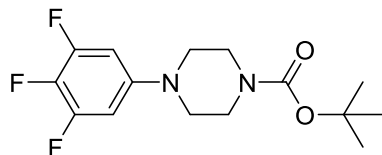
white solid containing a 1:1 mixture of methyl 2,3,5,6-tetrafluorobiphenyl-4-carboxylate and methyl 2,3,5,6-tetrafluorobenzoate. To this white solid was added, iodobenzene (0.39 mL, 3.50 mmol), Pd(OAc)₂ (0.039 g, 0.18 mmol), PPh₃ (0.092 g, 0.35 mmol) and silver carbonate (0.960 g, 3.50 mmol), and deionised water (15 mL) and the reaction repeated. Column chromatography using silica gel with hexane and DCM (2:3) as the eluent afforded *methyl 2,3,5,6-tetrafluorobiphenyl-4-carboxylate* (0.75 g, 38 %) as a white solid; GC-MS *m/z* (% relative intensity, ion): 284 (81, [M]⁺), 253 (100), 224 (59), 206 (36); ¹H NMR (400 MHz, CDCl₃): δ 4.01 (3H, s, O-CH₃), 7.42-7.57 (5H, m, Ar-H); ¹⁹F NMR (376 MHz, CDCl₃/CFCl₃): δ -140.0- -140.2 (2F, m, Ar-F), -143.0- -143.2 (2F, m, Ar-F); data in agreement with literature.²³

2,3,5,6-Tetrafluorobiphenyl-4-carboxylic Acid, 127

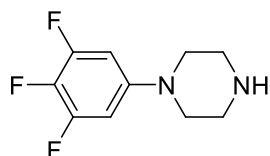


Methyl 2,3,5,6-tetrafluorobiphenyl-4-carboxylate (0.750 g, 2.64 mmol) was added to THF (20 mL) and methanol (20 mL) and stirred for 1 minute at room temperature. KOH solution (2M, 5 mL) was then added drop wise and the resulting solution stirred at room temperature overnight. The organic layer was removed *in vacuo* and the aqueous layer acidified with HCl solution (2M, 20 mL). The formed precipitate was filtered, washed thoroughly with water and dried, affording *2,3,5,6-tetrafluorobiphenyl-4-carboxylic acid* (0.50 g, 70 %) as a white solid; mp 201-203 °C [lit²⁴ 200-201 °C]; Anal. Calcd for C₁₃H₆F₄O₂: C, 57.79; H, 2.24. Found: C, 57.61; H, 2.21; HRMS-ASAP *m/z*: [M⁺] calcd for C₁₃H₆F₄O₂ 270.0304; found 270.0293; ASAP *m/z* (% relative intensity, ion): 271 (100, [M + H]⁺), 270 (84, [M]⁺), 254 (42), 253 (97), 250 (61), 227 (39), 226 (35), 207 (47), 206 (16), 177 (5); IR (cm⁻¹): 2996, 2555, 1702, 1651, 1599, 1508, 1473; ¹H NMR (700 MHz, *d*₆-DMSO): δ 7.47-7.64 (5H, m, Ar-H); ¹³C NMR (176 MHz, *d*₆-DMSO): δ 112.8 (t, ²J_{CF} 17.3, 1-C), 122.4 (t, ²J_{CF} 17.3, 4-C), 126.2 (s, Ar-CH), 128.8 (s, Ar-CH), 129.8 (s, Ar-CH), 130.0 (s, Ar-CH), 143.4 (dm, ¹J_{CF} 245.9, Ar-CF), 143.8 (dm, ¹J_{CF} 251.2, Ar-CF), 160.3 (s, -COOH); ¹⁹F NMR (658 MHz, *d*₆-DMSO): δ -141.3- -141.5 (2F, m, Ar-F), -142.9- -143.1 (2F, m, Ar-F).

6.4.7 Synthesis of a Biaryl Piperazine Derivative

***Tert*-butyl 4-(3,4,5-Trifluorophenyl)piperazine-1-carboxylate, 144**

$\text{Pd}(\text{OAc})_2$ (0.053 g, 0.236 mmol), JohnPhos (0.141 g, 0.473 mmol), 1-Boc-piperazine (1.06 g, 5.69 mmol) and potassium *tert*-butoxide (0.745 g, 6.64 mmol) were charged to a flame dried flask which was purged with argon to create an inert atmosphere. Dry, degassed toluene (10 mL) and 3,4,5-trifluorobromobenzene (0.57 mL, 4.77 mmol) were added in sequence to the flask which was then heated to 90 °C for 21 hours. The reaction was cooled to room temperature, diluted with diethyl ether and filtered through Celite[®] with diethyl ether as the eluent. The organic washings were concentrated *in vacuo* to give a brown oil. Column chromatography using silica gel with a gradient of 0 to 20 % ethyl acetate in hexane afforded *tert*-butyl 4-(3,4,5-trifluorophenyl)piperazine-1-carboxylate (1.29 g, 86 %) as a light yellow solid; GC-MS *m/z* (% relative intensity, ion): 317 (10, $[\text{M} + \text{H}]^+$), 316 (52, $[\text{M}]^+$), 260 (46), 186 (50), 174 (67), 57 (100); ¹H NMR (400 MHz, CDCl_3): δ 1.48 (9H, s, $\text{C}(\text{CH}_3)_3$), 3.03-3.10 (4H, m, $\text{N}-\text{CH}_2\text{CH}_2$), 3.50-3.63 (4H, m, $\text{N}-\text{CH}_2\text{CH}_2$), 6.43-6.55 (2H, m, 2-*H*, 6-*H*); ¹⁹F NMR (376 MHz, $\text{CDCl}_3/\text{CFCl}_3$): δ -134.5 (2F, dd, ³*J*_{FF} 21.3, ³*J*_{FH} 11.3, 3-*F*, 5-*F*), -172.2 (1F, bs, 4-*F*).

1-(3,4,5-Trifluorophenyl)piperazine, 145

Tert-butyl 4-(3,4,5-trifluorophenyl)piperazine-1-carboxylate (1.15 g, 3.64 mmol) was dissolved in DCM (10 mL) and the resulting solution cooled in an ice bath. To this solution, TFA (3.20 mL, 41.8 mmol) was added drop wise and the resulting mixture stirred at room temperature, under argon, for 18 hours. The reaction solution was then

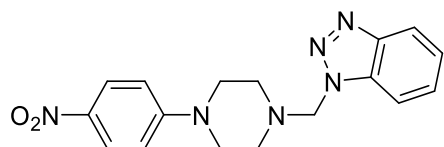
evaporated to a small volume *in vacuo* and partitioned between cold sodium bicarbonate solution (100 mL) and ethyl acetate (100 mL). The resulting aqueous solution was extracted with ethyl acetate (2×100 mL) and the combined organics dried (MgSO_4). Removal of the solvent *in vacuo* yielded *1-(3,4,5-trifluorophenyl)piperazine* (0.75 g, 96 %) as a brown solid; GC-MS m/z (% relative intensity, ion): 217 (5, $[\text{M} + \text{H}]^+$), 216 (39, $[\text{M}]^+$), 174 (100); ^1H NMR (400 MHz, CDCl_3): δ 3.01-3.11 (8H, m, CH_2), 6.38-6.52 (2H, m, 2-*H*, 6-*H*); ^{19}F NMR (376 MHz, $\text{CDCl}_3/\text{CFCl}_3$): δ -134.8- -135.1 (2F, m, 3-*F*, 5-*F*), -173.2 (1F, tt, $^3J_{\text{FF}}$ 21.6, $^4J_{\text{FH}}$ 5.8, 4-*F*).

6.4.8 Synthesis of Benzotriazolyl Derivatives

General Procedure for the Synthesis of Benzotriazolyl Derivatives

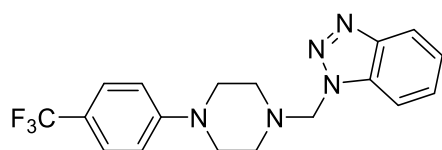
To a solution of *N*-aryl piperazine and benzotriazole in methanol:water (9:1) was added formaldehyde (37% aqueous solution) and the reaction mixture was stirred at room temperature. The precipitate formed was filtered and washed with cold diethyl ether to give benzotriazolyl product, which was directly used for subsequent reactions.

1-((4-(4-Nitrophenyl)piperazin-1-yl)methyl)-1H-benzo[d][1,2,3]triazole, 140



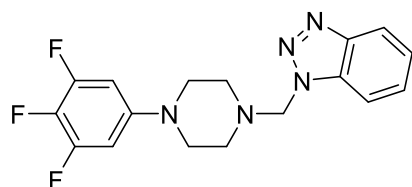
1-(4-Nitrophenyl)piperazine (0.414 g, 2.00 mmol), benzotriazole (0.238 g, 2.00 mmol), formaldehyde (0.324 g, 37 % aqueous solution, 4 mmol) and methanol:water (9:1, 10 mL), after 16 hours, afforded *1-((4-(4-nitrophenyl)piperazin-1-yl)methyl)-1H-benzo[d][1,2,3]triazole* (0.64 g, 95 %) as a yellow solid, which was used without further purification. The following spectroscopic data is for a mixture of isomers; ^1H NMR (400 MHz, CDCl_3): δ 2.74-2.92 (4H, m, $\text{N}-\text{CH}_2\text{CH}_2$), 3.36-3.50 (4H, m, $\text{N}-\text{CH}_2\text{CH}_2$), 5.46-5.67 (2H, m, $\text{N}-\text{CH}_2-\text{N}$), 6.73 (2H, dm, $^3J_{\text{HH}}$ 9.4, 2-*H*, 6-*H*), 7.33-8.11 (6H, m, Ar-*H*).

1-((4-(4-(Trifluoromethyl)phenyl)piperazin-1-yl)methyl)-1H-benzo[d][1,2,3]triazole, 142



1-(4-(Trifluoromethyl)phenyl)piperazine (0.460 g, 2.00 mmol), benzotriazole (0.238 g, 2.00 mmol), formaldehyde (0.324 g, 37 % aqueous solution, 4 mmol) and methanol:water (9:1, 10 mL), after 20 hours, afforded 1-((4-(4-(trifluoromethyl)phenyl)piperazin-1-yl)methyl)-1H-benzo[d][1,2,3]triazole (0.59 g, 82 %) as an off-white solid, which was used without further purification. The following spectroscopic data is for a mixture of isomers; ^1H NMR (400 MHz, CDCl_3): δ 2.77-2.92 (4H, m, N- CH_2CH_2), 3.23-3.35 (4H, m, N- CH_2CH_2), 5.48-5.67 (2H, m, N- CH_2 -N), 6.85 (2H, dm, $^3J_{\text{HH}}$ 8.8, 2-*H*, 6-*H*), 7.36-8.14 (6H, m, Ar-*H*); ^{19}F NMR (376 MHz, $\text{CDCl}_3/\text{CFCl}_3$): δ -62.0 (s).

1-((4-(3,4,5-Trifluorophenyl)piperazin-1-yl)methyl)-1H-benzo[d][1,2,3]triazole, 146



1-(3,4,5-Trifluorophenyl)piperazine (0.732 g, 3.40 mmol), benzotriazole (0.405 g, 3.40 mmol), formaldehyde (0.552 g, 37 % aqueous solution, 6.80 mmol) and methanol:water (9:1, 20 mL), after 18 hours, afforded 1-((4-(3,4,5-Trifluorophenyl)piperazin-1-yl)methyl)-1H-benzo[d][1,2,3]-triazole (0.67 g, 56 %) as an off-white solid, which was used without further purification. The following spectroscopic data is for a mixture of isomers; GC-MS m/z (% relative intensity, ion): 348 (1, $[\text{M} + \text{H}]^+$), 347 (5, $[\text{M}]^+$), 229 (86), 228 (100), 186 (50), 70 (40); ^1H NMR (400 MHz, CDCl_3): δ 2.77-2.86 (4H, m, N- CH_2CH_2), 3.09-3.18 (4H, m, N- CH_2CH_2), 5.54 (2H, s, N- CH_2 -N), 6.35-6.48 (2H, m, 2-*H*, 6-*H*), 7.37-7.46 (1H, m, Ar-*H*), 7.50-7.59 (1H, m, Ar-*H*), 7.61-7.70 (1H, m, Ar-*H*),

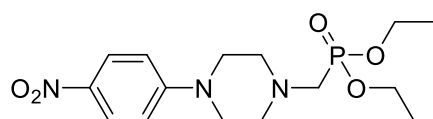
8.07-8.15 (1H, m, Ar-H); ^{19}F NMR (376 MHz, $\text{CDCl}_3/\text{CFCl}_3$): δ -134.7- -134.9 (2F, m, 3-F, 5-F), -172.9 (1F, tt, $^3J_{\text{FF}}$ 21.6, $^4J_{\text{FH}}$ 5.8, 4-F).

6.4.9 Synthesis of (Piperazin)phosphonates

General Procedure for the Synthesis of (Piperazin)phosphonates

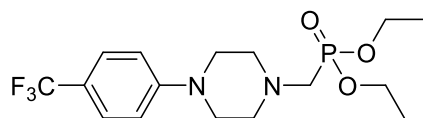
The benzotriazolyl derivative of *N*-aryl piperazine was dissolved in dry DCM at 0 °C and ZnBr_2 and triethyl phosphite were added successively. The reaction mixture was stirred at 0 °C for 2 h and then at room temperature. After this time the reaction was quenched with water and extracted with DCM. The combined organic layers were washed with 1M NaOH, brine and dried over anhydrous MgSO_4 . The resulting phosphonate was directly used for subsequent reactions.

Diethyl (4-(4-Nitrophenyl)piperazin-1-yl)methylphosphonate, 141



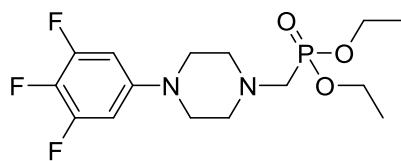
1-((4-(4-Nitrophenyl)piperazin-1-yl)methyl)-1*H*-benzo[*d*][1,2,3]triazole (0.600 g, 1.77 mmol), ZnBr_2 (0.479 g, 2.13 mmol), triethylphosphite (0.37 mL, 2.13 mmol) and dry DCM (40 mL), after 20 hours, afforded *diethyl (4-(4-nitrophenyl)piperazin-1-yl)methylphosphonate* (0.62 g, 98 %) as a yellow solid; GC-MS *m/z* (% relative intensity, ion): 358 (3, $[\text{M} + \text{H}]^+$), 357 (16, $[\text{M}]^+$), 220 (100), 180 (62), 178 (54), 177 (61), 70 (67); ^1H NMR (400 MHz, CDCl_3): δ 1.35 (6H, t, $^3J_{\text{HH}}$ 7.1, CH_2CH_3), 2.74-2.91 (6H, m, N- CH_2CH_2 , N- CH_2 -P), 3.37-3.50 (4H, m, N- CH_2CH_2), 4.10-4.23 (4H, m, CH_2CH_3), 6.81 (2H, dm, $^3J_{\text{HH}}$ 9.4, 2-*H*, 6-*H*), 8.11 (2H, dm, $^3J_{\text{HH}}$ 9.4, 3-*H*, 5-*H*); ^{31}P NMR (162 MHz, CDCl_3): δ 23.3 (s).

Diethyl (4-(4-(Trifluoromethyl)phenyl)piperazin-1-yl)methylphosphonate, 143



1-((4-(4-(Trifluoromethyl)phenyl)piperazin-1-yl)methyl)-1H-benzo[d][1,2,3]triazole (0.578 g, 1.61 mmol), ZnBr₂ (0.432 g, 1.91 mmol), triethylphosphite (0.33 mL, 1.93 mmol) and dry DCM (50 mL), after 21 hours, afforded *diethyl (4-(4-(trifluoromethyl)phenyl)piperazin-1-yl)methylphosphonate* (0.55 g, 91 %) as a yellow oil; GC-MS *m/z* (% relative intensity, ion): 381 (10, [M + H]⁺), 380 (48, [M]⁺), 244 (46), 243 (100), 214 (44), 206 (57), 201 (54), 200 (74), 194 (56), 180 (77), 172 (66), 152 (44), 145 (56), 70 (91), 42 (49); ¹H NMR (400 MHz, CDCl₃): δ 1.32 (6H, t, ³J_{HH} 7.1, CH₂CH₃), 2.75-2.88 (6H, m, N-CH₂CH₂, N-CH₂-P), 3.22-3.31 (4H, m, N-CH₂CH₂), 4.08-4.21 (4H, m, CH₂CH₃), 6.85-6.93 (2H, m, 2-*H*, 6-*H*), 7.40-7.49 (2H, m, 3-*H*, 5-*H*); ¹⁹F NMR (376 MHz, CDCl₃/CFCl₃): δ -61.8 (s); ³¹P NMR (162 MHz, CDCl₃): δ 23.6 (s).

Diethyl (4-(3,4,5-Trifluorophenyl)piperazin-1-yl)methylphosphonate, 147



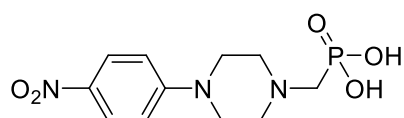
1-((4-(3,4,5-Trifluorophenyl)piperazin-1-yl)methyl)-1H-benzo[d][1,2,3]-triazole (0.400 g, 1.15 mmol), ZnBr₂ (0.311 g, 1.38 mmol), triethylphosphite (0.24 mL, 1.38 mmol) and dry DCM (30 mL), after 16 hours, afforded *diethyl (4-(3,4,5-trifluorophenyl)piperazin-1-yl)methylphosphonate* (0.36 g, 86 %) as a yellow oil; GC-MS *m/z* (% relative intensity, ion): 367 (4, [M + H]⁺), 366 (17, [M]⁺), 229 (100), 180 (49), 70(50); ¹H NMR (400 MHz, CDCl₃): δ 1.34 (6H, t, ³J_{HH} 7.1, CH₂CH₃), 2.76-2.88 (4H, m, N-CH₂-P and N-CH₂CH₂), 3.07-3.17 (4H, m, N-CH₂CH₂), 4.12-4.23 (4H, m, CH₂CH₃), 6.36-6.50 (2H, m, 2-*H*, 6-*H*); ¹⁹F NMR (376 MHz, CDCl₃/CFCl₃): δ -135.0 (2F, dd, ³J_{FF} 21.0, ³J_{FH} 11.4, 3-*F*, 5-*F*), -173.5 (1F, bs, 4-*F*); ³¹P NMR (162 MHz, CDCl₃): δ 23.7 (s).

6.4.10 Synthesis of (Piperazin)phosphonic Acids

General Procedure for the Hydrolysis of Phosphonates to Phosphonic Acids

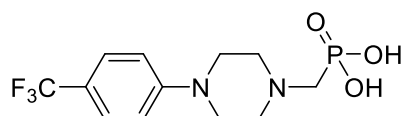
In a flame dried flask, under an inert atmosphere, the phosphonate was dissolved in dry DCM. Bromotrimethylsilane was added via syringe and the reaction stirred at room temperature. Volatile materials were removed under reduced pressure and the resulting product dissolved in an excess of 10:1 methanol:water and stirred overnight. Volatile materials were removed under reduced pressure and the crude product was purified by recrystallisation to yield the benzylphosphonic acid.

(4-(4-Nitrophenyl)piperazin-1-yl)methylphosphonic Acid, 131



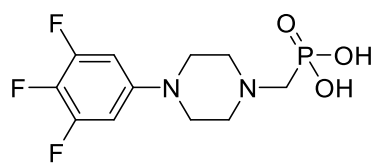
Diethyl (4-(4-nitrophenyl)piperazin-1-yl)methylphosphonate (0.650 g, 1.82 mmol), dry DCM (20 mL) and bromotrimethylsilane (0.71 mL, 5.38 mmol), after 20 hours and recrystallisation from water, yielded (4-(4-nitrophenyl)piperazin-1-yl)methylphosphonic acid (0.32 g, 58 %) as a yellow solid; mp > 250 °C; HRMS-ASAP m/z : $[M + H]^+$ calcd for $C_{11}H_{17}N_3O_5P$ 302.0906; found 302.0915; ASAP m/z (% relative intensity, ion): 302 (4, $[M + H]^+$), 208 (100); IR (cm^{-1}): 2282, 2022, 1740, 1587, 1510, 1480; 1H NMR (600 MHz, D_2O): δ 3.04 (2H, d, $^2J_{HP}$ 11.8, P- CH_2), 3.39-3.50 (4H, m, N- CH_2CH_2), 3.56-3.70 (4H, m, N- CH_2CH_2), 6.91 (2H, dm, $^3J_{HH}$ 9.4, 2- H), 8.02 (2H, dm, $^3J_{HH}$ 9.4, 3- H); ^{13}C NMR (176 MHz, D_2O): δ 44.3 (s, N- CH_2CH_2), 53.1 (d, J_{CP} 4.8, N- CH_2CH_2), 54.8 (d, $^1J_{CP}$ 127.4, P- CH_2), 114.0 (s, Ar-CH), 126.0 (s, Ar-CH), 138.9 (s, Ar-C), 154.1 (s, Ar-C); ^{31}P NMR (243 MHz, D_2O): δ 5.70 (s).

(4-(4-(Trifluoromethyl)phenyl)piperazin-1-yl)methylphosphonic Acid, 132



Diethyl (4-(4-(trifluoromethyl)phenyl)piperazin-1-yl)methylphosphonate (0.506 g, 1.34 mmol), dry DCM (20 mL) and bromotrimethylsilane (0.57 mL, 4.29 mmol), after 4 days and recrystallisation from water, yielded (4-(4-(trifluoromethyl)phenyl)piperazin-1-yl)methylphosphonic acid (0.23 g, 53 %) as an off white solid; mp > 250 °C; HRMS-ASAP m/z : $[M^+]$ calcd for $C_{12}H_{16}N_2O_3F_3P$ 324.0851; found 324.0858; ASAP m/z (% relative intensity, ion): 325 (19, $[M + H]^+$), 324 (8, $[M]^+$), 245 (65), 231 (100), 211 (34); IR (cm^{-1}): 3449, 2342, 1663, 1612, 1524, 1453; 1H NMR (700 MHz, D_2O): δ 3.02 (2H, d, $^2J_{HP}$ 11.7, P- CH_2), 3.39-3.48 (4H, m, N- CH_2CH_2), 3.55-3.66 (4H, m, N- CH_2CH_2), 6.88-6.93 (2H, m, 2- H , 6- H), 7.99-8.04 (2H, m, 3- H , 5- H); ^{19}F NMR (564 MHz, D_2O): δ -61.5 (s); ^{31}P NMR (243 MHz, D_2O): δ 5.98 (s). Due to solubility issues, ^{13}C NMR signals were too weak to be recorded.

(4-(3,4,5-Trifluorophenyl)piperazin-1-yl)methylphosphonic Acid, 133



Diethyl (4-(3,4,5-trifluorophenyl)piperazin-1-yl)methylphosphonate (0.355 g, 0.97 mmol), dry DCM (10 mL) and bromotrimethylsilane (0.41 mL, 3.10 mmol), after 25 hours and recrystallisation from water, yielded (4-(3,4,5-trifluorophenyl)piperazin-1-yl)methylphosphonic acid (0.24 g, 80 %) as an off white solid; mp > 250 °C; HRMS-ASAP m/z : $[M^+]$ calcd for $C_{11}H_{15}N_2O_3F_3P$ 311.0772; found 311.0762; ASAP m/z (% relative intensity, ion): 311 (100, $[M + H]^+$), 310 (34, $[M]^+$); IR (cm^{-1}): 2318, 2167, 2053, 2004, 1619, 1530, 1449, 1402; 1H NMR (700 MHz, D_2O): δ 3.21 (2H, d, $^2J_{HP}$ 12.7, P- CH_2), 3.31-3.57 (8H, bm, N- CH_2CH_2), 6.63 (2H, dd, $^3J_{HF}$ 10.4, $^4J_{HF}$ 5.8, 2- H , 6- H); ^{13}C NMR (176 MHz, D_2O): δ 46.2 (s, N- CH_2CH_2), 53.1 (d, $^3J_{CP}$ 5.2, N- CH_2CH_2), 53.2 (d, $^1J_{CP}$ 135.1, P- CH_2), 101.3 (dm, $^2J_{CF}$ 20.1, 2- C , 6- C), remaining ^{13}C peaks were too weak to observe; ^{19}F NMR (376 MHz, D_2O): δ -135.3 (2F, dd, $^3J_{FF}$ 21.4, $^3J_{FH}$ 11.0, 3- F , 5- F), -171.4 (1F, tt, $^3J_{FF}$ 21.4, $^4J_{FH}$ 6.1, 4- F); ^{31}P NMR (283 MHz, D_2O): δ 6.51 (s).

6.5 Experimental Data to Chapter 5

6.5.1 General Materials

Absolute ethanol, the solvent used for all sample incubations, was purchased from Merck KGaA, and diiodomethane, used for contact angle measurements, was purchased from Aldrich, all commercially bought solvents were used as received. Aluminium (0.2-0.7 mm, 99.9 %) was obtained from Thin Film Products and used as received. Microscope cover slides (10 x 20 mm) were purchased from Karl Hecht GmbH. All phosphonic acids used were synthesised following the procedures described within sections 3 and 4 of this chapter, with the exception of dodecylphosphonic acid which was purchased from Epsilon Chimie, and used as received.

6.5.2 Procedure for Al/glass Substrate Preparation

Microscope cover glasses (10 × 10 mm and 10 × 20 mm) were washed with distilled water and baked at 450 °C for 20 minutes. All Al films (110 nm) were deposited onto the glass slides using a resistant heater (Univex 350, Leybold Vakuum GmbH).

6.5.3 SAM Preparation

All Al/glass substrates were first cleaned by a solvent cleaning (SC) procedure that consisted of rinsing with ethanol, followed by sonication in ethanol for 4 minutes each, and concluded by drying in a flow of nitrogen gas. All ultraviolet ozone (UVO) cleaning was performed after the SC protocol, in an UVO cleaner (Jelight Company, Inc., model 42-220) for 10 minutes, followed by immediate reaction with the modifier. All oxygen plasma (OP) cleaning was performed after the SC protocol, in an oxygen fed plasma cleaner (GaLa Instrumente, model PlasmaPrep5) operated at 33 W for 4 minutes, followed by immediate reaction with the modifier.

The assembly procedure is as follows: after the pre-cleaning procedure, the Al/glass slides were immersed in a 4 mM ethanol solution of the corresponding phosphonic acid, so that the whole substrate was within the sample solution. The Al/glass substrate was left within this solution for 18-26 h. The Al/glass substrate was then rinsed copiously in

absolute ethanol to remove any unbound material, dried in a stream of nitrogen gas and either used immediately or stored under vacuum until required.

6.5.4 Contact Angle Measurements

Static contact angle goniometry measurements are performed using a drop shape analyzer (DSA-30) from Krüss GmbH (Hamburg, Germany) with an automated drop dispenser and image video capture system. [Figure 53] Immediately before data acquisition, the sample was rinsed with ethanol and dried in a nitrogen stream. Droplets of deionized water from a Millipore system (18.2 M Ω ·cm) and diiodomethane are deposited at different positions of each sample. Several drops (typically 3 repetitions) were quickly placed on the surface, the needle pulled back, and the drop shape captured immediately with the camera. Values reported are averages of measurements of at least three drops. Images were analysed with the Drop Shape Analysis software to determine the contact angle, by circle fitting, and averaging the results. Estimated uncertainties in the contact angles were $\pm 1^\circ$ for static angle measurements.

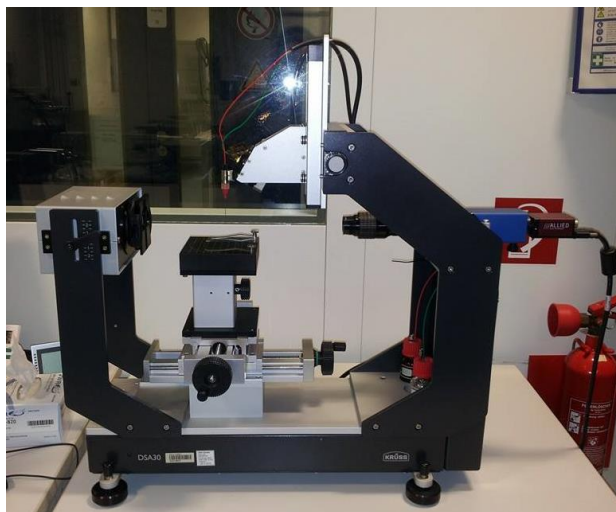


Figure 53. *Krüß Drop Shape Analysis System used for contact angle measurements*

6.5.5 PM-IRRAS Measurements

Polarization modulation infrared reflection-absorption spectra (PM-IRRAS) were acquired with a Bruker Vertex 80 spectrometer equipped with a PMA 50 polarization modulation unit including a nitrogen cooled mercury-cadmium-telluride (MCT)

detector and a ZnSe photoelastic modulator. [Figure 54] The IR beam was set at 82° incident to the AlO_x surface with maximum dephasing centred at 1500 cm^{-1} or 2900 cm^{-1} . The resolution was set to 4 cm^{-1} , and scan times of 30 min (2130 scans) per sample were used.



Figure 54. Bruker Vertex 80 fitted with a PMA 50 modulation unit, used for PM-IRRAS.

6.5.6 FT-IR Measurements

IR spectra were recorded as pellets (KBr) or films (CaF_2) using a Varian Cary 50 scan spectrophotometer, with blank and clean substrates as baselines, respectively.

6.5.6.1 Preparation of KBr Pellets

A mixture of KBr (~240 mg) and the phosphonic acid of interest (~50 mg) were ground to a fine powder in a pestle and mortar for 5 minutes. The mixture was then pressed for 1 hour at ~10 tonnes to form a pellet.

6.5.6.2 Preparation of CaF_2 Plates

CaF_2 plate was washed in detergent solution before rinsing with water and baking at $450\text{ }^\circ\text{C}$ for 10 minutes. After cooling in a stream of N_2 , a $20\text{ }\mu\text{L}$ aliquot of a 4 mM solution of the desired phosphonic acid in methanol was applied to a plate. Once

residual methanol had evaporated from the surface, the plate was inserted into a sample holder and the IR spectrum acquired immediately.

6.5.7 XPS Measurements

XP spectra are recorded using a Kratos Axis Ultra instrument equipped with a monochromated Al K_{α} emission source (1486.6 eV) operated at 15 kV and 180 W. [Figure 55] The photoelectrons are collected in normal emission geometry by a 165 mm mean radius hemispherical analyzer. With a monochromatized X-ray source and an analyzer pass energy of 40 eV, an instrumental energy resolution of ~ 0.5 eV is achieved. The energy scale is referenced to the Au $4f_{7/2}$ line at a binding energy (BE) of 84.0 eV. For all samples, a survey spectrum and high resolution spectra of the C $1s$, O $1s$, F $1s$, P $2s$, and Al $2p$ regions are acquired. The spectra are deconvoluted by Gauss-Lorentz profiles (Voigt functions with 50:50 Lorentzian:Gaussian ratio) after subtraction of a linear background. The line shape parameters are determined by least square fitting to carbon core level lines of known reference samples. To obtain elemental concentrations, XPS peak areas are normalized using instrumental relative sensitivity factors (RSF) calibrated with known reference samples. These ratios are related to those from *n*-dodecanethiol, methyl phosphonic acid and dodecylphosphonic acid SAMs, used here as a reference

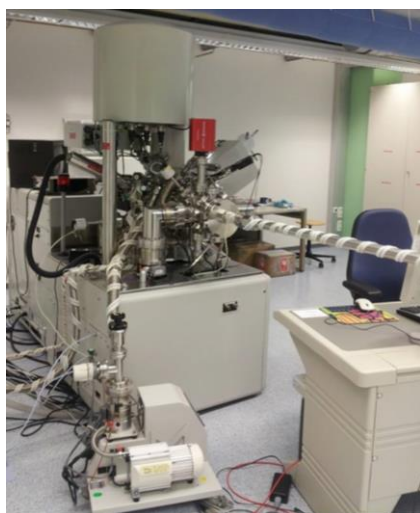


Figure 55. Kratos Axis Ultra, used for XPS measurements.

6.5.8 DFT Simulated IR Spectra

Molecular IR spectra were determined with ground state density functional theory (DFT) calculations performed with the nonlocal generalized gradient approximation. These calculations were done at the PBE theory level using a double numerical basis set that includes polarization functions (DNP). We utilised the DFT algorithm as implemented in the Dmol³ program (Accelrys, San Diego, CA).

6.6 Experimental Data for Calculated Dipole Moments

Surface dipole moments were determined with the Materials Studio package (Accelrys, San Diego, CA). All dipole moments were calculated with the phosphonic acid attached in a bidentate mode to an Al₆O₁₀ cluster, where 2 of the O-atoms are shared with the P-atom. The cartesian coordinates of the atoms in the cluster were fixed during calculations to observe a consistent cluster geometry throughout the calculations. Subsequently, the contribution of the cluster to the dipole moment should, to a first approximation, be the same for all compounds. The structure of cluster-P(O)CH₂CH₃ is shown. [Figure 56] All the atoms besides the cluster were allowed to relax during the calculations.

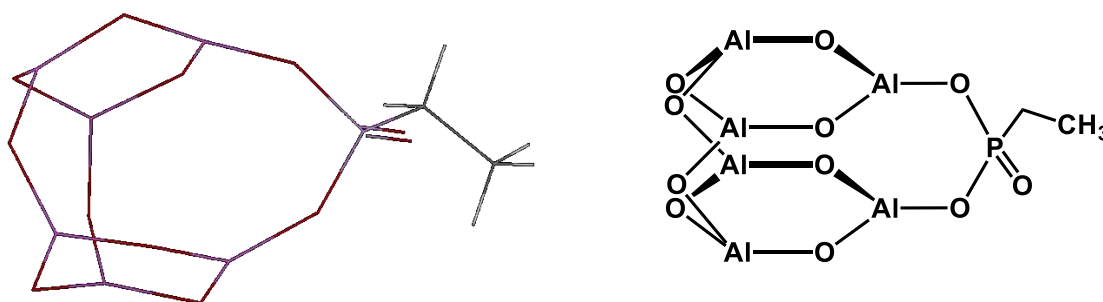


Figure 56. Structure of AlO_x cluster used for surface dipole calculations.

6.7 References

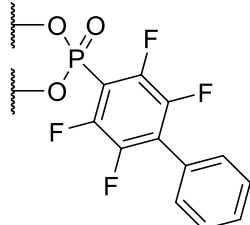
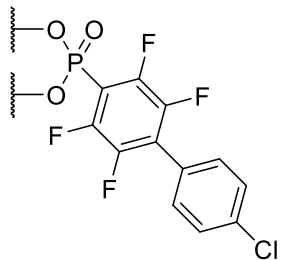
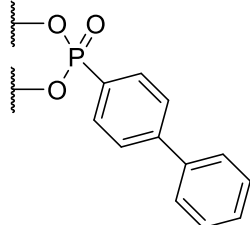
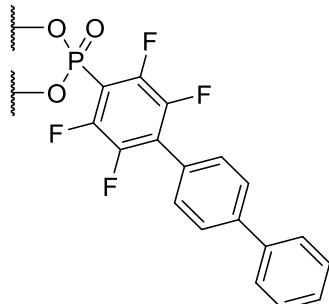
- (1) Becht, J.-M.; Drian, C. L. *Org. Lett.* **2008**, *10*, 3161–3164.
- (2) Chen, F.; Min, Q.-Q.; Zhang, X. *J. Org. Chem.* **2012**, *77*, 2992–2998.
- (3) Shang, R.; Fu, Y.; Wang, Y.; Xu, Q.; Yu, H.-Z.; Liu, L. *Angew. Chem. Int. Ed. Engl.*, **2009**, *48*, 9350–9354.
- (4) Oldham, P.; Williams, G. H. *J. Chem. Soc. C* **1970**, 1260–1263.
- (5) Fang, X.; Huang, Y.; Chen, X.; Lin, X.; Bai, Z.; Huang, K.-W.; Yuan, Y.; Weng, Z. *J. Fluorine Chem.* **2013**, *151*, 50–57.
- (6) Dutta, T.; Woody, K. B.; Watson, M. D. *J. Am. Chem. Soc.* **2008**, *130*, 452–453.
- (7) Yonekubo, S.; Fushimi, N. 1-Substituted-3-Beta-D-Glucopyranosylated Nitrogenous Hetero-cyclic Compounds and Medicines Containing the Same. Eur. Pat. Appl. 05806938.6, August 1, 2007.
- (8) Rice, B. L.; Guo, C. Y.; Kirchmeier, R. L. *Inorg. Chem.* **1991**, *30*, 4635–4638.
- (9) Khartulyari, A. S.; Kapur, M.; Maier, M. E. *Org. Lett.* **2006**, *8*, 5833–5836.
- (10) Hotchkiss, P. J.; Li, H.; Paramonov, P. B.; Paniagua, S. A.; Jones, S. C.; Armstrong, N. R.; Brédas, J.-L.; Marder, S. R. *Adv. Mater.* **2009**, *21*, 4496–4501.
- (11) Williams, A.; Naylor, R. A.; Collyer, S. G. *J. Chem. Soc., Perkin Trans. 2* **1973**, 25–33.
- (12) Xing, C.-H.; Lee, J.-R.; Tang, Z.-Y.; Zheng, J. R.; Hu, Q.-S. *Adv. Synth. Catal.* **2011**, *353*, 2051–2059.
- (13) Hoshiya, N.; Shimoda, M.; Yoshikawa, H.; Yamashita, Y.; Shuto, S.; Arisawa, M. *J. Am. Chem. Soc.* **2010**, *132*, 7270–7272.
- (14) Liu, L.; Zhang, Y.; Wang, Y. *J. Org. Chemistry* **2005**, *70*, 6122–6125.
- (15) Liu, N.; Liu, C.; Jin, Z. *J. Organomet. Chem.* **2011**, *696*, 2641–2647.
- (16) René, O.; Fagnou, K. *Org. Lett.* **2010**, *12*, 2116–2119.
- (17) Sandall, J.; Bolton, R.; Williams, G. *J. Fluorine Chem.* **1978**, *11*, 591–600.
- (18) Bandgar, B.; Bettigeri, S. V.; Phopase, J. *Tetrahedron Lett.* **2004**, *45*, 6959–6962.
- (19) Bouillot, A. M. J.; Dodic, N.; Gellibert, F. J.; Mirguet, O. 2,6-Disubstituted Pyridines as Soluble Guanylate Cyclase Activators. WO 071504, June 11, **2009**.
- (20) Urbani, M.; Ohkubo, K.; Islam, D.; Fukuzumi, S.; Langa, F. *Chem. Eur. J.* **2012**, *18*, 7473–7485.
- (21) Zimmerman, H. E.; Heydinger, J. A. *J. Org. Chem.* **1991**, *56*, 1747–1758.
- (22) Kosolapoff, G. M. *J. Am. Chem. Soc.* **1945**, *67*, 2259–2260.

- (23) Thunuguntla, S. S. R.; Subramanya, H.; Kunnam, S. R.; Sanivuru Vijay, S. R.; Bingi, C.; Kusanur, R.; Schwarz, M.; Arlt, M. Di hydroorotate Dehydrogenase Inhibitors. WO 115736, October 14, 2010.
- (24) Gerasimo, T. N.; Baturina, I. I.; Fomenko, T. V.; Chertok, V. S.; Kollegov, V. F.; Fokin, E. P. *Zh. Org. Khim.* **1974**, *10*, 2166–2171.

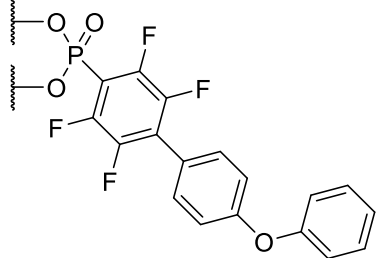
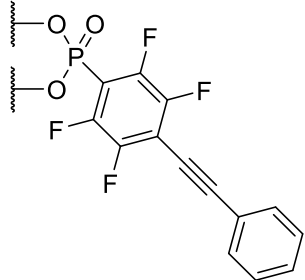
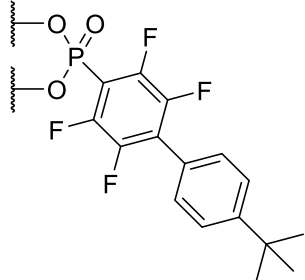
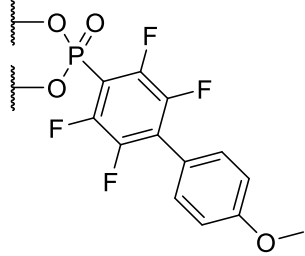
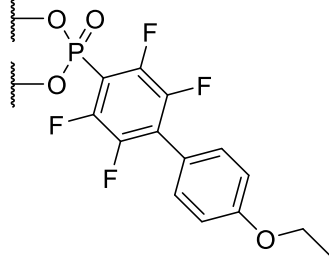
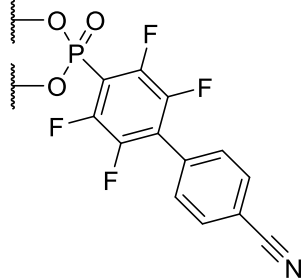
Appendix A

Calculated Dipole Moments of Phosphonic Acids
on AlO_x

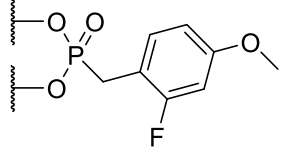
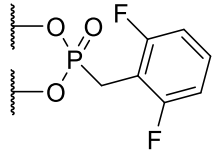
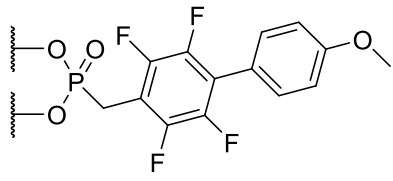
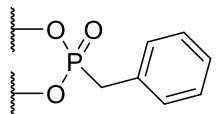
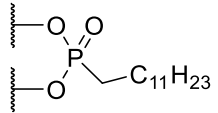
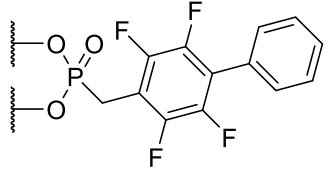
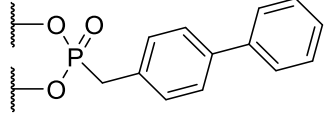
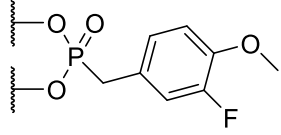
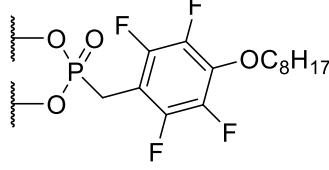
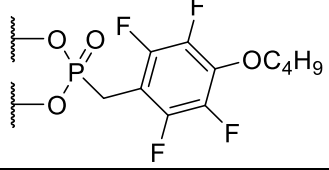
Biphenyl Phosphonic Acid Derivatives

Simulated Surface	Dipole Moment Vectors in Initial Coordinates (au)		Net Dipole Moment (D)
	19	x y z	0.320660 0.376806 0.596970 1.9708
	25	x y z	-0.788203 0.204099 0.426209 2.3359
	18	x y z	0.428834 0.412146 0.724121 2.3818
	20	x y z	0.531618 0.436021 0.661264 2.4247

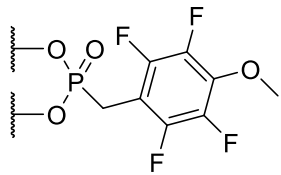
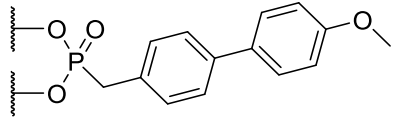
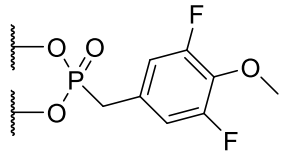
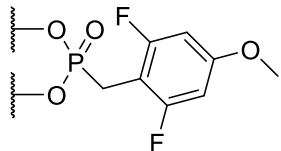
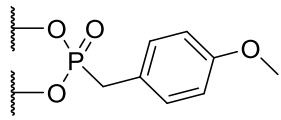
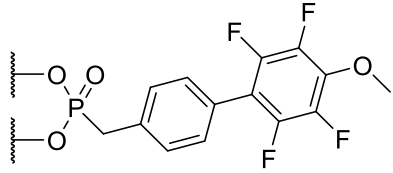
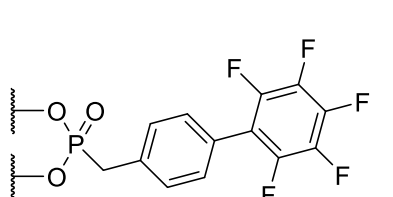
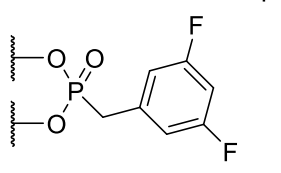
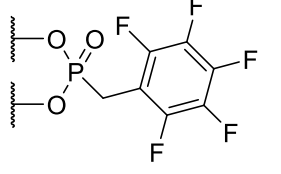
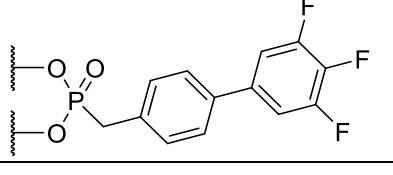
Appendix A: Calculated Dipole Moments of Phosphonic Acids on AlO_x

Simulated Surface	Dipole Moment Vectors in Initial Coordinates (au)	Net Dipole Moment (D)
	22 x -0.182846 y 0.676365 z 0.755327	2.6187
	27 x 0.069286 y 0.460899 z 0.978160	2.7541
	21 x 0.676491 y 0.484731 z 0.725491	2.8063
	23 x 0.036542 y 0.532172 z 1.517260	4.0879
	24 x 0.111303 y 0.676793 z 1.577451	4.3721
	26 x -1.957456 y -0.360594 z -0.296742	5.1150

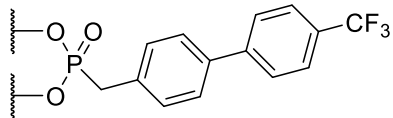
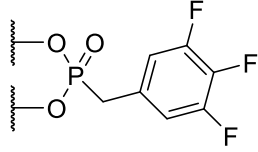
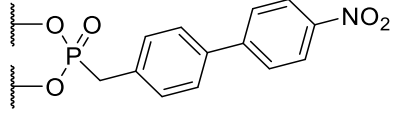
Benzylphosphonic Acid Derivatives

Simulated Surface	Dipole Moment Vectors in Initial Coordinates (au)	Net Dipole Moment (D)	Relative Dipole Moment (D)
	63 x -0.822541 y -0.385672 z 0.094773	2.3217	+1.5836
	66 x -1.197494 y -0.322738 z 0.669402	3.5822	+0.3231
	95 x -1.176318 y -0.366255 z 0.869961	3.8335	+0.0718
	58 x -1.457493 y -0.024051 z 0.632257	4.0386	-0.1333
	160 x -1.420110 y -0.027800 z 0.817704	4.1658	-0.2605
	94 x -1.547818 y -0.190104 z 0.584743	4.2333	-0.3280
	92 x -1.594062 y -0.044256 z 0.563479	4.2989	-0.3936
	65 x -1.525539 y 0.439598 z 0.639290	4.3502	-0.4449
	86 x -1.389991 y 0.087349 z 1.029757	4.4026	-0.4973
	85 x -1.463596 y 0.114500 z 0.991868	4.5033	-0.5980

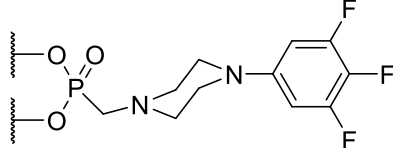
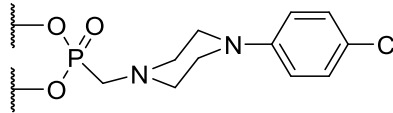
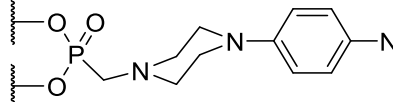
Appendix A: Calculated Dipole Moments of Phosphonic Acids on AlO_x

Simulated Surface		Dipole Moment Vectors in Initial Coordinates (au)	Net Dipole Moment (D)	Relative Dipole Moment (D)
	61	x y z	-1.580531 0.282013 0.845950	4.6126 -0.7073
	93	x y z	-1.478341 0.234125 1.041318	4.6346 -0.7293
	64	x y z	-1.665026 0.705521 0.437273	4.7288 -0.8235
	62	x y z	-1.268056 -0.822588 1.156739	4.8378 -0.9325
	60	x y z	-1.481472 -0.263767 1.166572	4.8395 -0.9342
	120	x y z	-1.777564 0.402171 1.022438	5.3115 -1.4062
	119	x y z	-2.128344 0.899837 0.123490	5.8818 -1.9765
	82	x y z	-2.290209 0.432253 0.207443	5.9474 -2.0421
	59	x y z	-2.456603 0.419905 0.303019	6.3813 -2.4760
	136	x y z	-2.293854 1.276702 -0.011131	6.6727 -2.7674

Appendix A: Calculated Dipole Moments of Phosphonic Acids on AlO_x

Simulated Surface		Dipole Moment Vectors in Initial Coordinates (au)		Net Dipole Moment (D)	Relative Dipole Moment (D)
	135	x	-2.295831	6.6961	-2.7908
		y	1.291832		
		z	0.023128		
	84	x	-2.720753	7.2258	-3.3205
		y	0.823928		
		z	-0.015953		
	134	x	-2.661898	8.6197	-4.7144
		y	2.074797		
		z	-0.331583		

Piperazine Benzylphosphonic Acid Derivatives

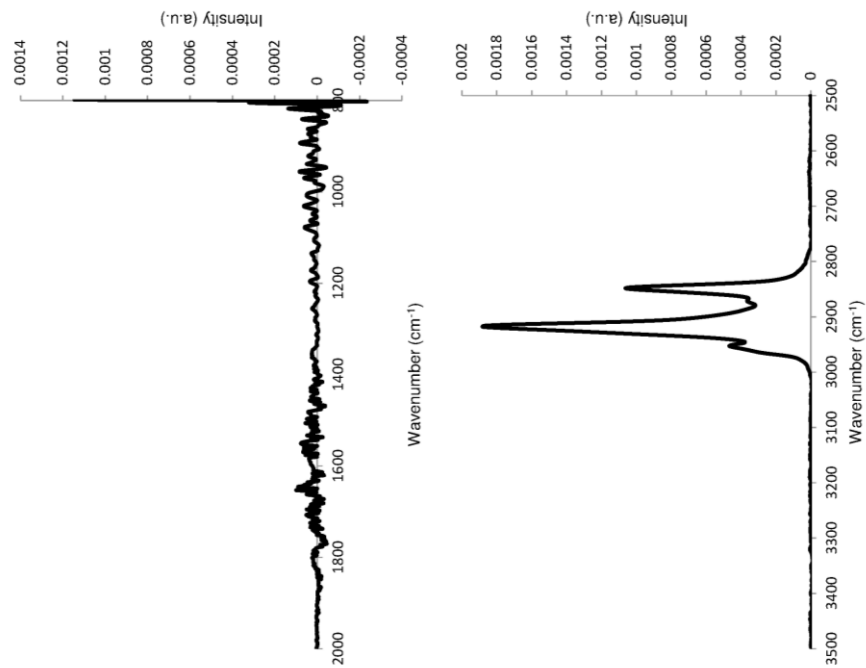
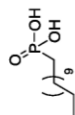
Simulated Surface		Dipole Moment Vectors in Initial Coordinates (au)		Net Dipole Moment (D)
	133	x	-0.097257	5.7318
		y	1.991397	
		z	1.053584	
	132	x	0.013272	6.0747
		y	2.116035	
		z	1.110855	
	131	x	-0.007077	8.6208
		y	3.267812	
		z	0.908104	

Appendix B

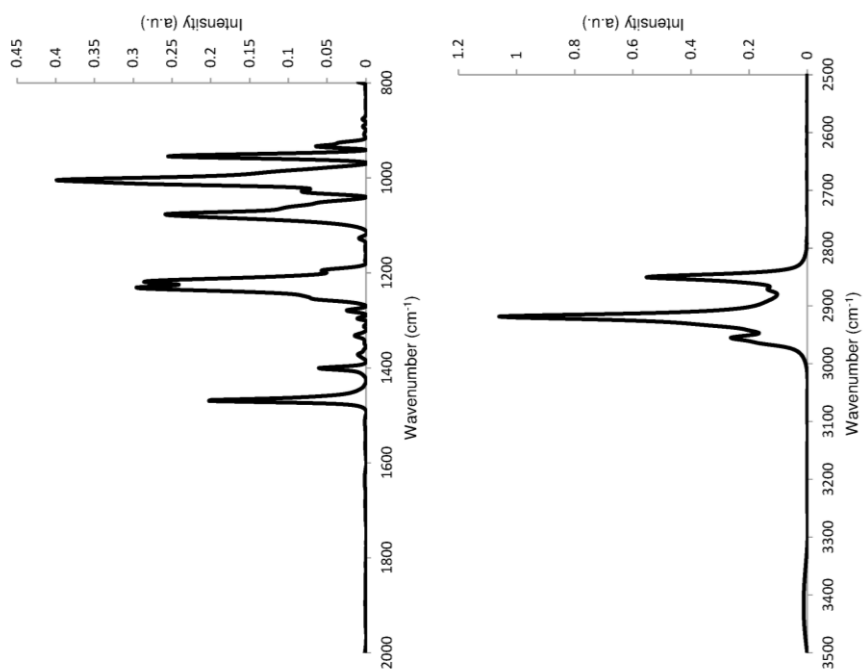
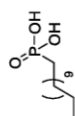
Transmission IR Spectra

Transmission IR spectra for bulk phosphonic acid samples studied in Chapter 5. IR spectra were recorded for both a thin film of the phosphonic acid deposited on a CaF₂ plate, and for the bulk powder within a KBr pellet.

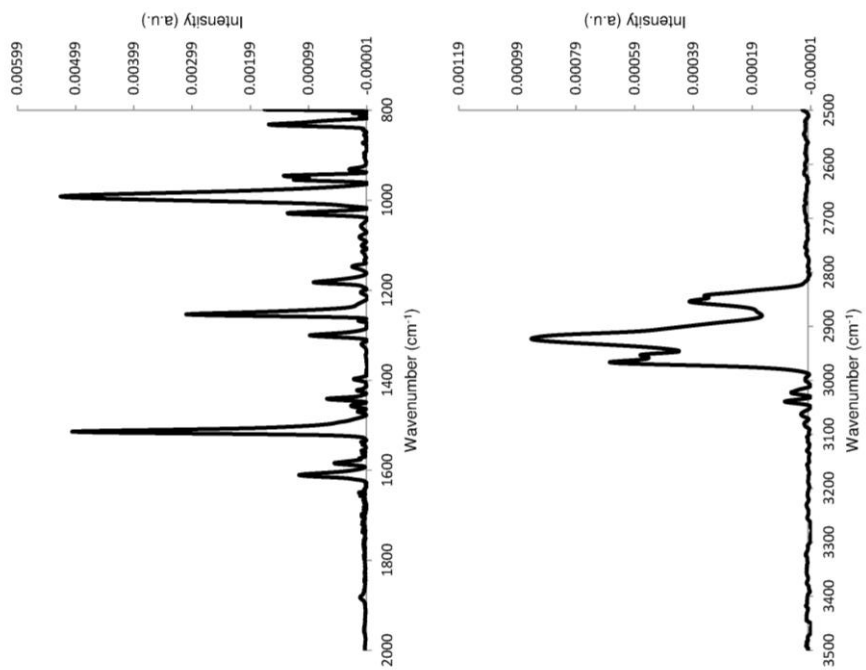
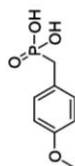
Dodecylphosphonic Acid, 160 (CaF₂)



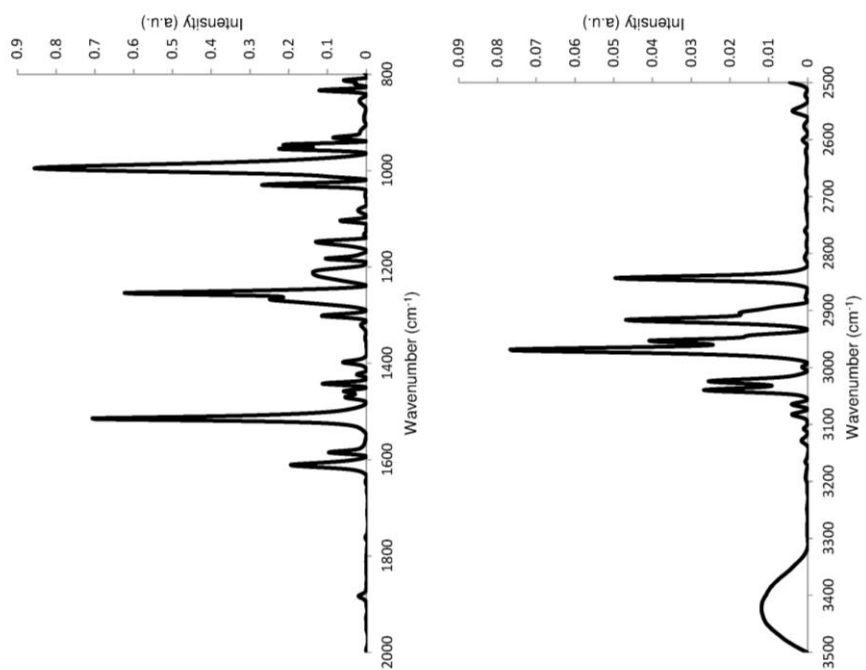
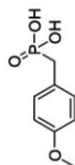
Dodecylphosphonic Acid, 160 (KBr)



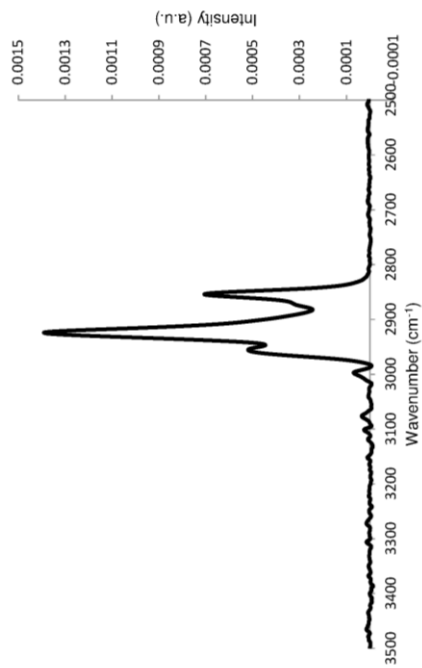
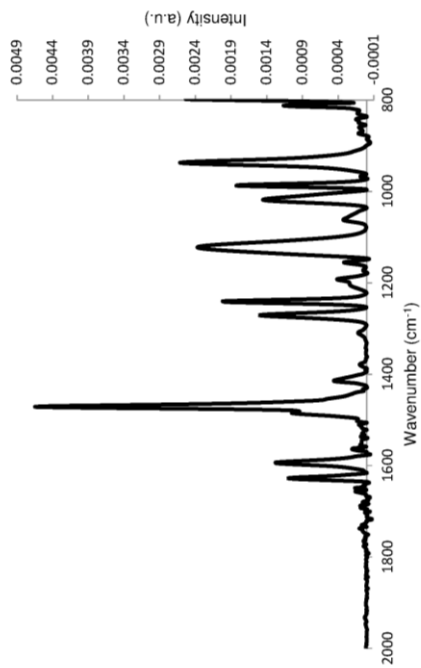
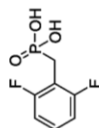
4-Methoxybenzylphosphonic Acid, 60 (CaF₂)



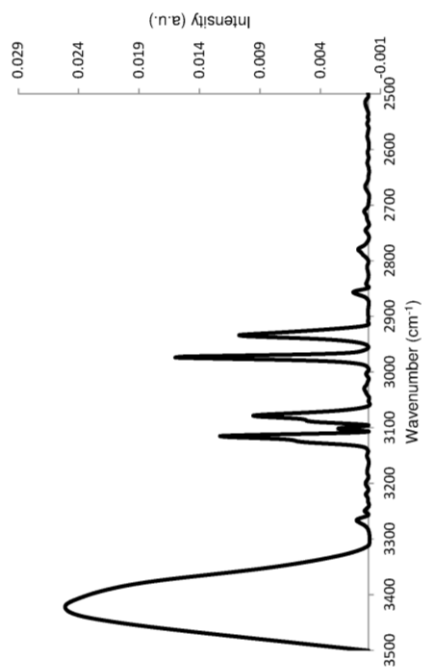
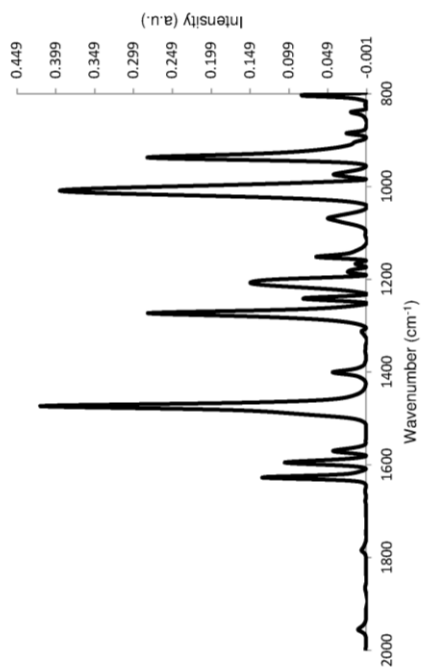
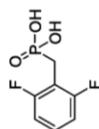
4-Methoxybenzylphosphonic Acid, 60 (KBr)



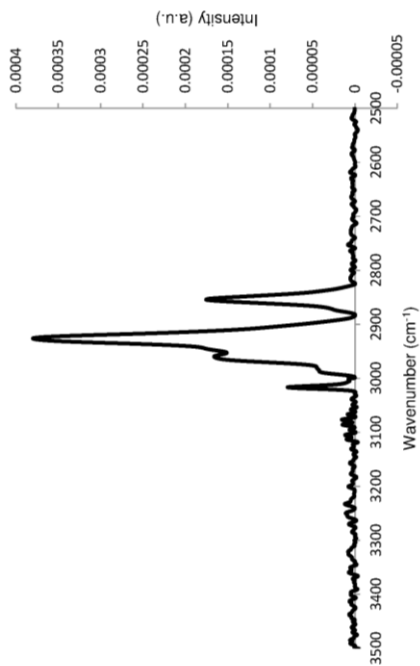
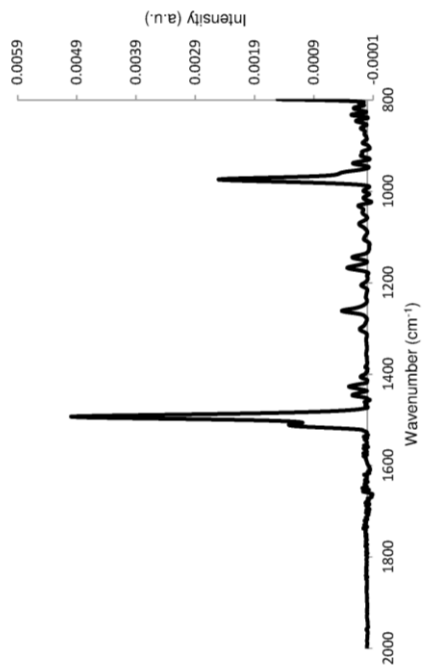
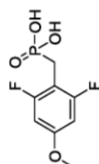
2,6-Difluorobenzylphosphonic Acid, 66 (CaF₂)



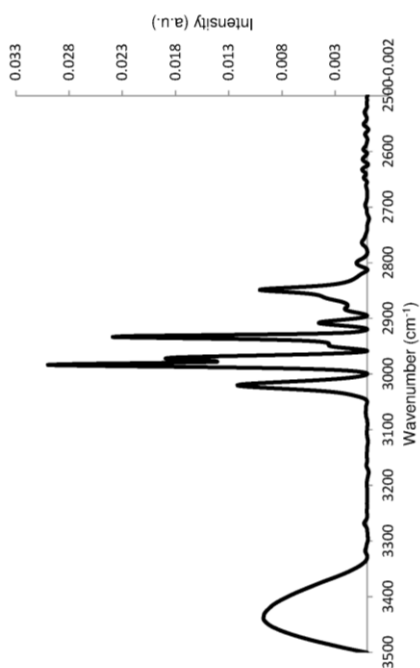
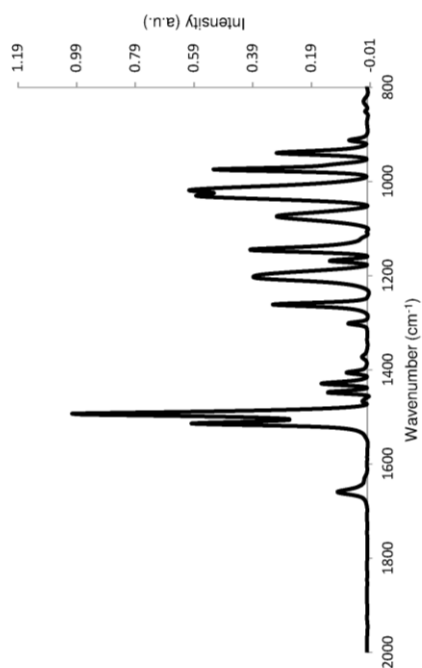
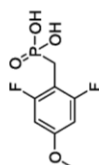
2,6-Difluorobenzylphosphonic Acid, 66 (KBr)



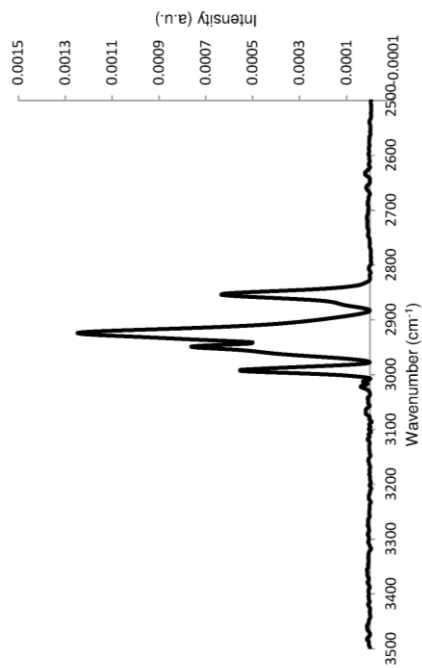
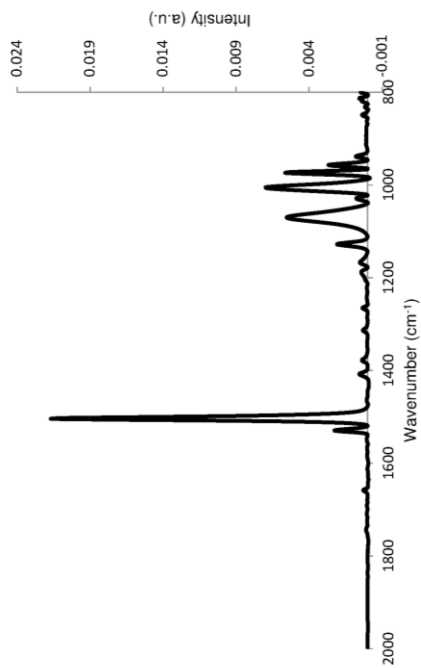
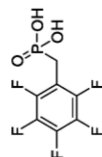
2,6-Difluoro-4-methoxybenzylphosphonic Acid, 62 (CaF₂)



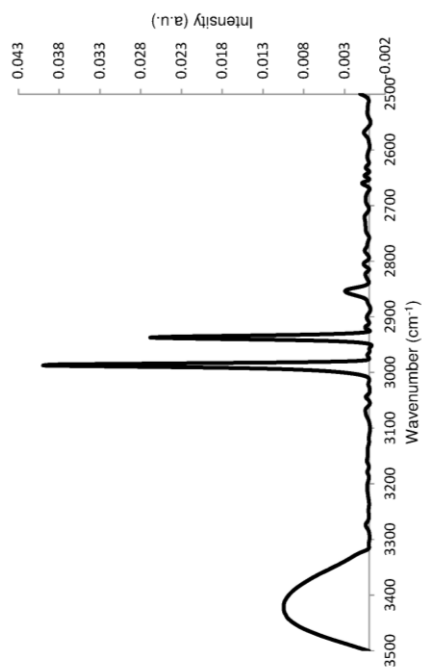
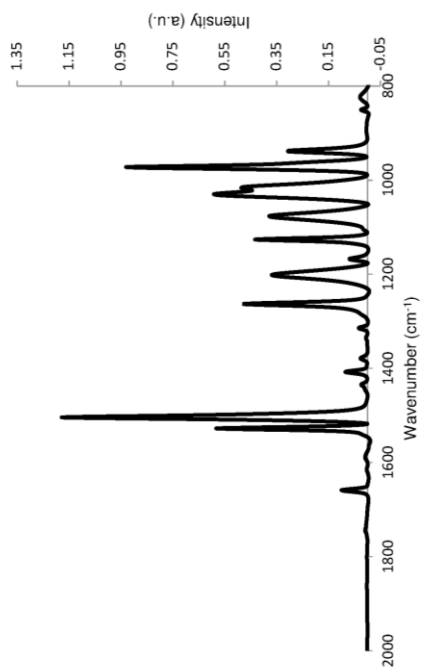
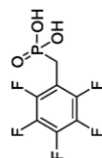
2,6-Difluoro-4-methoxybenzylphosphonic Acid, 62 (KBr)



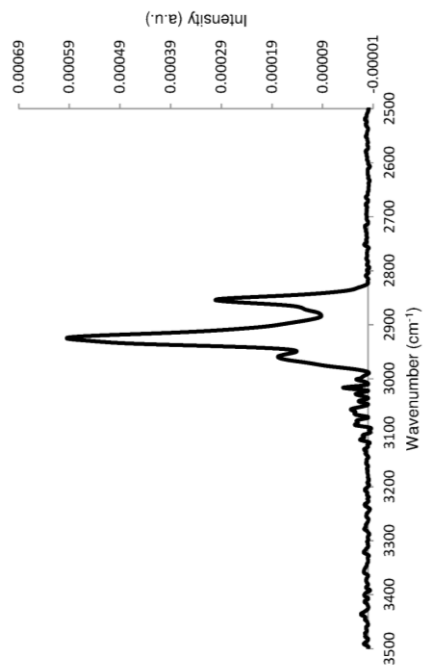
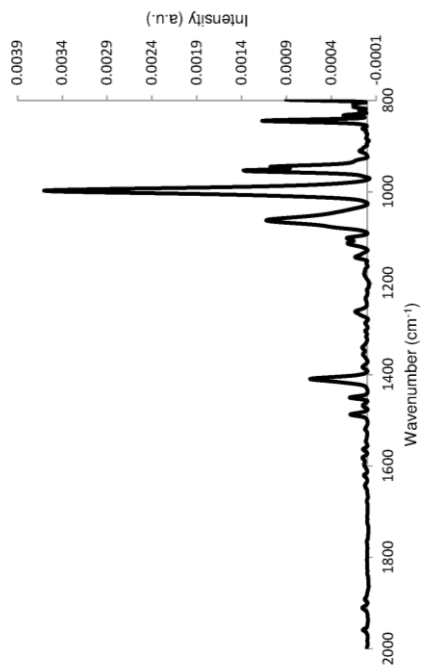
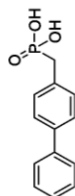
Pentafluorobenzylphosphonic Acid, 59 (CaF₂)



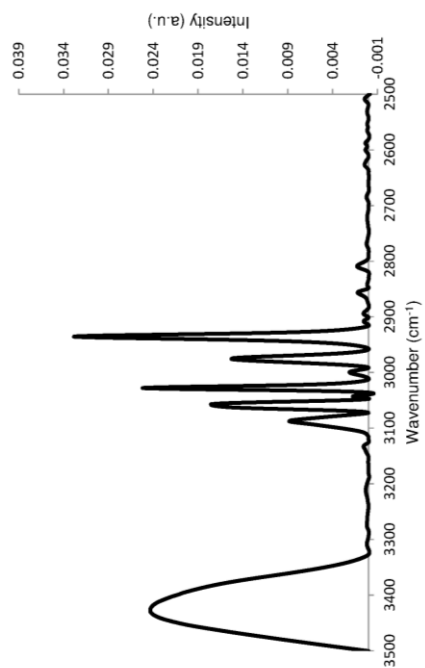
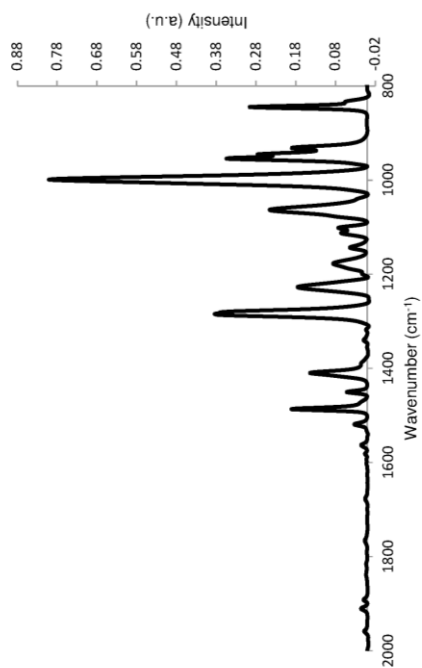
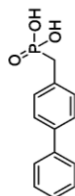
Pentafluorobenzylphosphonic Acid, 59 (KBr)



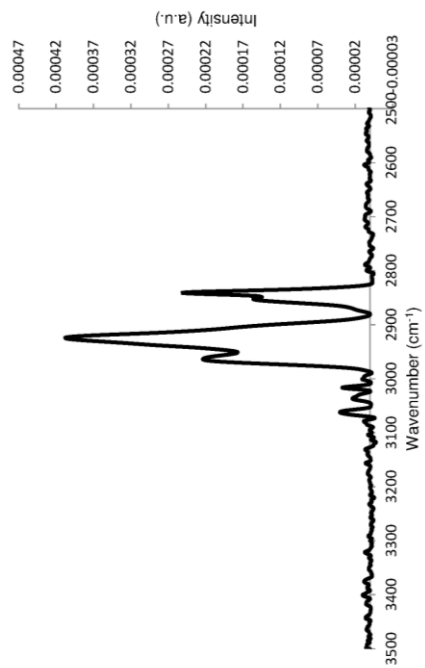
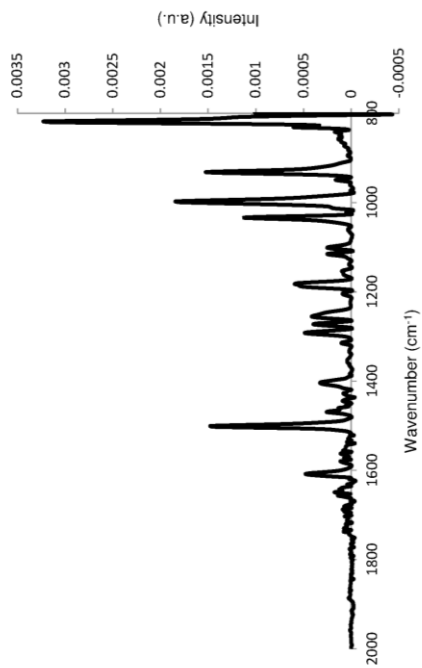
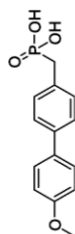
Biphenyl-4-ylmethylphosphonic Acid, 92 (CaF₂)



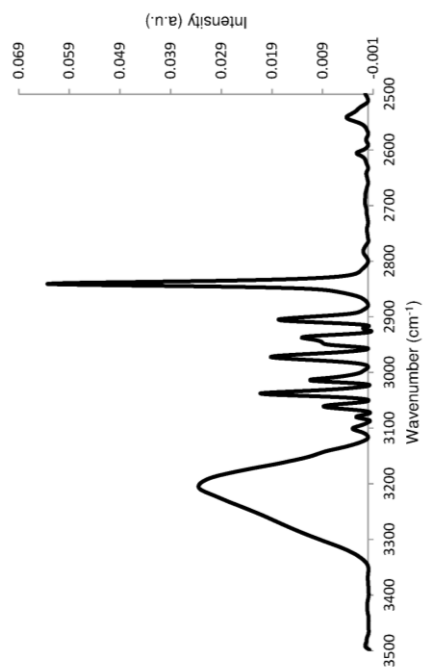
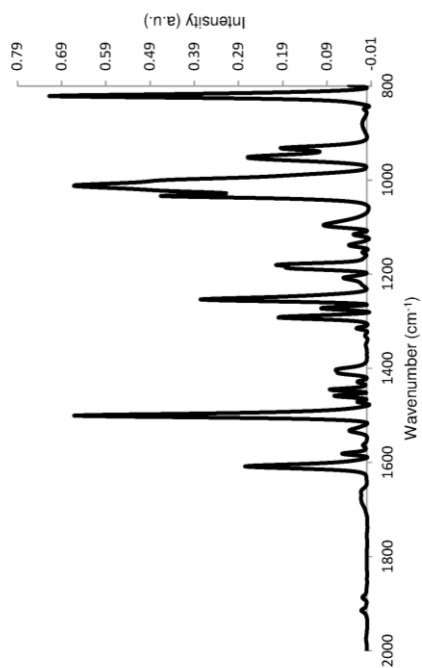
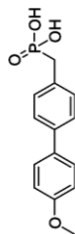
Biphenyl-4-ylmethylphosphonic Acid, 92 (KBr)



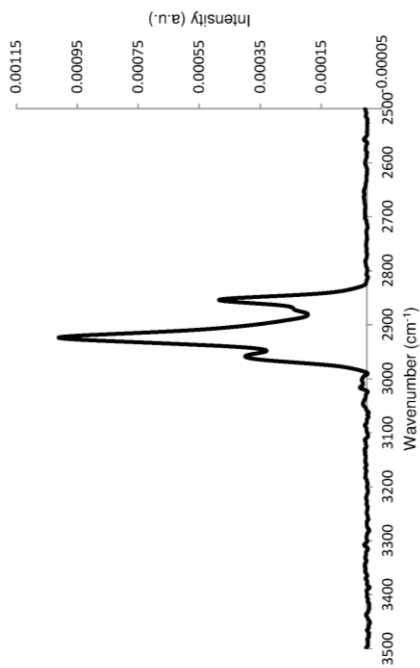
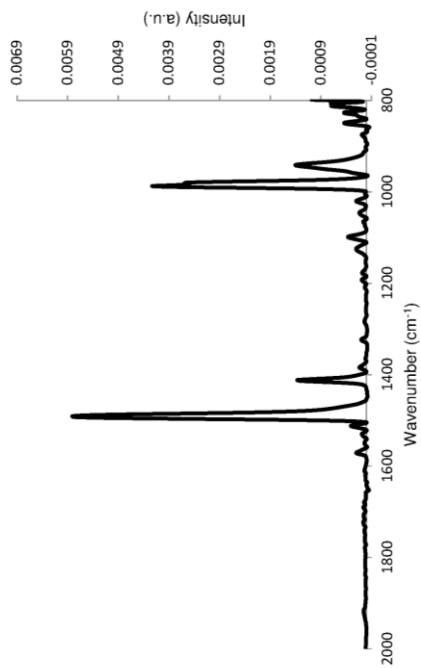
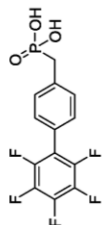
(4'-Methoxybiphenyl-4-yl)methylphosphonic Acid, 93 (CaF₂)



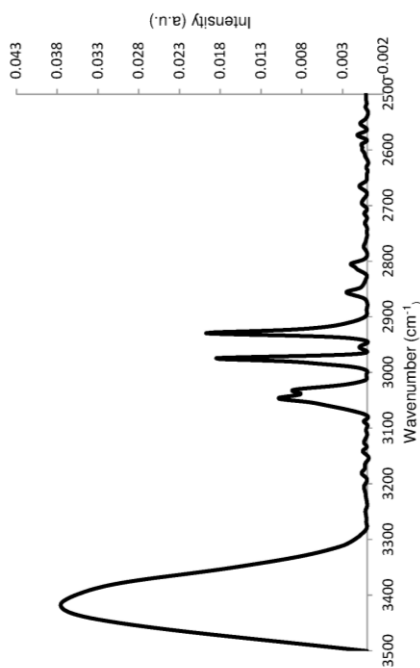
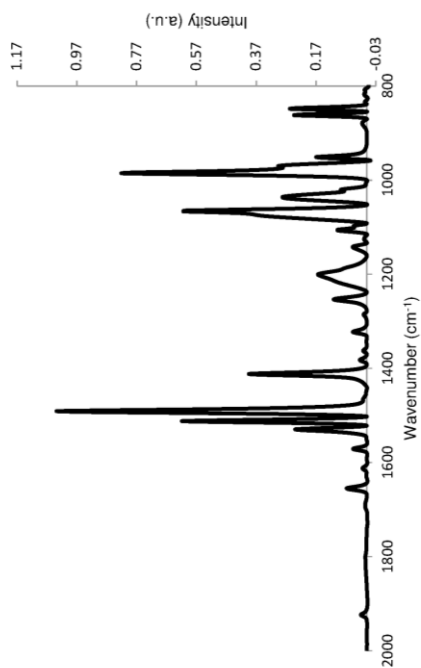
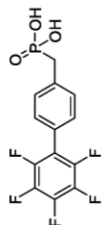
(4'-Methoxybiphenyl-4-yl)methylphosphonic Acid, 93 (KBr)



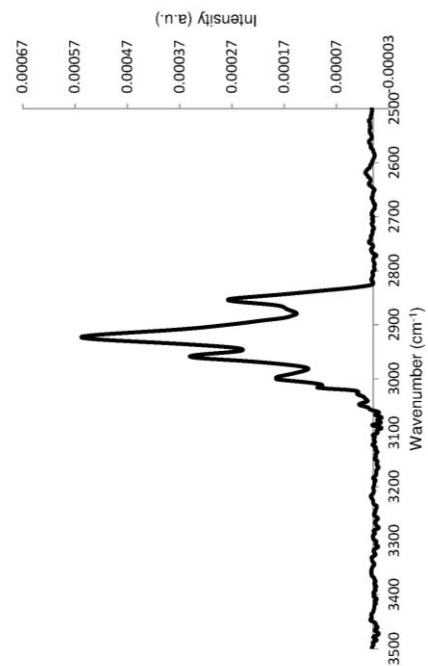
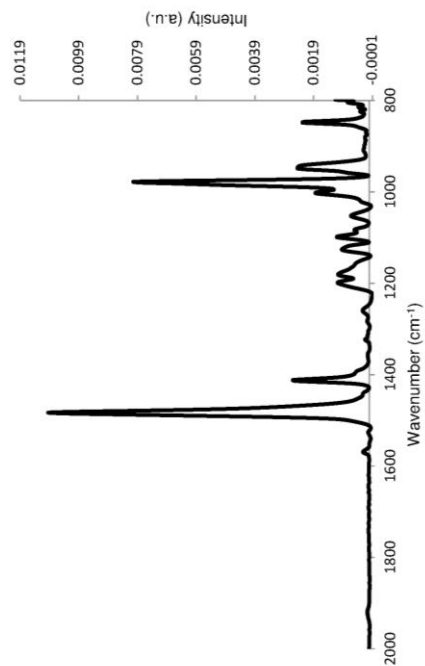
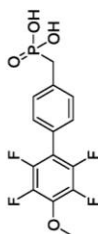
(2',3',4',5',6'-Pentafluorobiphenyl-4-yl)methylphosphonic Acid, 119 (CaF₂)



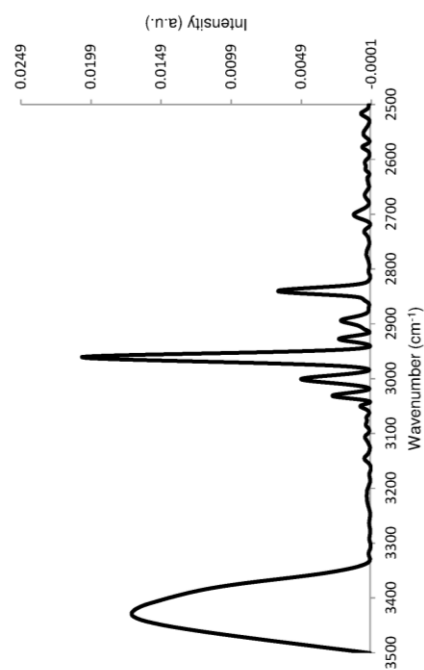
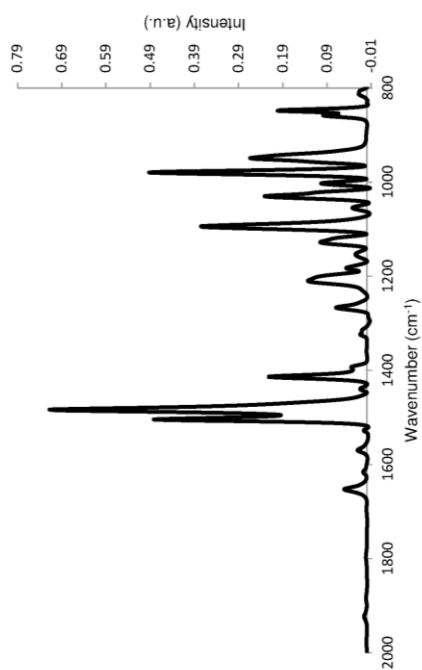
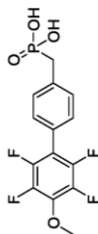
(2',3',4',5',6'-Pentafluorobiphenyl-4-yl)methylphosphonic Acid, 119 (KBr)



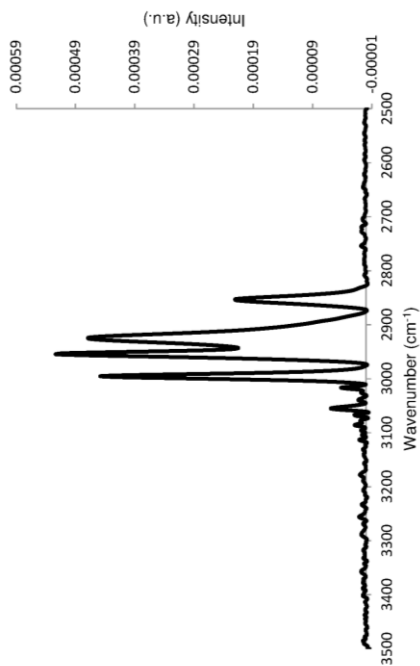
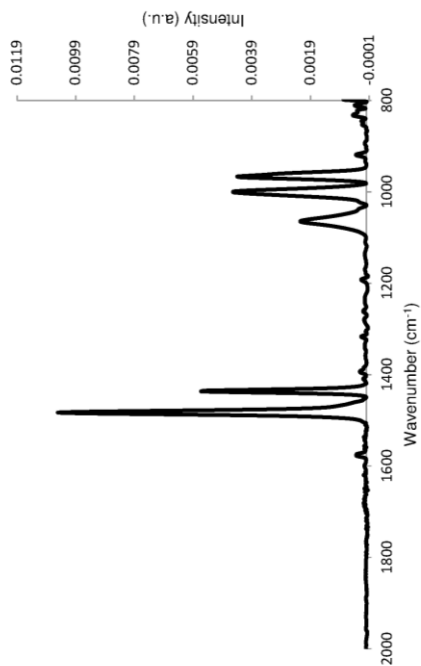
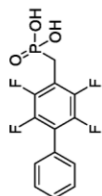
(2',3',5',6'-Tetrafluoro-4'-methoxybiphenyl-4-yl)methylphosphonic Acid, 120
(CaF₂)



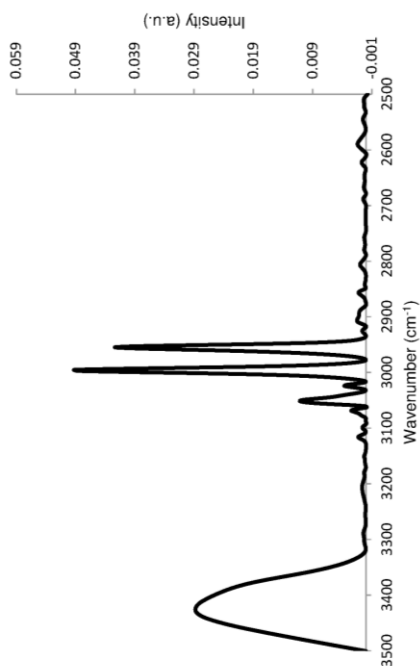
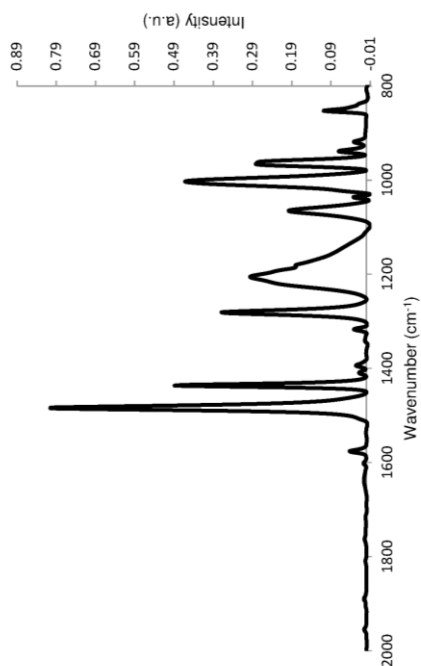
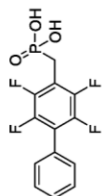
(2',3',5',6'-Tetrafluoro-4'-methoxybiphenyl-4-yl)methylphosphonic Acid, 120
(KBr)



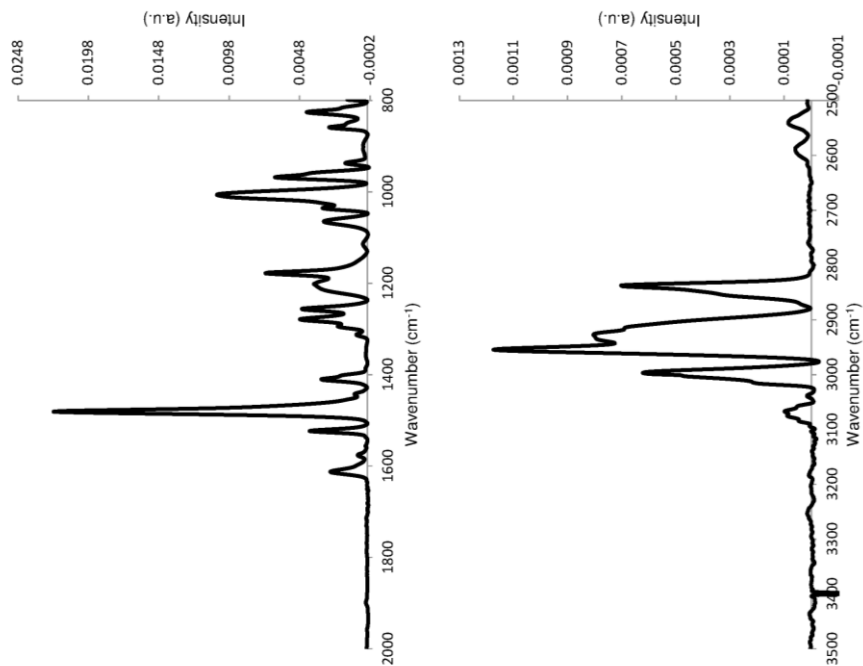
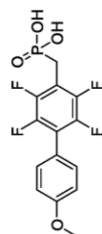
(2,3,5,6-Tetrafluorobiphenyl-4-yl)methylphosphonic Acid, **94** (CaF₂)



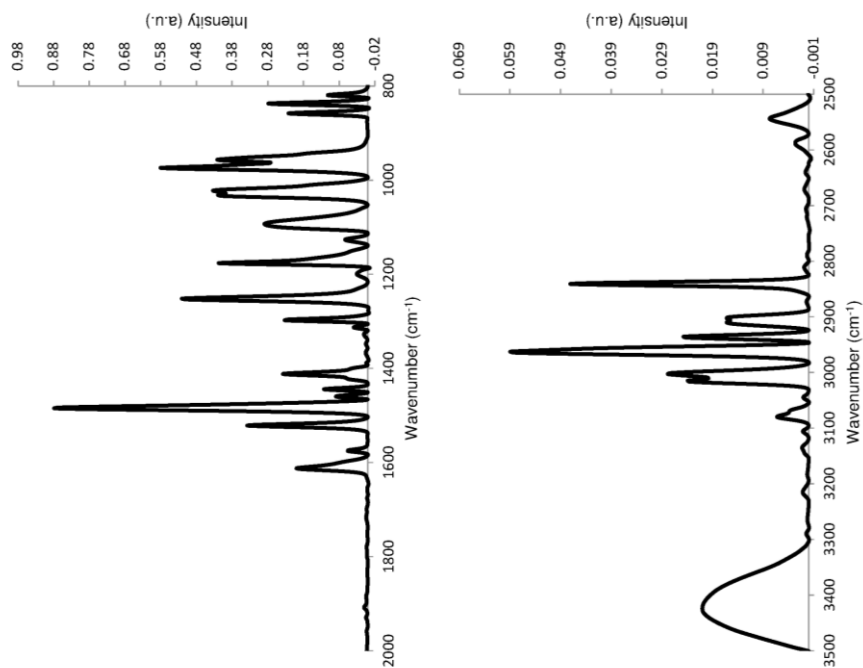
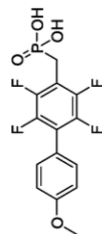
(2,3,5,6-Tetrafluorobiphenyl-4-yl)methylphosphonic Acid, **94** (KBr)



(2,3,5,6-Tetrafluoro-4'-methoxybiphenyl-4-yl)methylphosphonic Acid, 95 (CaF₂)



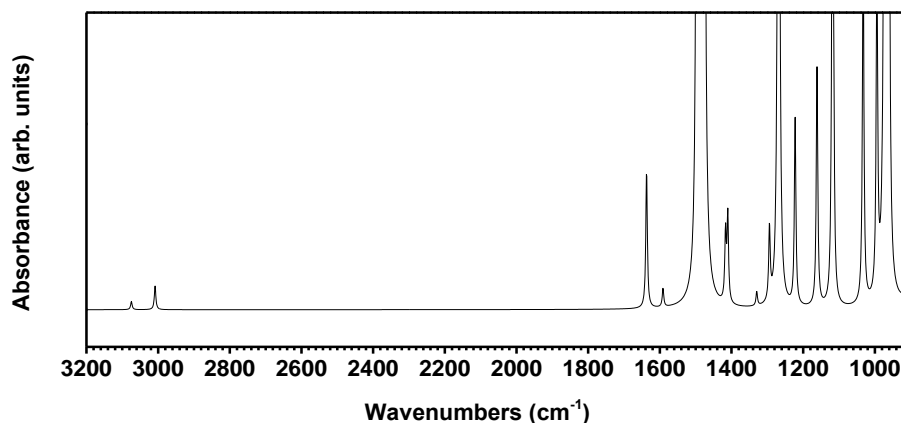
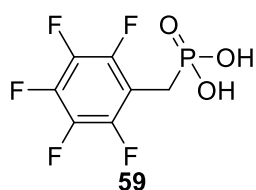
(2,3,5,6-Tetrafluoro-4'-methoxybiphenyl-4-yl)methylphosphonic Acid, 95 (KBr)



Appendix C

DFT Simulated IR Spectra

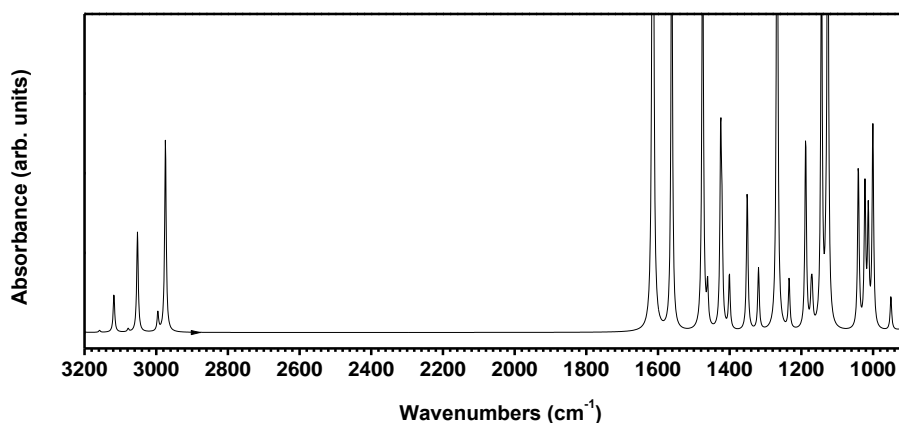
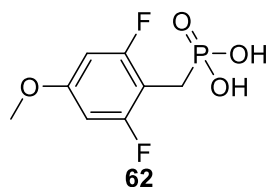
DFT simulated IR spectra for fluorinated benzylphosphonic acid derivatives **59**, **62**, **66**, **119** and **120**. It should be noted that only the relative peak shifts and not the absolute values, which deviate from experimental values depending on the choice of DFT function, are relevant for mode identification. All data compiled by Dr. Florian von Wrochem.



vibrational mode	au_amu	frequencies, cm ⁻¹	intensities, km/mol
1	-0.012747	-65.5	35.17
2	0.000000	0.0	0.10
3	0.000000	0.0	0.05
4	0.000000	0.0	0.12
5	0.000000	0.0	0.05
6	0.000000	0.0	0.03
7	0.000000	0.0	0.03
8	0.004778	24.6	2.52
9	0.010131	52.1	0.60
10	0.011587	59.6	1.06
11	0.024455	125.7	0.06
12	0.025775	132.5	0.03
13	0.033369	171.5	0.06
14	0.035136	180.6	16.72
15	0.040845	210.0	2.74
16	0.043366	222.9	10.71
17	0.051355	264.0	7.67
18	0.052731	271.1	10.37
19	0.053958	277.4	57.58
20	0.058397	300.2	0.79
21	0.063747	327.7	6.73

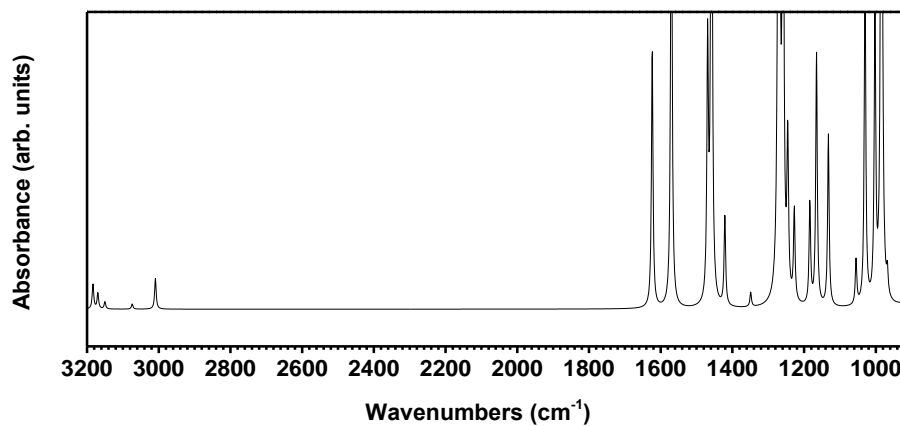
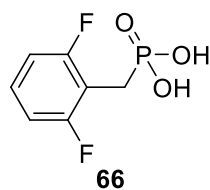
Appendix C: DFT Simulated IR Spectra

vibrational mode	au_amu	frequencies, cm ⁻¹	intensities, km/mol
22	0.065460	336.5	26.88
23	0.068831	353.8	6.40
24	0.070914	364.5	32.70
25	0.072628	373.3	0.55
26	0.077490	398.3	58.26
27	0.084947	436.7	53.17
28	0.085227	438.1	6.13
29	0.092310	474.5	12.96
30	0.109142	561.0	2.90
31	0.114692	589.6	17.06
32	0.124851	641.8	0.36
33	0.126804	651.8	4.51
34	0.135078	694.4	6.81
35	0.137541	707.0	1.34
36	0.144004	740.3	6.33
37	0.157650	810.4	169.17
38	0.163780	841.9	121.32
39	0.171863	883.5	205.71
40	0.187073	961.6	116.80
41	0.188948	971.3	226.91
42	0.193420	994.3	44.24
43	0.200894	1032.7	48.75
44	0.216968	1115.3	24.72
45	0.217661	1118.9	55.40
46	0.225933	1161.4	32.21
47	0.237821	1222.5	25.15
48	0.246788	1268.6	178.25
49	0.251743	1294.1	9.98
50	0.258660	1329.6	1.88
51	0.274375	1410.4	11.62
52	0.275605	1416.7	9.19
53	0.287670	1478.8	380.84
54	0.290854	1495.1	221.46
55	0.309537	1591.2	2.50
56	0.318454	1637.0	18.61
57	0.585284	3008.6	3.19
58	0.598139	3074.7	1.11
59	0.720217	3702.3	124.73
60	0.720844	3705.5	137.37



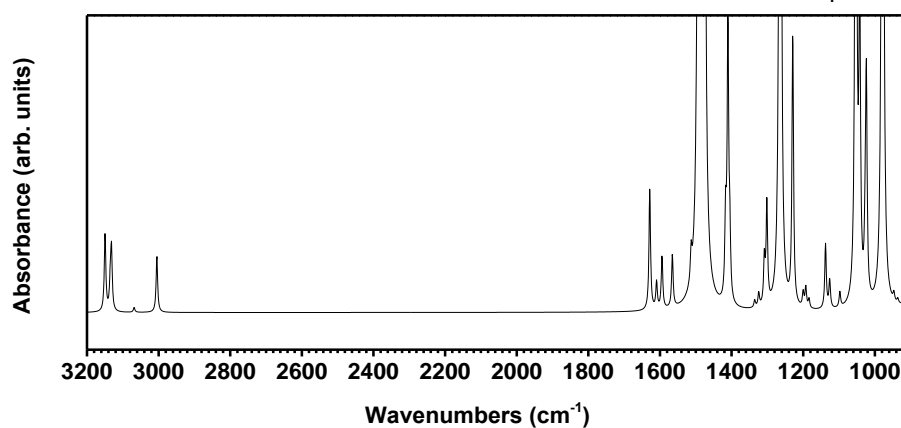
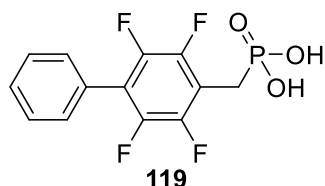
Appendix C: DFT Simulated IR Spectra

vibrational mode	au_amu	frequencies, cm-1	intensities km/mol
7	0.005148	26.5	0.03
8	0.007673	39.4	1.52
9	0.011291	58.0	0.53
10	0.014097	72.5	23.49
11	0.017352	89.2	8.85
12	0.025228	129.7	0.53
13	0.038289	196.8	11.27
14	0.040121	206.2	3.74
15	0.041782	214.8	1.28
16	0.043226	222.2	8.99
17	0.049840	256.2	0.12
18	0.057213	294.1	63.28
19	0.059069	303.6	5.97
20	0.061786	317.6	40.93
21	0.064375	330.9	5.51
22	0.066979	344.3	2.72
23	0.069871	359.2	24.73
24	0.076433	392.9	26.22
25	0.078625	404.2	56.45
26	0.086218	443.2	78.00
27	0.096794	497.6	8.07
28	0.101390	521.2	5.69
29	0.108709	558.8	3.41
30	0.112934	580.5	0.37
31	0.120080	617.3	5.07
32	0.123118	632.9	14.21
33	0.130587	671.3	2.50
34	0.141652	728.2	4.37
35	0.150556	773.9	18.41
36	0.155755	800.7	45.45
37	0.157995	812.2	2.36
38	0.159939	822.2	86.46
39	0.161107	828.2	206.03
40	0.169610	871.9	255.76
41	0.184835	950.1	10.60
42	0.194638	1000.5	63.27
43	0.197133	1013.4	35.43
44	0.198936	1022.6	43.90
45	0.202525	1041.1	51.13
46	0.219114	1126.4	169.69
47	0.220209	1132.0	8.19
48	0.222529	1143.9	123.17
49	0.227573	1169.8	10.17
50	0.228086	1172.5	9.24
51	0.231126	1188.1	60.05
52	0.240085	1234.2	15.77
53	0.246604	1267.7	181.82
54	0.256708	1319.6	19.47
55	0.262828	1351.1	43.77
56	0.272524	1400.9	17.31
57	0.276525	1421.5	26.30
58	0.277229	1425.1	59.10
59	0.284345	1461.7	12.54
60	0.287028	1475.5	142.42
61	0.287883	1479.9	0.82
62	0.303806	1561.7	143.65
63	0.314049	1614.4	269.71
64	0.578629	2974.4	60.45
65	0.582739	2995.6	5.83
66	0.593802	3052.4	31.53
67	0.598865	3078.5	1.00
68	0.606584	3118.1	12.02
69	0.614387	3158.3	0.62
70	0.621777	3196.2	0.07
71	0.718987	3695.9	127.52
72	0.722194	3712.4	111.66



vibrational mode	frequencies, intensities		
	au_amu	cm ⁻¹	km/mol
1	-0.005021	-25.8	9.31
2	0.000000	0.0	0.07
3	0.000000	0.0	0.04
4	0.000000	0.0	0.03
5	0.000000	0.0	0.01
6	0.000000	0.0	0.01
7	0.000000	0.0	0.05
8	0.009242	47.5	16.64
9	0.012346	63.5	1.86
10	0.015023	77.2	3.92
11	0.026837	138.0	0.74
12	0.038640	198.6	15.60
13	0.041356	212.6	17.99
14	0.046744	240.3	0.03
15	0.053630	275.7	81.61
16	0.055366	284.6	1.04
17	0.065192	335.1	24.29
18	0.067463	346.8	14.54
19	0.071221	366.1	31.42
20	0.077907	400.5	55.48
21	0.085795	441.0	62.30
22	0.095723	492.1	2.81
23	0.095829	492.6	7.44
24	0.104600	537.7	6.88
25	0.105744	543.6	7.49
26	0.114208	587.1	0.08
27	0.129905	667.8	1.31
28	0.136988	704.2	5.28
29	0.143030	735.2	27.92
30	0.152338	783.1	71.08
31	0.155576	799.7	105.31
32	0.159896	821.9	82.47
33	0.161874	832.1	83.75
34	0.164886	847.6	4.11
35	0.169255	870.1	218.10
36	0.188265	967.8	3.09
37	0.191445	984.1	124.97
38	0.195000	1002.4	40.22
39	0.200398	1030.1	45.47
40	0.205257	1055.1	6.03
41	0.220280	1132.3	23.18
42	0.226721	1165.5	34.23

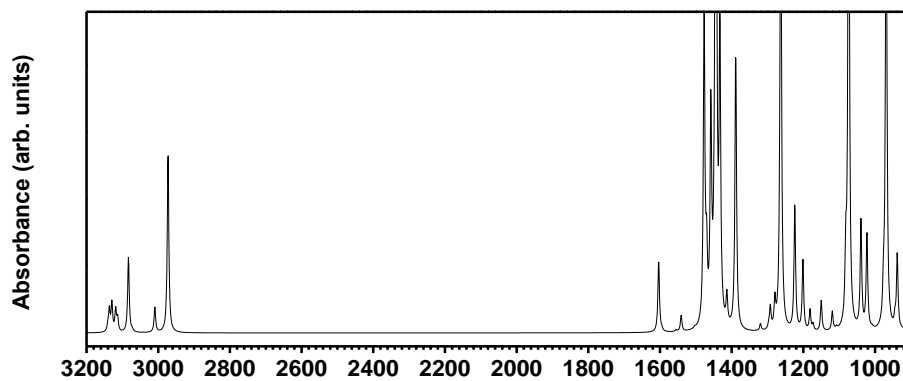
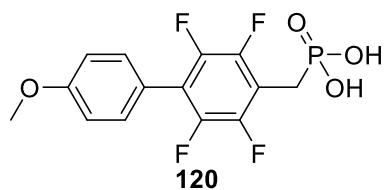
vibrational mode	au_amu	frequencies, cm ⁻¹	intensities, km/mol
43	0.230323	1184.0	13.73
44	0.238775	1227.4	12.38
45	0.242325	1245.7	21.39
46	0.244864	1258.7	77.70
47	0.247157	1270.5	160.28
48	0.262423	1349.0	1.95
49	0.276445	1421.1	12.08
50	0.283696	1458.3	92.60
51	0.285780	1469.0	34.39
52	0.305460	1570.2	70.01
53	0.315845	1623.6	35.40
54	0.585448	3009.5	4.16
55	0.598028	3074.2	0.70
56	0.612839	3150.3	0.97
57	0.616663	3169.9	2.15
58	0.619325	3183.6	3.37
59	0.718633	3694.1	127.56
60	0.721767	3710.2	116.99



vibrational mode	au_amu	frequencies, cm ⁻¹	intensities, km/mol
7	0.005767	29.6	0.12
8	0.006041	31.1	0.29
9	0.008725	44.9	1.06
10	0.013939	71.7	0.21
11	0.015469	79.5	0.04
12	0.016387	84.2	0.16
13	0.025845	132.9	0.02
14	0.028588	147.0	0.23
15	0.033677	173.1	1.01
16	0.036331	186.8	2.94
17	0.037428	192.4	2.89
18	0.039207	201.5	15.34
19	0.047496	244.2	7.05
20	0.051126	262.8	18.92
21	0.051895	266.8	0.04
22	0.053204	273.5	1.53
23	0.057628	296.2	39.91
24	0.059502	305.9	7.19
25	0.064166	329.8	13.19
26	0.065501	336.7	19.24

Appendix C: DFT Simulated IR Spectra

vibrational mode	au_amu	frequencies, cm ⁻¹	intensities km/mol
27	0.068652	352.9	8.41
28	0.071396	367.0	7.54
29	0.072766	374.1	0.72
30	0.075228	386.7	65.12
31	0.081185	417.3	5.44
32	0.082683	425.0	43.98
33	0.083057	427.0	55.61
34	0.084087	432.3	4.87
35	0.087967	452.2	38.26
36	0.093603	481.2	2.18
37	0.103334	531.2	43.78
38	0.110208	566.5	3.19
39	0.118984	611.6	7.90
40	0.123495	634.8	0.48
41	0.126021	647.8	0.13
42	0.127414	655.0	0.94
43	0.134162	689.7	12.83
44	0.140270	721.1	4.89
45	0.144561	743.1	3.63
46	0.149918	770.7	2.16
47	0.152962	786.3	135.50
48	0.156828	806.2	56.25
49	0.157542	809.8	10.26
50	0.161312	829.2	64.21
51	0.162843	837.1	149.09
52	0.166657	856.7	26.41
53	0.168773	867.6	213.08
54	0.182080	936.0	0.62
55	0.184199	946.9	1.13
56	0.190336	978.4	205.38
57	0.199164	1023.8	29.26
58	0.199793	1027.0	7.01
59	0.202764	1042.3	42.00
60	0.204853	1053.0	126.43
61	0.213537	1097.7	2.03
62	0.219058	1126.1	3.85
63	0.221333	1137.8	8.75
64	0.230296	1183.8	1.24
65	0.232049	1192.8	2.75
66	0.233476	1200.2	2.06
67	0.239135	1229.3	36.78
68	0.245972	1264.4	210.38
69	0.253192	1301.5	13.57
70	0.254553	1308.5	6.16
71	0.257611	1324.2	1.86
72	0.259801	1335.5	0.98
73	0.273338	1405.1	8.01
74	0.274353	1410.3	37.33
75	0.275629	1416.9	10.81
76	0.287592	1478.4	330.45
77	0.289940	1490.4	321.20
78	0.294320	1512.9	3.95
79	0.304524	1565.4	7.09
80	0.310143	1594.3	7.11
81	0.313100	1609.5	3.63
82	0.316799	1628.5	16.31
83	0.584576	3005.0	7.58
84	0.596928	3068.5	0.65
85	0.609245	3131.8	8.15
86	0.609898	3135.2	3.63
87	0.612710	3149.6	10.06
88	0.613049	3151.4	0.44
89	0.719580	3699.0	137.94
90	0.723577	3719.5	94.78



vibrational mode	Wavenumbers (cm ⁻¹)		
	au_amu	frequencies, cm ⁻¹	intensities km/mol
7	0.004719	24.3	0.41
8	0.005107	26.3	0.13
9	0.008504	43.7	0.40
10	0.011391	58.6	1.91
11	0.013309	68.4	0.23
12	0.015609	80.2	1.75
13	0.017455	89.7	4.00
14	0.023228	119.4	0.96
15	0.025539	131.3	0.59
16	0.030568	157.1	10.14
17	0.033821	173.9	25.67
18	0.035465	182.3	2.91
19	0.035686	183.4	4.91
20	0.038350	197.1	1.88
21	0.043308	222.6	5.27
22	0.046314	238.1	28.20
23	0.049853	256.3	43.15
24	0.053808	276.6	14.02
25	0.055847	287.1	8.44
26	0.057756	296.9	24.76
27	0.058685	301.7	4.80
28	0.061340	315.3	5.88
29	0.065976	339.2	1.65
30	0.069288	356.2	6.96
31	0.072468	372.5	10.88
32	0.074392	382.4	46.33
33	0.074791	384.5	1.71
34	0.079372	408.0	66.86
35	0.081261	417.7	2.57
36	0.083856	431.1	28.22
37	0.084791	435.9	9.88
38	0.089898	462.1	14.00
39	0.092814	477.1	3.26
40	0.102550	527.2	45.32
41	0.109448	562.6	3.74
42	0.118225	607.7	10.23
43	0.123220	633.4	0.03
44	0.126437	649.9	0.22
45	0.133197	684.7	1.48
46	0.134490	691.3	12.90
47	0.142632	733.2	8.20
48	0.146111	751.1	0.82
49	0.149653	769.3	2.79

Appendix C: DFT Simulated IR Spectra

vibrational mode	au_amu	frequencies, cm ⁻¹	intensities km/mol
50	0.152736	785.1	129.62
51	0.155809	800.9	71.04
52	0.159555	820.2	39.64
53	0.162590	835.8	112.70
54	0.163769	841.9	126.73
55	0.164670	846.5	18.92
56	0.169868	873.2	171.94
57	0.182493	938.1	27.64
58	0.183763	944.6	3.68
59	0.188492	968.9	183.84
60	0.189970	976.5	11.58
61	0.196102	1008.1	0.69
62	0.198948	1022.7	36.26
63	0.202186	1039.3	40.27
64	0.208843	1073.6	222.60
65	0.210417	1081.6	23.70
66	0.215488	1107.7	0.93
67	0.217739	1119.3	7.02
68	0.223753	1150.2	11.39
69	0.228182	1173.0	2.44
70	0.229819	1181.4	7.75
71	0.230875	1186.8	0.09
72	0.233679	1201.2	26.19
73	0.238096	1223.9	47.32
74	0.245720	1263.1	191.87
75	0.248902	1279.5	10.13
76	0.251395	1292.3	8.13
77	0.252222	1296.5	1.56
78	0.256761	1319.9	2.59
79	0.270065	1388.3	38.11
80	0.270212	1389.0	69.10
81	0.274974	1413.5	11.02
82	0.278752	1432.9	107.20
83	0.280978	1444.4	308.29
84	0.283662	1458.2	77.18
85	0.285977	1470.1	23.71
86	0.287311	1476.9	118.35
87	0.292398	1503.1	0.57
88	0.299775	1541.0	5.97
89	0.302553	1555.3	0.58
90	0.310228	1594.7	0.68
91	0.311971	1603.7	27.00
92	0.578296	2972.7	67.44
93	0.585458	3009.5	9.38
94	0.597689	3072.4	0.72
95	0.599787	3083.2	28.16
96	0.605663	3113.4	4.98
97	0.606730	3118.9	8.40
98	0.608790	3129.5	10.70
99	0.610160	3136.5	8.14
100	0.610971	3140.7	2.20
101	0.720475	3703.6	140.26
102	0.722015	3711.5	93.57